

# STUDIES ON STRETCHED ZONE WIDTH (SZW) AND FRACTURE TOUGHNESS IN LOW CARBON STEELS

A THESIS

*Submitted in fulfilment of the  
requirements for the award of the degree*

*of*

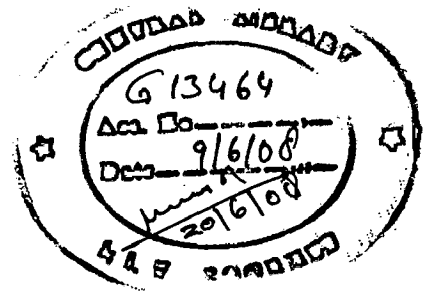
DOCTOR OF PHILOSOPHY

*in*

METALLURGICAL AND MATERIALS ENGINEERING

*by*

SANDEEP BANSAL



DEPARTMENT OF METALLURGICAL AND MATERIALS ENGINEERING  
INDIAN INSTITUTE OF TECHNOLOGY ROORKEE

ROORKEE-247 667 (INDIA)

FEBRUARY, 2007



# INDIAN INSTITUTE OF TECHNOLOGY ROORKEE ROORKEE


## CANDIDATE'S DECLARATION

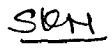
I hereby certify that the work which is being presented in the thesis entitled **STUDIES ON STRETCHED ZONE WIDTH (SZW) AND FRACTURE TOUGHNESS IN LOW CARBON STEELS** in fulfilment of the requirements for the award of the Degree of Doctor of Philosophy and submitted in the Department of Metallurgical and Materials Engineering of the Indian Institute of Technology Roorkee, Roorkee is an authentic record of my own work carried out during a period from July, 2001 to February, 2007 under the supervision of Dr. S. K. Nath, Professor & Head and Dr. Subrata Ray, Professor, Department of Metallurgical and Materials Engineering, Indian Institute of Technology Roorkee, Roorkee.

The matter presented in the thesis has not been submitted by me for the award of any other degree of this or any other Institute.

  
(SANDEEP BANSAL)

This is to certify that the above statement made by the candidate is correct to the best of our knowledge.

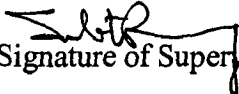
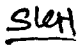
  
(Dr. Subrata Ray)  
Professor

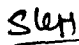
  
(Dr. S. K. Nath)  
Professor & Head

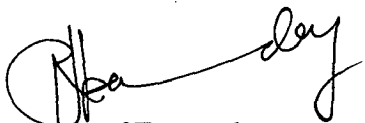
Date: 6-2-07.

Department of Metallurgical and Materials Engineering  
Indian Institute of Technology Roorkee  
Roorkee-247667

The Ph.D. Viva-Voce Examination of Mr. Sandeep Bansal, Research Scholar has been held on...June..22,,2007.....

   
Signature of Supervisor (s)

  
Signature of H.O.D.

  
Signature of External Examiner

A decorative line graphic consisting of a horizontal line on the left, a diagonal line sloping down to the right, and another horizontal line extending to the right. The word "ABSTRACT" is positioned to the right of the diagonal line, above the second horizontal line.

## ABSTRACT

The technological advancement in aerospace, nuclear, piping and oil tanker industry has put stringent demand on structural components leading to widespread failure. These failures often are catastrophic with serious consequences on important aspects of life like economy, ecology and safety. Fortunately, some of the potential dangers due to increasing technological complexity may, in many cases, be reduced or avoided through better understanding of materials. Earlier, the design engineers used the flow behavior of ductile materials under uni-axial loading as the basis of design although for brittle materials, the preexisting crack used to be taken into account. Cracks and crack like defects exist in both the brittle and the ductile materials, which escape attention because of size limitation of detection ability of different quality control methods. It is also well known that these defects often initiate at non-metallic inclusions or at casting, forging and welding defects and propagate rapidly causing structural failure. There are certain similar defects, which may remain benign and does not contribute to failure. The identification of potentially dangerous defects and the condition under which these defects start propagating, has become the focus of research in fracture mechanics and this knowledge is being increasingly incorporated in our approach to design and quality control.

Fracture toughness,  $J$ , has been identified as a measure of resistance to extension of a crack [ASTM E1823-96 1996] and it is a key concept fracture mechanics, which deals with the effect that a defect has on the load-bearing capacity of structures and materials. The fracture mechanics allows a quantitative assessment of the resistance of a material to fracture by determining the maximum load-bearing capacity of a structural element with a given crack size, subjected to monotonically increasing load. The fracture toughness may also provide an indicator that marks the onset of extension of a crack. In some cases, the curve describing the behaviour of stable extension of a crack is important from the application point of view.

In general, the fracture toughness helps to indicate the end point of the useful life of a material or structure. As such, it may be used as a parameter for determining the design conditions like allowable stresses in order to make material selection for a given application and also, to set inspection criteria for the corresponding maximum size of crack which could be tolerated in a safe structure.

Resistance to fracture of a ductile material is determined by its  $J$ - $R$  curve, which shows variation of fracture toughness,  $J$ , with the extension of crack and it is an important input to all elastic-plastic fracture analysis of structures.  $J$ - $R$  curve is determined experimentally through fracture toughness test of a specimen or component, which involves loading under bending or tension of fatigue pre-cracked specimens for the determination of  $J$  as a function of crack length during the process of crack growth.  $J$ - $R$  curve was earlier believed to be the material property. Thus, the  $J$ - $R$  curve obtained through the Compact Tension (CT) / Three Point Bend (TPB) specimens of the same material could as well be applied to estimate the limiting load for a prototype structure. However, it is increasingly been realized that real life structures exhibit fracture resistance which is different from that of CT/TPB specimens. The transferability of the  $J$ - $R$  curve obtained by CT/TPB specimens to component level is, thus, an important issue in fracture mechanics. As fracture mechanics parameters have become extremely important as design criteria, it is imperative to develop simple, easy and reproducible measurement method which could be undertaken without much specialized knowledge and also address the transferability issue of the  $J$ - $R$  curve to component level. During fracture in CT and TPB specimens it is observed that between fatigue pre-crack region and the region of stable crack propagation, there is a stretched zone, which develop during initial stage of tensile loading as a result of the blunting of fatigue pre-crack. It has been proposed that the stretched zone width ( $SZW$ ) could be used to determine the initiation fracture toughness,  $J_{IC}$ , of a material. Further, it has been claimed that  $J_{IC}$  determining on the basis of  $SZW$  is more reliable than that determined followed the procedure prescribed by ASTM.

The present study aims to explore the correlation between the initiation fracture toughness ( $J_{IC}$ ) and stretched zone width ( $SZW$ ) in high toughness ferrous material system. The distribution of  $SZW$  along the thickness of a test specimen has been explored in SA333 Gr. 6 and SAILMA HI 410 steel under investigation in order to extract a reliable parameter of  $SZW$ . The impact of variation of the thickness and the extent of fatigue pre-crack on  $SZW$  and  $J-R$  curve has been examined to arrive at a reasonable understanding of the effect of these parameters on the transferability of the laboratory data to real life components. The negative crack extension in the  $J-R$  curve often observed in ductile specimen as an artifact, has been tackled by appropriate shifting of the  $J-R$  curve [Rosenthal *et al*, 1990; Bowman *et al*, 1988; Voss and Mayville, 1985 and Seok, 2000]. The initiation fracture toughness and  $J-R$  curves, which are important from design point of view, have been investigated in SA333 Gr. 6 and SAILMA steel with special attention of the transferability issue.

The dissertation has been organized into chapters with contents as outlined below.

Chapter-1 contains the introductory remarks about the fracture toughness and its importance for the design. The problems associated with the measurement of fracture toughness are also briefly discussed.

Chapter-2 begins with the survey of the existing literature outlining the evolution of concepts of fracture mechanics leading to elastic plastic fracture mechanics based on  $J$ -integral. The acceptance of fracture parameter relevant to engineering applications is dependent upon how easily it can be measured on test specimens. The various procedures to determine the  $J-R$  curve and the initiation fracture toughness have been critically examined. The effects of specimen geometry on initiation fracture toughness have been highlighted as it provides a context for the present study because of their importance in the context of transferability. An exhaustive survey of literature has been carried out to understand the existing knowledge about the formation of stretched zone and the role that its width may play in determining

initiation fracture toughness. After reviewing the available literature, the problem under the current investigation has been formulated.

Chapter-3 presents the experimental techniques and procedure employed for fracture toughness testing and stretched zone width measurement in the two types of steel investigated. This chapter also highlights various methodologies applied in respect of microstructure characterization, tensile testing and cleaning and preservation of fractured surfaces.

The materials investigated, as mentioned earlier are SA333 Gr. 6 steel pipes of 16" diameter and wall thickness of 32 mm, SAILMA HI-410 micro-alloyed steel plate of thickness 32 mm. The SA333 Gr. 6 steel pipes have been procured from Bhaba Atomic Research Centre (BARC). SAILMA HI-410 micro-alloyed steel plate is a product of SAIL, India and has been procured from Govt. Irrigation Workshop, Roorkee. Test on compact tension (CT) and Single Edge Notch (SENB) [also called Three point Bend (TPB)] specimens carried out to generate the  $J$ - $R$  curves for SA333 Gr. 6 and SAILMA micro alloyed steel (HI 410) materials have been described including the procedure used to incorporate a wide range of crack tip triaxiality in order to see its effect on  $J$ - $R$  curve in specimens having different constraints ahead of the crack tip.

$J$ - $R$  curve is determined experimentally through fracture toughness test of a specimen, which involves determination of load versus load-line displacement recorded digitally as the basic data of the test. The  $J$ -integral is determined at different load-displacement points from the load by the relevant analytical expression for a given mode of loading and it is plotted against crack extension,  $\Delta a_p$ , as determined through compliance within specified limits of crack growth. These data are plotted as  $J$  versus crack extension, which reflects the resistance of a material to crack growth. The  $J$  versus crack extension behaviour is approximated with the best-fit power law relationship. A blunting line is drawn, approximating crack tip stretch effects, following ASTM standard E 813. The blunting line is defined as a line that

approximates apparent crack advance as given by change in compliance due to crack tip blunting. The equation for the blunting line is given by ASTM as  $J = 2\sigma_f \Delta a$ , where,  $\sigma_f = \frac{1}{2}(\sigma_Y + \sigma_U)$ . The value of  $J$  on  $J$ - $R$  curve marking the initiation of the actual ductile crack extension is termed as initiation fracture toughness ( $J_{IC}$ ). The initiation fracture toughness has been taken to be a point on the  $J$ - $R$  curve corresponding to physical crack extension of 0.2 mm, which could be identified by an offset construction line at 0.2 mm with the same slope that is defined in the test method [ASTM E 813, 1995].

After testing for  $J$ - $R$  curves, the fractured surfaces of the CT/TPB specimens have been separated by dipping it in liquid nitrogen and pulling apart to cause brittle fracture in the remaining area, not fractured during the test. These surfaces have been cleaned before examining the surfaces under *SEM* to measure Stretched zone width (*SZW*).

Chapter-4 describes the results of the studies on materials characterization and stretched zone observed on the fractured surface of the tested CT and TPB specimens of the two steels used in the present investigation. In SA333 Gr. 6 steel the carbon content is 0.16 wt% which is lower than the specified 0.18 wt% and the silicon content is more than the specified level. A small amount of aluminium is also observed in the pipe material and it could have originated from de-oxidation practice or been added intentionally for grain size control. Sulphur and phosphorus contents in the material are at acceptable levels. The chemical composition of SAILMA HI-410 micro-alloyed steel shows that the plates are having micro alloying of Cr (0.003-0.011 wt%) and Ni (0.031-0.035 wt%) along with Cu (0.033-0.042 wt%). The carbon content of the steel is 0.14 wt%. The micrographs of SA333 Gr. 6 steels show the presence of ferrite (white) and pearlite (black) in the matrix with banded morphology. The microstructures of as received SAILMA HI 410 steel plate obtained by controlled rolling, revealed ferrite-pearlite (dark) microstructure with relatively finer grains and the presence of pearlite is primarily along the bands observed in typical rolled structure. The yield strength of all the pipes of SA333 Gr. 6 steel is greater than 280 MPa and the tensile strength is around

420 MPa. The percent elongation is more than 36% as specified. The yield strength of SAILMA HI 410 steel plate is 440 MPa, the tensile strength is about 574 MPa but elongation is about 29 %.

The widths of the stretched zone have been measured by scanning electron microscopy at low magnification under tilted condition. There are two prevalent methods for measuring stretched zone width (*SZW*) – the nine point method of ESIS and three point method. To determine the adequacy of the methods in the present context, the stretched zone width (*SZW*) has been measured from micrographs along the thickness on the fracture surface at close intervals of about 200  $\mu\text{m}$  and the average, which is taken as the true average *SZW*<sub>t</sub>, has been compared with that determined by three point (*SZW*<sub>3</sub>) and nine point methods (*SZW*<sub>9</sub>) for different specimens. It has been observed that the stretched zone width estimated by nine point method is almost similar to the true stretched zone width while the stretched zone width estimated by three point method are generally lower than the true stretched zone width. Thus, it appears that nine point method is more likely to give a representative estimate of stretched zone width.

In the present study, the variations of stretched zone width, both true as well as those measured by the nine point method, with the thickness at different pre-crack depths of the two steel have been studied. In view of mixed trends and variation limited to 95% confidence interval, no significant trend in the variation of stretched zone with thickness of the specimens could be inferred.

The variation of stretched zone width, both true as well as those measured by the nine point method, with the pre-cracked depth have also been studied at different thicknesses of the two steels. Here, again no definite conclusion could be drawn about the dependence of *SZW* on the depth of pre-cracking. Thus, one may arrive at a mean value of *SZW* over different thickness and depths of pre-cracking and use it for the determination of fracture toughness.



The effect of composition and heat treatment on the observed stretched zone width in low carbon steels shows a limited variation within the observed standard deviation of the measurements. However, it was interesting to note higher standard deviation in the measurement of *SZW* in normalized SA333 Gr. 6 steel which has relatively higher difference in mechanical properties of phase constituents in the microstructure compared to that in either annealed or as received steels.

Chapter-5 describes the finding of the study regarding the initiation fracture toughness of the two steels investigated in the present study. The *J-R* curves have been obtained for CT and TPB specimens by compliance technique using the compliance equation for crack extension. Sometimes, the initial crack extension ( $\Delta a$ ) data points in the *J-R* curve have anomalous negative values, which are often encountered in ductile materials during partial unloading compliance test. This is an artifact of the method of measurement. ASTM standard does not discuss this problem of the apparent negative crack growth phenomenon or specify any procedure for treating *J-R* curve with such features. These *J-R* curves have been corrected by a constant by shift of all *J* versus  $\Delta a$  data points along the  $\Delta a$  direction so that the most negative  $\Delta a$  point falls on the blunting line from origin as proposed by Seok [2000].

The initiation fracture toughness ( $J_{IC}$ ) based on the offset blunting line equation with 0.2 mm offset as prescribed by ASTM could not be determined in highly ductile steel, since this offset line has a relatively smaller slope as estimated from the material flow stress and does not intersect the *J-R* curve within the valid region as prescribed by ASTM standard. Thus, there is a need to establish an accurate slope for the blunting line for highly ductile materials. The slope have been evaluated from the observed *SZW* and its variation with strain hardening coefficient has been fitted by regression to find an empirical expression of slope in term of strain hardening coefficient. It is observed that the fracture toughness measured by the *SZW* method and fracture toughness measured by the blunting line as obtained from the regression equation are comparatively similar, showing consistency of the blunting line equation with individual measurements.

The variation of initiation fracture toughness, measured either by the blunting line method or by the stretched zone width method, with increasing specimen thickness and pre-crack depth have been studied for the two steels under investigation. The variation of the initiation fracture toughness ( $J_{IC}$ ) with the pre-crack depth ( $a/W$  ratio) for CT specimens of SA333 Gr. 6 steel shows that in a relatively thin specimen there is drastic reduction in  $J_{IC}$  when pre-crack depth increases from  $a/W$  ratio of 0.4 to 0.6 but beyond 0.6,  $J_{IC}$  changes marginally till  $a/W$  ratio of 0.8. But at larger thickness, there is continuous reduction in  $J_{IC}$  with increasing  $a/W$  ratio in the entire range from 0.4 to 0.8. The results on the effect of  $a/W$  ratio on  $J_{IC}$  in CT specimens of SAILMA steel show similar trends of variation as observed in SA333 Gr. 6 steel. The fracture toughness of three point bend specimen of SA333 Gr. 6 steel increases with increasing  $a/W$  ratio, but the extent of increase is relatively small and becomes still smaller at lower thickness. This trend is contrary to that observed on CT specimens.

The influence of specimen thickness on the initiation fracture toughness  $J_{IC}$  for CT specimens of SA333 Gr. 6 steel show that fracture toughness decreases with increasing thickness but it is observed only in the range of thickness between 15 and 25 mm. At relatively lower thickness, initiation fracture toughness increases significantly with increasing specimen thickness between 10 and 15 mm. The variation of the initiation fracture toughness,  $J_{IC}$ , with the specimen thickness of CT specimens of SAILMA steel shows that in thinner specimens with lower pre-crack depth the fracture toughness increases drastically but on increasing the thickness the fracture toughness decreases. However, at higher pre-crack depth, the initiation fracture toughness increases steadily with increasing specimen thickness. The variation of the initiation fracture toughness,  $J_{IC}$ , measured on TPB specimens of SA333 Gr. 6 steel, with increasing specimen thickness show that the initiation fracture toughness measured by either 0.2 mm offset blunting line or *SZW* method, is more or less insensitive to increasing thickness.

The observed *J-R* curves leads one to infer that *J-R* curves for CT specimens of different thicknesses and pre-crack depths show mixed trends in both SA333 Gr.6 and

SAILMA steel but TPB specimens of SA333 Gr. 6 steel show consistent trends of lower  $J$ - $R$  curves for thinner specimens of higher pre-crack depth, which are also observed in CT specimens in certain limited ranges of thickness and pre-crack depth.

The effect of different composition and heat treatments like annealing and normalizing on fracture behavior of different carbon steels reveals that the variation in initiation fracture toughness in CT specimens of 25 mm thickness and pre-crack depth of 0.6, closely follows the trend of variation in ductility obliterating the effect of strength, possibly because of limited variation of mechanical properties in the steels investigated.

At relatively high crack extension, the annealed SA333 Gr. 6 steel having relatively lower strength, has relatively much higher slope of  $J$ - $R$  curve compared to that in as received SA333 Gr. 6 steel which has shown a relatively higher strength and ductility, possibly because of the difference in morphology of phases. The normalized SA333 Gr. 6 steel has a  $J$ - $R$  curve lower than that of as received steel at higher crack extension reflecting the importance of ductility, which is more emphasized in the lowest observed  $J$ - $R$  curve in SAILMA steel.

Chapter 6 presents the major conclusions of the current study in two segments. The first segment includes conclusions relating to materials characterization and stretched zone width observed on the fractured surface of the tested CT and TPB specimens of the two steels used in the present investigation. The conclusions related to the initiation fracture toughness and  $J$ - $R$  curves have been outlined in the second segment.



## ACKNOWLEDGEMENTS

The author is pleased to express his immense sense of gratitude to *Dr. S. K. Nath*, Professor and Head and *Dr. Subrata Ray*, Professor, Department of Metallurgical and Materials Engineering, Indian Institute of Technology Roorkee, Roorkee for their invaluable guidance, constructive criticism, thought provoking discussions and painstaking efforts throughout the course of this work. Their invaluable and prompt remarks at the time of preparation of the manuscript are especially appreciated.

The to author acknowledges his deep sense of gratitude *Dr. P.K. Ghosh*, Professor, Department of Metallurgical and Materials Engineering and *Dr. K. Chandra*, Professor, Institute Instrumentation Centre for their invaluable help and advice from time to time as when needed.

The author is grateful to the Head, Metallurgical and Materials Engineering Department, Institute Instrumentation Centre for providing him the facilities during the course of experimental work.

The author is highly obliged and wishes to express his sincere thanks to the technical staff of the Metallurgical & Materials Engineering Department and Institute Instrumentation Centre, especially to *Mr. R.K.Sharma*, *Mr. J.S. Saini*, *Mrs. Rekha Sharma*, *Mr. Ramesh Chand*, *Mr. Sukhmal Giri*, *Mr. H.K. Ahuja*, *Mr. Ram Kishan*, *Mr. Shakti Gupta*, *Mr. S.K. Seth*, *Mr. Rajendra Sharma*, *Mr. Balesh Sharma*, *Mr. Vidya Prakash*, *Mr. Shamsher Singh* and *Mr. A. Kush*, who have helped him in all possible ways during the experimental work. Thanks are also due to *Mr. Sunil Sharma*, the Librarian of Metallurgical and Materials Engineering Department for providing help at crucial times.

The author wishes to register his sincere thanks to *Mr. H.S. Kushwaha* and *Dr. J. Chattopadhyay*, BARC, Mumbai, *Prof. R. K. Pandey*, Applied Mechanics Department, Indian Institute of Technology Delhi and *Dr. S. Tarafdar*, National Metallurgical

Laboratory, Jamshedpur, whose critical and timely suggestions proved to be helpful at the time of preparation of this thesis.

The financial support provided by BRNS, Bhaba Atomic Research Center, Mumbai is highly acknowledged.

When hurdles appeared insurmountable and targets unachievable, the encouragement and camaraderie of friends helped keep things in perspective. Author wishes to thank many friends and colleagues who helped lighten the burden, especially to *Dr. Rajneesh Tyagi, Mr. Vinay Kumar Goyal, Dr. Sanjay Panwar, Dr. Amrish Panwar, Mr. Deepak Tyagi, Dr. Vivesh, Mr. Amit Tyagi, Mr. Ritesh Srivastava, Mr. Abhay Sharma, Mr. Narendra, Mr. Rajkumar Sharma, Mr. Kuldeep, Ms. Priti Singh, Ms. Archana Mishra, Mr. Ramesh, Mr. Manoj, Mr. Krishna and Mr. Vijay.*

The author also wishes to register his sincere thanks to *Sonal*, who made his surrounding vivacious enough to ensconce perfectly. In a jiffy that spent in each other company, author enjoyed every moment.

The author would like to express his reverence and great admiration for his parents, to whom he owes everything. They have been a guiding force all his life and the author has tried to measure up to their expectations. The author humbly dedicates this work to them. The author wishes to express his sincere thanks to his sisters, brothers in law and other family members who have shown patience during the entire duration of this work.

At last thanks to the almighty god who has given the author spiritual support and courage to carry out this work.

**(Sandeep Bansal)**

# CONTENTS

	Page No.
Candidate's declaration	i
Abstract	ii
Acknowledgements	xi
Contents	xiii
List of Figures	xvi
List of Tables	xxiv
<i>Chapter 1 INTRODUCTION</i>	<i>1</i>
<i>Chapter 2 REVIEW OF LITERATURE</i>	<i>7</i>
2.1 THEORY OF FRACTURE TOUGHNESS	9
2.1.1 Linear Elastic Fracture Mechanics	9
2.1.2 Crack tip Opening Displacement (CTOD)	22
2.1.3 Compliance and crack size	23
2.1.4 Fracture Toughness	25
2.1.5 Thickness- Plane Strain to Plane Stress	26
2.1.6 Fracture in Thin Plate Sheets	26
2.1.7 Limitation of LEFM	29
2.1.8 Elastic Plastic Fracture Mechanics	29
2.1.9 Relationship between $J$ and Potential energy	32
2.1.10 Relation between $J$ and Crack tip Stress Field	32
2.1.11 Relation between $J$ and CTOD	33
2.1.12 $J$ integral as Fracture parameter	37
2.2 FRACTURE CHARACTERISTICS OF DUCTILE METALS – $J$ - $R$ CURVE AND $J_{IC}$	42
2.3 EFFECT OF SPECIMEN GEOMETRY ON INITIATION FRACTURE TOUGHNESS ( $J_{IC}$ )	53
2.4 STRETCHED ZONE WIDTH	68

2.4.1	Stretched Zone width Measurement	70
2.4.2	Determination of SZW and its relationship with $J_{IC}$	71
2.5	INFLUENCE OF DIFFERENT PARAMETERS ON SZW	82
2.5.1	Effect of thickness and width of specimens on SZW	82
2.5.2	Effect of $a/W$ ratio on SZW	83
2.5.3	Effect of notch root radius on SZW	86
2.5.4	Effect of loading rate on SZW	87
2.5.5	Effect of fatigue precracking stress	87
2.5.6	Effect of Temperature on Fracture Toughness	87
2.5.7	Effect of Rolling Direction	89
2.5.8	Effect of Grain Size	89
2.6	PROBLEM FORMULATION	90
	<b>Chapter 3 EXPERIMENTAL WORK</b>	<b>93</b>
3.1	TEST MATERIALS	93
3.2	MICROSTRUCTURAL STUDIES	93
3.3	TENSILE TESTING	94
3.4	FRACTURE TOUGHNESS TESTING	96
3.4.1	Test Specimens	96
3.4.2	Fatigue Pre-cracking	97
3.4.3	Test Procedure for $J_{Ic}$	100
3.4.4	Calculation and Interpretation of Results	101
3.5	PREPARATION AND PRESERVATION OF FRACTURE SPECIMENS	104
3.5.1	Care and Handling of Fracture Surface	105
3.5.2	Sectioning Fracture Surface	106
3.5.3	Fractured Surface Cleaning with ENDOX-214 before Stretched Zone Width (SZW) Measurement	106
3.6	MEASUREMENT OF STRETCHED ZONE WIDTH (SZW)	107

<b>Chapter 4</b>	<b>RESULTS AND DISCUSSIONS: STRETCHED ZONE WIDTH</b>	<b>108</b>
4.1	MATERIAL CHARACTERISATION	108
4.1.1	Chemical Composition	108
4.1.2	Microstructural Studies	109
4.1.3	Mechanical Properties	109
4.2	STRETCHED ZONE WIDTH	116
4.2.1	Stretched zone width and methods of measurement	119
4.2.2	Influence of specimen thickness on <i>SZW</i> of SA333 Gr. 6 steel	125
4.2.3	Influence of pre-crack depth ( <i>a/W</i> ) on <i>SZW</i> of SA333 Gr. 6 steel	126
4.2.4	Influence of specimen thickness on <i>SZW</i> of SAILMA steel	132
4.2.5	Influence of pre-crack depth ( <i>a/W</i> ) on <i>SZW</i> of SAILMA steel	133
4.3	DISCUSSION	133
<b>Chapter 5</b>	<b>RESULTS AND DISCUSSIONS: FRACTURE TOUGHNESS</b>	<b>142</b>
5.1	DETERMINATION OF INITIATION FRACTURE TOUGHNESS ( $J_{IC}$ )	142
5.2	INFLUENCE OF SPECIMEN THICKNESS AND PRE-CRACK DEPTH ON INITIATION FRACTURE TOUGHNESS ( $J_{IC}$ )	157
5.2.1	Fracture toughness of SA333 Gr. 6 steel	157
5.2.2	Fracture toughness of SAILMA steel	169
5.3	INFLUENCE OF COMPOSITION AND HEAT TREATMENT ON $J_{IC}$	174
5.4	INFLUENCE OF SPECIMEN THICKNESS AND PRE-CRACK DEPTH ON <i>J-R</i> CURVE	175
5.4.1	<i>J-R</i> curves for SA333 Gr. 6 Steel	175
5.4.2	<i>J-R</i> curves of SAILMA Steel	185
5.5	INFLUENCE OF COMPOSITION AND HEAT TREATMENT ON <i>J-R</i> CURVE	186
5.6	DISCUSSION	192
<b>Chapter 6</b>	<b>CONCLUSIONS</b>	<b>204</b>
	<b>REFERENCES</b>	<b>211</b>





## LIST OF FIGURES

<b>No.</b>	<b>Title</b>	<b>Page No.</b>
Fig. 2.1	A cracked body of an arbitrary shape loaded by a point load $P$ resulting in a displacement along the load-line, $V$	10
Fig. 2.2	The relationship between load and displacement and the definition of compliance.	12
Fig. 2.3	The three modes of loading a cracked body	17
Fig. 2.4	Crack-tip coordinate system and the stresses acting on an element ahead of the crack-tip.	17
Fig. 2.5	Elastic and elastic-plastic crack tip stress distribution in front of the crack tip and plastic zone sized $r_y$ and $r_p$ .	18
Fig. 2.6	Plastic zone shapes for plane stress and plane strain conditions according to (a) Von-Mises criterion and (b) Tresca criterion.	21
Fig. 2.7	Crack tip opening displacement (CTOD). An initially sharp crack blunts with plastic deformation, resulting in a finite displacement ( $\delta$ ) at the crack tip.	24
Fig. 2.8	The hinge model for estimating CTOD from three-point bend specimens.	24
Fig. 2.9	The relationship between non-dimensional compliance (CBE) and crack size for compact type specimens.	27
Fig. 2.10	An arbitrary displacement measurement location on a compact-type specimen for which the compliance relationship can be computed by equation.	27
Fig. 2.11	A schematic relationship between fracture toughness and specimen thickness illustrating $K_{IC}$ , the plane strain fracture toughness value.	28
Fig. 2.12	(a) $K$ -resistance curve as a function of crack size; (b) $K_R$ vs. crack size curve superimposed on the $K$ vs. crack size trend for different stress level illustrate instability.	28
Fig. 2.13	A counter-clockwise closed contour, $\Phi$ .	31

<b>Fig. 2.14</b>	A two dimensional cracked body with a contour $\Gamma$ originating from the lower crack surface and going counterclockwise and terminating at the upper crack surface. The traction vector at any point on the contour is marked T.	31
<b>Fig. 2.15</b>	A closed contour around a cracked tip with four distinct segments.	34
<b>Fig. 2.16</b>	The Dugdale model for deformation at the crack tip in a thin sheet in an elastic perfectly plastic material.	34
<b>Fig. 2.17</b>	Defination of crack tip opening displacement (CTOD)	35
<b>Fig. 2.18</b>	Schematic representation of crack tip events during stable, ductile tearing.	40
<b>Fig. 2.19</b>	Schematic representation of crack tip deformation zones for a growing crack.	40
<b>Fig. 2.20</b>	Sketch of various specimens (a) CT, (b) TPB	45
<b>Fig. 2.21</b>	Schematic diagram of the orientation code for identify testing direction.	45
<b>Fig. 2.22</b>	Determination of $d_n^*$ , [Heerens <i>et al</i> , 1988]	54
<b>Fig. 2.23</b>	(a) $J$ - $R$ curves for 25, 10, 3 and 0.5 mm thick specimens of A533B-1 (b) The change of fracture toughness $J_{IC}$ with thickness of specimen [Mao, 1991].	57
<b>Fig. 2.24</b>	Effect of specimen size on fracture toughness $J_Q$ [Ono <i>et al</i> , 2004]	57
<b>Fig. 2.25</b>	$J_i$ of specimens with shallow and deep notches [Zhang and Wang, 1987]	60
<b>Fig. 2.26</b>	$J$ resistance ( $J_{0.2}$ ) as a function of $a/W$ [Shen <i>et al</i> , 2001]	60
<b>Fig. 2.27</b>	Variation of $J$ - $R$ curves with the level of crack tip constraints [Chao and Zhu, 2000].	61
<b>Fig. 2.28</b>	$T_{stress}$ solutions for TPB and CT specimens [Sherry <i>et al</i> , 1995].	64
<b>Fig. 2.29</b>	$J$ and $J - A_2$ dominant zones and its relation to $J$ or $J - A_2$ controlled crack growth [Chao and Zhu, 2000].	67
<b>Fig. 2.30</b>	Illustration of stretched zone geometry [Smith <i>et al</i> , 1995]	72
<b>Fig. 2.31</b>	Schematic of the crack profile depicting the stretched zone components.	72
<b>Fig. 2.32</b>	Stretched zone of a broken specimen half showing relationship with COD	75
<b>Fig. 2.33</b>	Nine Point Stretch zone width measurement procedure	78
<b>Fig. 2.34</b>	Comparison of initiation fracture toughness obtained from stretch zone measurements, with initiation fracture toughness, obtained graphically from the blunting line, for SENB specimen . $W = 50$ mm, $B = 25$ mm of SA333 steel.[Tarafder <i>et al</i> , 2003]	79
<b>Fig. 2.35</b>	Comparison of initiation fracture toughness values according to different test standards. [Roos <i>et al</i> 2000]	79

<b>Fig. 2.36</b>	Effect of Specimen size on <i>SZW</i> [Putatunda and Rigsbee, 1985].	84
<b>Fig. 2.37</b>	Variation of Stretch zone width with pre-crack depth [Hyatt and Matthews, 1994]	85
<b>Fig. 2.38</b>	Variation of stretch zone width with loading rate [Hyatt and Matthews, 1994].	88
<b>Fig. 2.39</b>	<i>SZW</i> vs. test temperature of the 304L steel [Marengo and Ipina, 1996]	88
<b>Fig. 2.40</b>	Influence of Rolling Direction on Stretch zone Width, XC35 steel [Pluvinage and Lanvin, 1993]	91
<b>Fig. 3.1</b>	The schematic diagram of the tensile specimen.	95
<b>Fig. 3.2</b>	Schematic diagram of the orientation of the specimens collected from the pipe for testing.	98
<b>Fig. 3.3</b>	Schematic diagram of the orientation of the specimens collected from the plate for testing	98
<b>Fig. 3.4</b>	Schematic diagram of the Compact Tension (CT) specimen.	99
<b>Fig. 3.5</b>	Schematic diagram of the Three Point Bend (TPB) specimen.	99
<b>Fig. 4.1</b>	Typical microstructure of SA333 Gr. 6 pipes. (a) X100 and (b) X200.	111
<b>Fig. 4.2</b>	Typical microstructure of annealed SA333 Gr. 6 (a) X100 and (b) X200.	111
<b>Fig. 4.3</b>	Typical microstructure of normalized SA333 Gr. 6 (a) X100 and (b) X200.	112
<b>Fig. 4.4</b>	Typical microstructure of SAILMA HI 410. (a) X100 and (b) X200.	112
<b>Fig. 4.5</b>	Typical Stress Strain diagrams of SA333 Gr. 6 steel	113
<b>Fig. 4.6</b>	Typical Stress Strain diagrams of annealed SA333 Gr. 6 steel	113
<b>Fig. 4.7</b>	Typical Stress Strain diagrams of normalized SA333 Gr. 6 steel	114
<b>Fig. 4.8</b>	Typical Stress Strain diagrams of SAILMA HI 410 steel	117
<b>Fig. 4.9</b>	Typical appearance of the <i>SZW</i> in SA333 Gr. 6 steel.	118
<b>Fig. 4.10</b>	Variation of <i>SZW</i> measured at regular interval of 200 $\mu\text{m}$ along the thickness of CT specimen of SA333 Gr. 6 steel at $a/W$ ration of 0.6 and specimen thickness of 25 mm.	121
<b>Fig. 4.11</b>	Comparison of <i>SZW</i> , and standard deviation of different steels, SA333 Gr. 6 steels with or without heat treatment and SAILMA steel in 25 mm thick CT specimens with pre-crack depth of $a/W = 0.6$	122

<b>Fig. 4.12</b>	The comparison of stretched zone widths measured by nine point ( $SZW_9$ ) and three point methods ( $SZW_3$ ) with those given by average of measurements at close intervals ( $SZW_t$ ) along the thickness on the fractured surface of CT specimens of SA333 Gr. 6 material.	123
<b>Fig. 4.13</b>	The comparison of the stretched zone widths measured by nine point and three point methods with those given by average of measurements at close intervals along the thickness on the fractured surfaces of <i>TPB</i> specimens of SA333 Gr. 6 material	124
<b>Fig. 4.14</b>	The comparison of standard deviations determined by nine point ( $SZW_9$ ) and three point methods ( $SZW_3$ ) with the standard deviation determined from measurements at close intervals, $(SD)_t$ , along the thickness on the fractured surface of CT specimens of SA333 Gr. 6 material.	124
<b>Fig. 4.15</b>	The comparison of standard deviations determined by nine point and three point methods with the standard deviation determined from measurements at close intervals along the thickness on the fractured surface of <i>TPB</i> specimens of SA333 Gr. 6 material	127
<b>Fig. 4.16</b>	The comparison of standard deviations in hardness with the standard deviation determined from measurements at close intervals along the thickness on the fractured surface of CT specimens of SA333 Gr. 6 material.	127
<b>Fig. 4.17</b>	The variation of the stretched zone width with the specimen thickness at $a/W$ ratio of 0.4 in the CT specimens	128
<b>Fig. 4.18</b>	The variation of the stretched zone width with the specimen thickness at $a/W$ ratio of 0.6 in the CT specimens.	128
<b>Fig. 4.19</b>	The variation of the stretched zone width with the specimen thickness at $a/W$ ratio of 0.8 in the CT specimens.	129
<b>Fig. 4.20</b>	The variation of the stretched zone width with the specimen thickness at $a/W$ ratio of 0.4 in the <i>TPB</i> specimens.	129
<b>Fig. 4.21</b>	The variation of the stretched zone width with the specimen thickness at $a/W$ ratio of 0.6 in the <i>TPB</i> specimens.	130
<b>Fig. 4.22</b>	The variation of the stretched zone width with the specimen thickness at $a/W$ ratio of 0.8 in the <i>TPB</i> specimens.	130

<b>Fig. 4.23</b>	The variation of the stretched zone width, averaged over different thickness, with the pre-crack depth ( $a/W$ ratio) for CT specimens of SA333 Gr. 6 material.	131
<b>Fig. 4.24</b>	The variation of the stretched zone width, averaged over different thickness, with the pre-crack depth ( $a/W$ ratio) for TPB specimens of SA333 Gr. 6 material.	131
<b>Fig. 4.25</b>	The comparison of the stretched zone width, averaged over same thickness and same pre-crack depth ( $a/W$ ratio) for CT and TPB specimens of SA333 Gr. 6 material.	134
<b>Fig. 4.26</b>	The variation of the stretched zone width with the specimen thickness at $a/W$ ratio of 0.4 in the CT specimens of SAILMA steel.	134
<b>Fig. 4.27</b>	The variation of the stretched zone width with the specimen thickness at $a/W$ ratio of 0.6 in the CT specimens of SAILMA steel	135
<b>Fig. 4.28</b>	The variation of the stretched zone width with the specimen thickness at $a/W$ ratio of 0.8 in the CT specimens of SAILMA steel.	135
<b>Fig. 4.29</b>	The variation of the stretched zone width, averaged over different thickness, with the pre-crack depth ( $a/W$ ratio) for CT specimens of SAILMA steel.	136
<b>Fig. 5.1</b>	Typical $J$ - $R$ curve of SA333 Gr. 6 having thickness of 25 mm and $a/W$ ratio of 0.4 with the blunting line drawn by ASTM procedure	144
<b>Fig. 5.2 (a)</b>	Relationship of $M$ with strain hardening coefficient ( $n$ ) when value of offset is taken as 0.2 mm	148
<b>Fig. 5.2 (b)</b>	Relationship of $M$ with strain hardening coefficient ( $n$ ) when value of offset is taken as 0.1 mm	148
<b>Fig. 5.3</b>	Typical $J$ - $R$ curve of SA333 Gr. 6 having thickness of 25 mm and $a/W$ ratio of 0.4 with the blunting line drawn by Equation 4.3. Line A indicates the stretched zone width and the dotted line on both sides indicate the 95 % confidence interval.	149
<b>Fig. 5.4</b>	Typical $J$ - $R$ curve of SA333 Gr. 6 having thickness of 25 mm and $a/W$ ratio of 0.4 with the blunting line drawn by Equation 4.3.	149
<b>Fig. 5.5</b>	The comparison of the fracture toughness measured by blunting line method and $SZW$ method in the CT specimens of SA333 Gr. 6 steel material.	155
<b>Fig. 5.6</b>	The comparison of the fracture toughness measured by blunting line method and $SZW$ method in the TPB specimens of SA333 Gr. 6 steel material.	155
<b>Fig. 5.7</b>	Typical $J$ - $R$ curve of SAILMA steel having thickness of 25 mm and $a/W$ ratio of 0.4	156

<b>Fig. 5.8</b>	Typical $J$ - $R$ curve of SAILMA steel having thickness of 25 mm and $a/W$ ratio of 0.4	156
<b>Fig. 5.9</b>	The comparison of the fracture toughness measured by blunting line method and $SZW$ method in the CT specimens of SAILMA steel material.	160
<b>Fig. 5.10</b>	The variation of the fracture toughness ( $J_{IC}$ ) with the pre-crack depth ( $a/W$ ratio) for 25 mm thickness of the CT specimens of SA333 Gr. 6 steel.	160
<b>Fig. 5.11</b>	The variation of the fracture toughness ( $J_{IC}$ ) with the pre-crack depth ( $a/W$ ratio) for 15 mm thickness of the CT specimens of SA333 Gr. 6 steel.	161
<b>Fig. 5.12</b>	The variation of the fracture toughness ( $J_{IC}$ ) with the pre-crack depth ( $a/W$ ratio) for 10 mm thickness of the CT specimens of SA333 Gr. 6 steel.	161
<b>Fig. 5.13</b>	The variation of the fracture toughness ( $J_{IC}$ ) with the pre-crack depth ( $a/W$ ratio) for 25 mm thickness of the TPB specimens of SA333 Gr. 6 steel.	162
<b>Fig. 5.14</b>	The variation of the fracture toughness ( $J_{IC}$ ) with the pre-crack depth ( $a/W$ ratio) for 15 mm thickness of the TPB specimens of SA333 Gr. 6 steel.	162
<b>Fig. 5.15</b>	The variation of the fracture toughness ( $J_{IC}$ ) with the pre-crack depth ( $a/W$ ratio) for 10 mm thickness of the TPB specimens of SA333 Gr. 6 steel.	163
<b>Fig. 5.16</b>	The variation of the fracture toughness ( $J_{IC}$ ) with the specimen thickness at $a/W$ ratio of 0.4 in the CT specimens of SA333 Gr. 6 steel.	166
<b>Fig. 5.17</b>	The variation of the fracture toughness ( $J_{IC}$ ) with the specimen thickness at $a/W$ ratio of 0.6 in the CT specimens of SA333 Gr. 6 steel.	166
<b>Fig. 5.18</b>	The variation of the fracture toughness ( $J_{IC}$ ) with the specimen thickness at $a/W$ ratio of 0.8 in the CT specimens of SA333 Gr. 6 steel.	167
<b>Fig. 5.19</b>	The variation of the fracture toughness ( $J_{IC}$ ) with the specimen thickness at $a/W$ ratio of 0.4 in the TPB specimens of SA333 Gr. 6 steel.	167
<b>Fig. 5.20</b>	The variation of the fracture toughness ( $J_{IC}$ ) with the specimen thickness at $a/W$ ratio of 0.6 in the TPB specimens of SA333 Gr. 6 steel.	168
<b>Fig. 5.21</b>	The variation of the fracture toughness ( $J_{IC}$ ) with the specimen thickness at $a/W$ ratio of 0.8 in the TPB specimens of SA333 Gr. 6 steel.	168
<b>Fig. 5.22</b>	The variation of the fracture toughness ( $J_{IC}$ ) with the pre-crack depth ( $a/W$ ratio) for 25 mm thickness of the CT specimens of SAILMA steel.	171
<b>Fig. 5.23</b>	The variation of the fracture toughness ( $J_{IC}$ ) with the pre-crack depth ( $a/W$ ratio) for 20 mm thickness of the CT specimens of SAILMA steel.	171

<b>Fig. 5.24</b>	The variation of the fracture toughness ( $J_{IC}$ ) with the pre-crack depth ( $a/W$ ratio) for 10 mm thickness of the CT specimens of SAILMA steel.	172
<b>Fig. 5.25</b>	The variation of the fracture toughness ( $J_{IC}$ ) with the specimen thickness at $a/W$ ratio of 0.4 in the CT specimens of SAILMA steel.	172
<b>Fig. 5.26</b>	The variation of the fracture toughness ( $J_{IC}$ ) with the specimen thickness at $a/W$ ratio of 0.6 in the CT specimens of SAILMA steel.	173
<b>Fig. 5.27</b>	The variation of the fracture toughness ( $J_{IC}$ ) with the specimen thickness at $a/W$ ratio of 0.8 in the CT specimens of SAILMA steel.	173
<b>Fig. 5.28</b>	The initiation fracture toughness of SA333 Gr. 6 steel with or without heat treatment and SAILMA steel as observed in CT specimens of 25 mm thickness and pre-crack depth of 0.6.	176
<b>Fig. 5.29</b>	Power law fit for a Typical $J$ - $R$ curve in CT specimen of SA333 Gr. 6 steel.	177
<b>Fig. 5.30</b>	$J$ - $R$ curve plotted after averaging the coefficients of fitted experimental curves of similar parameter from different CT specimens of as received SA333 Gr. 6 steel.	177
<b>Fig. 5.31</b>	The averaged $J$ - $R$ curve at pre-crack depth of 0.4 at different thickness of the CT specimens of SA333 Gr. 6 steel.	178
<b>Fig. 5.32</b>	The averaged $J$ - $R$ curve at pre-crack depth of 0.6 at different thickness of the CT specimens of SA333 Gr. 6 steel.	178
<b>Fig. 5.33</b>	The averaged $J$ - $R$ curve at pre-crack depth of 0.8 at different thickness of the CT specimens of SA333 Gr. 6 steel.	179
<b>Fig. 5.34</b>	The averaged $J$ - $R$ curve of 25 mm thickness at different $a/W$ ratio of the CT specimens of SA333 Gr. 6 steel.	182
<b>Fig. 5.35</b>	The averaged $J$ - $R$ curve of 15 mm thickness at different $a/W$ ratio of the CT specimens of SA333 Gr. 6 steel.	182
<b>Fig. 5.36</b>	The averaged $J$ - $R$ curve of 10 mm thickness at different $a/W$ ratio of the CT specimens of SA333 Gr. 6 steel.	183
<b>Fig. 5.37</b>	The averaged $J$ - $R$ curve at pre-crack depth of 0.4 at different thickness of the TPB specimens of SA333 Gr. 6 steel.	183
<b>Fig. 5.38</b>	The averaged $J$ - $R$ curve at pre-crack depth of 0.6 at different thickness of the TPB specimens of SA333 Gr. 6 steel.	184

<b>Fig. 5.39</b>	The averaged <i>J-R</i> curve at pre-crack depth of 0.8 at different thickness of the TPB specimens of SA333 Gr. 6 steel.	184
<b>Fig. 5.40</b>	The averaged <i>J-R</i> curve of 25 mm thickness at different <i>a/W</i> ratio of the TPB specimens of SA333 Gr. 6 steel.	187
<b>Fig. 5.41</b>	The averaged <i>J-R</i> curve of 15 mm thickness at different <i>a/W</i> ratio of the TPB specimens of SA333 Gr. 6 steel	187
<b>Fig. 5.42</b>	The averaged <i>J-R</i> curve of 10 mm thickness at different <i>a/W</i> ratio of the TPB specimens of SA333 Gr. 6 steel	188
<b>Fig. 5.43</b>	The averaged <i>J-R</i> curve at pre-crack depth of 0.4 at different thickness of the CT specimens of SAILMA steel.	188
<b>Fig. 5.44</b>	The averaged <i>J-R</i> curve at pre-crack depth of 0.6 at different thickness of the CT specimens of SAILMA steel.	189
<b>Fig. 5.45</b>	The averaged <i>J-R</i> curve at pre-crack depth of 0.8 at different thickness of the CT specimens of SAILMA steel.	189
<b>Fig. 5.46</b>	The averaged <i>J-R</i> curve of 25 mm thickness at different <i>a/W</i> ratio of the CT specimens of SAILMA steel.	190
<b>Fig. 5.47</b>	The averaged <i>J-R</i> curve of 20 mm thickness at different <i>a/W</i> ratio of the CT specimens of SAILMA steel.	190
<b>Fig. 5.48</b>	The averaged <i>J-R</i> curve of 10 mm thickness at different <i>a/W</i> ratio of the CT specimens of SAILMA steel.	191
<b>Fig. 5.49</b>	The averaged <i>J-R</i> curve of SA333 Gr. 6 steel with or without heat treatment and SAILMA steel as observed in CT specimens of 25 mm thickness and pre-crack depth of 0.6.	191





## LIST OF TABLES

<b>No.</b>	<b>Title</b>	<b>Page No.</b>
<b>Table 2.1</b>	Variation of <i>SZW</i> with specimen thickness [Kobayashi <i>et al</i> , 1977].	84
<b>Table 2.2</b>	Stretched Zone size for StE 690. [Zheng <i>et al</i> , 2000b]	85
<b>Table 4.1</b>	The chemical composition of SA333 Gr. 6 steel.	110
<b>Table 4.2</b>	The chemical composition of SAILMA HI 410 steel	110
<b>Table 4.3</b>	Mechanical Properties of SA333 Gr. 6 steel	114
<b>Table 4.4</b>	Mechanical Properties of SAILMA HI 410 steel	117
<b>Table 5.1</b>	Slope of the blunting line with offset distance.	147
<b>Table 5.2</b>	Initiation Fracture toughness based on stretched zone width method and blunting line equation of CT specimens of SA333 Gr. 6 steel	152
<b>Table 5.3</b>	Initiation Fracture toughness based on stretched zone width method and blunting line equation of TPB specimens of SA333 Gr. 6 steel	154
<b>Table 5.4</b>	Initiation Fracture toughness based on stretched zone width method and blunting line equation of CT specimens of SAILMA steel	159
<b>Table 5.5</b>	The initiation fracture toughness as observed in different low carbon steels along with their mechanical properties.	174

# Chapter 1

## *INTRODUCTION*

The emergence of fracture mechanics preceded some well known disasters. About 400 liberty ships out of 2700 ships built during World War II, suffered from serious fracture problem when the method of joining was changed from riveting to welding. The crash of comet jet in 1954 due to structural failure during a severe storm has led to considerable investigation on fracture. Kings Bridge in Melbourne failed in 1962 when a loaded vehicle weighing 45 tons crossed one of the spans, causing it to collapse by extensive fracture. From the early concepts of fracture in brittle material forwarded by Griffith [1920] and its extension to ductile materials by Orōwan [1948], the progress of the understanding of fracture has led to two distinct types of fracture mechanics –linear elastic fracture mechanics (LEFM), applicable to brittle elastic materials like high strength steels, glass, ceramics etc. and elesto-plastic fracture mechanics (EPFM) which is applied to ductile materials like low carbon steels, stainless steels, certain aluminium alloys and polymers. Present study involves low carbon steels and so falls within the regime of elesto-plastic fracture mechanics.

In classical engineering design, the load bearing capacity or ultimate strength of a structure is normally judged by the load-elongation diagram of the material, in terms of a limit stress or load calculated on the basis of yield strength or tensile strength depending on the definition of failure in a given context of application. The next step then is to impose a partial safety factor on this limit load combined with minimum tensile elongation requirements. As long as this load bearing capacity of the material exceeds the applied stress, integrity of the component is assured. It is implicitly assumed that the component is defect-free but the design margins provide some protection against defects. However, in some cases, classical

design rules have proved to be inadequate or unsafe as described in the previous paragraph. For this reason, fracture mechanics has gained a major attention in sectors where catastrophic failure can have serious consequences on important aspects of life like economy, ecology and safety. Fortunately, some of the potential dangers due to increasing technological complexity may, in many cases, be reduced or avoided through better understanding of materials, design and fracture driving forces.

Modern design and operation philosophies, however, take explicit account of the possible presence of defects in engineering components. Such defects may arise from fabrication, e.g., during casting, welding or forming processes, or may develop during operation. These defects may extend during operation and eventually lead to failure, which, in the ideal case, occurs beyond the design life of the component. Failure assessment methods are based upon the behaviour of sharp cracks in structures. For this reason all flaws or defects found in structures have to be treated as if they are sharp planar cracks. In fracture mechanics there are two structural variables - design stress and flaw size and fracture toughness replaces strength as the material characteristic property. Fracture mechanics quantifies the critical combination of these three variables. Fracture mechanics is the science of progressive crack extension in real structures, which contain discontinuities. Thus, fracture mechanics approaches allow development of safer, more reliable and more economical structures by providing quantitative bases for decisions on quality control in design, material selection, manufacture, heat treatment, inspection and repair during manufacture and service. Fracture mechanics also provides a powerful diagnostic aid in the investigations of service failures.

The first milestone in the fracture mechanics has been set by Griffith [1920] in his famous paper that quantitatively relates the flaw size to the fracture stresses. However, Griffith's approach is too primitive for engineering applications and is only good for brittle materials. For ductile materials, Irwin [1948] has set another milestone by developing the

concept of strain energy release rate,  $G$ , which is defined as the rate of change in potential energy near the crack area for a linear elastic material. When the strain energy release rate reaches the critical value,  $G_c$ , the crack will grow. Later, the strain energy release rate has been replaced by the stress intensity factor,  $K$ , while developing a similar approach. After the fundamentals of fracture mechanics were established around 1960, scientists began to concentrate on the plasticity at the crack tips. In 1968, Rice modeled the plastic deformation as a nonlinear elastic behaviour and extended the method of energy release rate to nonlinear materials. It was demonstrated by him that the energy release rate can be expressed as a path-independent line integral, called the  $J$  integral. Rice's theory has since dominated the development of fracture mechanics of ductile materials in United States. Meanwhile, Wells proposed a parameter called crack tip opening displacement ( $CTOD$ ), which provided the central concept for the fracture mechanics research in Europe. Thereafter, many experiments have been conducted to verify the accuracy of the models of fracture mechanics, with the aim to convert theories of fracture mechanics to fracture design guidelines.

Ductile fracture in engineering materials is usually characterized by the fracture initiation toughness,  $J_{IC}$ , and the fracture resistance curve (i.e.,  $J$ - $R$  curve) beyond the onset of the propagation of crack. For a cracked component or structure,  $J_{IC}$  dictates the condition under which the crack propagation is initiated and the  $J$ - $R$  curve determines how far the crack can grow in a stable manner at an applied load characterized by  $J$ . These single-parameter fracture criteria based on  $J$ , namely, the  $J_{IC}$  and the  $J$ - $R$  curve, have been widely used in fracture analyses of engineering structures when the ductile tearing is dominant. Therefore, the  $J_{IC}$  and the  $J$ - $R$  curves obtained from the laboratory specimens must be reasonably accurate and applicable to full-scale structures. The fracture criteria are based on single-parameter  $J$ , which characterizes the crack tip stress conditions. As long as the plastic zone at the crack tip is limited compared to the geometry of the component or specimen, satisfying the so called small scale yielding, a single parameter fracture mechanics approach could be applied.

Resistance to fracture of a ductile material is determined by its  $J$ - $R$  curve, which shows variation of fracture toughness,  $J$ , with the extension of crack and it is an important input to all elastic-plastic fracture analysis of structures. The fracture toughness data are generally obtained experimentally through fracture toughness tests of standard specimens, following the procedure specified by ASTM standards [ASTM E 1820-01, 2001]. The test involves loading under bending or tension of fatigue pre-cracked specimens for the determination of  $J$  as a function of crack length during the process of crack growth.  $J$ - $R$  curve was earlier believed to be a material property. Thus, the  $J$ - $R$  curve obtained through the Compact Tension (CT) / Three Point Bend (TPB) specimens of the same material could as well be applied to estimate the limiting load for a prototype structure. However, it has now been realized that the fracture toughness and the fracture resistance properties are dependent on test specimen design and the standard fracture mechanics test procedures are designed to have high constraint in order to reproduce the worst conditions, more favorable to crack propagation. This dependency is often referred as the effect of crack tip constraint. It is understood that the nonstandard specimens and actual cracked structures may have low constraint configurations. Accordingly, the constraint effect on the  $J$ - $R$  curve must be considered when it is applied to a structure in service for flaw stability evaluation.

In general, the fracture initiation toughness  $J_{IC}$  and the  $J$ - $R$  curve could be functions of test specimen geometry and loading configurations. As a consequence of these observations, two fundamental issues appear. The first issue is that of characterization of crack growth resistance of specimens and structural components having low constraint. The second issue pertains to the transferability of the fracture toughness data that are measured on a specific specimen to component level, referred in the literature as ‘transferability problem’.

As fracture mechanics parameters have become extremely important as design criteria, it is imperative to develop simple, easy and reproducible measurement method which could

be undertaken without much specialized knowledge and also address the transferability issue of the  $J$ - $R$  curve to component level. During fracture in CT and TPB specimens it is observed that, between fatigue pre-crack region and the region of stable crack propagation, there is a stretched zone, which develops during initial stage of tensile loading as a result of the blunting of fatigue pre-crack. It has been proposed that the stretched zone width ( $SZW$ ) could be used to determine the initiation fracture toughness,  $J_{IC}$ , of a material. The blunting line drawn by the procedure recommended by ASTM for the determination of  $J_{IC}$ , aims to simulate the resulting apparent  $\Delta a$ , which results due to stretching of the fatigue crack (introduced by pre-fatiguing) under tensile load, before the onset of propagation of crack. However, the procedure involves arbitrary elements like an offset of 0.2 mm, which does not have any apparent justification. Therefore, many investigators have suggested direct measurement of the stretched zone width which is clearly recognized under microscope as distinct region between regions of fatigue fracture and dimpled ductile fracture. Since  $SZW$  remains constant after the onset of crack propagation, it provides a convenient marker for identifying the crack initiation point, even in a material component at any time after completion of the fracture process. Thus, estimation of the material fracture toughness in a material is possible on the basis of direct measurement of stretched zone width. Further, it has been claimed that  $J_{IC}$  determined on the basis of  $SZW$  is more reliable than that determined followed the procedure prescribed by ASTM.

The present study aims to explore the correlation between the initiation fracture toughness ( $J_{IC}$ ) and stretched zone width ( $SZW$ ) in highly ductile low carbon steels. The distribution of  $SZW$  along the thickness of a test specimen has been explored in SA333 Gr. 6 and SAILMA HI 410 steel under investigation in order to extract a reliable parameter of  $SZW$ . The impact of variation of constraints in terms of thickness and the extent of fatigue pre-crack on  $SZW$  has been examined in CT and TPB specimens. The effect of changing thickness and pre-crack depth on initiation fracture toughness,  $J_{IC}$ , and  $J$ - $R$  curves has been examined to arrive at a

reasonable understanding of the effect of these parameters on the transferability of the laboratory data to real life components in the context of SA333 Gr. 6 and SAILMA steel. A limited study on the effect of heat treatment on  $SZW$ ,  $J_{IC}$  and  $J-R$  curve has also been carried out to develop some understanding of the metallurgical aspects.

## Chapter 2

# REVIEW OF LITERATURE

The technological advancement in aerospace, nuclear, piping and oil tanker industry has put stringent demand on structural components leading to widespread failure. These failures often are catastrophic with serious consequences on important aspects of life like economy, ecology and safety. Fortunately, some of the potential dangers due to increasing technological complexity may, in many cases, be reduced or avoided through better understanding of materials. Earlier, the design engineers used the flow behaviour of ductile materials under uni-axial loading as the basis although for brittle materials, the preexisting crack used to be taken into account. Cracks and crack like defects exist in both the brittle and the ductile materials, which escape attention because of limitation of the ability to detect by different quality control methods. It is also well known that these defects initiate rapidly at non-metallic inclusions or in casting, forging, and welding defects causing structural failure. There are certain similar defects which may remain benign and does not contribute to failure. The identification of potentially dangerous defects and the condition under which these defects starts propagating, has become the focus of research in fracture mechanics and this knowledge is being increasingly incorporated in our approach to design and quality control.

Fracture toughness has been defined as a “generic term for a measure of resistance to extension of a crack” [ASTM E 1823-96, 1996]. The term fracture toughness is associated with the fracture mechanics method, which deals with the effect of defects on the load-bearing capacity of structures and materials. Fracture toughness is an empirical material property that is determined by a standard fracture-toughness test. Different standard test methods or test procedures have been developed by different organizations for fracture-toughness testing



including American Society for Testing and Materials (ASTM) in USA, British Standards Institution (BSI) in UK, European Society of Structural Integrity (ESIS) in Europe, and Japanese Standards Association (JSA) in Japan.

Fracture-toughness values are generated for a variety of reasons. The fracture mechanics methods allow a quantitative assessment of the resistance of a material to fracture. As such, the fracture-toughness value can determine a point of maximum load-bearing capacity for a critical crack size in a structural element subjected to monotonically increasing load. The fracture toughness may be measured as an indicator that marks the separation of the material into two or more pieces or that marks the onset of a stable extending defect. In some cases, the curve describing the fracture process of a stable extending crack is important from application point of view. In general, the fracture toughness indicates the end point of the useful life of a material or structure. As such, it may be used as a parameter for determining the design conditions like allowable stresses in order to make material selection and also, for determining the critical defect sizes to set inspection criteria in order to identify the conditions leading to failure during failure analysis.

During the space race of the 1960s, failures of rocket motor cases provided the motivation and urgency to develop a standard test method for the prediction of fracture. The first widely recognized fracture-toughness standard evolved to provide plane-strain fracture-toughness method [ASTM E 399-70T, 1970] for the measurement of  $K_{IC}$ , first published in 1970 as a tentative standard. The crack-tip stress intensity factor,  $K$ , has been fairly established by then for characterizing fracture-toughness values quantitatively, in order to predict final failure conditions in metallic materials. This standard is limited to the materials, which could be described by linear-elastic fracture mechanics (LEFM), and also to highly constrained geometries approaching the plane-strain constraint. The ASTM method to measure  $K_{IC}$  has become a paradigm for other standards. For example, BSI (BS 1977), JSA (JISG 1999), and ISO (ISO 1996) have developed standards for plane-strain fracture

toughness  $K_{IC}$  testing having many of the features of the original ASTM standard. For many materials including most metals used in structural applications, linear elastic fracture mechanics cannot describe the stress state around the crack because of their ability to undergo significant amount of plastic deformation. Approaches and parameters that can be used to characterize fracture toughness in these relatively ductile materials have already been developed. The approach, developed initially by Wells [1961], involves crack-tip opening displacement (CTOD) parameter, which has been basis of the first standard evolved by BSI in 1979 (BS 1979). In a parallel development the concept of  $J$ -integral is developed [Rice, 1968] and forwarded as an alternative fracture parameter [Begley and Landes, 1972]. The method to measure  $J_{IC}$  has evolved into ASTM standard in 1981 [ASTM E 813-81, 1982].

The fracture-toughness tests, depending on the deformation behaviour of materials, are used to evaluate the resistance of a material quantitatively for the extension of a crack-like defect. This involves the testing of a specimen containing a crack-like defect under monotonically increasing force or displacement. The test continues until the specimen reaches or passes a point or region over which the fracture toughness is defined.

## **2.1 THEORY OF FRACTURE TOUGHNESS**

### **2.1.1 Linear Elastic Fracture Mechanics**

There are two alternative approaches for fracture analysis under dominantly linear-elastic conditions; one is energy criterion and other is stress intensity approach. Both approaches are equivalent in certain circumstances.

#### **(a) Energy Balance Approaches to Fracture**

Inglis [1913] introduced stress concentration at geometrical discontinuity. Seven years later, Griffith [1920] realized its importance in failure of brittle materials where failure takes

place by fracture following elastic deformation. The discrepancy between theoretically estimated strength and the observed ones in brittle materials like glass has inspired Griffith [1920] to draw attention to the role of preexisting cracks in the process of fracture. He has proposed the quantitative connection between fracture stress and flaw size and is acknowledged as the father of the fracture mechanics approach. Griffith, [1920] has shown that a flaw become unstable when the decrease in the elastic strain energy change due to increment of crack growth is sufficient to overcome the surface energy required to create fracture surfaces in a brittle material. His concept can be explained in the context of a body of arbitrary shape having crack of area  $A$  under point load  $P$  resulting in load line displacement,  $V$  (Fig. 2.1).

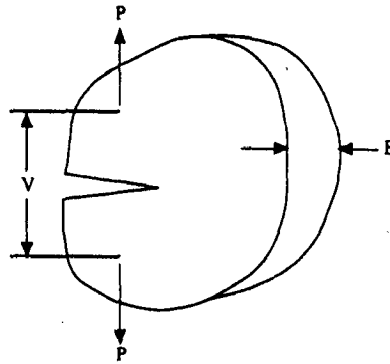


**Fig. 2.1** A cracked body of an arbitrary shape loaded by a point load  $P$  resulting in a displacement along the load-line,  $V$

Energy balance in the body is given in terms of rate by

$$\dot{W} = \dot{U} + \dot{K}_E + 2\dot{\gamma}_s A \quad (2.1)$$

where,

$\dot{W}$  = work performed by the external loads;

$\dot{U}$  = Elastic energy stored in the cracked body =  $\dot{U}_e$

$\dot{K}_E$  = Kinetic energy of the body

$\dot{\gamma}_s$  = energy per unit surface area required to create the crack.

$U$  was later modified to accommodate for some plastic deformation between elastic deformation and fracture by including the part of the energy,  $U_p$ , required to be spent out of stored elastic energy to perform work of plastic deformation before propagation of crack causing fracture.

Sir Nevil Mott [1948] introduced the kinetic energy term,  $K_E$ , to lay the foundation of dynamic fracture mechanics.

If the load is not time dependent and KE change is negligible then,

$$\frac{\partial}{\partial t} = \frac{\partial}{\partial A} \frac{\partial A}{\partial t} = A \frac{\partial}{\partial A} \quad (2.2)$$

and so one may write,

$$\frac{\partial W}{\partial A} = \left[ \frac{\partial U_e}{\partial A} + \frac{\partial U_p}{\partial A} \right] + 2\gamma_s \quad (2.3)$$

By rearranging,

$$\frac{\partial W}{\partial A} - \frac{\partial U_e}{\partial A} = \frac{\partial U_p}{\partial A} + 2\gamma_s \quad (2.4)$$

if one writes  $\frac{\partial U_p}{\partial A} = 2\gamma_p$  and  $\gamma_p + \gamma_s = \gamma$ , as proposed by Irwin [1948] and Orowan [1948]

independently, the final form of the equation becomes,

$$\frac{\partial W}{\partial A} - \frac{\partial U_e}{\partial A} = 2\gamma \quad (2.5)$$

or, 
$$\frac{\partial}{\partial A} (W - U_e) = 2\gamma = G \quad (2.6)$$

where,  $G$  is defined as the Griffith crack extension force. This equation (2.6) states that fracture can only occur if the difference between the work done by external forces and the increase in elastic strain energy of the body is sufficient to supply the energy required for fracture. The energy required for fracture is the sum of the energy used for plastic deformation before the propagation of crack and the energy needed to form new surfaces resulting due to advancement of crack. For metals, the plastic energy term is much larger as compared to the surface energy term.

During loading of the specimen with a given size of crack, as shown in Fig.2.2, load ( $P$ ) is linearly related to load-line displacement ( $V$ ) as,

$$V = CP \tag{2.7}$$

where,  $C$  is the compliance of the specimen, which depends on crack size and body but independent of applied load and distance. The elastic energy stored on the specimen with a given crack size,  $U_e$  is obtained by integrating the area under the straight line in Fig. 2.2 as,

$$U_e = -\frac{1}{2}PV = -\frac{P^2C}{2} \tag{2.8}$$

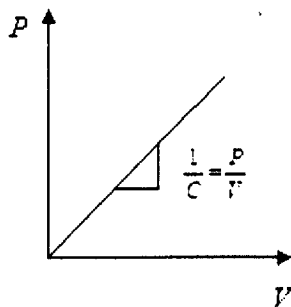


**Fig. 2.2 The relationship between load and displacement and the definition of compliance.**

As load increases, the amount of elastic energy stored increases following equation (2.8) till the condition under equation (2.6) is fulfilled and the crack, so far dormant, starts to

advance by a length  $da$ . The change in area cracked caused by this advance is  $B da$  where  $B$  is the width of the specimen as defined in Fig. 2.1.

If  $\Delta W = 0$  during crack advance which corresponds to fixed grip situation,

$$-\frac{\partial U_e}{\partial A} = G = \frac{1}{B} \frac{\partial U_e}{\partial a} = \frac{P^2}{2B} \frac{dC}{da} \quad (2.9)$$

Under fixed grip condition energy needed for fracture is balanced by decrease in strain energy.

However, for fixed load situation,

$$W = PV \quad (2.10)$$

$$U_e = \frac{1}{2} PV \quad (2.11)$$

$$W - U_e = \frac{1}{2} PV \quad (2.12)$$

$$\frac{\partial(W - U_e)}{\partial A} = \frac{1}{B} \frac{\partial}{\partial a} \left( \frac{1}{2} PV \right) = \frac{P^2}{2B} \frac{dC}{da} \quad (2.13)$$

Under fixed load condition, the external work goes to supply energy for both fracture and for increase in strain energy due to displacement. Under both these conditions, the energy per unit area required to be released for fracture,  $G$ , is the same and is also known as the strain energy release rate.

## (b) Stress Intensity Parameter Approaches

Westergaard, [1939] has shown that stresses at the tip of the crack in elastic body varies as a function of  $\frac{1}{\sqrt{r}}$  where,  $r$  is the distance from the crack tip. Irwin [1957] has extended this theory to almost brittle material accommodating for a limited plastic

deformation and led finally to the development of the fracture mechanics based on crack-tip stress field analysis. Irwin has shown that stresses and displacements near the crack tip can be described through a single parameter that is related to the energy release rate, namely, the crack-tip stress intensity factor,  $K$ .

There are three modes of application of load under which crack may open up, as shown in Fig. 2.3. In mode I, the stress and strain fields are symmetric with respect to the x-y and x-z plane while anti-symmetrical fields are there in mode II and mode III.

For mode I, the stresses and displacement near the crack tip are given by

$$\sigma_x = \frac{K_I}{\sqrt{2\pi r}} \cos \theta \left( 1 - \sin \frac{\theta}{2} \sin \frac{3\theta}{2} \right) \quad (2.14a)$$

$$\sigma_y = \frac{K_I}{\sqrt{2\pi r}} \cos \theta \left( 1 + \sin \frac{\theta}{2} \sin \frac{3\theta}{2} \right) \quad (2.14b)$$

$$\tau_{xy} = \frac{K_I}{\sqrt{2\pi r}} \cos \theta \sin \frac{\theta}{2} \sin \frac{3\theta}{2} \quad (2.14c)$$

Under plane strain condition:  $\sigma_z = \nu(\sigma_x + \sigma_y)$  while under plane stress condition:  $\sigma_z = 0$

Also,  $\tau_{yz} = \tau_{xz} = 0$

The principal stresses in radial coordinates are:

$$\sigma_1 = \frac{K_I}{\sqrt{2\pi r}} \cos \frac{\theta}{2} \left( 1 + \sin \frac{\theta}{2} \right) \quad (2.15a)$$

$$\sigma_2 = \frac{K_I}{\sqrt{2\pi r}} \cos \frac{\theta}{2} \left( 1 - \sin \frac{\theta}{2} \right) \quad (2.15b)$$

The general expression for stress distribution which is valid ahead of crack-tip region is given by Williams [1957] as,

$$\sigma_{ij} = \frac{K}{\sqrt{r}} f_{ij}(\theta) + \sum_{m=0}^{\alpha} A_m r^{m/2} g_{ij}^{(m)}(\theta) \quad (2.16)$$

Where,  $f_{ij}$  and  $g_{ij}$  are angular functions.  $A_m$  is the amplitude which depends on the geometry of the crack. Both the equations (2.14) and (2.16) indicate  $\sigma \propto \frac{1}{\sqrt{r}}$  where  $r$  is small.

Higher order terms change with geometry but near the crack tip, it only makes a second order contribution to the stresses. The distance up to which the second term in equation (2.16) can be neglected could give us an idea of the size of the region ahead of crack where the stress intensity parameter,  $K$ , alone will determine the level of stress. A numerical study has been conducted by Talug and Reifsnider [1977] for a specimen where  $\sigma_y$  has been estimated by equations (2.14) and (2.16) as function of  $r$  from the crack tip for two sizes (lengths) of crack (a)  $a = 0.25$  mm (small) and (b)  $a = 6.25$  mm (long) in 25 mm wide single edge notch subjected to uniform stress under mode-I loading. It has been observed that till  $r = 0.15a$ , both the estimates match very closely. Thus, in other words,  $K_I$ -dependent stress field, for the given geometry of the specimen, develops within a region of about  $0.15a$  ahead of the crack where  $a$  is the crack length. It is also interesting to note that at  $r = 0$ , there is a stress singularity and  $K_I$  also signifies the amplitude of this singularity.

The elastic displacement fields in  $x$  and  $y$  directions in Fig. 2.4, near the crack tip are

$$u = \frac{K_I}{2G} \sqrt{\frac{r}{2\pi}} \cos \frac{\theta}{2} \left( \kappa - 1 + 2 \sin^2 \frac{\theta}{2} \right) \quad (2.17a)$$

$$v = \frac{K_I}{2G} \sqrt{\frac{r}{2\pi}} \sin \frac{\theta}{2} \left( \kappa - 1 + 2 \cos^2 \frac{\theta}{2} \right) \quad (2.17b)$$



where,

$G$  = shear modulus

$$\kappa = 3 - 4\nu \quad \text{for plane strain condition}$$

$$= \frac{3 - \nu}{1 + \nu} \quad \text{for plane stress condition}$$

and,  $\nu$  = Poisson's ratio

Thus, it is shown that the stress intensity parameter,  $K_I$ , also controls the displacement fields that develop ahead of the crack tip.  $K_I$  depends linearly on the applied load or stress and is also a function of the crack size and geometric parameter of the specimen.

$$K = \frac{P}{BW^{\frac{1}{2}}} F(a/W) = \sigma \sqrt{\pi a} f(a/W) \quad (2.18)$$

Irwin [1957] has performed a crack closure analysis and has shown a general relationship of  $G$  to  $K$  for Mode I loading as

$$G = \frac{K^2}{E} \quad \text{for plane stress} \quad (2.19a)$$

$$G = \frac{K^2}{E} (1 - \nu^2) \quad \text{for plane strain} \quad (2.19b)$$

For other modes of crack extension such as mode II and III similar relationships as in equation (2.19) may also be derived.

The stress intensity factor, therefore, provides a measure of the stress and strain fields developing in the vicinity of the crack tip in a elastic material. However, its use in the context of crack in a real material, which may undergo some plastic deformation in the most highly stressed region at the tip, has to be considered to evolve the condition for validity of this approach. The elastic stress distribution,  $\sigma_y$ , near a crack as given by equation (2.20) is shown in Fig. 2.5 and the stress singularity at the crack tip cannot be supported by real materials, which, if capable, will undergo plastic deformation to relax the stress there.

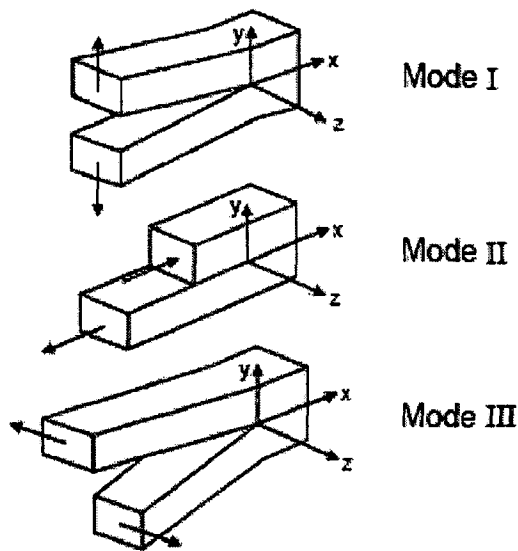


**Fig. 2.3 The three modes of loading a cracked body**

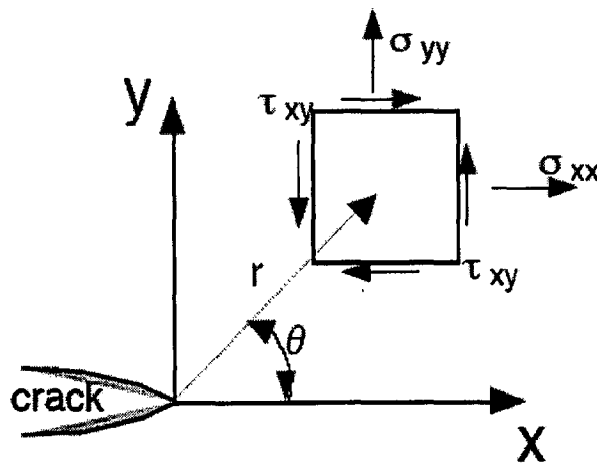


**Fig. 2.4 Crack-tip coordinate system and the stresses acting on an element ahead of the crack-tip**



For an elastic perfectly plastic material, the stress will be limited to the yield stress,  $\sigma_y = \sigma_0$ , and under plane stress condition, the boundary of the zone under plastic deformation characterized by radial distance  $r_y$ , will satisfy the condition

$$\sigma_y = \frac{K_I}{\sqrt{2\pi r_y}} = \sigma_0 \quad (2.20)$$

Thus, the size of the plastic zone is

$$r_y = \frac{1}{2\pi} \left( \frac{K}{\sigma_0} \right)^2 \quad (2.21)$$

This is incorrect because it is based on elastic stress distribution. Under elastic-plastic stress distribution, force equilibrium in  $y$  direction leads to

$$r_p = 2r_y = \frac{1}{\pi} \left( \frac{K}{\sigma_0} \right)^2 \quad (2.22)$$

To arrive at the correct elastic stress distribution outside the region under plastic deformation, the effective position of the crack tip is at  $r = r_y$  and so the crack length is not  $a$  but is  $a_{eff} = a + r_y$ . The plastic zone does not allow the elastic stress to develop within it and is unable to transmit any stress across their surfaces. It is a region behaving in between crack and elastic material.

For strain-hardening materials, the size of the plastic zone,  $r_y = r_p$ , is estimated to be

$$r_p = \frac{m-1}{m+1} \cdot \frac{1}{\pi} \left( \frac{K}{\sigma_0} \right)^2 \quad (2.23)$$

The stress distribution now becomes

$$\sigma_y = \begin{cases} \sigma_0 & \text{for } 0 \leq r \leq r_p \\ \frac{K_p}{\sqrt{2\pi(r-r_y)}} & \text{for } r > r_p \end{cases} \quad (2.24)$$

Equation (2.23) and (2.24) are for plane stress conditions where  $\sigma_3 = 0$  and  $\sigma_1 = \sigma_0$  for yielding to occur.

Under plane strain condition, the stress in the thickness or z-direction for  $\theta = 0$ , is given by

$$\sigma_3 = \sigma_z = 2\nu \frac{K}{\sqrt{2\pi r}} \quad (2.25)$$

For  $\nu = 1/3$ ,  $\sigma_1 = 3\sigma_0$  for yielding to occur. If one substitute  $3\sigma_0$  in place of  $\sigma_0$  in equation (2.22) the plane strain plastic zone size will be nine times smaller than the plane stress plastic zone. But Irwin argued that plane strain condition does not exist either at the specimens surface or at the crack tip so effective yield strength is  $\sigma_1 \approx 1.68\sigma_0$  and it gives an estimate for  $r_p$  as

$$r_p|_{\text{plane strain}} = \frac{1}{6\pi} \left( \frac{K}{\sigma_0} \right)^2 \quad (2.26)$$

Plastic zone under plane strain is much smaller than that under plane stress.

Large plastic zone results in unconstrained yielding. If plastic zone size is equal to plate thickness free yielding will cause plane stress condition to develop.

The shape of the plastic zone size can be derived by substituting the Von Mises and Tresca yield criteria into crack tip field equations. Plastic zone shapes for plane stress and plane strain conditions according to the two criteria are shown in Fig. 2.6. The extent of plastic zone along  $\theta = 0$  is independent of yield criterion but the shapes are dependent on it.

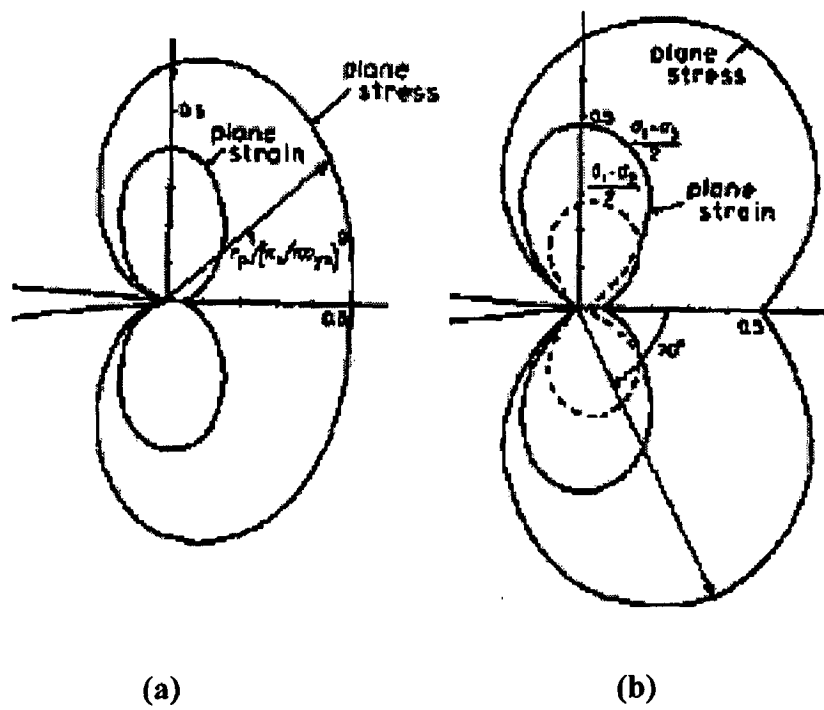


Fig. 2.6 Plastic zone shapes for plane stress and plane strain conditions according to (a) Von-Mises criterion and (b) Tresca criterion.

## 2.1.2 Crack tip Opening Displacement (CTOD)

Wells [1961] has noticed that the crack faces moves apart prior to fracture as blunting occurs at initially sharp crack due to plastic deformation (Fig. 2.7). The degree of crack blunting increases in proportional to the toughness of the material. Based on this observation Wells [1961] has proposed the opening at the crack tip as a measure of fracture toughness.

It is obtained by putting  $\theta = 180^\circ$  and  $r = r_y$  in  $v$  and putting  $CTOD = 2v$

$$CTOD = 2v_0 = \frac{4K^2}{\pi E \sigma_0} \quad (2.27)$$

Where value of  $v$  is  $v_0$  at the crack tip.

CTOD may also be related to the energy release rate as

$$CTOD = \frac{4G}{\pi \sigma_0} \quad (2.28)$$

Thus, in the limit of small scale yielding, CTOD is related to  $G$  and  $K_I$ . Wells, [1961] have recommended that CTOD is an appropriate crack tip characterizing parameter when LEFM is no longer valid.

### CTOD in Specimen

The crack tip opening displacement (CTOD) of a crack at the edge of a three-point bending specimen is shown in Fig. 2.8.

where  $CTOD_m$  is the measured crack tip opening displacement, usually near the edge of the specimen for ease of access, CTOD is the real crack tip opening displacement,  $a$  is the length of the crack, and  $b$  is the width of the rest of the specimen. From simple geometry of two similar triangles:

$$CTOD = \frac{\rho b}{a + \rho b} CTOD_m \quad (2.29)$$

$$\delta = \frac{\rho b}{a + \rho b} \Delta \quad (2.30)$$

where  $\rho$  is a dimensionless rotational factor used to locate the center of the hinge.

For simplicity, it is assumed that the center of the hinge locates at the center of  $b$ , i.e.,  $\rho \sim 1/2$ .

The CTOD then becomes

$$\delta = \frac{b}{2a+b} \Delta \quad (2.31)$$

The above hinge model may not be accurate when the displacement is mostly elastic.

A more accurate approach is to separate the CTOD into an elastic part and a plastic part:

$$\begin{aligned} \delta &= \delta_{elastic} + \delta_{plastic} \\ &= \frac{K_I^2}{m\sigma_{ys}E} + \frac{\rho_{plastic}b}{a + \rho_{plastic}b} \Delta \end{aligned} \quad (2.32)$$

where  $\sigma_{ys}$  is the small scale yielding stress and  $m$  is a dimensionless constant that depends on the material properties and the stress states.

### 2.1.3 Compliance and crack size:

$$\frac{V}{P} = C = \frac{1}{BE} f(a/W) \quad (2.34)$$

The dimensionless quantity  $CBE$  is dependent only on  $a/W$  provided planer geometry of the body remains the same.

$$BEC = \frac{BEV}{P} \quad (2.35)$$

If  $V$  is measured not on load-line but at a distance  $x$  from the load line

$$C_x BE = \frac{BEV_x}{P} = \frac{\frac{BEV_0}{P} \left| \frac{x_0}{W} - \frac{x}{W} \right|}{\left| \frac{x_0}{W} + 0.25 \right|} \quad (2.36)$$



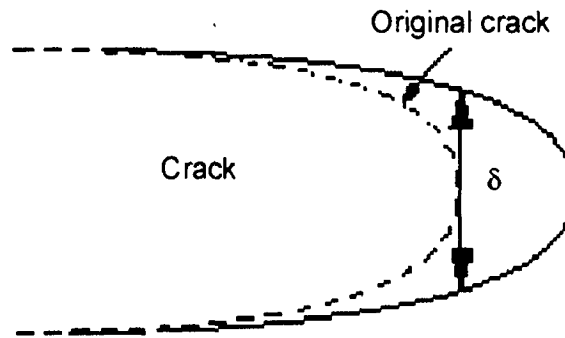


**Fig. 2.7** Crack tip opening displacement (CTOD). An initially sharp crack blunts with plastic deformation, resulting in a finite displacement ( $\delta$ ) at the crack tip.

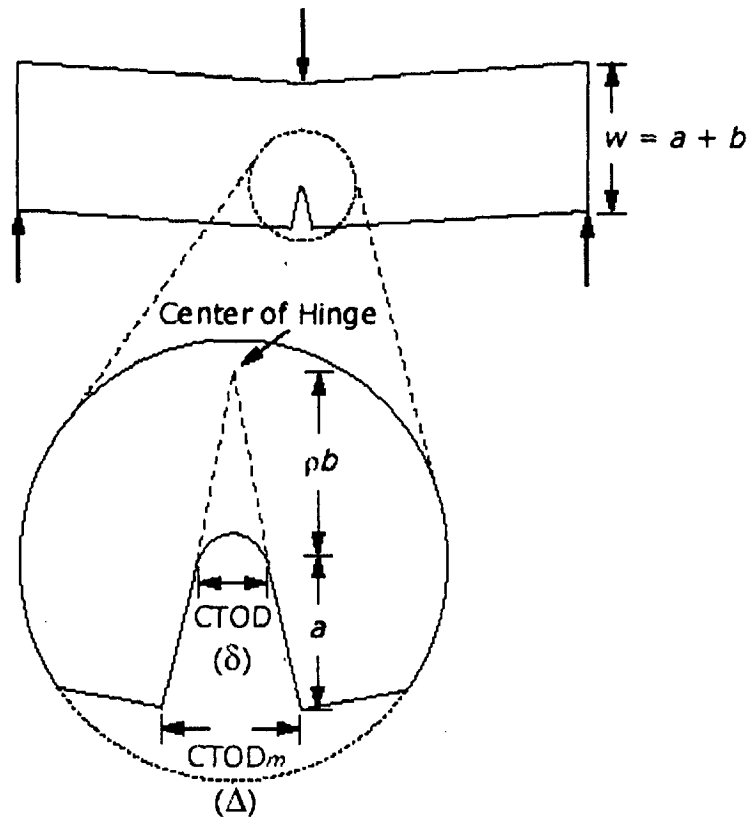


**Fig. 2.8** The hinge model for estimating CTOD from three-point bend specimens.

$x$  is positive towards the crack tip and negative towards the front face of CT specimen.  $x_0$  is the point of rotation

$$\frac{x_0}{W} = \left[ 0.09953 + 3.02437(a/W) - 7.95768(a/W)^2 + 13.546(a/W)^3 - 10.6274(a/W)^4 + 3.1133(a/W)^5 \right] \quad (2.37)$$

$$a/W = \left[ C_0 + C_1 U_x + C_2 U_x^2 + C_3 U_x^3 + C_4 U_x^4 + C_5 U_x^5 \right] \quad (2.38)$$

where

$$U_x = \frac{1}{[C_x B E]^{1/2} + 1}$$

$C_x$  corresponding to measurement location  $x_0$ . The value of  $C_0, C_1$  etc. for different  $x$  value are available.

### 2.1.4 Fracture Toughness

$K$  uniquely determines

1. The magnitude of stresses in the crack tip region
2. Size and shape of the crack tip plastic zone
3. Strain energy available for crack extension

When applied  $K$  is equal or greater than critical  $K$ , crack extension occurs and this critical  $K$  is called the fracture toughness.

### 2.1.5 Thickness- Plane Strain to Plane Stress:

The plastic zone size increases as thickness decreases to create plane stress condition. So the fracture toughness should depend on thickness as shown in Fig. 2.11.

Under plane strain condition the material shows the lowest fracture toughness value  $K_{IC}$  which is regarded as material constant. Thus, limiting the plastic zone size is extremely important. The standard requires that the uncracked ligament and the crack length itself be not less than  $25 r_p$  at the point of fracture. To ensure plane-strain conditions along most of the crack edge except near the faces, it is also required that the specimen thickness be at least  $25 r_p$ . Small-scale yielding will be in force at the onset of crack growth if the applied load is less than half the limit load. For high strength, relatively brittle metal alloys, values of  $r_p$  at fracture initiation in the range 0.1 to 1 mm are typical in plane strain. Thus the specimen with crack lengths on the order of 2.5 to 25 mm will suffice to ensure small scale yielding. All the pertinent dimensions of the specimen (ASTM E-399)  $B, W - a \geq 2.5 \left( \frac{K_Q}{\sigma_0} \right)^2$  must be more than 50 times the plastic zone size under plane strain condition.

### 2.1.6 Fracture in Thin Plate Sheets:

In thin specimens, due to plastic deformation, instability in crack growth is preceded by a stable crack growth. So  $R$ -curve or  $K$ -resistance curve is used to arrive at the condition of instability in crack propagation. The crack growth resistance curve in which the crack extension  $\Delta a$ , is correlated with  $K$ , is shown in Fig. 2.12 (a). Fig. 2.12 (b) shows the  $K$ -resistance curve on which the applied  $K$  vs crack size curves for various stress levels are superimposed. For instability, the applied  $K$  must exceed the fracture resistance of the material.

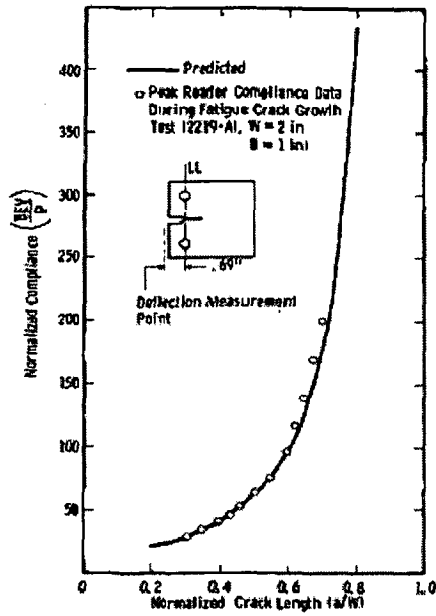


Fig. 2.9 The relationship between non-dimensional compliance (CBE) and crack size for compact type specimens

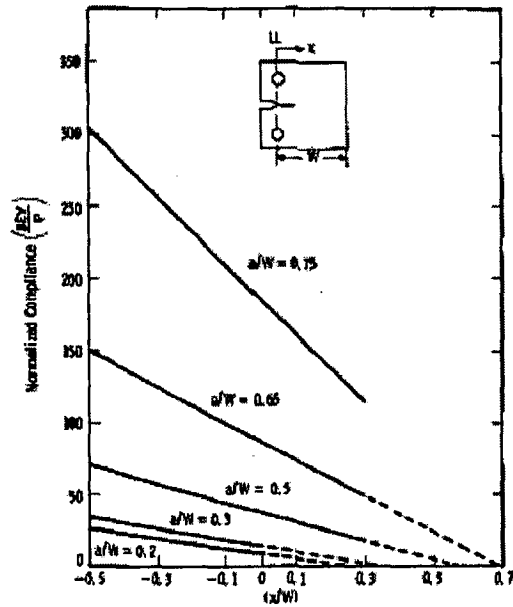


Fig. 2.10 An arbitrary displacement measurement location on a compact-type specimen for which the compliance relationship can be computed by equation.

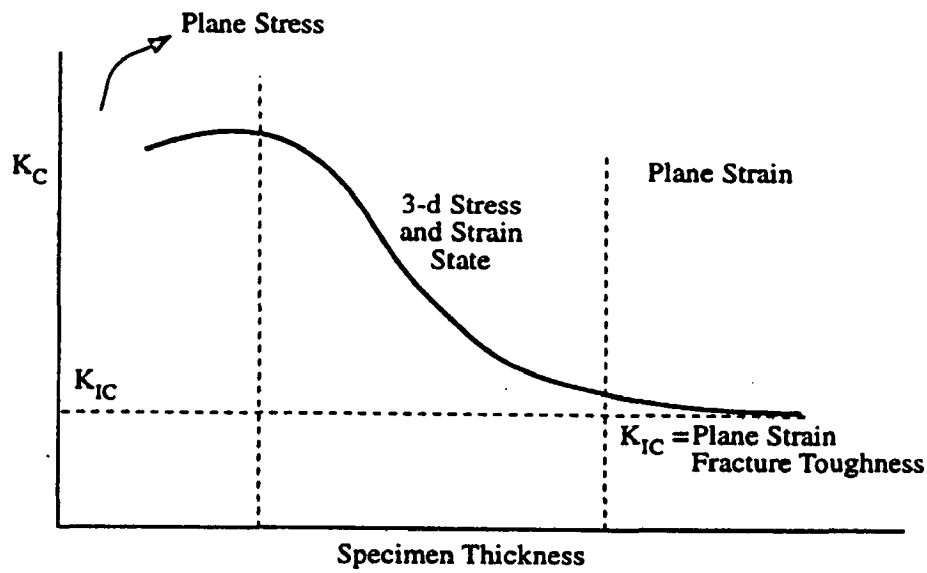


Fig. 2.11 A schematic relationships between fracture toughness and specimen thickness illustrating  $K_{IC}$ , the plane strain fracture toughness value.

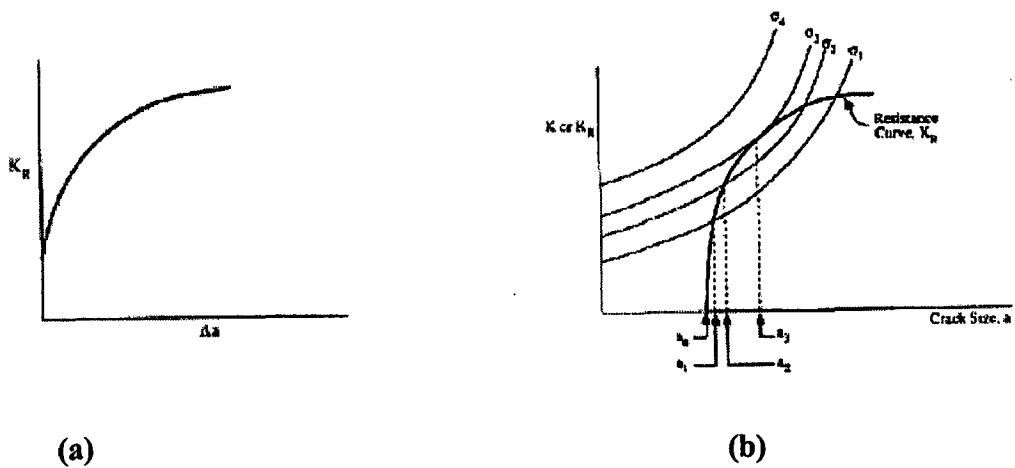


Fig. 2.12 (a)  $K$ -resistance curve as a function of crack size; (b)  $K_R$  vs. crack size curve superimposed on the  $K$  vs. crack size trend for different stress level illustrate instability.

As stress increases from  $\sigma_1 \rightarrow \sigma_2$ ,  $a$  increases from  $a_1$  to  $a_2$  and at this stress applied  $K$  level drops below  $K_R$  curve as crack length increases so there is no crack extension.

But at  $\sigma \rightarrow \sigma_3$  the crack extends to  $a_3$  and increase in crack length keeps applied  $K$  above  $K_R$  curve so crack length increases giving rise to instability.

The condition for instability is

$$\frac{dK}{da} \geq \frac{dK_R}{da} \quad \text{and } K > K_R \quad (2.39)$$

### 2.1.7 Limitation of LEFM

Early developments of fracture mechanics have focused on plain strain, linear elastic fracture mechanics (LEFM) and on relatively high strength brittle materials. Attention was concentrated on  $K_{IC}$  and  $K_{Ia}$  values, which relate well to instability conditions for materials which exhibit relatively brittle fracture behavior. However, for a broader structure reliability spectrum of applications and materials, variants disqualifying LEFM such as lower strength and higher toughness materials, thinner section, higher localized stress region, large scale plasticity developed prior to fracture have to be considered and included. Many structural alloys may qualify for LEFM at room temperature but at elevated temperatures, fracture does not develop before a significant yielding, disqualifying it for description under LEFM. An alternative fracture mechanics model has been developed to account for some of these variants through elastic-plastic fracture analysis.

### 2.1.8 Elastic Plastic Fracture Mechanics

This pertains to fracture in ductile material where scale of plasticity may not impose any limitation.

Elastic-plastic fracture mechanics (EPFM) has been developed in 1968 and three papers of considerable significance to the development of elastic-plastic fracture mechanics have appeared. Rice [1968] have idealized plastic deformation as a nonlinear elastic behavior for mathematical purposes and is able to generalize the energy release rate for such materials in terms of a path-independent contour integral  $J$ . This has the form identical to energy-momentum tensor for characterising general forces on dislocations and point defects by Eshelby [1956]. Nonlinear elastic materials have similar behavior to plastic material under unidirectional loading.

$$J_\phi = \oint_\phi \left( W n_1 - \vec{T} \frac{\partial \vec{u}}{\partial x_1} \right) ds \quad (2.40)$$

$W$  = Elastic strain energy density

$$= \int_0^{\epsilon_{ij}} \sigma_{ij} d\epsilon_{ij} \quad \text{or, } \sigma_{ij} = \frac{\partial W}{\partial \epsilon_{ij}}$$

$T$  = Traction vector along the outer normal to contour  $\Phi$

$u$  = displacement vector =  $u_1 i + u_2 j$

$$T_i = \sigma_{ij} - n_j$$

In the absence of body forces and under small deformations it can be shown (Fig. 2.13) that

$$J_\phi = 0$$

For a cracked body Rice defined  $J$  integral as

$$J = \int_\Gamma \left( W n_1 - T_i \frac{\partial u_i}{\partial x_1} \right) ds \quad (2.41)$$

Where  $\Gamma$  is a counter clockwise contour as shown in Fig. 2.14 which begins at a point on lower crack surface and ends on a point on the upper crack surface.

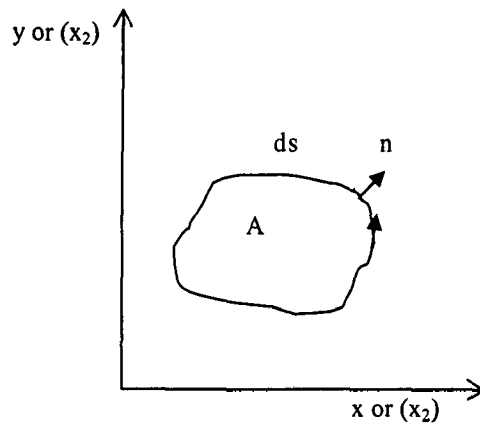


**Fig. 2.13** A counter-clockwise closed contour,  $\Phi$

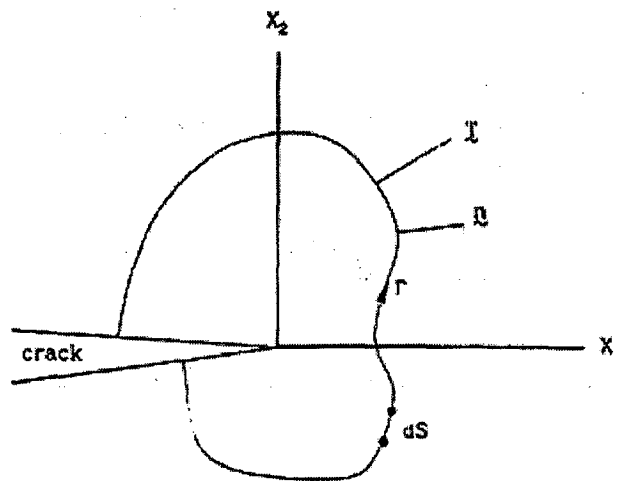


**Fig. 2.14** A two dimensional crackd body with a contour  $\Gamma$  originating from the lower crack surface and going counterclockwise and terminating at the upper crack surface. The traction vector at any point on the contour is marked  $T$ .



## Path independence of $J$ -integral

$J$  is path independent as shown in Fig. 2.15

$$J_{\Gamma_1} + J_{\Gamma_2} + J_{\Gamma_3} + J_{\Gamma_4} = 0. \quad (2.42)$$

Along  $\Gamma_2$  &  $\Gamma_4$ ;  $n_1 = \frac{dy}{ds}$  and  $dy = 0$  so  $n_1 = 0$

Also, on free crack surface the traction force  $T_i = 0$  so,

$$J_{\Gamma_1} = -J_{\Gamma_3} \quad (2.43)$$

## 2.1.9 Relationship between $J$ and Potential energy

It has been shown that  $J$  is related to the rate of change of potential energy,  $U$

$$U = \int_A W(x, y) dA - \int T_i u_i ds \quad (2.44)$$

$A$  is the area of the body;  $T_i$  and  $u_i$  are the traction and displacement, respectively, applied along the boundary  $\Gamma$ .

$$J = -\frac{1}{B} \frac{dU}{da} \quad (2.45)$$

so under elastic regime  $J$  will correspond to  $G$ , the crack extension force of Griffith.

## 2.1.10 Relation between $J$ and Crack tip Stress Field

Crack tip stress fields,

$$\sigma_{ij} = \sigma_0 \left( \frac{J}{\alpha \sigma_0 \varepsilon_0 I_m r} \right)^{\frac{1}{1+m}} \hat{\sigma}_{ij}(\theta, m) \quad (2.46)$$

Crack tip strain fields,

$$\varepsilon_{ij} = \alpha \varepsilon_0 \left( \frac{J}{\alpha \sigma_0 \varepsilon_0 I_m r} \right)^{\frac{m}{1+m}} \hat{\varepsilon}_{ij}(\theta, m) \quad (2.47)$$

The material follows a nonlinear stress-strain relationship under uniaxial loading as

$$\frac{\varepsilon}{\varepsilon_0} = \alpha \left( \frac{\sigma}{\sigma_0} \right)^m \quad (2.48)$$

$\varepsilon_0$ ,  $\sigma_0$  are strain and stress at yield point and  $m$  is the plasticity exponent.  $\hat{\varepsilon}_{ij}(\theta, m)$  and  $\hat{\sigma}_{ij}(\theta, m)$  are angular functions.

$$I_m = \begin{cases} 6.568 - 0.4744m + 0.0404m^2 - 0.001262m^3 & \text{for plane strain} \\ 4.546 - 0.2827m + 0.0175m^2 - 0.45816 \times 10^{-4} m^3 & \text{for plane stress} \end{cases} \quad (2.49)$$

When  $m = 1$ ,  $J = \frac{K^2}{E}$  so  $\frac{\sigma}{\varepsilon} \propto \frac{K/\sqrt{r_0}}{K/\sqrt{r}}$

Hutchinson [1968 a, b] and Rice and Rosengren [1968] in the same year, have related the  $J$ -integral to crack tip stress, strain, and displacement fields for nonlinear materials in a similar manner as the crack tip fields are related to  $K$  under linear-elastic conditions. Since  $J$  is derived for nonlinear elastic materials, it is considered to have severe limitations for characterizing fracture in elastic-plastic materials.

### 2.1.11 Relation between $J$ and CTOD

For a perfect plastic material ( $m = \infty$ ) Dugdale [1960] in his model to strip deformation zone at the crack-tip has shown (Fig. 2.16) that if we take an integration path along the boundary of the strip deformation zone at the crack tip along which  $dy = 0$ , the  $J$ -integral simplifies to

$$J = \int_a^{a+c} \sigma_0 \frac{\partial}{\partial x} (u_2^+ - u_2^-) dx = \sigma_0 (u_2^+ - u_2^-) \Big|_a^{a+c} = \sigma_0 \delta \quad (2.50)$$

where  $\delta$  is the crack tip opening displacement (CTOD).

Shih, [1981], took a step further and showed that a unique relationship exists between  $J$  and CTOD beyond the validity limits of LEFM. He has evaluated the displacements at the crack tip implied by the HRR solution and related the displacement at the crack tip to  $J$  and flow properties. According to the HRR solution, the displacements near the crack tip are given by

$$u_i = \frac{\alpha \sigma_{ys}}{E} \left( \frac{EJ}{\alpha \sigma_{ys}^2 I_m r} \right)^{\frac{m}{m+1}} r \hat{u}_i(\theta, m) \quad (2.51)$$

Shih [1981] introduced the 90° intercept definition of CTOD, as shown in Fig. 2.17.

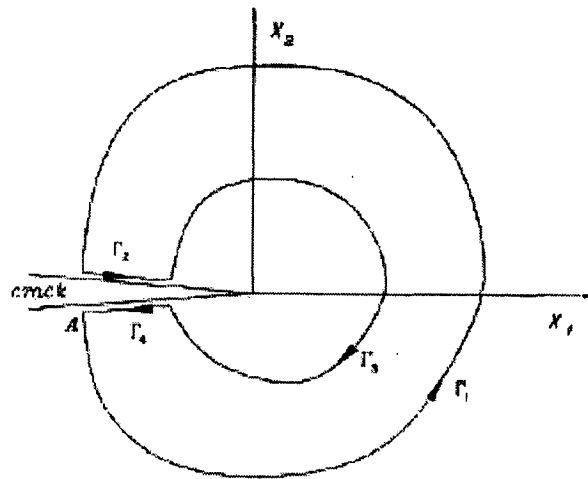


Fig. 2.15 A closed contour around a cracked tip with four distinct segments.

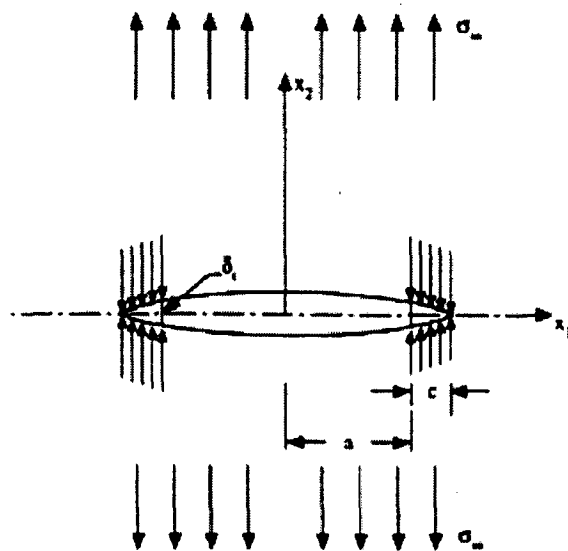
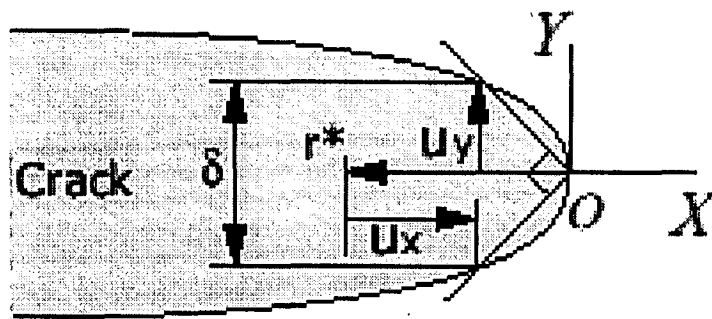


Fig. 2.16 The Dugdale model for deformation at the crack tip in a thin sheet in an elastic perfectly plastic material.



**Fig. 2.17** Definition of crack tip opening displacement (CTOD)

The CTOD is evaluated from  $u_x$  and  $u_y$  at  $r = r^*$  and  $\theta = \pi$

$$\frac{\delta}{2} = u_y(r^*, \pi) = r^* - u_x(r^*, \pi) \quad (2.52)$$

Since

$$r^* = \left( \frac{\alpha \sigma_{ys}}{E} \right)^{\frac{1}{m}} \left\{ \tilde{u}_x(\pi, m) + \tilde{u}_y(\pi, m) \right\}^{\frac{m}{m+1}} \frac{J}{\sigma_{ys} I_m} \quad (2.53)$$

and Shih has obtained

$$\delta = \frac{d_m}{\sigma_{ys}} J = \frac{2\tilde{u}(\pi, m) \left\{ \frac{\alpha \sigma_{ys}}{E} [\tilde{u}_x(\pi, m) + \tilde{u}_y(\pi, m)] \right\}^{\frac{1}{m}}}{I_m \sigma_{ys}} J \quad (2.54)$$

where  $d_m$  is a strong function of  $m$  but weakly dependent of  $\sigma_{ys}/E$ . for most engineering materials,  $0 < d_m \leq 1$  for plane stress and  $0 < d_m < 0.8$  for plane strain [Lloyd and McClintock, 2003]

The Shih analysis shows that there is a unique relationship between  $J$  and CTOD for a given material. Thus these two quantities are equally valid crack tip characterizing parameters for elastic-plastic materials. The fracture toughness of a material can be quantified either by a critical value of  $J$  and CTOD. Dawes [1979] has also acknowledged that the two parameters are related and represented different ways of measuring the same toughness.

Gullerud *et al* [1999] have expressed equations (2.50) and (2.54) as

$$J = m \sigma_y \delta \quad (2.55)$$

Where  $m$  can be a constant for a specific material. Differentiating equation (2.55) with respect to the crack length ( $a$ ), with additional approximation that  $m$  remains unchanged during limited amount of crack extension, Gullerud *et al* [1999] and Omidvar *et al* [1997] have established the relationship between CTOA and slope of the  $J$ - $R$  curve as

$$CTOA = d\delta / da = (dJ / da) / m \sigma_y \quad (2.56)$$

Lam *et al* [2005] have observed that value of  $m$  is not exactly constant due to fluctuation of the experimental data points, but depends on the crack tip constraint. The value of  $m$  derived by this process is 1.27, 1.16 and 1.01, respectively for specimens with  $a/W$  of 0.32, 0.59 and 0.71.

### **2.1.12 $J$ integral as Fracture parameter**

Path independent  $J$  integral can be interpreted as the rate of release of potential energy for non-linear elastic materials. It is identical to  $G$  in LEFM and has all the characteristics of  $K$  in the linear elastic limit so the theory may apply to plasticity if the loading is monotonic and no unloading occurs. In addition, small deformation is assumed to show path independence of  $J$ , the relation between  $J$  and the potential energy and between crack tip stress field and also with CTOD. In ductile metals, fracture occurs in a region where deformation may not be considered small ( $\epsilon < 0.1$ ).  $J$  can be used to correlate the initiation of crack growth in true elastic-plastic solids, one must be sure that the following two conditions are met. First, the deformation theory of plasticity must be an adequate model of the small-strain behavior of real elastic-plastic materials under the monotonic loads. Second, the regions in which finite strain effects are important and in which the microscopic processes occur must each be contained well within the region of the small-strain solution dominated by the singularity fields. The later condition is  $J$ -dominance condition and is analogous to small-scale yielding requirement for linear fracture mechanics.

Landes and Begley [1972] have published the results of their study on the use of  $J$  to predict the initiation of fracture under elastic-plastic conditions and this work led to the publication of a standard procedure for testing  $J$ . They hypothesized the relation between  $J$  and  $\Delta a$  as shown in Fig. 2.18. Clarke *et al* [1976] have simplified this approach and proposed partial unloading technique, where the extent of crack extension is determined from the change of the elastic compliance by repeated small unloading during test carried out on a single specimen. Following these studies, the field of elastic-plastic fracture mechanics has progressed rapidly due to persistent efforts of Landes and Begley and also, some land-mark work by Shih [1981] and by

Hutchinson and Paris [1979]. The latter two pieces of work provide a rigorous theoretical justification for characterizing stable crack growth using the  $J$ -integral. When crack extension occurs the material plasticity deformed ahead the crack moves behind the crack-tip, gets unloaded which is not permissible if  $J$ -integral has to qualify as a fracture parameter. Hutchinson and Paris [1979] have noted that crack growth involves elastic unloading and non-proportional plastic deformation near the crack tip. As they accept the validity of the  $J$  integral only within the deformation theory of plasticity, they conclude that for  $J$ -controlled crack growth it would be necessary that nearly proportional plastic deformation occurs everywhere except in a small neighborhood around the crack tip. In this case the differences between a deformation theory of plasticity and the corresponding flow theory of nonlinear elasticity would be negligible. Based on this proposition, criteria for  $J$ -controlled growth (small relative crack extension, large slope of the  $J$ - $\Delta a$  curve) have been developed so that  $J$  uniquely measures, or physically controls, the stress and strain field surrounding the crack tip. As the plastic zone is a problem in LFM, the zone of intense deformation extending over one CTOD distance ( $\delta_I$ ) beyond the crack tip is the problem for  $J$ . Around this region there is a larger zone, where stress and strain fields are controlled by  $J$  (Fig. 2.19).

So the pertinent dimensions of the specimens

$$a, W - a, B \geq C \frac{J}{\sigma_0}$$

where,  $C = 20$ .

McClintock [1971] argued on the basis of slip line fields in perfectly plastic material specimens of different geometries that crack tip stress and strain fields are geometry dependent. Strain hardening may result in clear  $J$ -dominance but the extent of regions of  $J$  dominance depends on specimen geometry.

Finite element analysis shows that

$$b = W - a \geq 200 \frac{J}{\sigma_0} \quad \text{for CCT specimens}$$

$$\geq 30 \frac{J}{\sigma_0} \quad \text{for Bend specimens}$$

It is now apparent that  $J$  could be accepted as a fracture parameter at the onset of ductile crack initiation. Hutchinson and Paris [1979] argued that several metals sustain only small amount of crack extension compared to pertinent dimensions of the specimen which characterize the mechanics of the problem. If crack growth is controlled by  $J$ , it is necessary as well as sufficient that nearly proportional plastic deformation occurs everywhere except in the small region near the crack tip or  $\partial \varepsilon$  must be uniquely related to  $\partial J$  for the dominant portion of the body.

For power law hardening material

$$\varepsilon_{ij} = K_m \left(\frac{J}{r}\right)^{\frac{m}{1+m}} \hat{\varepsilon}_{ij}(\theta) \quad (2.57)$$

we are concerned with crack increment in an element of material which was originally at  $r + da$  but is now only a distance  $r$  away from the crack tip.

$$d\varepsilon_{ij} = \frac{m}{m+1} K_m \left(\frac{1}{r}\right)^{\frac{m}{1+m}} J^{\frac{1}{m+1}} dJ \hat{\varepsilon}_{ij}(\theta) - K_m J^{\frac{1}{m+1}} da \cdot \frac{\partial}{\partial x} \left(r^{-\frac{m}{1+m}} \hat{\varepsilon}_{ij}(\theta)\right) \quad (2.58)$$

where  $\frac{\partial}{\partial x} = \cos \theta \frac{\partial}{\partial r} - \frac{\sin \theta}{r} \frac{\partial}{\partial \theta}$

or, 
$$d\varepsilon_{ij} = K_m \left(\frac{J}{r}\right)^{\frac{m}{1+m}} \left(\frac{m}{1+m} \frac{dJ}{J} \hat{\varepsilon}_{ij}(\theta) + \frac{da}{r} \hat{\beta}_{ij}(\theta)\right) \quad (2.59)$$

there are two terms - the first is proportional to  $dJ$  and the second is non proportional term.



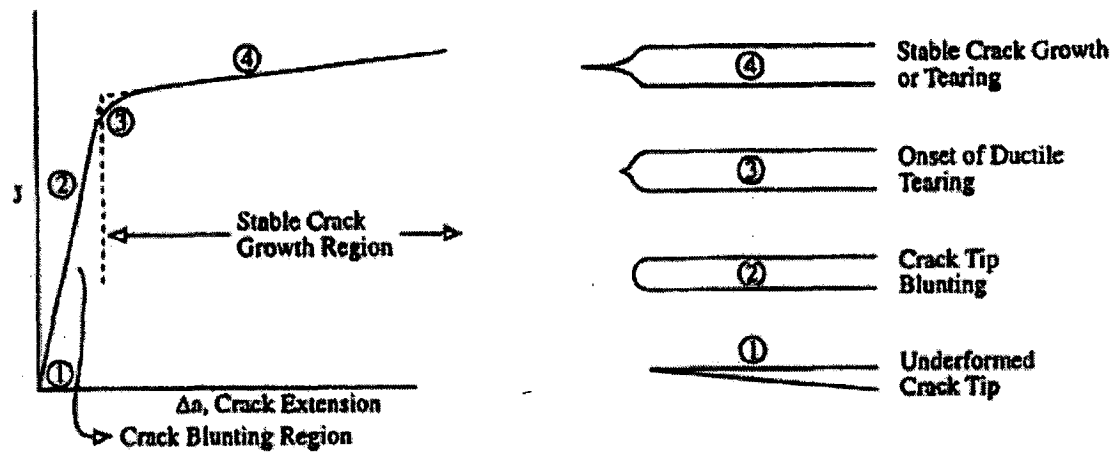


Fig. 2.18 Schematic representation of crack tip events during stable, ductile tearing.

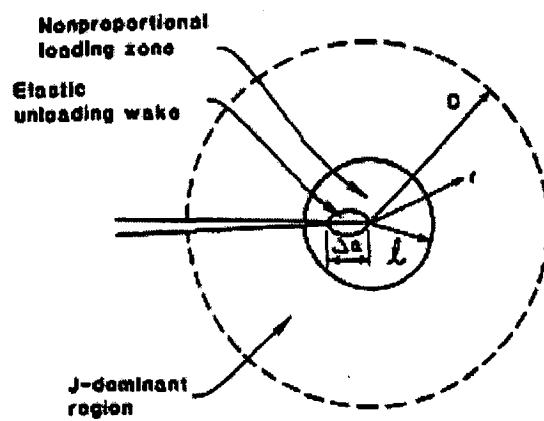


Fig. 2.19 Schematic representation of crack tip deformation zones for a growing crack.

So for  $J$  controlled crack growth to occur

$$\frac{dJ}{J} \gg \frac{da}{r}$$

or, 
$$\frac{1}{J} \frac{dJ}{da} \gg \frac{1}{r}$$

so,  $J / \frac{dJ}{da}$  should remain small in comparison to region  $R$  where  $J$  field dominate for

$J$ -controlled crack growth to occur. For fully yielded specimen,  $R = W - a$ , the uncracked ligament size.

So, 
$$\frac{J}{dJ/da} \ll R = W - a$$

or, 
$$\frac{W - a}{J} \frac{dJ}{da} = \omega \gg 1$$

higher the  $\frac{dJ}{da}$  in a specimen, there will be larger extent of crack growth characterized by  $J$  in a specimen of a given size. Shih *et al* [1979] has shown that for bend specimen  $J$  controlled condition exist for

$$\Delta a \leq 0.06(W - a) \text{ and for } \omega \geq 10$$

In the subsequent years, much progress has been occurred in the development of test methods using the  $J$ -integral approach and in the development of methods for estimating  $J$ -integral, making elastic-plastic fracture mechanics a viable engineering tool for assessing structural integrity.

## 2.2 FRACTURE CHARACTERISTICS OF DUCTILE METALS

### - $J$ - $R$ CURVE AND $J_{IC}$

Resistance to Fracture of a material is determined by its  $J$ - $R$  curve, which is an important input to all elastic-plastic fracture analyses of structures.  $J$ - $R$  curve is determined experimentally through fracture test of a specimen or component. Fracture test involves loading under bending or tension of fatigue pre-cracked specimens and determination of  $J$  as a function of crack length during the process of crack growth. Load versus load-line displacement is recorded digitally as the basic data of the test. The  $J$ -integral is determined from the load and the mode of loading at different load-displacement points, to plot it against crack growth,  $\Delta a_p$ , within specified limits, as determined physically or through properties like compliance. These data reflect the materials resistance to crack growth. The  $J$  versus crack growth behaviour is approximated with a best-fit power law relationship. A blunting line is drawn, approximating crack tip stretch effects, following ASTM standard E-813. Blunting line has been defined as a line that approximates apparent crack advance due to crack tip blunting in the absence of slow stable crack tearing [ASTM E 1823, 1996]. The blunting line is given by the equation,

$$J = 2\sigma_f \Delta a \quad (2.60)$$

where,  $\sigma_f = \frac{1}{2}(\sigma_Y + \sigma_U)$

The single point on  $J$ - $R$  curve related to the initiation of the ductile crack extension is termed as initiation fracture toughness ( $J_{IC}$ ). The initiation fracture toughness can be a point on  $J$ - $R$  curve at physical crack extension point, e.g., 0.2 mm of crack extension is most often used. It can also be at an offset point modeled by the crack-tip blunting geometry, e.g., a point defined by an offset construction line at 0.2 mm with a slope that is defined in the test method [ASTM E 813, 1995].

Usually single edge notch bend (SENB or three-point bend) or the compact tension (CT) specimens are tested for fracture toughness test, as shown in Fig. 2.20. The measurement of displacement is carried out generally on the load line to avoid correction, which will be required since  $J$  is an energy based parameter. Therefore, provision has to be made in the specimens to allow a direct measurement of displacement along the load-line. The position and orientation of the specimen is important and also, the location and orientation of the notch is critical. Typically, the notch along which fatigue pre-cracking takes place is positioned so as to propagate the crack through the chosen microstructure. The notch is oriented with respect to (a) the weld axis for welded joints, (b) the rolling direction in a rolled product or (c) forging axis in a forged component, as shown in Fig. 2.21. All the specimen dimensions are proportioned to the width,  $W$ . For SENB and CT specimens the dimensions obey  $1 \leq W/B \leq 4$  and  $2 \leq W/B \leq 4$  respectively.

Specimens are required to be pre-cracked under cyclic load before carrying out the test for fracture toughness in order to ensure reproducibility. Pre-cracking is done to introduce a sharp crack from a machined notch, which may be a straight one through the thickness of the specimen or in the shape of a chevron. All standard test methods have some requirements for fatigue pre-cracking, given as under:

- Applied load during pre-cracking be lower than the limit load so that the specimen is not overloaded,
- Maximum stress intensity factor,  $K_{max}$ , be lower than a specified value,
- $K_{max}$  lower than a specified percentage of the measured fracture toughness,
- Additional requirements be met when the test temperature is different from the pre-cracking temperature,
- Minimum pre-cracking length be met,
- Specified range of load ratio ( $R = P_{min}/P_{max}$ ) be maintained,
- More severe requirements be met while approaching the final stage of pre-cracking.

Theoretical justification given by Scibetta *et al* [2002] may help to understand these requirements specified in various standards. During fatigue pre-cracking a plastic zone is created. As long as pre-cracking is performed in the linear elastic regime, the square root of the plastic zone size,  $r_y$ , is proportional to the applied stress intensity factor,  $K$ , under fatigue.

$$K = f\sigma_{ys}\sqrt{6\pi r_y} \quad (2.61)$$

Where  $\sigma_{ys}$  is the yield strength,  $f$  is a function of the strain hardening exponent and the ratio of yield strength to Young modulus. Fracture toughness may artificially increase due to compression residual stresses induced at the crack tip during pre-cracking. The residual stress affects fracture toughness and it is supported by experiments conducted in different studies [Hsing and Ji-Liang, 1993; Kaufman and Schilling, 1973 and May, 1970]. Therefore, the plastic zone size during fracture must be larger than the plastic zone size during fatigue. Several requirements are given to satisfy this condition in terms of:

$$K_{\max} \leq \gamma K_{Jc} \quad (2.62)$$

where  $K_{Jc}$  is the  $J$ -integral at initiation converted to  $K$  following equation  $J_{IC} = \frac{K_{IC}^2}{E}$  and  $\gamma$  a constant varying from 0.6 to 0.8.

Fracture toughness increases due to an overloading at a temperature above the testing temperature [Pickles and Cowan, 1983]. When the test temperature,  $T_{test}$ , is lower than the pre-cracking temperature,  $T_{fatigue}$ , the plastic zone generated during pre-cracking has size larger than the one that would be obtained during fracture toughness test at the test temperature,  $T_{test}$ . Therefore, the ratio  $\sigma_{ys}(T_{fatigue})/\sigma_{ys}(T_{test})$ , which is lower than one, is generally taken into account to make the requirements on equation (2.54) more stringent. Tobler and Shimada [1991] have tested two austenitic steels 13 Mn (low toughness material) and 22 Mn (high toughness material) at 4 K that are pre-cracked at 295, 77 and 4 K. No effect of pre-cracking has been observed on low toughness material (cleavage fracture) as long as

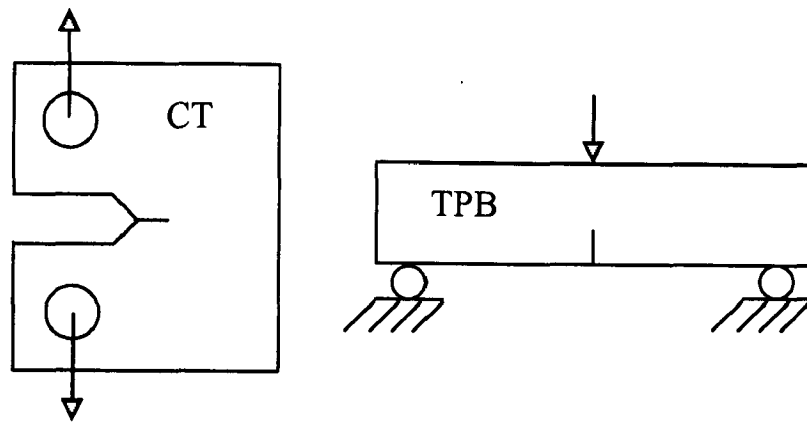


Fig. 2.20 Sketch of various specimens (a) CT, (b) TPB

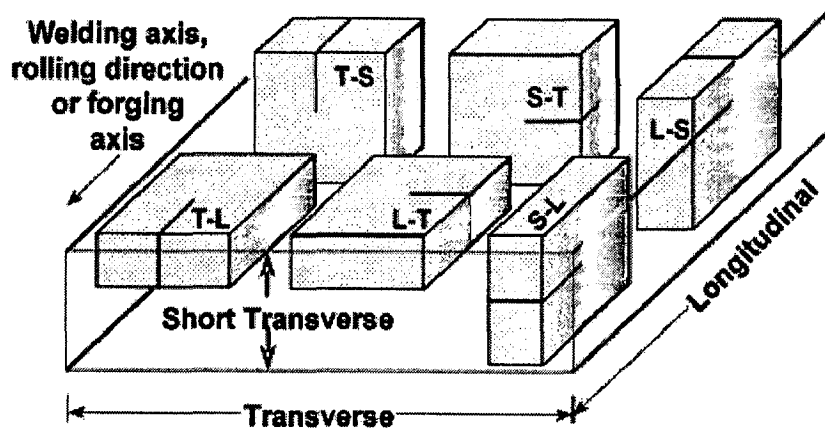


Fig. 2.21 Schematic diagram of the orientation code for identify testing direction.

$K_{max} \leq 0.7\sigma_{YS} (T_{fatigue})/\sigma_{ys} (T_{test})K_{IC}$ . When  $K_{max} > 0.7\sigma_{YS} (T_{fatigue})/\sigma_{ys} (T_{test})K_{IC}$  a strong effect of pre-cracking has been observed. In high toughness material (ductile fracture), no effect of pre-cracking has been observed even for specimen pre-cracked up to  $46 \text{ MPa}\sqrt{m}$  at room temperature. All tests were performed with  $K_{max} \leq 0.80.7\sigma_{YS} (T_{fatigue})/\sigma_{ys} (T_{test})K_{IC}$ , where  $K_{Jc}$  is the  $J$ -integral at initiation converted to  $K$ .

In order to apply linear elastic fracture mechanics to the pre-cracking requirements, it is required that the load be lower than the limit load. Loads higher than the limit load could result in permanent deformation caused by pre-cracking. Therefore, several requirements are given in terms of:

$$P_{max} \leq \kappa P_{lim} \quad (2.63)$$

Where,  $P_{lim}$  is the limit load and  $\kappa$  a constant varying from 0.4 to 1.

In order to avoid any interaction of the machined notch with the stress field at the crack tip, the length of the crack due to fatigue should be long enough. For the purpose of each specific test method, crack length to width ratio requirement is set.

## 2.2.1 Single and Multi Specimens Tests

Two techniques are used to determine  $J$ - $R$  curve of a material. The first is the multiple specimen method, in which four or more identically prepared (including pre-cracking) specimens are loaded to different displacements and plotted as a single curve to obtain the desired plot. The value of  $J$  is estimated from the area under the load vs. load-line displacement curve by the equation

$$J = J_{el} + J_{pl} \quad (2.64)$$

where,  $J_{el}$  = elastic component of  $J$

$J_{pl}$  = plastic component of  $J$ .

For a given load-displacement point,  $(i)$ ,  $J_{el}$  is calculated following the equation,

$$J_{el(i)} = \frac{K^2_{(i)}(1-\nu^2)}{E} \quad (2.65)$$

For CT specimens of width  $W$ ,

$$K_{(i)} = \left[ P_i / (BB_N W)^{1/2} \right] f(a_0/W) \quad (2.66)$$

Where,  $P_i$  = Load at point  $(i)$

$B_N$  = net specimen thickness ( $B_N = B$  if no side grooves are present), and,

$$f(a_0/W) = \left[ \frac{(2 + a_0/W)(0.886 + 4.64a_0/W - 13.32(a_0/W)^2 + 14.72(a_0/W)^3 - 5.6(a_0/W)^4)}{(1 - a_0/W)^{3/2}} \right] \quad (2.67)$$

For three point bend specimens of width  $W$ ,

$$K_{(i)} = \left[ \frac{P_i S}{(BB_N)^{1/2} W^{3/2}} \right] f(a_0/W) \quad (2.68)$$

Where,  $B_N$  = net specimen thickness ( $B_N = B$  if no side grooves are present)

$S$  = Span between the loading points, and,

$$f(a_0/W) = \left[ \frac{3(a_0/W)^{1/2} \left[ 1.99 - (a_0/W)(1 - a_0/W)X(2.15 - 3.93(a_0/W) + 2.7(a_0/W)^2) \right]}{2(1 + 2a_0/W)(1 - a_0/W)^{3/2}} \right] \quad (2.69)$$



From the area under the load-displacement curve  $J_{pl}$  at a point corresponding to each loading unloading cycle has been calculated using equation

$$J_{pl} = \frac{\eta A_{pl(i)}}{B_N b_0} \quad (2.70)$$

Where,

$i$  = point on the load-displacement curve

$A_{pl(i)}$  = area under the load-displacement curve up to the point  $i$

$b_0$  = uncracked ligament

$\eta = 2 + 0.522 b_0/W$  for CT specimens and 2 for TPB specimens.

In multiple specimen technique crack extension is determined from measurements taken on the fractured surface of the test specimen. The final crack length is usually identified as being at the end of the ductile crack extension region. This is identified by special marking such as heat tinting at about 300 °C for 30 minutes for steels and titanium alloys before breaking it into two. Without heat tinting, the sample may be broken under cyclic load. The region under fatigue fracture could be easily distinguished from the region under ductile tearing by their physical appearance. Usually the crack front for each region (i.e. fatigue pre-crack region, region of ductile crack extension and a final fast crack extension region) is curved. For obtaining the single-length value, the crack is measured at different points on fixed interval through the thickness and these are averaged. In nine point average method, the crack length is measured at the fractured surface along the thickness at seven intervals of size 1/8th thickness. The two surface lengths are averaged to give one value and the seven middle lengths are averaged to give another value. The average of these two values gives the length of crack extension,  $\Delta a$ . From the estimated  $J$  and  $\Delta a$  data points at different load-displacement level in at least four specimens,  $J$ - $R$  curve is fitted using construction procedure specified in standard test

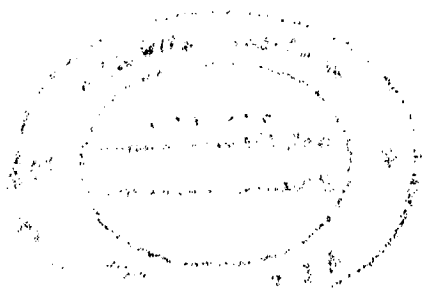
methods for further analysis. Multiple specimen technique is costly due to requirement of large number of specimens.

The second technique requires only one specimen and is called “Single specimen technique”. There is fundamental difference between multiple and single specimen test methods. Since the  $J$ - $R$  curve in the multiple specimen method is determined only at a few specific load-displacement points, one, therefore, gets a crack growth resistance behavior and the initiation parameter, which is averaged over the inhomogeneity of the specimen. The single specimen method, on the other hand, gives results on a much closer interval providing information on the impact of material inhomogeneity. The single-specimen test technique is also based on same principle as that of multiple specimen technique, but this technique uses elastic compliance or potential drop techniques for measurement of crack growth at various stages of loading without breaking the specimens.

The partial unloading compliance technique is the commonly used method to measure the crack growth under increasing loading during fracture mechanics tests on compact tension (CT) and three point bend (TPB) specimens. The crack length is computed at regular intervals during the test by partially unloading the specimen and measuring the compliance. The specimen compliance changes with the growth of a crack. However, one pre-requisite of using this technique is to have a compliance function correlating the crack length and depth with compliance. Correlations are available for CT, TPB and some other types of specimens. The relation for CT specimen is as follows [Saxena and Hudak, 1978]

$$a/W = [1.000196 - 4.06319\mu + 11.242\mu^2 - 106.043\mu^3 + 464.335\mu^4 - 650.677\mu^5]$$

(2.71)



where,  $\mu = \frac{1}{[B_e EC_i]^{1/2} + 1}$

$$B_e = B - \left(\frac{B - B_N}{B}\right)^2$$

where,  $B_N$  = net specimen thickness, for the non side grooved specimens  $B_e$  is taken as  $B$ .  $E$  is the Young's Modulus of the specimen and  $C_i$  is the compliance at corresponding loading unloading cycle. The compliance correlation for the TPB specimen is as follows [Wu, 1984]:

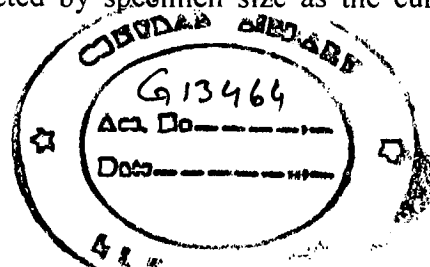
$$a/W = [0.999748 - 3.9504\mu + 2.9821\mu^2 - 3.21408\mu^3 + 51.51564\mu^4 - 113.031\mu^5] \quad (2.72)$$

Where,

$$\mu = \frac{1}{\left[\frac{B_e WE' C_i}{S/4}\right]^{1/2} + 1}$$

$S$  is the loading span and  $W$  is the width of the TPB specimen. The other symbols have the same meaning as in equations (2.71).

The potential drop technique utilizes a voltage change to infer about the extent of crack growth. If a constant alternating or direct current passes through the uncracked ligament of a test specimen, the voltage increases as the crack grows, due to increased electrical resistance across the crack contributed by decrease in remaining ligament cross-section. Crack extension can be determined accurately using either AC or DC potential drop [Okumura *et al*, 1981]. However, there are particular advantages of each of these techniques, which govern the most suitable one for a given application [Gibson, 1987]. There are two main advantages of using AC rather than DC potential drop. Firstly, the sensitivity of AC potential drop to changes in crack length is less affected by specimen size as the current



passes around the surface of the specimen, while in DC technique, the current passes through the specimen. Therefore, for a given voltage resolution, a smaller increase in current is required in AC technique while testing larger specimen. The second advantage is that there are no thermal induced emfs when testing at temperatures other than ambient; although this problem can also be avoided by repeatedly reversing the current flow in DC technique. There are two main disadvantages of using AC potential drop. Firstly, the potential drop signals have to be corrected for contributions due to the effect of stress on electrical resistance. No such step is required for DC potential drop. The second disadvantage of using AC potential drop concerns the lowest detectable  $J_I$  value. The value has been found to be about twice as high in AC compared to that in DC potential drop [Gibson, 1987].

The potential drop technique is not very popular as it requires additional instrumentation and sometimes, it is difficult to separate the voltage change due to crack growth and that due to plastic energy near the crack tip of a ductile material.

$J$ - $\Delta a$  data points estimated from either multi specimen technique or single specimen technique is joined to get  $J$ - $R$  curve experimentally. This  $J$ - $R$  curve can be used directly to evaluate the fracture behavior and determine the fracture-toughness,  $J_{IC}$ , of a ductile metallic material. The valid  $J$ - $R$  curve is drawn following a construction procedure prescribed by ASTM [ASTM E 1820, 2001], which uses a two parameter power law for fitting the experimental  $J$ -  $\Delta a$  points.

$$J = C_1 (\Delta a)^{C_2} \quad (2.73)$$

where  $C_1$  and  $C_2$  are constants. All the points cannot be used for power law fit. Only those points below  $J_{limit} = (W-a_0)\sigma_f / 15$  and falling between the exclusion lines, drawn at crack extension of  $\Delta a = 0.15$  and  $\Delta a = 1.5$  mm with the same slope as that of blunting line, are taken. It should be ensured that the available data are uniformly distributed. At least one data

point lies in between the 0.15 and 0.5 mm offset lines and at least one point lies between 0.5 mm and 1.5 mm lines.

The International Organization for Standardization (ISO) and European Society of Structural Integrity (ESIS) recommends a fitting procedure using three parameter power law as,

$$J = \alpha + \beta(\Delta a)^\gamma \quad (2.74)$$

Where  $\alpha$ ,  $\beta$  and  $\gamma$  are constants. The equation of the blunting line used in the ESIS procedure is

$$J = \left( \frac{1}{d_n^*} \right) (\Delta a \cdot E) \quad (2.75)$$

where,  $d_n^*$  is a function of material tensile properties, like strain hardening coefficient  $n$ , proof stress at strain 0.2 percent and  $E$ , the Young's modulus. For materials with  $\nu = 0.3$ , the value of  $d_n^*$  may be determined graphically using Fig. 2.22 [Heerens *et al*, 1988]. Alternatively,  $d_n^*$  can be determined using equation [ESIS-92, 1992a]

$$d_n^* = \varepsilon_0^{n-1} \cdot D_n \quad (2.76)$$

$$\text{and } D_n = 0.787 + 1.554n - 2.45n^2 + 16.952n^3 - 38.206n^4 + 33.13n^5$$

where  $\varepsilon_0$  is reference strain equivalent to  $(\sigma_0 / E)$ , where  $\sigma_0$  is the reference stress taken as flow stress,  $[(\sigma_U + \sigma_Y)/2]$ .

In this procedure only those points, which fall below the  $J_{max} = (W-a_0) \sigma_f/20$  and lies in between the 0.1 mm and exclusion line at  $\Delta a_{max} = 0.10 (W-a_0)$ , are considered for fitting, where  $W$  is the width of the specimen and  $a_0$  is the initial crack length.

Since many assessment methods are based on a single-point fracture toughness value, it is often desirable to arrive at a single-point fracture-toughness value which could be used as a characteristics of a material and used for design purposes. Although in all the approaches, there is an effort to choose the point associated with initiation of the ductile crack extension, still there are variations in the choice of a point on the  $J$ - $R$  curve to characterize the fracture toughness. The initiation point can be determined directly from the microstructure but a point corresponding to 0.2 mm of crack extension is most often used. It can also be an offset point determined by modeling the extension caused by crack-tip blunting. The point of intersection between the  $J$ - $R$  curve and an offset line constructed at  $\Delta a = 0.2$  mm, with the same slope as the blunting line [ASTM E 813, 1982]. As mentioned earlier, a microscopic procedure may also be used. The stretched zone width is clearly identified by the boundary of fatigue fracture obtained during pre-fatiguing and the ductile fracture obtained during crack propagation. The stretched zone width may be used to identify the initiation value of crack extension and used as a value of crack extension that should correspond to single-point fracture-toughness value  $J_Q$  [ESIS-92, 1992 a, b].

The  $J_Q$  is the candidate for  $J_{IC}$  value determined by these methods and it qualifies to become  $J_{IC}$  if the following size requirement is satisfied

$$B, W - a_0 \geq 25 \frac{J_Q}{\sigma_Y}$$

## 2.3 EFFECT OF SPECIMEN GEOMETRY ON INITIATION FRACTURE TOUGHNESS ( $J_{IC}$ )

Ductile fracture in engineering materials is usually characterized by the fracture initiation toughness  $J_{IC}$  as it has been described earlier but the detailed fracture resistance behaviour is given by the entire  $J$ - $R$  curve. For a cracked component or structure, the  $J_{IC}$  dictates the condition of stress under which crack propagation is initiated and the  $J$ - $R$  curve determines how far the crack can grow in a stable manner under increasing load

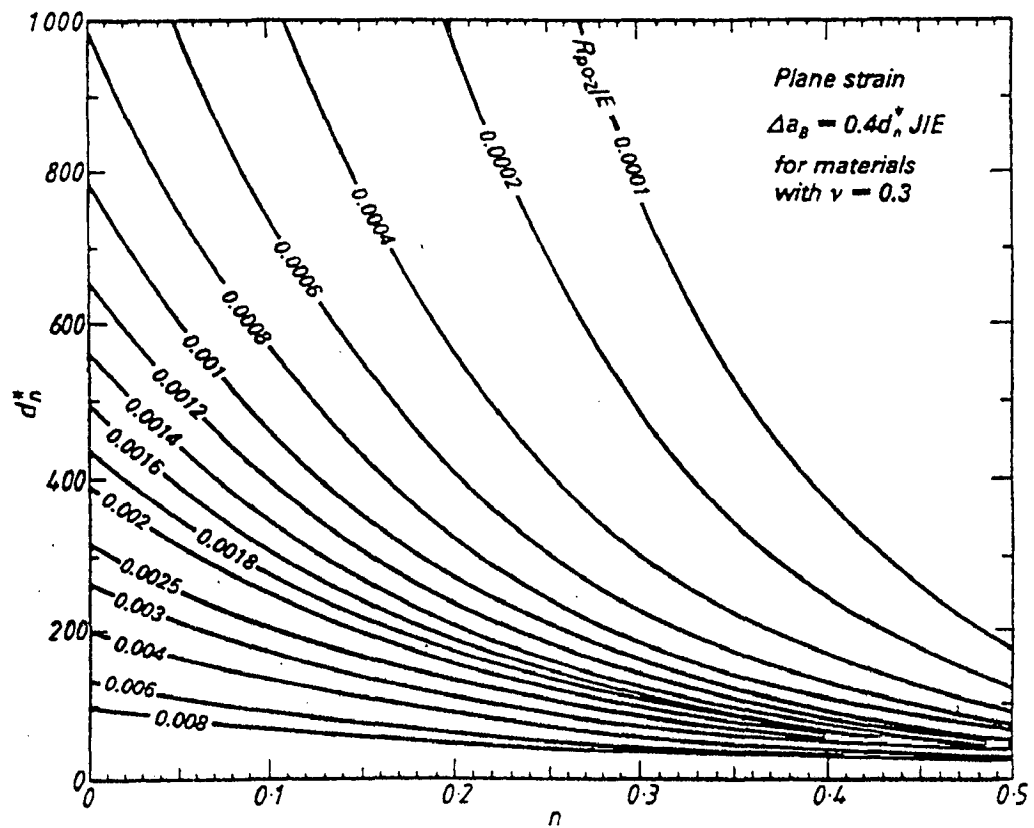


Fig. 2.22 Determination of  $d_n^*$ , [Heerens *et al*, 1988]

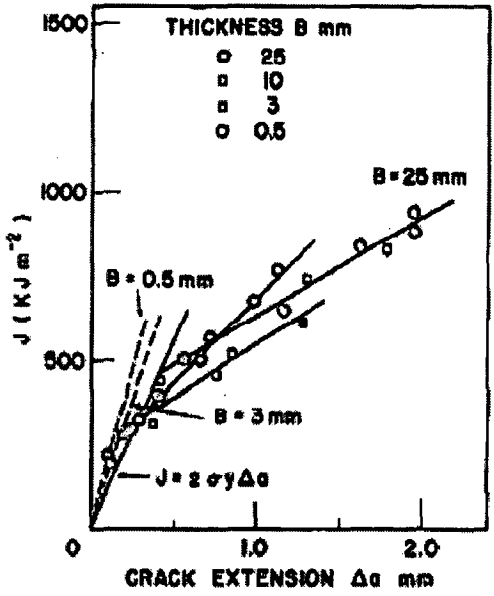
characterized by  $J$ . Earlier, the fracture criteria, namely, the  $J_{IC}$  and the  $J$ - $R$  curve, have been widely considered as a material property in the analysis of fracture of engineering structures. It is assumed that  $J_{IC}$  and the material  $J$ - $R$  curves are independent of geometry and type of loading. However, it is now well-known that material  $J$ - $R$  curve is geometry dependent. This dependence of fracture toughness is a result of the varying degree of triaxiality of the stresses at the crack tip which is referred to as the “constraint”. The original concept of constraint is related to the thickness of a specimen. It is experimentally observed that thicker specimens usually give lower fracture-toughness values than similar thinner specimens. Hence, fracture-toughness testing is conducted on specimens, which has a thickness requirement that would place the fracture-toughness result in a category of high-constraint, approaching plane strain, so that the result would be conservative relative to the application. The requirements of high constraint for fracture testing often create difficulties in practical applications of test results to real structure components with low crack-tip constraints. The transferability of the laboratory data to the component level is, thus, an important issue yet to be tackled satisfactorily in the field of elastic-plastic fracture mechanics (EPFM).

A number of research worker have used non-standard fracture specimens to study the effect of crack-tip constraints (thickness) on the fracture behavior of ductile crack growth. Mao [1991] has tested CT specimens of A533B-1 steel with thickness ( $B$ ) of 25, 10, 3 and 0.5 mm having width ( $W$ ) of 50, 20, 10 and 10 mm respectively. Some specimens tested do not satisfy the ASTM requirement for the minimum thickness of the specimen, given by  $B = 25J_{Ic} / \sigma_f$ .  $J$ - $R$  curves (Fig. 2.23) for specimens of A533B-1 show that the initiation fracture toughness decreases with decreasing specimen thickness while maintaining the same width. Initiation fracture toughness is independent of specimen thickness if specimen width is also reduced maintaining the same  $B/W$  ratio. However, the slope of  $J$ - $R$  curve increases with decreasing thickness of the specimen. Ono *et al* [2004] have also studied the effect of specimen size on  $J$ - $R$  curve for CT specimens of reduced activation ferritic steel, JLF-1. Four different sizes of

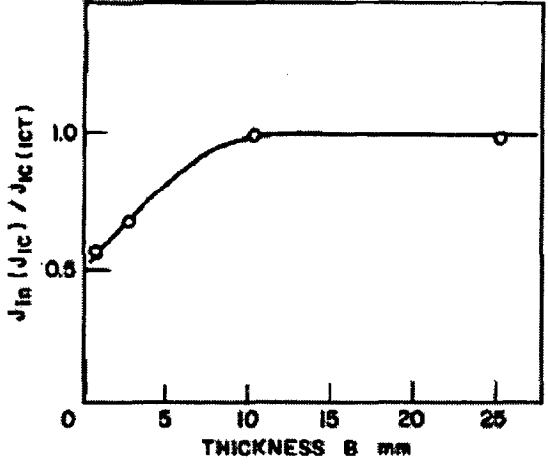


compact tension (CT) specimens, 1T-1CT, 1/2T-1CT, 1/2CT and 1/4CT have been tested for the fracture toughness at room temperature by means of the unloading compliance method referring to the ASTM E1820-01 [2001]. The  $J_Q$  values obtained for the 1T-1CT and 1/2T-1CT (different thickness, same width) specimens are found to be 404 and 623 kJ/m<sup>2</sup> (Fig. 2.24), respectively, indicating that the  $J_Q$  value increases with decreasing specimen thickness because of approaching the plane stress state where the plastic zone size at the crack tip increases near specimen side surfaces. Since the energy spent on the plastic deformation increases, the fracture toughness also increases.

On the other hand,  $J_Q$  decreases with decreasing specimen thickness while maintaining the same  $B/W$  ratio. Ono *et al* [2004] have explained it with the help of slip-line field analysis for the static loading given by Rice [1968], the plastic zone size at the crack tip is around 1.6 mm for a standard size specimen which is described by  $2(J/\sigma_{YS})$ , where  $\sigma_{YS}$  is the yield stress of the material. It is considered that almost half of the ligament length is occupied by the plastic zone in the 1/4CT specimen, while there is enough ligament length left without plastic deformation in the 1T-1CT specimen. When the specimen size becomes extremely small like 1/4CT size, the ligament size becomes too small to suppress gross yielding, resulting in flow instability and a decrease in the  $J_Q$  values for the smaller specimens. However, Jitsukawa *et al* [1999] have not found any appreciable change in  $J_Q$  value with the specimen thickness (with the same width) on three point bend bar specimens of 7075-T6 high strength aluminum alloy. Seok and Kim [2002] have also studied the effect of specimen thickness on the  $J$ - $R$  curve of side grooved specimens of thickness ranging from 12.7 mm to 50.8 mm.  $J$ - $R$  curves obtained from their studies show no significant difference. This may be due to side grooving of the specimens, which produces the plane strain condition at the crack tip.



(a)



(b)

Fig. 2.23 (a)  $J$ - $R$  curves for 25, 10, 3 and 0.5 mm thick specimens of A533B-1 (b) The change of fracture toughness  $J_{IC}$  with thickness of specimen [Mao, 1991].

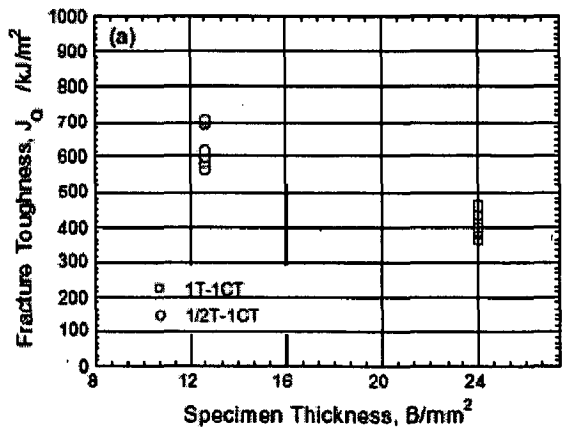


Fig. 2.24 Effect of specimen size on fracture toughness  $J_Q$  [Ono *et al*, 2004]

Also, the constraint of the specimen is influenced by  $a/W$  ratio more than thickness. Lower constraint is found for shorter cracks i.e. when ratio of crack length to planar width,  $a/W$ , is small. For the measurement of fracture toughness according to the ASTM standard, bending or compact tension specimens with relatively deep notches (the ratio of notch depth to specimen depth  $a/W$  is approximately 0.5) are preferred. However, in engineering practice, many defects encountered are shallow cracks and investigations on shallow notches indicate that  $J_{Ic}$  values of shallow cracks are significantly higher than those of deep cracks. Li *et al* [1986] have performed a series of tests on a high strength and high toughness alloy steel by varying the  $a/W$  ratio from about 0.1 to 0.5, keeping  $W$  constant. The results indicate that  $J_{Ic}$  is insensitive to  $a/W$  when  $a/W \geq 0.2$  and becomes dependent on  $a/W$  as  $a/W \leq 0.15$ . Zhang and Wang [1987] has also studied the effect of  $a/W$  on the  $J_{Ic}$  in the structural steel in three point bend specimens. This study has also reported that in specimen with shallow notches, the  $J$ -integral at initiation is greater than those in specimens with deep notches as shown in Fig. 2.25. When  $a/W = 0.1$ , the  $J$ - integral at initiation is about twice as large as that for  $a/W = 0.5$ . Zhang and Huang [1988] through experimental and finite element analysis, have shown that different plastic deformation pattern leads to larger plastic work needed for the onset of crack propagation in specimens with shallow notches and it contributes significantly to the difference in behavior observed between specimens with shallow and deep cracks.

Zheng *et al* [2000a] have tested the fracture toughness of St 69 steel by changing the crack length ( $a/W$ ) of the TPB specimens and shown that the critical  $J$  integral for physical crack initiation varies from one specimen to another which indicates the dependence of critical  $J$  integral on stress state or geometry strongly. Kikuchi [1997] has also observed that  $J_{Ic}$  increases due to the decrease of the crack tip constraint on CT, TPB and CCT specimens made of A533B steel and aluminium alloy with different crack length. Shen *et al* [2001] have also made the same observation after testing TPB specimens of CSA grade G40.21 350WT plate materials that shallow cracks have much higher fracture toughness than deep cracks as shown in Fig. 2.26. However, Jitsukawa *et al* [1999] have not noticed any appreciable change in  $J_Q$  value with  $a/W$  ratio (from 0.125 to 0.5) on three point bend bar specimens of 7075-T6 high strength aluminum alloy.

Using A533B, HY-100 and HY-80 structural steels, Joyce and Link [1995, 1997] presented the experimental data of ductile crack growth for TPB, ICT, single edge-notch tensile (SENT) specimen, and double edge-notched tensile (DENT) specimen with shallow to deep cracks over a range of crack length ratios from 0.13 to 0.83. In spite of wide range of variation of constraint presented over this range of  $a/W$  ratio, it is surprising that no significant effect of constraint on initiation toughness could be found but the slope of  $J$ - $R$  curve after a relatively large crack extension is considerably affected by the change in constraint through  $a/W$  ratio.

The same conclusion has been made through experiments using large-sized specimens, by Marschall *et al* [1989] for 3 CT and 10 CT in a stainless steel, Eisele *et al* [1992] and Roos *et al* [1991, 1993] for CT, TPB, CCP, DENT and SENT in KS01 (22NiMoCr37) steel, and through experiments using small or sub-sized specimens by Elliot *et al* [1991], Alexander [1993] and Gilbert *et al* [1997]. Similar results have also been reported by Kordisch *et al* [1989], Klemm *et al* [1991], Henry *et al* [1996], Decamp *et al* [1997], Haynes and Gangloff [1997]. All experimental data reported in literature suggest that the  $J$ - $R$  curves vary with the level of constraint. The  $J$ - $R$  curve for high constraint specimen geometry is lower than that for low constraint specimen geometry as shown in Fig. 2.27 [Chao and Zhu, 2000]. Quantitatively, at a fixed crack extension ( $\Delta a$ ), the value of the  $J$ -integral of a high-constraint specimen is less than that of a low-constraint specimen. In other words, the low-constraint specimen exhibits higher load carrying capacity [Lam *et al*, 2003].

To simulate the experimental results of ductile crack growth, two and three dimensional finite element analyses [FEA] have been carried out. Most of these studies use macroscopic plasticity theory [Yuan and Brocks, 1989; Brocks *et al*, 1994; Henry *et al*, 1996; Shan *et al*, 1996; Kikuchi, 1997; Yan and Mai, 1997]. Void growth models, local damage

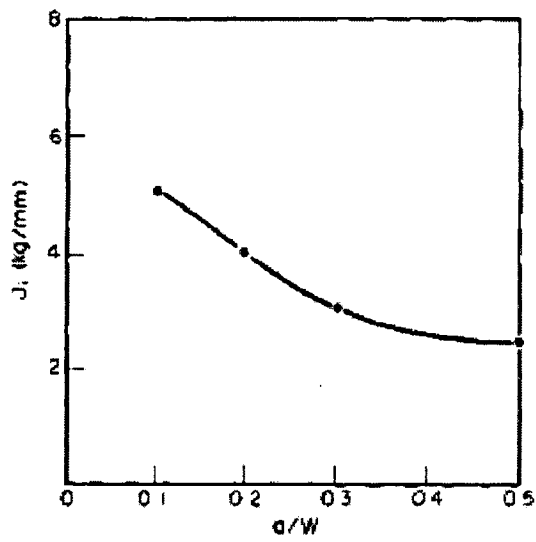


Fig. 2.25  $J_i$  of specimens with shallow and deep notches [Zhang and Wang, 1987]

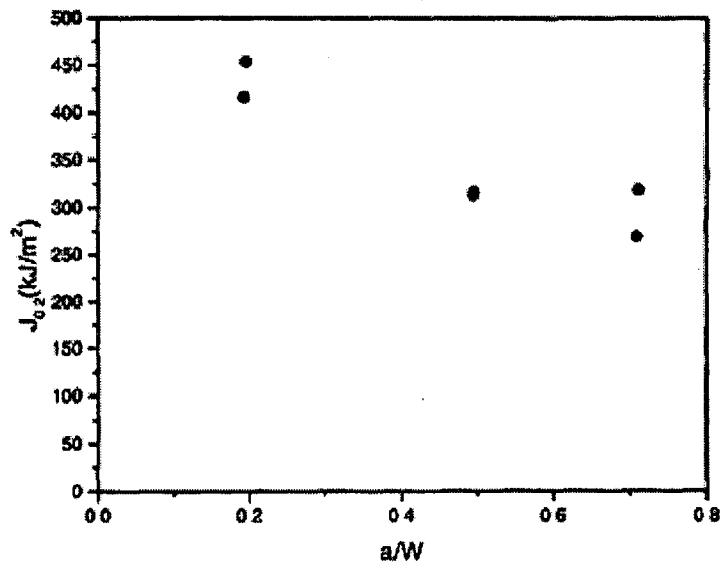


Fig. 2.26  $J$  resistance ( $J_{0.2}$ ) as a function of  $a/W$  [Shen *et al*, 2001]

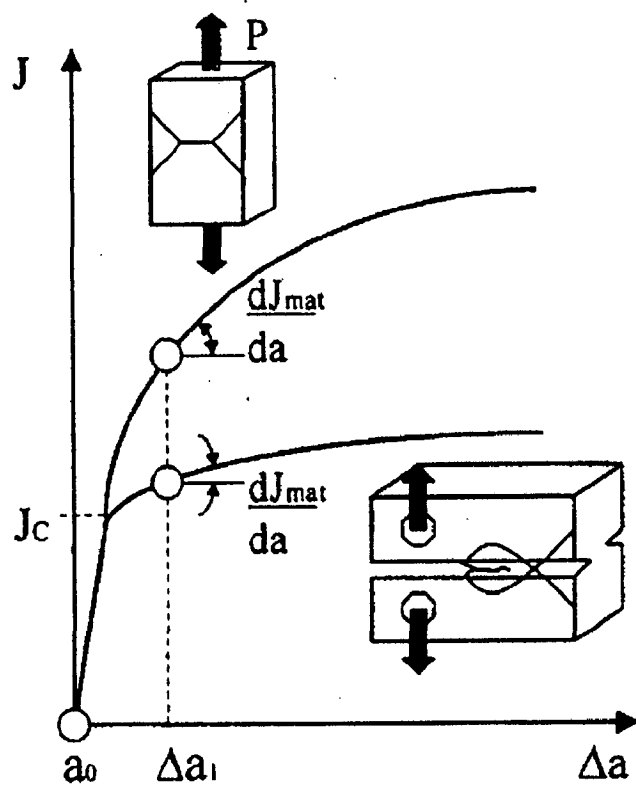


Fig. 2.27 Variation of  $J$ - $R$  curves with the level of crack tip constraints [Chao and Zhu, 2000]

models or micro-mechanics approach have been employed [Sun and Schmitt, 1990; Xia *et al*, 1995; Xia and Shih, 1995a, 1995b; Moyer *et al*, 1997; Sun *et al*, 1997]. FEA simulations for different specimens, such as CT, TPB, SENT, DENT and CCP, show that ductile crack growth is sensitive to the crack-tip constraints and the amount of  $J$ -controlled crack growth is different for different specimens. At the stage of fracture initiation, the fracture toughness  $J_{IC}$  increases somewhat with the crack-tip constraints, and is weakly and linearly related to constraint level. During the crack growth, the tearing resistance of  $J$ - $R$  curve increases with decreasing constraint level.

The three most commonly used methods to quantify crack-tip constraints are

- (1)  $J$ - $T$  approach proposed by Betegon and Hancock [1991],
- (2)  $J$ - $Q$  approach by O'Dowd and Shih [1991, 1992, 1994], and
- (3)  $J$ - $A_2$  approach by Yang *et al* [1993] and Chao *et al* [1994].

Williams [1957] has proposed an expression for the full-field crack tip stress distribution ahead of the crack tip in a cracked elastic solid. The proposed stress field in the vicinity of crack tip can be expressed as an infinite power series, with leading term exhibiting a  $1/\sqrt{r}$  singularity, the second term independent of  $r$  and the third term proportional to  $\sqrt{r}$  and so on as given by the expression

$$\sigma_{ij}(r, \theta) = Ar^{-\frac{1}{2}} f_{ij}(\theta) + Bg_{ij}(\theta) + Cr^{\frac{1}{2}} h_{ij}(\theta) + \dots \quad (2.77)$$

The terms  $B$  and  $C$  are dependent on the geometry of the cracked body while the first singular term which dominates the crack tip stress as  $r \rightarrow 0$ , depends only on  $K$ . The third and higher terms in Williams solution have positive exponent of  $r$ , and so becomes zero at the crack tip but the second term remains finite [Larsson and Carlsson, 1973].

Williams two term solution for a crack in an isotropic elastic material subjected to plane strain Mode I loading is given by

$$\sigma_{ij}(r, \theta) = \frac{K}{\sqrt{2\pi r}} f_{ij}(\theta) + T\delta_{ij} \quad \text{as } r \rightarrow 0 \quad (2.78)$$

$T$  is elastic  $T$ -stress and proportional to the applied stress. It is dependent on the geometry and size of the body. Using different combination of the two loading parameters,  $K_I$  and  $T$ , different near crack-tip fields can be generated. Thus,  $(K_I / \sigma_0)^2$  or equivalently  $(J / \sigma_0)$  provides the only length scale in the two-parameter formulation. Fields of different crack-tip stress triaxialities can be induced by applying different levels of  $T / \sigma_0$ . Thus, the near-tip field depends on distance only through the  $r / (J / \sigma_0)$ .

This implies that the stress parameter  $T$  provides a convenient means to parameterize specimen geometry effects on crack-tip stress triaxiality (constraint) under condition of well contained yielding [Betegon and Hancock, 1991]. The  $T_{\text{stress}}$  can be used as a constraint parameter under SSY conditions. The  $T_{\text{stress}}$ , compared with others constraint parameters, has the advantage of simplicity, requiring only a linear-elastic analysis of the cracked body. Sherry *et al* [1995] have presented a compendium of  $T_{\text{stress}}$  solutions for different cracked geometries. Figure 2.28 gives  $T_{\text{stress}}$  values in TPB and CT specimens as a function of the crack-depth, indicating a significant difference of  $T_{\text{stress}}$  (positive values) in deeply cracked TPB and CT. The  $T_{\text{stress}}$  values in Fig. 2.28 are normalized by the remote applied stresses.

A simple equation for the  $T_{\text{stress}}$  at limit load has been developed for the CT specimen by Wallin [2001]. He has combined the constraint solutions of Kfoury [1986] with the standard  $K_I$  and limit load solutions for the CT-specimen, resulting in the polynomial equation (2.79) giving  $T_{\text{stress}}/\sigma_Y$  for  $a/W \leq 0.7$ .

$$\frac{T_{\text{stress}}^{CT}}{\sigma_Y} = -2.15 + 15.07 \cdot \frac{a}{W} - 27.02 \cdot \left(\frac{a}{W}\right)^2 + 15.08 \cdot \left(\frac{a}{W}\right)^3 \quad (2.79)$$

The corresponding expression for the TPB specimens using the  $T_{\text{stress}}$  solutions of Sham [1991] is given in equation (2.80), which is valid for  $a/W \leq 0.9$ :

$$\frac{T_{\text{stress}}^{TPB}}{\sigma_Y} = -1.13 + 5.96 \cdot \frac{a}{W} - 12.68 \cdot \left(\frac{a}{W}\right)^2 + 18.31 \cdot \left(\frac{a}{W}\right)^3 - 15.7 \cdot \left(\frac{a}{W}\right)^4 + 5.6 \cdot \left(\frac{a}{W}\right)^5 \quad (2.80)$$



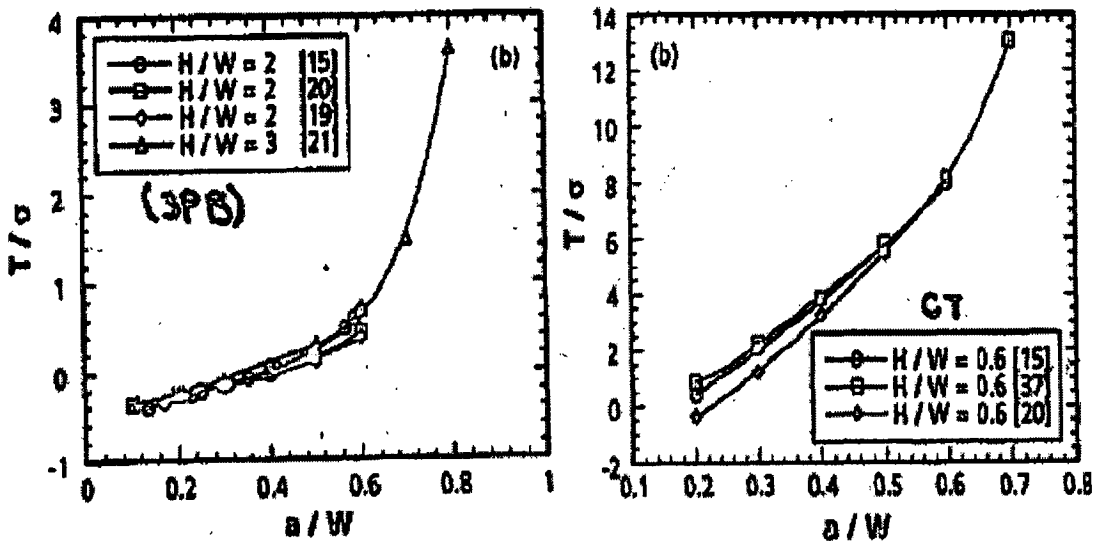


Fig. 2.28  $T_{\text{stress}}$  solutions for TPB and CT specimens [Sherry *et al*, 1995]

Hancock *et al* [1993] have used a fracture mechanics approach based on the  $J$ - $T$  theory to characterize the crack-tip conditions in different cracked geometries.

The  $J$ - $T$  approach is based on the elasticity theory and it may be extended to situations where plastic deformation is limited to a small region ahead of the crack tip.

O'Dowd and Shih [1991, 1992, 1994] have proposed the  $Q$  factor concept, in which the  $J$ -integral scales the crack tip singular field, and the  $Q$  factor is a measure of the stress triaxiality at the crack tip. O'Dowd and Shih have proposed that some combination of these two parameters gives a satisfactory fracture criterion under the constraint condition. Due to simplification, the  $J$ - $Q$  theory is applied extensively to the constraint analysis of stationary cracks [Dodds *et al*, 1993; Henry *et al*, 1996; Joyce and Link, 1997; Kikuchi, 1997; O'Dowd, 1995; Yan and Mai, 1997 and Yuan and Brocks, 1998].

Through full-field FEA analysis, O'Dowd and Shih [1991, 1992] have observed that the difference in stress field between the full-field solution  $\sigma_{ij}$  and the HRR field  $(\sigma_{ij})_{HRR}$  is approximately a uniform hydrostatic stress ahead of the crack tip. Accordingly, near-tip stress fields is given by

$$\sigma_{ij} = (\sigma_{ij})_{HRR} + Q\sigma_0\delta_{ij} \quad \text{for } r > J/\sigma_0 \quad |\theta| \leq \pi/2 \quad (2.81)$$

However, Sharma *et al* [1995] and Nikishkov *et al* [1995] have pointed out that the parameter  $Q$  in (2.81) is distance-dependent under large applied loads. To reduce the distance-dependence of  $Q$ , O'Dowd and Shih [1994] later have suggested choosing a small-scale yielding solution  $(\sigma_{ij})_{SSY}$  as the difference field and (2.81) is modified to become

$$\sigma_{ij} = (\sigma_{ij})_{SSY} + Q\sigma_0\delta_{ij} \quad \text{for } r > J/\sigma_0 \quad |\theta| \leq \pi/2 \quad (2.82)$$

O'Dowd [1995] has showed that the difference of two  $Q$  values:  $Q_{HRR}$  from equation (2.81) and  $Q_{SSY}$  from equation (2.82) is a constant  $a_0(n)$ , which is a function of the hardening exponent  $n$ , or

$$Q_{HRR} = Q_{SSY} + a_0(n) \quad (2.83)$$

For  $n = 10$ ,  $a_0 = -0.2$ , as seen in the Fig. 5 (b) of O'Dowd [1995]. Although the parameter  $Q$  is distance-dependent (that is, there is no unique  $Q$  near a crack tip), the  $J$ - $Q$  solution can be used as a 'first-order' engineering approximation. For example, Joyce and Link [1995, 1997] used  $Q$  as a constraint parameter to rank the constraint effect on different specimens at the fracture initiation. It should be noted that the parameter  $Q$  is also load-dependent and varies with change of loading, and thus cannot remain constant during the crack extension. As a result,  $Q$  cannot be a reasonable constraint parameter in the analysis of ductile crack growth.

However, this theory has a serious restriction in ductile crack growth because the constraint parameter  $Q$  depends on the magnitude of applied loads [Faleskog, 1995]. If there is a modified constraint parameter  $Q^*$  instead of  $Q$  in the  $J$ - $Q$  theory and  $Q^*$  is load independent, then for a crack growing through ductile fracture, one can extend the single parameter  $J$ -controlled crack growth to the two-parameter  $J$ - $Q^*$  controlled crack growth with  $J$  being the driving force and  $Q^*$  a constraint parameter. Moreover, it is anticipated that under a certain amount of crack extension the  $J$ - $Q^*$  approach can approximately characterize the effect of crack-tip constraints on ductile crack growth.

The  $J$ - $A_2$  approach developed by Yang *et al* [1993] and Chao *et al* [1994] is based on a rigorous asymptotic solution and also holds promise for a two-parameter fracture testing [Chao and Zhu, 1998]. Moreover,  $A_2$  is nearly independent of its position near the crack tip [Nikishkov *et al*, 1995] and has been successfully used to quantify the effect of constraints on fracture toughness for different geometry and loading configurations [Chao and Zhu, 1998; Zhu and Chao, 1999]. Accordingly, it is believed that the  $J$ - $A_2$  approach is a preferable methodology for the quantitative description of constraint effect. For a crack growing in a ductile material, similar to the concept of  $J$ -controlled crack growth, one can envision that within certain amount of crack extension the  $J$ - $A_2$  description can still approximately characterize the crack-tip fields with  $J$  being the driving force and  $A_2$  a parameter to quantify the constraint level. As demonstrated in Fig. 2.29, the amount of  $J$ - $A_2$  controlled crack growth should be much larger than that of the  $J$ -controlled crack growth since the zone dominated by  $J$ - $A_2$  at the crack tip is much larger than that controlled by  $J$  alone [Chao and Zhu, 1998].

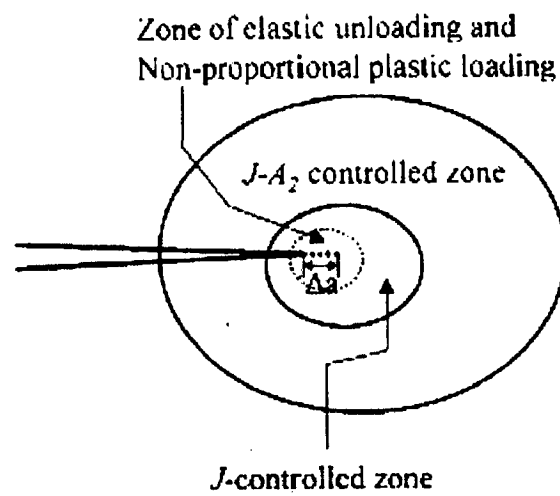


**Fig. 2.29  $J$  and  $J - A_2$  dominant zones and its relation to  $J$  or  $J - A_2$  controlled crack growth [Chao and Zhu, 2000].**

## 2.4 STRETCHED ZONE WIDTH

The blunting line drawn by the procedure recommended by ASTM for the determination of  $J_{IC}$  aims to simulate the  $\Delta a$  which results due to stretching of the fatigue crack (introduced by pre-fatiguing) under tensile load, before the initiation of crack. However, the procedure involves arbitrary elements like an offset of 0.2 mm, which does not have any apparent justification. Therefore, many investigators have suggested direct measurement of the stretched zone width which is clearly recognized under microscope between the ductile fracture region and the fatigue fracture region resulting during pre-cracking by fatigue [Spitzig, 1968]. The stretched zone possesses a number of unique properties, the main of which are as follows:

- since  $SZW$  remains constant after crack initiation, it provides a convenient marker for identifying the crack initiation point, even in a material component at any time after completion of the fracture process;
- width of any stretched zone is available for measurement, as a function of its position along the crack front (this is especially required for the investigation of heterogeneous materials, welding seams, etc.);
- estimation of the material fracture toughness in a material is possible on the basis of direct measurement of stretched zone width

The main purpose of fracture testing in a laboratory is to transfer the test results to full-scale service structures. If fracture toughness value obtained from  $J-R$  curves does not represent a valid material characteristic but is specimen dependent, then the testing on laboratory specimen is of no use. Therefore, the transferability of fracture toughness value from laboratory specimens to component level is an important issue to be dealt satisfactorily before undertaking design of components on this basis.

In both the methods prescribed by ASTM and ESIS,  $J_{IC}$  is determined as an intercept of the blunting line at an offset of 0.2 mm with the  $J$ - $R$  curve. Clearly the accuracy of determining  $J_{IC}$  will depend on the accuracy with which the offset line represents the process of stretching or blunting. The problem of accurate choice of the slope of blunting line is accentuated in the case of ductile and tough materials for which the crack growth due to the physical tearing of the material may be virtually indistinguishable from the extensive crack tip blunting. Kobayashi *et al* [1977] and Landes and Begley [1974] have proposed a procedure for the determination of  $J_{IC}$  in terms of stretched zone width, which is especially suited for the highly ductile materials. They considered stretched zone width to be the most accurate value close to the onset of crack initiation for the measurement of initiation fracture toughness. When examined at relatively high image magnifications, the crack stretch zone exhibits a typical featureless appearance easily distinguishable from the prior pre-crack surface and the subsequent main fracture by ductile tearing or eventual brittle cleavage. Being a precise indication of the extent of the plastic blunting process, the stretch zone width ( $SZW$ ) is now recognized as an alternative method for determining the fracture toughness of the material. Indeed, it has been very well correlated with the critical values of energetic and geometric criteria,  $J_{IC}$  and  $CTOD_c$  respectively, involved in fracture mechanics.

Two groups of research workers have used  $SZW$  differently in their studies on fracture mechanics. A number of research workers have correlated stretched zone width ( $SZW$ ) to either  $K_{IC}$  in linear elastic fracture mechanics or  $J_{IC}$  in elastic plastic fracture mechanics. Another group of research workers use  $SZW$  merely to estimate the initiation point of fracture accurately.

### 2.4.1 Stretched Zone width Measurement

The stretched zone detected for the first time by Spitzig [1968], is considered to be an important parameter resulting from the behavior of the fatigue pre-crack tip of the specimen subjected to increasing tensile load leading to fracture. A stretched zone is formed at the initial crack tip due to the stretching of the tip under tension before fracture occurs. In ductile materials, the initial fine crack resulting from fatigue gradually blunts due to application of load giving rise to a stretched zone. The stretched zone grows in size with the load increment and at the same time, voids are nucleated ahead of the crack tip and grow. When voids coalesce giving rise to a crack on the stretched surface, the stretched zone ceases to develop further, and extension (generally stable) of the crack takes over. Stretching through fully developed *SZW* makes  $J$  to attain the critical value of  $J_{IC}$  for crack propagation. The observations have shown that stretched zone on the fracture surfaces comprises of two distinct parts (Fig. 2.30) [Smith *et al*, 1995]. The first part is a deformed zone which is nearly parallel to the original fatigue crack surface. This region is formed by deformation of the fatigue crack surface behind the crack tip, as reported by the investigators [Cao and Lu, 1984; Luo and Embury, 1988]. The second part forms inclined at an average angle  $\theta$  to the fatigue crack surface. Studies utilizing scanning electron microscopy [Kobayashi *et al*, 1979], stereo fractography [Broek, 1974] and sectioning techniques [Kobayashi *et al*, 1977] indicate that  $\theta$  is typically within 35-45 degrees. Smith *et al* [1995] has determined  $\theta$  to be 35 degrees by measuring the inclined stretch zone at various tilt angles. Sivaprasad *et al* [2002] have considered stretched zone in terms of its overall horizontal component called the stretched zone width (*SZW*) and the overall vertical component called the stretched zone depth (*SZD*) as shown in Fig. 2.31 [Sivaprasad *et al*, 2002]. Both the stretched zone width and stretched zone depth are claimed to have a good correlation with ductile fracture toughness of a material.

Most of the research workers engaged in *SZW* measurement favor its use for estimating ductile fracture-toughness. However, some others argue that *SZD* measurements are more appropriate [Sreenivasan *et al*, 1996; Cao and Lu, 1984; Broek, 1974] for obtaining ductile fracture toughness through a mathematical correlation. But *SZD* measurements are difficult due to the problem identification while observing the specimen end-on.

#### **2.4.2 Determination of *SZW* and its relationship with $J_{IC}$**

The stretched zone width is determined by post test examination of fractured specimens under scanning electron microscope (SEM). It appears as a distinct region under SEM and could be measured easily using a tilting stage. Local inhomogeneity, fractured large particles ahead of a crack tip and the irregularity of crack front may bring about an irregularly shaped stretched zone. This implies that the *SZW* is not uniform across the crack front and also, it will vary at the side ends due to deviation from plane strain condition. It has also been reported that large grain size and the presence of second phase particles produce large errors in the evaluation of the *SZW* [Bassim *et al*, 1992]. Therefore, it is not only desirable to have experience in interpreting scanning electron micrographs but also a suitable statistical measure for stretched zone width [Schwalbe *et al*, 1993; ESIS 1992a; Halim *et al*, 1988].

Halim *et al* [1988] have shown that it is sufficient to measure only one specimen half to obtain the value of *SZW*. For elastic-plastic specimens, the width of the stretched zone varies across the crack front. It is maximum near the centre and minimum near the edges of the test specimen. On specimens with side grooves, the stretched zone width across the thickness is constant [Halim *et al*, 1988]. Also, as the specimen size shrinks and plastic conditions dominate, the width of the stretched zone becomes more uniform across the crack front [Bassim *et al*, 1992]. Similarly, Schwalbe *et al* [1993] have demonstrated through the analysis of an experimental round robin results that the difference in the measurements of two specimen halves is in all cases smaller than the width of the scatter band of all specimens.



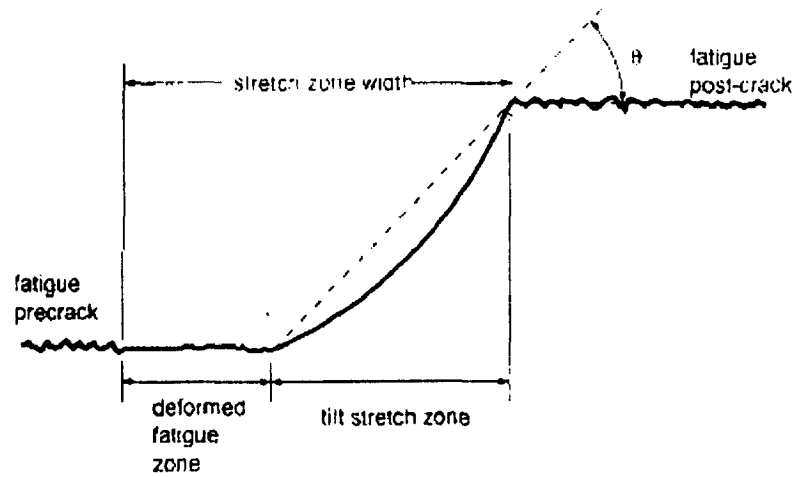


Fig. 2.30 Illustration of stretched zone geometry [Smith *et al*, 1995].

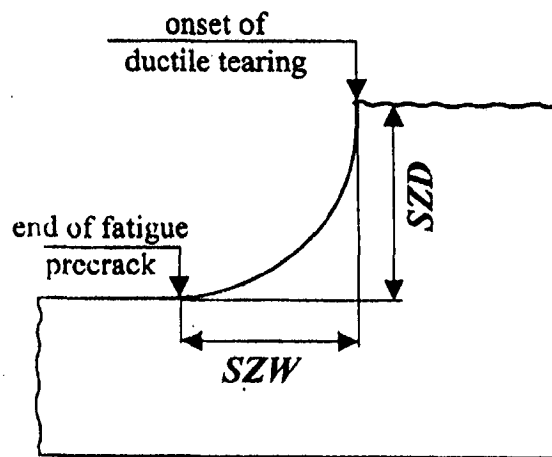


Fig. 2.31 Schematic of the crack profile depicting the stretched zone components. [Sivaprasad *et al*, 2002]

From this it is concluded that the examination of one specimen half is sufficient. Schwalbe *et al* [1993] have also recommended that care should be taken during defining the beginning next to the fatigue fracture region and the end of the stretch zone. When fixing the transition line between the stretch zone and the tearing surface, dimple, broken second phase particles and similar feature should be carefully identified and left aside, to be sure that only stretching or blunting contributes to the measurement of stretched zone width.

Pandey and Banerjee [1973] have examined the fractographic features in Fe-Mn base alloys. For the measurement of *SZW*, the replicas are prepared from the fractured surface, which include transition region between the fatigue and fast fracture. An area of nearly 2 mm has been scanned very carefully. About 15-20 readings have been taken from the representative regions on each fractograph to allow a reasonable estimate of stretched zone width. A maximum variation of  $\pm 40$  percent from the average width has been observed.

Landes and Begley [1972] have shown that the apparent crack extension  $(\Delta a)_{SZ}$  associated with stretched zone can be approximated by assuming that the stretched zone size is equal to half the crack opening displacement (COD).

This can be expressed as

$$(\Delta a)_{SZ} \approx \frac{1}{2}(COD) \quad (2.84)$$

The crack opening displacement is then related to *J* by the following relationship

$$J = m\sigma_Y(COD) \quad (2.85)$$

where  $\sigma_Y$  is the yield strength of the material and *m* is the constraint factor. The flow stress  $\sigma_f$  customarily is substituted for the yield strength  $\sigma_Y$  in this equation to take into account

the strain hardening effect [Knott, 1980]. Combining these equations one gets the blunting line equation given by

$$J = 2m\sigma_y(\Delta a)_{SZ} \quad (2.86)$$

Nguyen-Duy and Bayard [1981] have derived an equation relating to stretch zone width,  $SZW$ , to the crack-opening displacement ( $COD$ ),

If  $AB$  in Fig. 2.32 is the stretched zone width, it can be shown that this width is related to critical  $COD$  as

$$SZW = \frac{d}{\cos(\theta - \delta)} \frac{1}{G} \quad (2.87)$$

where,

$$(COD)_c = \frac{2d}{\cos \delta + \sin \delta} \frac{1}{G} \quad (2.88)$$

where  $d$  is the measured length of the stretched zone on the micrographs,  $\delta$  is the incident angle of the beam (the tilt angle),  $\theta = 45^\circ$  and  $G$  is the magnification. Under plane strain conditions, the critical value of the  $J$  integral,  $J_{Ic}$ , is related to  $(COD)_c$  by

$$J_{Ic} = m\sigma_f(COD)_c \quad (2.89)$$

where  $\sigma_f$  is the flow stress (the average of the yield stress and the ultimate tensile stress) and  $m$  a constraint factor due to plane strain loading. If equation (2.88) is substituted into equation (2.89), with  $m$  equal to 2, equation (2.89) becomes

$$J_{Ic} = \frac{4\sigma_f d}{\cos \delta + \sin \delta} \frac{1}{G} \quad (2.90)$$

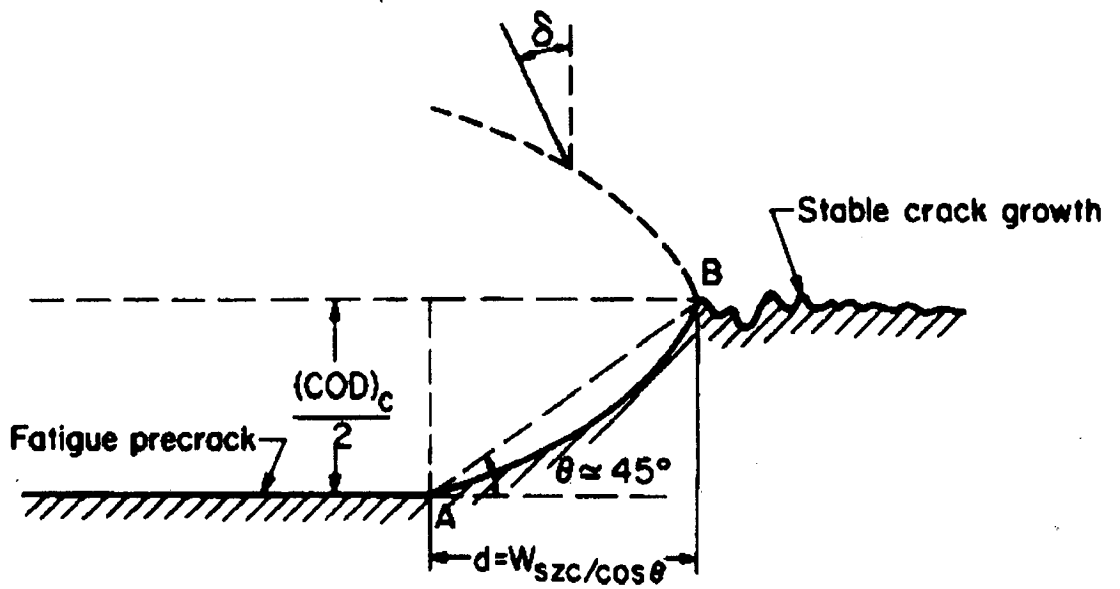


Fig. 2.32 Stretched zone of a broken specimen half showing relationship with COD.

Amouzouvi and Bassim [1982] have measured the stretched zone width with the scanning electron microscope at a tilt angle of  $45^0$  and a magnification of about 250-380. The stretched zone width has been measured at different points along the crack front and the results are averaged to calculate the value of  $J_{IC}$  using equation (2.90).

Putatunda [1986] has measured the stretch zone width by SEM on fracture surface of AISI 4340 steels after cleaning it in acetone. The stretched zone has been measured at 20-25 points on each half of the specimens. Statistical analysis of the stretched zone width measurement has shown that a minimum of 25 readings is necessary for measurement of  $SZW$  with a 95% confidence limit [Putatunda and Rigsbee, 1985]. The  $SZW$  in each specimen is determined by holding the specimen at  $45^0$  to the incident beam. The measurements are carried out in the mid thickness portion of the crack front. The measured  $SZW$  value has been multiplied by a factor of  $\sec 45^0$  to convert to its true value. From the average value of  $SZW$ , the fracture toughness  $J_{IC}$  has been measured by using Landes and Begley's [1974] approximation.

A method [ESIS 1992a] has been proposed to measure the fracture toughness using  $SZW$ . In this method, local stretched zone width,  $SZW$ , is measured at 9 positions using calibrated photographs taken in SEM (Fig. 2.33).

At each position the SEM magnification has been adjusted so that both the start and end of the stretch zone are visible at the same time. At least 5 measurements are required at each position giving the local stretch zone width

$$\Delta a_{SZW_L} = \frac{1}{k} \sum_{i=1}^k \Delta a_{SZW_L,i} \quad \text{for } k \geq 5 \quad (2.91)$$

The stretched zone width of the specimen is determined by averaging the local measurements over nine positions as,

$$\Delta a_{SZW} = \frac{1}{9} \sum_{i=1}^9 \Delta a_{SZW_L,i} \quad (2.92)$$

a line parallel to the  $J$ -axis is constructed through the critical stretch zone width on  $J$ - $R$  curve. The intercept of the  $J$ - $R$  curve with the parallel line defines  $J_{IC}$ .

The JSME [Japanes Society of Mechanical Engineers] method for the determination  $J_{IC}$ , depends mainly on the measurement of  $SZW$ . The *JSME* procedure includes loading the specimens to selected different displacement levels as in multi-specimen procedure prescribed by the ASTM and ESIS. The difference, however, is that two or more specimens are loaded to displacement levels that are lower than those at the onset of ductile tearing, where only stretched zone has formed. The other specimens, three or more, are loaded to crack propagation region similar to those in the ASTM and ESIS. Fatigue cycling is again applied at the end of tensile loading to fracture the specimen and mark the extent of stretching or crack extension clearly. The  $SZW$ s are measured before it is fully developed and the corresponding  $J$ -integral values are calculated as above. The  $J$ - $SZW$  data of the group of specimens unloaded before the onset of ductile tearing are used to establish the blunting line, which is the best-fit through the origin. On the other hand, the fully developed stretched zone width ( $SZW$ ) is determined as the average of  $SZW$  of the other group of specimens where crack propagation has taken place. The intersection of the blunting line and the line indicating development of  $SZW$  up to its fully developed value, defines the value of  $J_{IC}$  of the material.

Tarafder *et al* [2003] in their investigation on TPB specimens of 25 mm thickness of SA333 Gr. 6 steel has shown that the initiation fracture toughness measured by the  $SZW$  method gives a conservative value of initiation fracture toughness compared to that measured by blunting line without offset, drawn following ASTM procedure (Fig. 2.34).

From the crack resistance curve,  $J$ - $R$  curve, initiation fracture toughness can be derived by different procedures, ASTM E-813, ESIS and  $SZW$  method. Roos *et al* [2000] have reported the initiation fracture toughness as determined by the various procedures as shown in Fig. 2.35.

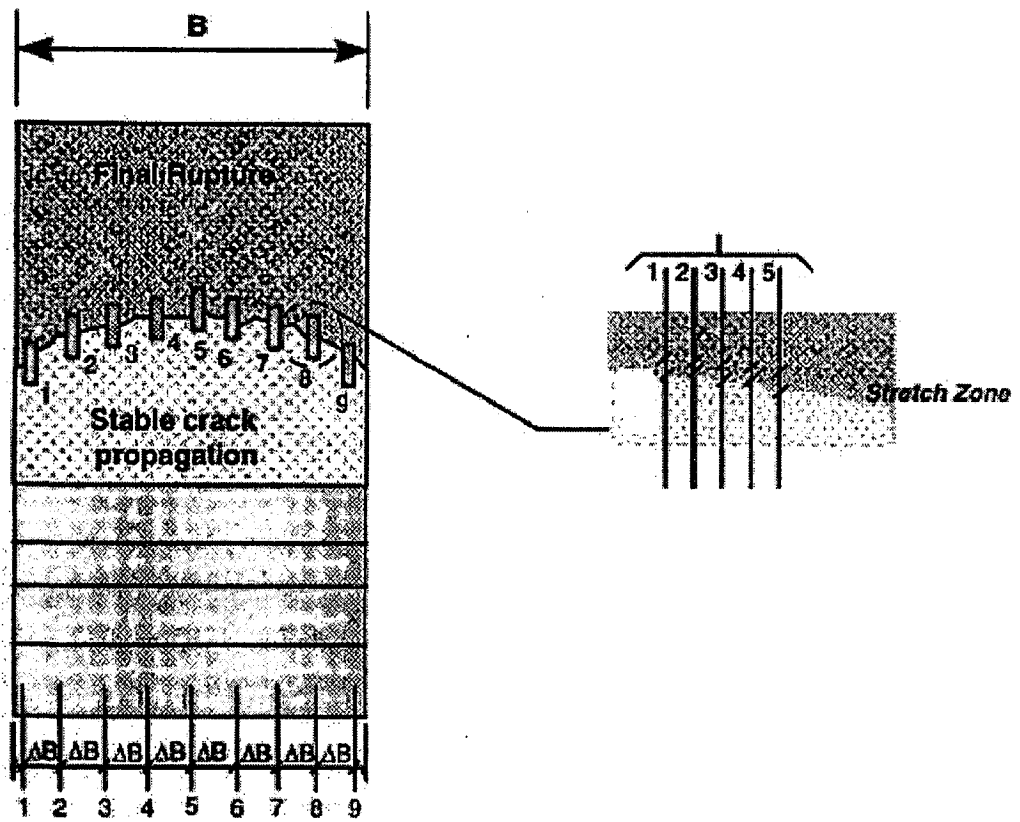


Fig. 2.33 Nine Point Stretch zone width measurement procedure.

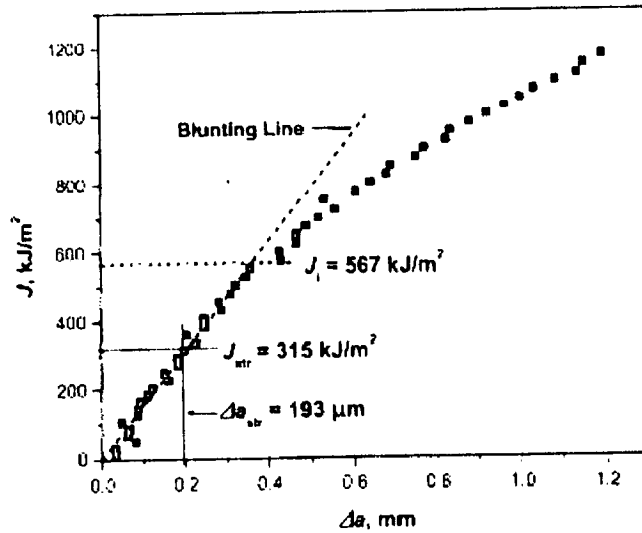


Fig. 2.34 Comparison of initiation fracture toughness obtained from stretch zone measurements, with initiation fracture toughness, obtained graphically from the blunting line, for SENB specimen .W = 50 mm, B = 25mm of SA333 Gr. Steel [Tarafer *et al* 2003]

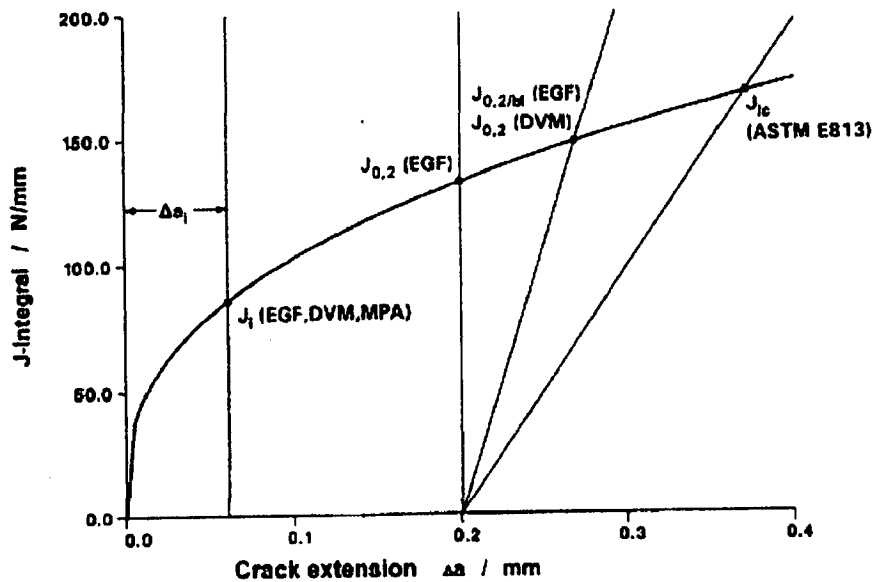


Fig. 2.35 Comparison of initiation fracture toughness values according to different test standards [Roos *et al* 2000].



Many experimental studies [Mills, 1981; Yin *et al*, 1983; Kolednik and Stuwe, 1986] have shown that the offset line as prescribed by ASTM, overestimates the crack extension due to the blunting process, especially for materials with low strength and high strain hardening. Yin *et al* [1983] have investigated on three point bend specimens of carbon steel (St52-3) to determine the slope of the blunting line and their results demonstrate that the slope of the blunting line obtained by the *SZW* method is steeper than the blunting line predicted by the ASTM method. This results in lower values for both  $J_{IC}$  and  $\Delta a_c$  when determined by the *SZW* method, as compared with those obtained by the ASTM method.

Several experimental relationships between the fracture toughness  $J_{IC}$  and stretched zone width have been published, taking into account the influence of Young's modulus. Kobayashi *et al* [1977] have conceived that stretched zone develops as the loading progresses and its width reaches *SZW* when fracture initiates. Later, for a wide range of metallic materials including steels, copper, aluminium and titanium alloys, having high as well as low strengths, blunting behaviours have been examined in terms of the development of the stretched zone with increasing  $J$  and it is observed that the blunting depends not on  $\sigma_{ys}$  but on Young's modulus ( $E$ ). The thickness of the stretched zone,  $SZT$ , increases with increasing  $J$  as given by the following expression [Kobayashi *et al*, 1979] before attaining the *SZW*.

$$SZT = 89 \frac{J}{E} \quad (2.93)$$

The coefficient 89 is an average value lying in the interval 54-143. The results show that the change of  $E$  from 70.6 to 206 has little influence on the relation between  $SZT$  and  $J/E$  and there is no influence of the test temperature on this relationship. Kobayashi *et al* [1977] have found that the relation between  $SZT$  and  $J$  for two geometries, compact tension (1/5 CT, 1/2 CT, 1 CT) and TPB specimens, at room temperature is identical. A  $SZT$  versus  $J$  curve is independent of test temperature at low temperature range as *SZW* decreases with test temperature hence,  $J_{IC}$  values corresponding of these *SZW* decrease with decreasing temperature. Cao and Lu [1984] have

reported that the  $SZW$  versus  $J/E$  relation can not be represented by unique straight line over all the range of  $J/E$ . The linear regression analysis of the experimental data revealed that  $SZW$  versus  $J/E$  has been represented by the following relationships:

$$\begin{aligned}
 J_{Ic} / E > 0.7 \text{ mm} \quad \text{then} \quad SZW(\text{mm}) &= 91 \frac{J_{Ic}}{E} - 0.0043 \\
 J_{Ic} / E < 0.7 \text{ mm} \quad \text{then} \quad SZW(\text{mm}) &= 47 \frac{J_{Ic}}{E} - 0.00056
 \end{aligned}
 \tag{2.94}$$

Several researchers have found it difficult to define the beginning and end of the stretched zone; therefore they have preferred to measure the height of the stretch zone ( $H_{SZ}$ ). Cao and Lu [1984] on broken three point bending samples made of steels, copper, aluminium and titanium alloys have obtained the following relationship:

$$H_{SZ} = J_{Ic} / 6\sigma_0 \tag{2.95}$$

Krassowsky *et al* [1981] on two different steels have found:

$$H_{SZ} = (0.2, \dots, 1.15) J_{Ic} / (2E\sigma_Y)$$

Pluvillage and Lanvin [1993] have studied the stretched zone width and height by using five different methods (Transmission Electron Microscopy, Retrodiffused Electron Microscopy, Nickel Plating, Roughness Measurement, Ondulation Method) and found the following relationships between stretched zone width and height and the initiation fracture toughness parameter  $J_{IC}$ :

$$SZW = 1.75 H_{SZ}$$

$$J_{Ic} = 1.91 SZW \sigma_Y \quad \text{and} \quad J_{Ic} = 3.2 H_{SZ} \sigma_Y$$

these relationships are different from earlier relationships found in literature but the coefficients are of the same order of magnitude.

## 2.5 INFLUENCE OF DIFFERENT PARAMETERS ON SZW

### 2.5.1 Effect of thickness and width of specimens on SZW

The thickness effect on stretched zone size has been studied by the various workers [Gilmore *et al*, 1983; Kobayashi *et al*, 1977, 1979; Ohji *et al*, 1978]. Gilmore *et al* [1983] have reported a larger value of stretched zone width in 12.7 mm specimen prepared from martensitic stainless steel HT80 than for 2.5 mm specimens of the same material. In contrast, Ohji *et al* [1978] and Kobayashi *et al* [1977] found the stretched zone width to be virtually independent of specimen thickness. Kobayashi *et al* [1977] have done the fracto-graphic analysis at the mid thickness of the specimens where plain strain conditions exist and stable crack growth occurs initially, using a two stage plastic carbon replica with chromium shadowing. The results obtained by Kobayashi *et al* [1977] have shown in Table-2.1. Putatunda and Rigsbee [1985] has measured stretched zone width in the mid thickness region at 20-25 points on each half of the specimens. The size of the stretched zone in each specimen is determined by holding the specimen at  $45^{\circ}$  to the incident beam. The measurement is carried out in the mid thickness portion of the crack front with confidence. It is reported in this investigation that the specimen thickness has little influence on the stretched zone in AISI-4340 steel, which is in agreement with the results by Ohji *et al* [1978] and Kobayashi *et al* [1977]. Putatunda and Rigsbee [1985] have measured the stretched zone width in specimens with different thicknesses  $B$  of about 12, 6 and 4 mm. All these specimens have a constant width of about 100 mm. Figure 2.36 shows plots of stretch zone size versus  $J$  and critical stretch zone size versus  $J$  respectively for three specimen thickness and three specimen widths. It is evident from the Fig. 2.36 that the specimen thickness has no apparent influence on the stretch zone size.

Fig. 2.36 also shows the effect of the specimen width on the stretch zone size. All these specimens had a constant thickness  $B$  of about 12 mm. The stretch zone sizes as measured on these specimens are comparable with the measured values on specimens with different thickness. It is clear from Fig. 2.36 that specimen width also has little or virtually no effect on the stretch zone size when loaded to comparative  $J$  values. However, the scatter in the measured stretch zone values is somewhat lower than was found for the specimen with varying thicknesses.

A study [Mao, 1991] of higher magnification SEM fractographs indicates that the crack extension region can be primarily divided into two fracture modes, the fracture region is mixed modes of (1) anti-plane shear mode ( $B_s$ ) near the specimen surface and (2) the flat fracture region by simple open mode ( $B_f$ ) in the centre region (mid-thickness). Thus fracture in small specimens was dominated by mixed modes I and III. Fracture toughness of  $J_{IC}$  is based on mode I. A thin specimen has a thickness effect on  $J_{IC}$  because of fracture mode III. Therefore, the more fracture mode III occurs, the more the thickness effect on fracture toughness.

## 2.5.2 Effect of $a/W$ ratio on SZW

Zheng *et al* [2000b] have tested the fracture toughness of St 690 steel by changing the crack length ( $a/W$ ) of the TPB specimens with the size of 13X26 mm and the ratio of loading span ( $S$ ) to the width ( $W$ ) of specimen is 4. Their results are shown in Table 2.2 and this study shows that the stretched zone size measured is indeed an invariable, which is independent on the relative precrack size.

Similar observations are found in the investigation of Hyatt and Matthews [1994]. Hyatt and Matthews [1994] have measured the stretched zone width by nine point method in which the averaging scheme used is one half the sum of the stretch zone on each edge of the specimen plus sum of the other seven positions, all divided by eight.  $SZW$  are measured only at predetermined points, not at nearby points where the stretch zones are well formed and attractive. In this investigation change in precrack depth do not produce measurable changes in  $SZW$  as shown in Fig. 2.37.

Table -2.1 Variation of  $SZW$  with specimen thickness [Kobayashi *et al*, 1977].

Specimen	B, mm	$SZW$ , $\mu\text{m}$
1CT	25.5	6.06
1/2 CT	12.5	6.31
1/5 CT	5.5	5.91

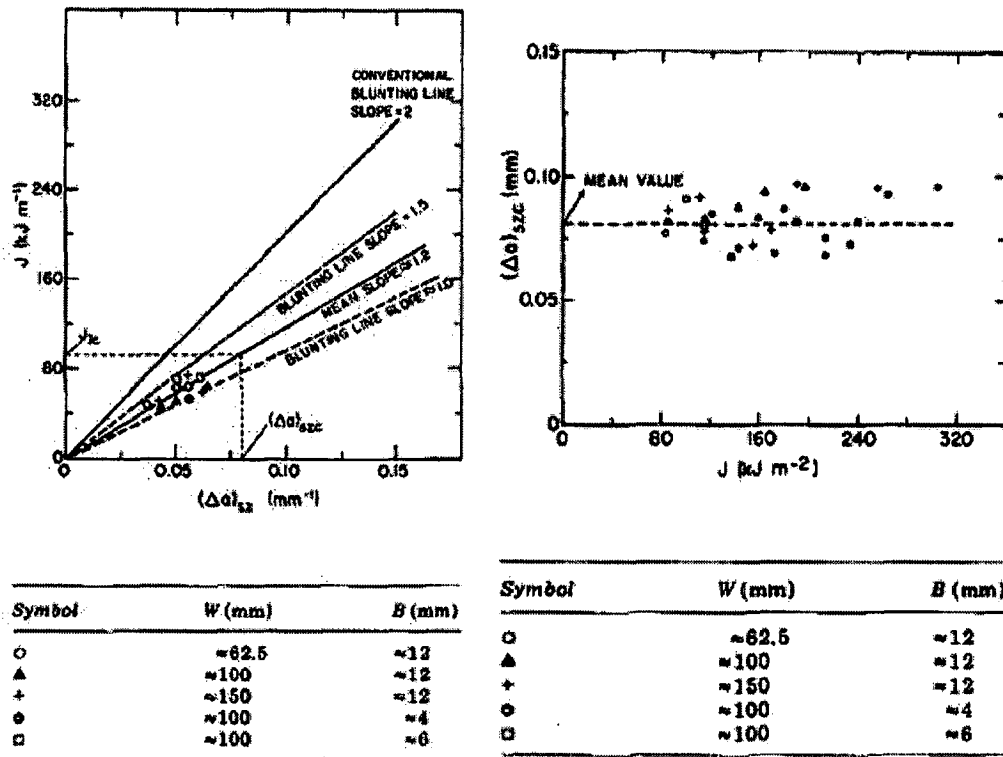
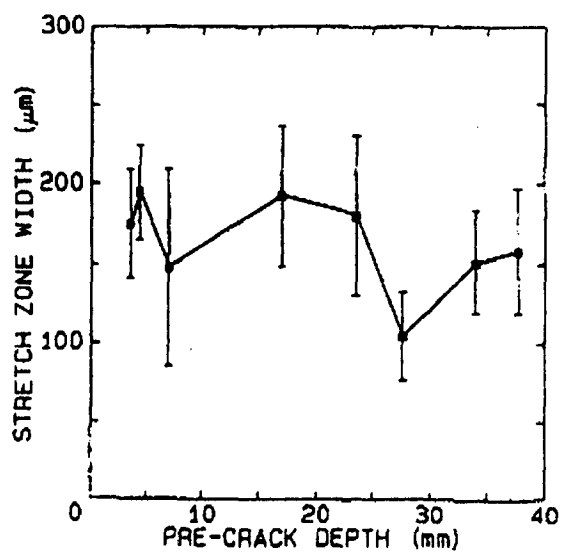


Fig. 2.36 Effect of Specimen size on  $SZW$  [Putatunda and Rigsbee, 1985]

**Table 2.2** Stretched Zone size for StE 690. [Zheng *et al*, 2000b]

a/W	0.5	0.4	0.3	0.2	0.1	Average
SZW( $\mu\text{m}$ )	51	56	57	56	53	54.6



**Fig. 2.37** Variation of Stretch zone width with pre-crack depth [Hyatt and Matthews, 1994].

### 2.5.3 Effect of notch root radius on SZW

For six commercial metals, with micrographic analysis, Srinivas *et al* [1992, 1994] also shows that the apparent  $J_{IC}$  is a linear function of notch root radius, but it is interesting to note from his results that that if notch root radius is subtracted from the measured critical stretch zone width corresponding to that notch root, the resulting value is independent of the notch root radius for all materials.

The stretched zone width is related to the critical crack tip opening displacement (CTOD) by the following expression [Robinson and Tetelman, 1976]

$$2SZW_c = CTOD_c \quad (2.96)$$

the above statement is valid for the specimens which are fatigue cracked having initial notch root radius zero. In case of notched specimens, without fatigue precracked, the measured  $SZW$  can be related to the CTOD as [Srinivas *et al*, 1994]

$$2(SZW_c - \rho) = CTOD_c \quad (2.97)$$

where,  $\rho$  is notch root radius.

The correct index of fracture toughness of material, therefore is the parameter  $(SZW_c^{measured} - \rho)$  or  $SZW_c^{corrected}$ . Equation can be written as

$$SZW_c^{measured} = \rho + CTOD/2 \quad (2.98)$$

Therefore the corrected stretched zone width in specimens with a finite notch root radius,  $\rho$ , can be converted to the critical stretched zone width in the fatigue precracked specimen,  $SZW_c^{corrected}$  using the following relation:

$$SZW_c^{corrected} = (SZW_c^{measured} - \rho) \quad (2.99)$$

The usefulness of this technique is that it eliminates the requirement of fatigue precracking and provides a way for measuring ductile initiation fracture toughness  $J_{IC}$  using a single specimen for high ductility materials exhibiting stretched zone formation during fracture toughness testing.

## 2.5.4 Effect of loading rate on SZW

Hyatt and Matthews [1994] have studied effect of loading rate on stretched zone width on TPB specimens of ASTM A710, Grade A steel. At a narrow range of loading velocities (1.2-4.9 m/s) no significant change in *SZW* is observed. However with the addition of specimens deformed at lower rates, a trend can barely be discerned as shown in Fig. 2.38. At low rate specimen stretch zone width is  $224 \pm 17$  and for high rate specimens the value of stretch zone is  $173 \pm 25$ . Thus, a measurable drop in stretch zone width has been observed with loading rate. Bayoumi *et al* [1984] and Bassim *et al* [1987] in their study on the fracture behavior of annealed AISI 1045 steel, subject to tensile loading rates ranging from quasi-static to dynamic, using compact tension specimens having three different *a/W* ratio, have reported experimental results based on stretch zone measurements which indicate a significant decrease in fracture toughness for AISI 1045 steel at high loading rates as well as a slight dependence of the stretch zone with *a/W*.

## 2.5.5 Effect of fatigue precracking stress

Smith *et al* [1995] studied the effect of the fatigue precracking stress intensity range ( $\Delta K$ ) on the formation of stretch zone in AISI4340 steel. In their investigation compact tension specimens were fatigue precracked at 62%, 100% and 147% of the  $\Delta K$  limit prescribed by ASTM E813-93, then loaded to levels of  $J \leq J_{IC}$ . It is found that the precracking reduces the *SZW* formed at a given value of *J* in proportion to the maximum applied *J* during precracking. The magnitude of this reduction,  $SZW_0$ , is well-approximated by  $SZW_0 = J_0 / 2m\sigma_f$  adding  $SZW_0$  to the measured *SZW* corrects for this effect.

## 2.5.6 Effect of Temperature on Fracture Toughness

Marengo and Ipina [1996] has studied the effect of high temperature on fracture toughness on 304 L steel specimens. They measured the  $SZW_c$  as stated by ESIS P2-92 [1992b]. Their results are shown in Fig. 2.39. The  $SZW_c$  values increase with an increase in temperature and reach a maximum at about 200°C. For higher temperatures, the  $SZW_c$  decreases continuously. Pluvinage and Lanvin [1993] have found that the stretch zone width increases linearly with the temperature in the case of heat treated XC35 steel.



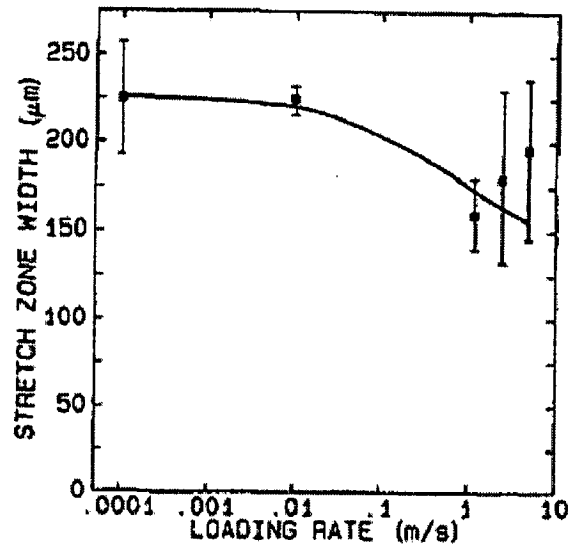


Fig. 2.38 Variation of stretch zone width with loading rate [Hyatt and Matthews, 1994].

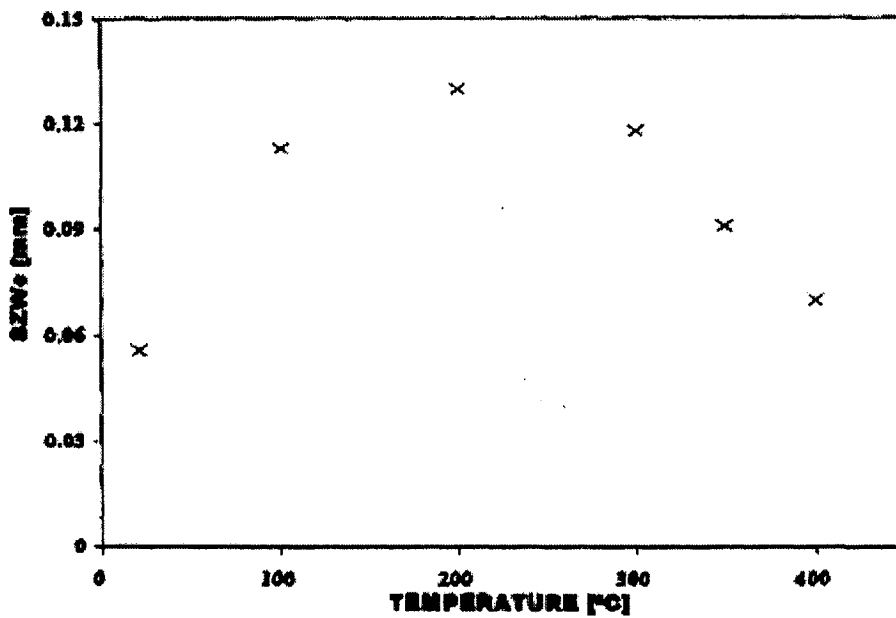


Fig. 2.39 SZW vs. test temperature of the 304L steel [Marengo and Ipina, 1996]

## 2.5.7 Effect of Rolling Direction

Rolling direction is also an important parameter. Pluinage and Lanvin [1993] have found during *SZW* measurement of specimens in two rolling direction that the stretched zone is a little smaller for the transverse direction as shown in Fig. 2.40.

## 2.5.8 Effect of Grain Size

Srinivas *et al* [1987] have studied the influence of polycrystal grain size on fracture toughness on Armco iron over a grain size range 40 to 1050  $\mu\text{m}$ . They found that the blunting line suggested in ASTM E-813 standard test procedure for  $J_{IC}$  determination is not applicable for Armco iron, therefore, they established a blunting line experimentally through stretch zone width measurements as the *SZW* across the thickness is found to be quite uniform. The fracture toughness of Armco iron increases with decreasing grain size and the variation can be expressed by the relationship similar to that for Hall-Petch for strength as

$$J_{Ic} = 52 + 1.28d^{-1/2} \quad (2.100)$$

where  $J_{IC}$  is in  $\text{kJ/m}^2$  and  $d$  in meters. The variation of ductile fracture toughness with grain size can be understood in terms of its plastic zone size at the crack tip. At finer grain sizes plastic zone size encompasses more number of grains which implies more energy input in order to activate slip in grains oriented differently. Pluinage and Lanvin [1993] have inflicted different thermal treatment on XC35 which cause different grain sizes from 20 to 125  $\mu\text{m}$ . They have found a linear relationship in stretch zone width versus the square root of the average grain size. This relationship agrees to the relationship obtained by Srinivas *et al* [1987]. The stretch zone width is a linear function of the fracture toughness  $J_{IC}$  and the fracture toughness decreases with increasing yield stress is a well known experimental fact. For this reason any parameters influencing the yield stress have an influence on stretch zone width. The relationship between the stretch zone with square root of grain size is similar to the famous Hall-Petch relationship between the yield stress and square root of the grain diameter.

## 2.6 PROBLEM FORMULATION

The design of engineering structures and components made of materials is based on the behavior of dormant cracks of size which depends on the detection limit of quality inspection tools. The failure of the structure or the component depends on the dormant crack becoming active to start propagating even in a ductile material. The objective of the design is to keep the stress at the crack tip within such limit that the crack does not start propagating. The stress field at the crack tip is characterized by a single parameter  $J$  and the crack propagation starts when  $J$  takes the value of  $J_{IC}$ , the initiation fracture toughness. Earlier, it has been thought that  $J_{IC}$  is a material property and the ease of propagation is determined by the  $J$  vs. crack extension curve, called  $J$ - $R$  curve, which has also been considered a material characteristics. With passage of time, it has been observed that both  $J_{IC}$  and  $J$ - $R$  curve depend on the geometrical characteristics of the test specimen like its thickness and pre-crack depth. The stress distribution at the crack-tip is not uniquely determined by the single parameter  $J$  but requires at least another parameter. Thus, for a safe design, it is required to determine the lower limit of  $J_{IC}$  and  $J$ - $R$  curve in respect of the geometrical variables of the test specimen.

The tests for fracture toughness involves various types of specimen and loading conditions. The most popular ones involve CT and TPB specimens under tensile and bending type of loading. The specimens of recommended dimensions as to ensure plane strain condition under each type of loading, are machined with notch, from where fatigue crack is generated upto a given pre-crack depth. The specimen with pre-crack is then loaded under tensile or three point bending load. The first step during loading involves a shape change of the fine fatigue crack to a blunted one by a process of stretching and creation of a plastic zone around the crack-tip to exhaust its ductility. Thereafter, the second step, which involves the onset of crack propagation, starts. The determination of initiation fracture toughness,  $J_{IC}$ , involves the value of  $J$  at the transition between step 1 and step 2. Determination of this

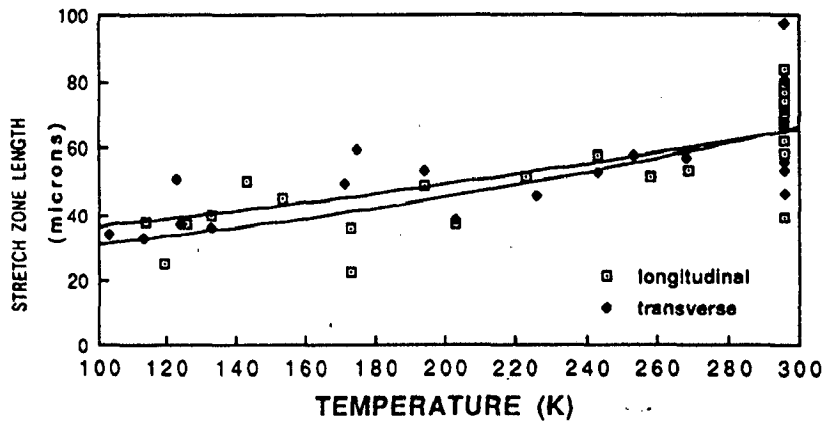


**Fig. 2.40** Influence of Rolling Direction on Stretch zone Width, XC35 steel [Pluinage and Lanvin, 1993]

transition in ASTM recommended procedure depends on the assumed blunting behavior given by a linear blunting line equation from the origin. The intersection of blunting line with the  $J$ - $R$  curve extrapolated from larger crack extension indicates the onset of crack propagation. Since the onset of crack propagation does not take place at the same  $J$  across the entire thickness, an offset blunting line is drawn with 0.2 mm offset and its intersection with the extrapolated  $J$ - $R$  curve is taken as initiation fracture toughness,  $J_{IC}$ , to ensure the onset of crack propagation almost everywhere across the crack front. The assumed blunting behavior in ASTM procedure does not always represent the actual blunting behavior particularly in highly ductile material. This problem has been realized and ASTM, in its subsequent recommendation, has asked for determination of the slope of blunting line depending on its strain hardening characteristics. On the other hand, ESIS has recommended the slope of the blunting line based on strain hardening coefficient of the material as well as well. But JSME takes an altogether different approach and recommends determination of initiation fracture toughness based on the development of stretched zone width with loading.

The present study aims to evolve a unified procedure by introducing a blunting line equation based on the mean stretched zone width in the context of the fracture behavior of low carbon steels like SA333 Gr. 6 steel and SAILMA steel. If the blunting line based on strain hardening coefficient shows adequate consistency then, the behavior of initiation fracture toughness in respect of the influence of geometrical variables like thickness and pre-crack depth will be determined in the context of some contrary observations in the literature. The variation in the slope and position of  $J$ - $R$  curves with thickness and pre-crack depth will also be determined. The study will be carried out in highly ductile low carbon steel where the elastic-plastic fracture mechanics is at the other extreme from the boundary of linear elastic fracture mechanics.

## Chapter 3

# EXPERIMENTAL WORK

This chapter describes the experimental procedures used in the present investigation for materials characterization, fracture toughness testing and stretched zone width measurement of the different materials investigated.

### 3.1 TEST MATERIALS

The materials investigated are SA333 Gr. 6 steel pipes of 16" diameter and wall thickness of 32 mm, SAILMA HI-410 micro-alloyed steel plate of thickness 32 mm. The SA333 Gr. 6 steel pipes have been procured from Bhaba Atomic Research Centre (BARC). SAILMA HI-410 micro-alloyed steel plate has been procured from Govt. Irrigation Workshop, Roorkee. The chemical analysis of the steels used in the present study has been carried out under simultaneous spark emission spectrometer (Thermo Jarrell Ash TJA181) with a spot size of about 3 mm.

### 3.2 MICROSTRUCTURAL STUDIES

The microstructures of SA333 Gr. 6 and HI-410 steels have been examined under optical microscope to find the amount and the distribution of phases in the microstructure.

For metallographic examination, samples are manually polished following the standard metallographic procedures described below. The surface of the specimen that is to be examined is first made flat by means of a specially designed motor-driven emery belt. The sharp edges of the specimen are then beveled to avoid the tearing of the emery paper during subsequent polishing. The specimens were then polished manually using metallographic emery papers (120, 240, 400 and 600 grit) containing abrading silicon carbide particles.

During polishing on each emery paper, the direction of polishing was such as to introduce scratches at right angles to those introduced by the preceding paper. The final polishing was carried out on a rotating polishing wheel with sylvet-cloth mounted on it. The polishing medium was 0.1  $\mu\text{m}$  size alumina powder suspension. After polishing, all the samples were etched with 5 pct nital (5 pct  $\text{HNO}_3$  + 95 pct Methanol), washed, dried and finally examined under  $\text{MeF}_3$  Reichert-Jung optical microscope made in Austria. Typical microstructural features of all the samples are photographed. These optical micrographs are presented and discussed in Chapter-4.

### 3.3 TENSILE TESTING

The tensile tests were carried out at ambient temperature, conforming to ASTM specification. The dimensions of the tensile specimens are shown schematically in Fig. 3.1. Tests were carried out using a crosshead speed of 1 mm/min on a hydraulic universal testing machine. The diameter and gauge length of each specimen was measured prior to and after the test. The yield strength was generally estimated from the yield point noticed on the load-displacement plot. The ultimate tensile strength of the specimens was evaluated by dividing the maximum tensile force by the initial cross-sectional area of the specimens in units of  $\text{MN}/\text{m}^2$  or MPa.

The stress-strain diagrams of all the specimens were further analyzed, in between the yield strength and ultimate tensile strength, according to the Ramberg-Osgood expression as given below

$$\left[ (\varepsilon / \varepsilon_0) = (\sigma / \sigma_0) + \alpha (\sigma / \sigma_0)^n \right] \quad (3.1)$$

Where,  $\varepsilon$  is the observed strain in the material at a given stress of  $\sigma$  at any instant.  $\sigma_0$  is the reference stress taken as flow stress,  $[(\sigma_U + \sigma_Y)/2]$ , and,  $\varepsilon_0$  is  $(\sigma_0 / E)$ .  $\alpha$  is a dimensionless material constant and  $n$  is the strain hardening exponent.

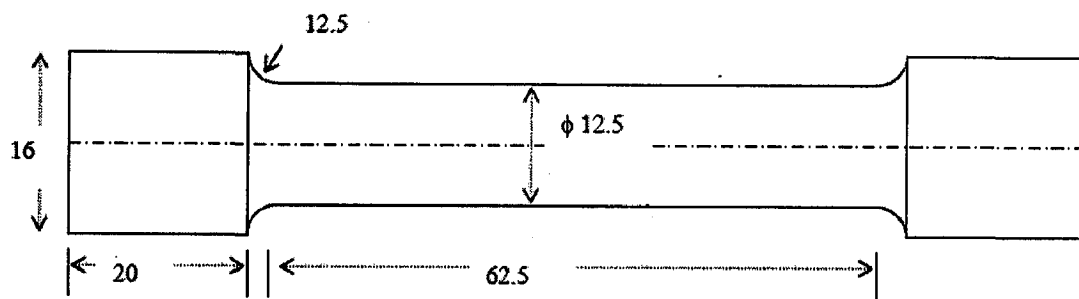


**Fig. 3.1 Schematic diagram of the round tensile specimens.**



## 3.4 FRACTURE TOUGHNESS TESTING

Fracture toughness tests were carried out on Servo hydraulic universal testing machine of make Instron Model 8800 using Fast track  $J_{Ic}$  program. The  $J_{Ic}$  fracture toughness Program runs under an environment set-up by the LabVIEW programming application from National Instruments. LabVIEW is a programming environment that provides the interface between the program and the Instron Model 8800.

The method involves loading under three-point bending and pin loading of fatigue precracked specimens and determination of  $J$  as a function of crack growth. Load versus load-line displacement is recorded digitally. The  $J$ -integral is determined and plotted against physical crack growth,  $\Delta a_p$ , using at least four data points within specified limits of crack growth. These data reflect the materials resistance to the crack growth. Prior to  $J$ - $R$  test each specimen was fatigue pre-cracked. After fatigue pre-cracking but prior to  $J$ - $R$  testing each specimens were side-grooved to the extent of 20 % of the thickness. The single specimen technique was employed for the determination of  $J$ - $R$  curve of the pre-cracked specimens. The detail of the test process and various test parameters are described in the following subsection.

### 3.4.1 Test Specimens

For fracture toughness testing, specimens required for two types of tests - compact tension (CT) and three point bend (TPB), have been used. The orientations of the specimens taken from the pipes and from plates are shown in Fig. 3.2 and Fig. 3.3. The dimensions of the CT and TPB specimens, conforming to ASTM specification, are shown schematically in Fig. 3.4 and Fig. 3.5 respectively. CT and TPB specimens were machined for specimens of varying thickness ( $B$ ) from 10 to 25 mm. The tests were carried out on both standard and non-standard samples with respect to ASTM E 813. The objective of this study is to incorporate a wide range of crack tip triaxiality. The nominal specimen width ( $W$ ) of 50.0 mm

for CT and 50 mm for TPB was chosen in order to allow for measurement of valid  $J$  at large crack extensions, in accordance with ASTM E 813.

### 3.4.2 Fatigue Pre-cracking

Prior to fracture toughness tests, all specimens were precracked by fatigue, up to varying crack aspect ratio of about  $a/W \approx 0.4, 0.6$  and  $0.8$ , for each thickness using a servo hydraulic machine. The frequency of precracking was kept 10 Hz and the stress ratio  $R = 0.1$ . Precracking was done at constant stress intensity range  $\Delta K$ . The loading criterion was kept in accordance with the ASTM specifications conforming to a maximum load less than  $0.4 P_L$ , where  $P_L$  is the load limit ( $N$ ), defined as

For three- point bend specimens:

$$P_L = \left[ \left( \frac{4}{3} \right) \left( \frac{Bb_0^2 \sigma_{yeff}}{S} \right) \right] \quad (3.2)$$

For compact specimen:

$$P_L = \left[ \frac{Bb_0^2 \sigma_{yeff}}{(2W + a)} \right] \quad (3.3)$$

where,  $B$  is the thickness of the specimen (mm),  $W$  is the width of the Specimen (mm),  $b_0$  is the initial uncracked ligament (mm),  $a$  is the initial crack length (mm) and  $\sigma_{yeff}$  is the effective yield strength of the specimen ( $N/mm^2$ ).  $\sigma_{yeff}$  is estimated as  $(\sigma_y + \sigma_u) / 2$ , where  $\sigma_y$  is the yield strength ( $N/mm^2$ ) and  $\sigma_u$  is the ultimate tensile strength ( $N/mm^2$ ).  $S$  is the support span of bend table (mm).

The measurements of crack length were carried out by compliance, using a clip gauge. The control of load and frequency was executed through a microprocessor controlled Instron Fast Track Console.

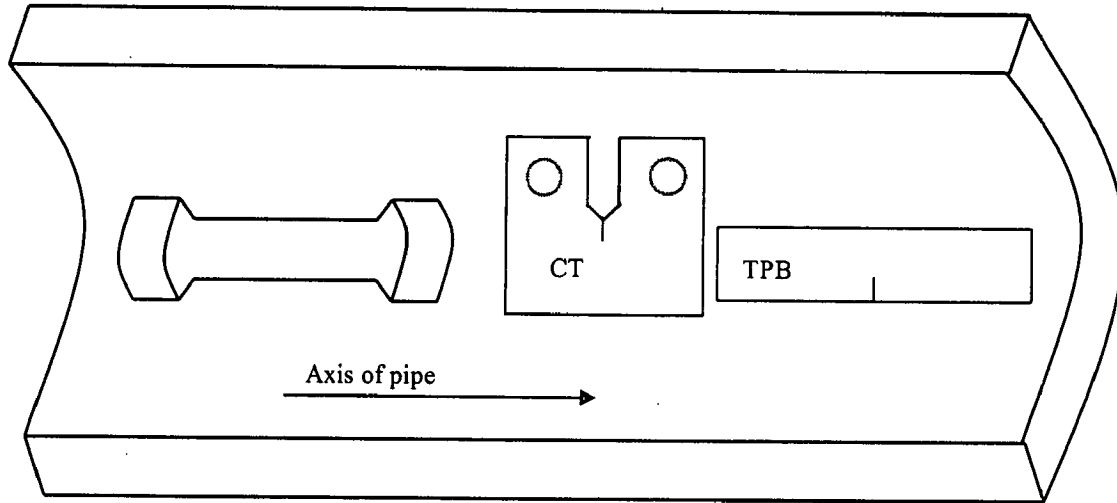


**Fig. 3.2** Schematic diagram of the orientation of the specimens collected from the pipe for testing.

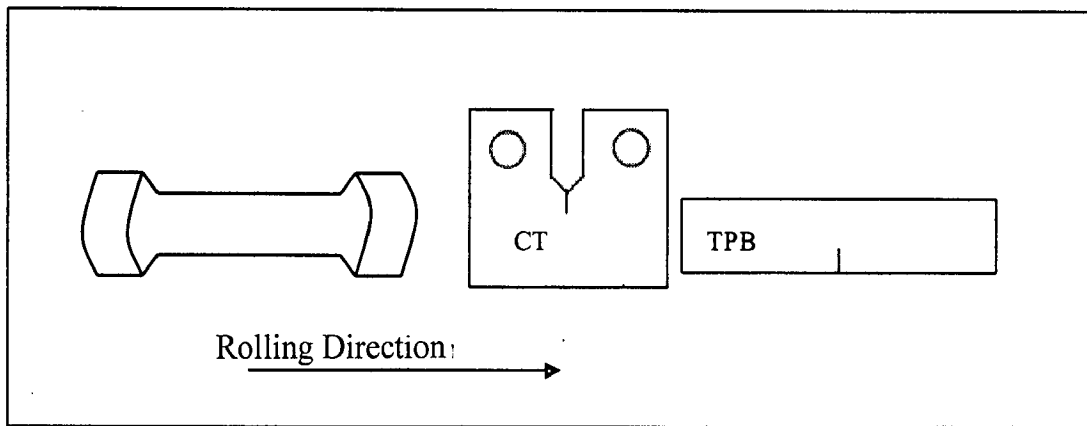


**Fig. 3.3** Schematic diagram of the orientation of the specimens collected from the plate for testing

All Dimensions are in mm.

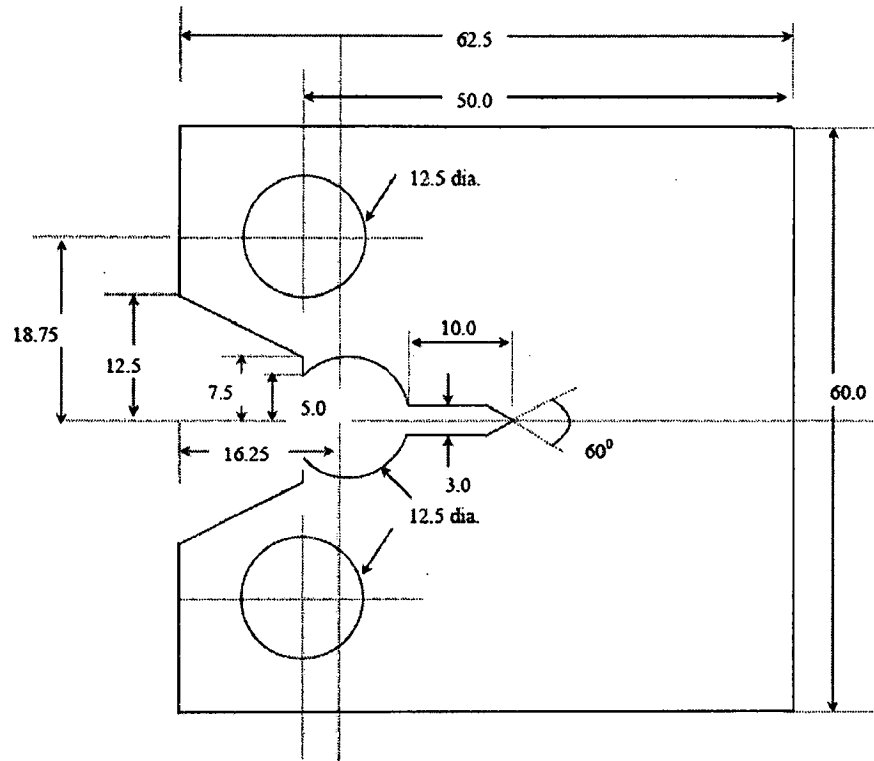


**Fig. 3.4 Schematic diagram of the Compact Tension (CT) specimen.**

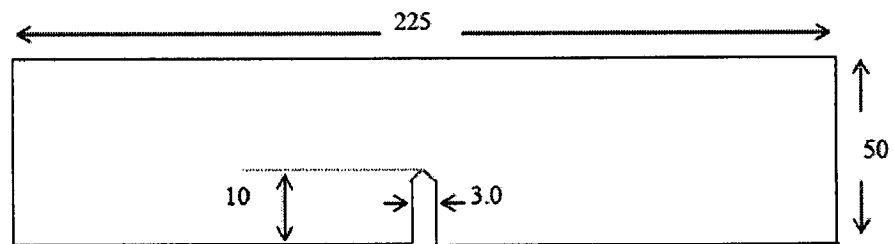


**Fig. 3.5 Schematic diagram of the Three Point Bend (TPB) specimen.**

### 3.4.3 Test Procedure for $J_{IC}$

Fracture toughness tests were performed at room temperature on an Instron Universal machine model 8800 under displacement control with a crosshead speed of 0.5 mm/min., as prescribed by ASTM E 813. Crack length measurements were made by unloading compliance (UC) method. The load line crack opening displacement was measured with an inboard clip gage attached to front notches at the load line. After testing, optical crack length measurements were made and used to transcribe experimental crack length data as per ASTM E 813. In the unloading compliance technique, a specimen was partially unloaded and then reloaded at specified intervals during the test. The unloading slopes, which tend to be linear and independent of prior plastic deformation, were used to estimate the crack length at each unloading from analytical elastic compliance relationships.

Following steps were carried out on each test specimen individually:

- I. Crack length estimations from initial elastic compliance were carried out with a peak load in the range of 0.5 to 1.0 times the maximum precracking load. Estimation of the original crack length,  $a_0$ , from compliance measurements were repeated three times. The peak loads for other two sequences were 60 % and 80 % of this peak. The individual values should be within a limited range from the mean. After estimating the original crack length, the load was returned to a low value maintaining the fixture alignment.
- II. The test was preceded in a manner such that the unloading/reloading sequences produce  $J$  versus crack extension data points evenly spaced over the prescribed test region. The unloading for crack extension measurements were carried out till 40 % of the current load from where reloading is done.

- III. After completing the final unloading, the load had to be returned to zero without additional crosshead displacement beyond the then current maximum displacement.
- IV. The specimens were removed and completely broken in liquid nitrogen. The fracture surfaces were studied for crack length measurements and fractographic analyses. The fracture surfaces of broken specimens were examined in detail using a scanning electron microscope.
- V. Along the front of fatigue crack and the front of the marked region of slow-stable crack extension, measurement of the crack size were carried out at nine equally spaced points centered about the specimen centerline and extending to  $0.005 W$  from the root of the side groove or surfaces of plane-sided specimens. Calculation of the original crack size,  $a_0$ , and the final physical crack size,  $a_p$ , was carried out as follows: average the two near-surface measurements were taken, this average was combined with the result of remaining seven crack length measurements and determine the average.

#### **3.4.4 Calculation and Interpretation of Results**

Calculations of  $J$ -integral were made from load, load-line displacement curves obtained from the procedure outlined in previous section. From the load vs. load line displacement data  $J$ - $R$  curve was plotted in following steps:

##### **(a) Calculating crack length**

- (i) From load vs. load line displacement data of different loading and unloading cycles, the slopes was determined by linear least square fit of the data points of loading and unloading cycle taken together data. From the slopes of different loading-unloading cycles the compliance was calculated:

- (ii) This compliance was used to find the value of  $\mu$  according to equation

For CT specimens

$$\mu = \frac{1}{[B_e EC_i]^{1/2} + 1} \quad (3.4)$$

For TPB specimens,

$$\mu = \frac{1}{\left[ \frac{B_e WE' C_i}{S/4} \right]^{1/2} + 1} \quad (3.5)$$

where

$$B_e = B - \left( \frac{B - B_N}{B} \right)^2$$

where,  $B_N$  is the net specimen thickness after excluding the side grooving depth of the specimen.  $E$  is the Young's Modulus of the specimen and  $C_i$  is the compliance at corresponding loading unloading cycle.  $E'$  is the  $E/(1-\nu^2)$ , where  $\nu$  is Poisson's ratio.  $S$  is the loading span and  $W$  is the width of the TPB specimen

- (iii) From the value of  $\mu$  at each loading-unloading cycle, the ratio of crack length to width ( $a/W$ ) has been calculated using inverse relationship between crack size and compliance as given by

For CT specimen

$$a/W = [1.000196 - 4.06319\mu + 11.242\mu^2 - 106.043\mu^3 + 464.335\mu^4 - 650.677\mu^5] \quad (3.6)$$

For TPB specimen

$$a/W = [0.999748 - 3.9504\mu + 2.9821\mu^2 - 3.21408\mu^3 + 51.51564\mu^4 - 113.031\mu^5] \quad (3.7)$$

The crack extension after each cycle is calculated by multiplying  $a/W$  ratio with the width of the specimen tested.

### (b) Calculating $J$ value

$J$  was calculated according to the equation:

$$J = J_{el} + J_{pl} \quad (3.8)$$

Where,  $J_{el}$  and  $J_{pl}$  are the elastic and plastic components of  $J$ .

For a given load-displacement point,  $(i)$ ,  $J_{el}$  and  $J_{pl}$  are calculated following the equations,

For CT specimens:

$$J_{el(i)} = \frac{K^2_{(i)}(1-\nu^2)}{E} \quad (3.9)$$

where

$$K_{(i)} = \left[ \frac{P_i}{(BB_N W)^{1/2}} \right] \cdot f(a_0/W) \quad (3.10)$$

where,

$$f(a_0/W) = \left[ \frac{(2 + a_0/W)(0.886 + 4.64a_0/W - 13.32(a_0/W)^2 + 14.72(a_0/W)^3 - 5.6(a_0/W)^4)}{(1 - a_0/W)^{3/2}} \right] \quad (3.11)$$

and,

$$J_{pl} = \frac{\eta A_{pl(i)}}{B_N b_0} \quad (3.12)$$

where,  $K$  is the stress intensity factor,  $\nu$  is the Poisson's ratio,  $E$  the modulus of elasticity,  $P$  the value of load at the unloading point,  $i$  point on the load vs displacement curve,  $A_{pl(i)}$  is the



area under the load-displacement curve,  $B_N$  is the net specimen thickness ( $B_N = B$  if no side grooves are present),  $b_0$  is the length of uncracked ligament, and  $\eta = (2 + 0.522 b_0/W)$ .

For TPB Specimens:

$$J_{el(i)} = \frac{K_{(i)}^2 (1-\nu^2)}{E} \quad (3.13)$$

where,

$$K_{(i)} = \left[ \frac{P_i S}{(BB_N)^{1/2} W^{3/2}} \right] \cdot f(a_0/W) \quad (3.14)$$

$$f(a_0/W) = \left[ \frac{3(a_0/W)^{1/2} [1.99 - (a_0/W) \cdot (1 - a_0/W) \cdot (2.15 - 3.93(a_0/W) + 2.7(a_0/W))^2]}{2(1 + 2a_0/W)(1 - a_0/W)^{3/2}} \right] \quad (3.15)$$

and,

$$J_{pl(i)} = \frac{2A_{pl(i)}}{B_N b_0} \quad (3.16)$$

where,  $K$  is the stress intensity factor,  $\nu$  is the Poisson's ratio,  $E$  the modulus of elasticity,  $P$  the value of load at the unloading point,  $i$  point on the load vs displacement curve,  $A_{pl(i)}$  area under the load-displacement curve,  $B_N$  is the net specimen thickness ( $B_N = B$  if no side grooves are present),  $b_0$  is the length of uncracked ligament, and  $S$  is the bend span ( $4W$ ).

The  $J$ -integral values obtained were plotted against the corresponding measured crack growth  $\Delta a$  values to construct the  $J$ - $R$  curve.

### 3.5 PREPARATION AND PRESERVATION OF FRACTURE SPECIMENS

Fracture surfaces are fragile and subject to mechanical and environmental damage that can destroy microstructural features. Consequently, fracture specimens must be carefully

handled during all stages of analysis. This section discusses the care and handling of fracture surfaces, procedure for sectioning fracture surfaces and surface cleaning techniques.

### **3.5.1 Care and Handling of Fracture Surface**

Because of fracture surface contains a wealth of information, it is important to understand the type of damage that can obscure or obliterate fracture features and obstruct interpretation. These type of damages are usually classified as chemical and mechanical damage. Chemical and mechanical damage of the fracture surface can occur during or after the fracture event.

Chemical damage of the fracture surface occurs due to environmental conditions. If the environment is corrosive to the base metal, the fracture surface in contact with the environment will be chemically damaged. Humid air is considered to be aggressive to most of the iron base alloys and will cause oxidation to occur on steel fractured surfaces in a brief period of time. Touching the fracture surface with the fingers will introduce moisture and salts that may chemically attack the fracture surface.

Mechanical damage of the fracture surface that occurs after the fracture event usually results from handling or transporting of the fracture surfaces. It is easy to damage a fracture surface while opening, sectioning the fracture surface from the total part and transporting the fracture surface. Careful handling and transporting of the fracture are necessary to keep the damage to a minimum.

Once mechanical damage occurs on the fracture surface, nothing can be done to remove its obliterating effect on the original fracture morphology. However, if chemical damage occurs and if it is not too severe, can be implemented that will remove the oxidized or corroded surface layer and will restore the fracture surface to a state representative of its original conditions.

### 3.5.2 Sectioning Fracture Surface

It is necessary to remove the portion containing fracture surface to reduce the specimen to a convenient size for scanning electron microscopy because of the specimen chamber that limit specimen size.

Power saw cutting machine was used for cutting the specimens fracture surface. A coolant is used to avoid heat damage to the fractured region. Fractured surface is cleaned with solvent (acetone) and dried immediately after cutting.

### 3.5.3 Fractured Surface Cleaning with ENDOX-214 before Stretched Zone Width (SZW) Measurement

Fracture surfaces contain unwanted surface debris, corrosion or oxidation products and accumulated artifacts that must be removed before meaningful fractography can be performed. The fracture surface was cut into a suitable size from the fractured CT or TPB specimens and degreased in an ultrasonic bath with acetone before electrolytic cleaning.

A working solution of ENDOX-214 was prepared by adding 230 gms of ENDOX-214 powder to 1000 ml of cold water followed by stirring until it was completely dissolved. The working temperature of the solution was the room temperature.

A glass beaker with 250 ml of ENDOX-214 solution was placed in the electrolytic bath, the specimen was connected as cathode and a stainless strip was used as anode. Current density of about  $250 \text{ mA/cm}^2$  was applied for one minute. The specimen was removed from the electrolyte and washed in clean flowing water. The specimen was then dipped in methanol and dried in hot air.

The above procedure was carried out for one cycle and the cycle could be repeated if necessary, to achieve the desired cleaning as observed under optical microscope. The cleaning process was regulated only to remove the rust without any damage or disturbance to the underlying features of the fracture surface. Immediately after cleaning and drying, the specimens were studied under scanning electron microscope to avoid any further rusting on the specimen under ambient condition.

### **3.6 MEASUREMENT OF STRETCHED ZONE WIDTH (SZW)**

The stretched zone width (*SZW*) along the thickness direction of the fractured specimens was studied under LEO, 435 VP Scanning Electron Microscope (*SEM*). The studies were carried out at different magnification, so that the stretched zone prior to initiation of typical ductile fracture under static loading could be clearly identified by its unique stretched feature in contrast to dimpled region under ductile fracture.

The total length of the stretched zone along the thickness as it appeared in the fractograph, was photographed in parts and the width of the *SZW* was measured on the digital photographs directly on the screen at intervals of 200  $\mu\text{m}$  along the thickness. From these micrographs, the stretched zone width has also been measured by two other methods customarily followed. In nine point method, the local stretched zone width is determined by averaging five measurements taken at each of nine positions. The stretched zone width of the specimen is determined by averaging the local measurements over nine positions. In three point method stretched zone width is determined by averaging the three values of the local stretched zone widths taken at the center and two sides of the fractured specimen along the thickness.

## Chapter 4

# **RESULTS AND DISCUSSIONS: STRETCHED ZONE WIDTH**

## **4.1 MATERIAL CHARACTERISATION**

### **4.1.1 Chemical Composition**

The chemical composition of pipe material of SA333 Gr. 6 from 16" diameter supplied by BARC and SAILMA HI-410 micro-alloyed steel plate of thickness 34 mm, has been determined by emission spectroscopy (Thermo Jarrel Ash TJA 181).

The chemical composition of SA333 Gr. 6 steel which is a carbon-manganese steel is given in Table 4.1. If the carbon content is 0.18% the manganese content should increase to 0.89 wt% as specified in ASTM A 333 standards. It is observed that a carbon level of pipe material is lower than the specified 0.18 wt% and silicon content is more than the specified level. A small amount of aluminium is also observed in the pipe material and it could have originated from de-oxidation practice or added intentionally for grain size control. Sulphur and phosphorus contents in all the pipe materials are at acceptable levels.

The chemical composition of SAILMA HI-410 micro-alloyed steel is given in Table 4.2. The table shows that the plates are having micro alloying of Cr (0.003-0.011 wt%) and Ni (0.031-0.035 wt%) along with Cu of the order of 0.033-0.042 wt%. The carbon content of the steel is 0.14 wt%.

### 4.1.2 Microstructural Studies

Typical microstructures of as received in SA333 Gr. 6 pipe material of nominal bore (NB) of 16" as revealed in the low and high magnifications of X100 and X200 have been shown in Figs. 4.1 (a) and (b). The micrographs show the presence of ferrite (white) and pearlite (black) in the matrix with banded morphology. The banded morphology develops due to inter-dendritic segregation of manganese leading to segregation of carbon, caused by lowering of its activity in presence of manganese.

Table shows SAILMA ?

Typical microstructures of annealed and normalized SA333 Gr. 6 revealed in the low and high magnifications of X100 and X200 have been shown in Figs. 4.2 (a) and (b) and Figs. 4.3 (a) and (b). The annealed and normalized conditions the microstructure of the steels consists of homogenize ferrite and pearlite in the matrix. However, the grain size in normalized steel is small compared to annealed steel. In normalized steel fine pearlite is observed.

The microstructures of as received SAILMA HI 410 steel plate obtained by controlled rolling revealed under low and high magnifications of X100 and X200, are shown in Figs. 4.4 (a) and (b). The figures show that the plates are having ferrite-pearlite (dark) microstructure of relatively finer grains with the presence of pearlite primarily along the bands typical of rolled structure.

### 4.1.3 Mechanical Properties

The typical stress-strain plots of various specimens of as received, annealed and normalized SA333 Gr. 6 steels from straight pipe material are shown in Figs. 4.5, 4.6 and 4.7.

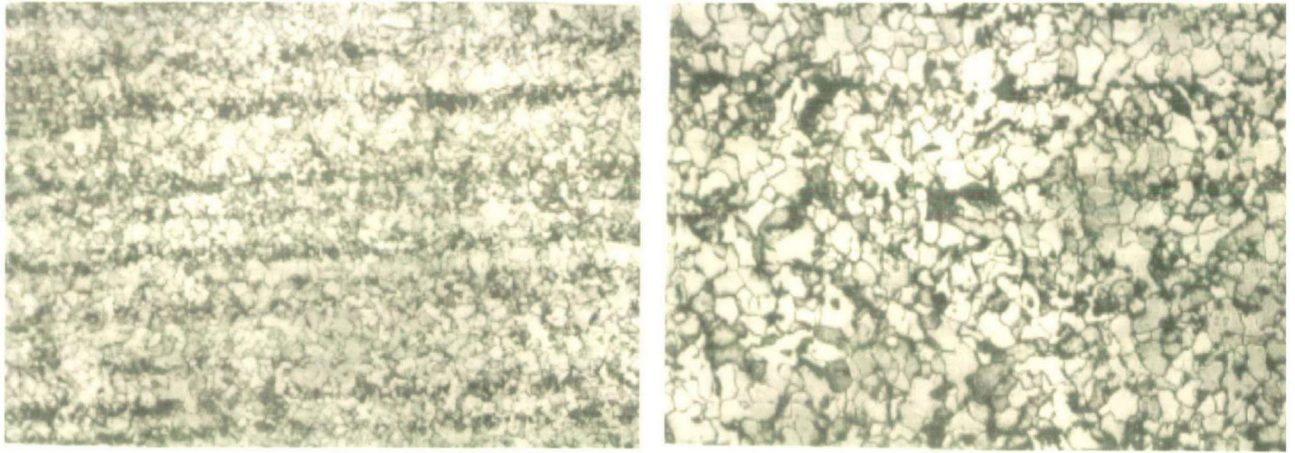
Tensile properties of 16 inch pipe materials are shown in Table 4.3. The design of high strength low alloy C-Mn steel has been based initially on tensile strength alone as joining has

**Table 4.1 The chemical composition of SA333 Gr. 6 steel**

<b>Chemical composition (Wt. %)</b>			
<b>C</b>	<b>Mn</b>	<b>Si</b>	<b>Al</b>
0.1680	0.8804	0.1189	0.0489
0.1697	0.8887	0.1208	0.0499

**Table 4.2 The chemical composition of SAILMA HI-410 steel**

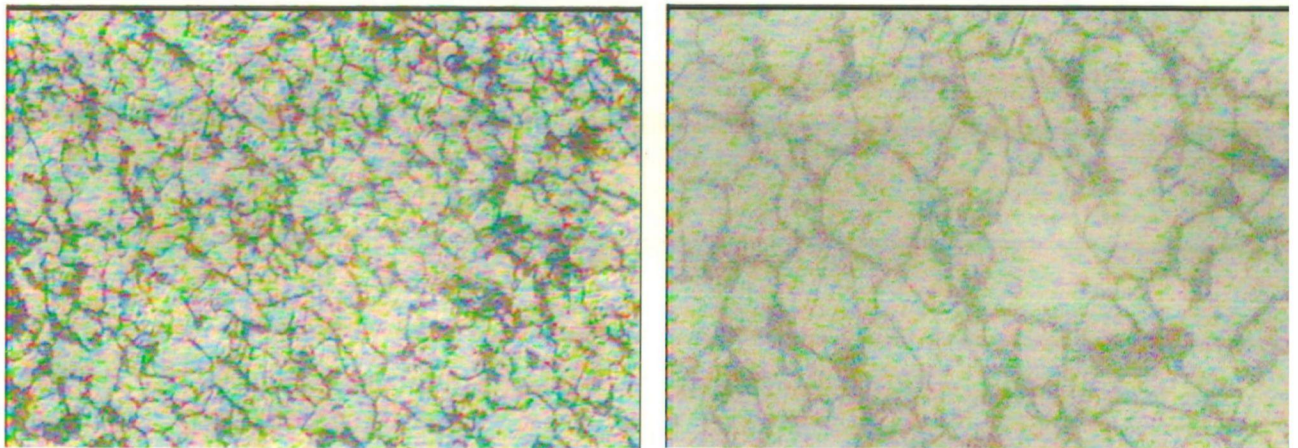
<b>Chemical composition (Wt. %)</b>										
<b>C</b>	<b>Mn</b>	<b>Si</b>	<b>S</b>	<b>P</b>	<b>V</b>	<b>Ti</b>	<b>Cu</b>	<b>Al</b>	<b>Nb</b>	<b>Ce</b>
0.14	1.45	0.30	0.012	0.021	0.01	0.03	0.02	0.027	0.05	0.39



(a)

(b)

**Fig. 4.1** Typical microstructure of SA333 Gr. 6 pipes. (a) X100 and (b) X200.

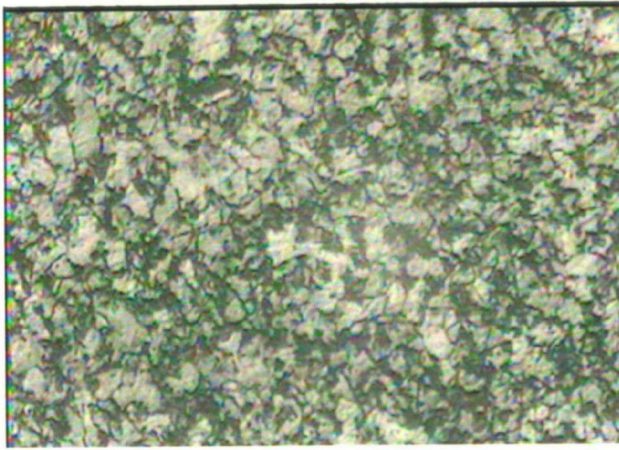


(a)

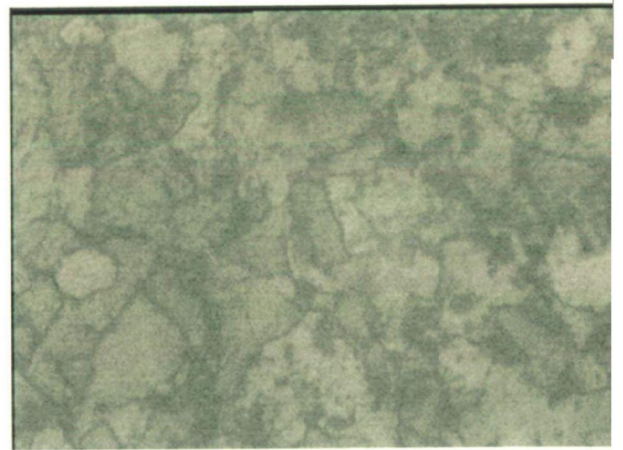
(b)

**Fig. 4.2** Typical microstructure of annealed SA333 Gr. 6 (a) X100 and (b) X200.



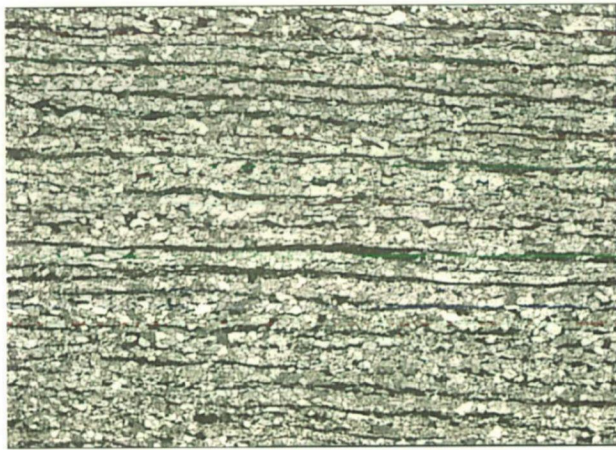


(a)

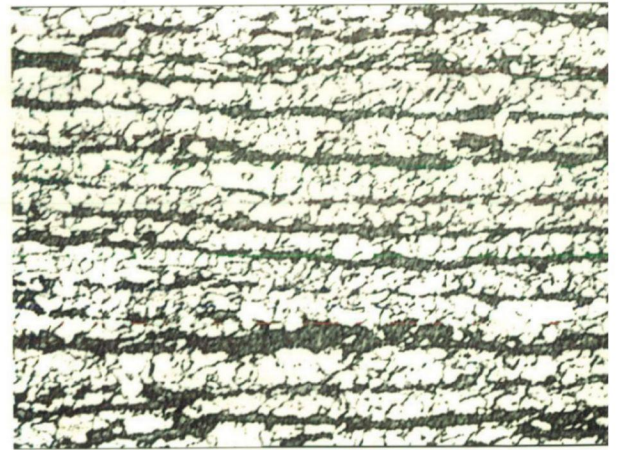


(b)

**Fig. 4.3** Typical microstructure of normalized SA333 Gr. 6 (a) X100 and (b) X200.



(a)



(b)

**Fig. 4.4** Typical microstructure of SAILMA HI 410. (a) X100 and (b) X200.

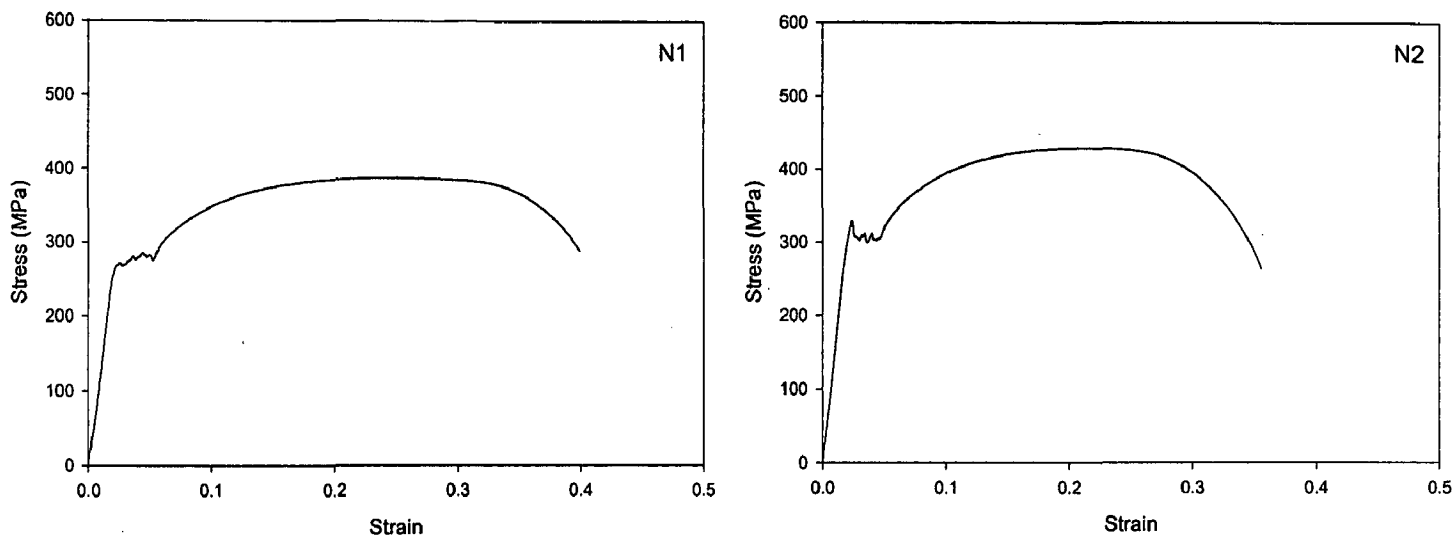


**Fig. 4.7** Typical Stress Strain diagrams of normalized SA333 Gr. 6 steel

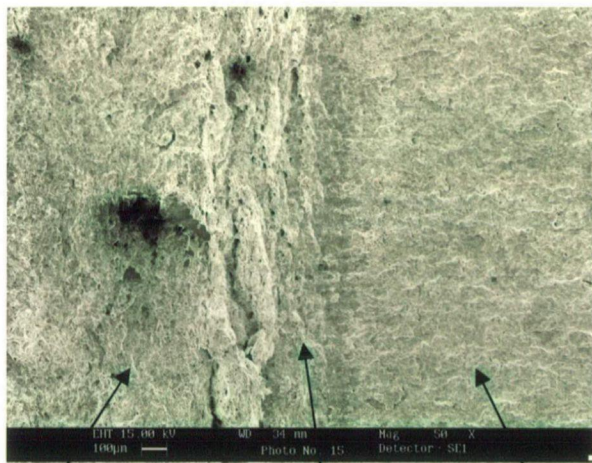
**Table 4.3** Mechanical Properties of SA333 Gr. 6 steel

Material	Yield Strength (MPa)	Tensile Strength (MPa)	Elongation (%)	n	$\alpha$
As received	318.47	445.86	38.0	4.37	10.70
Annealed	306.00	415.00	36.7	4.83	10.63
Normalized	327.00	428.00	34.2	5.23	11.36

been based on riveting. Carbon, being the cheapest alloying element, has been mainly used along with manganese to develop tensile strength. The advent of welding rather than riveting as a method of joining has necessitated lower carbon content. The strength could then be maintained by increasing manganese content. Failure of welded structures by brittle fracture has led to recognition of the importance of impact and fracture toughness in these materials. A need for low impact transition temperature is apparent. It has been further recognized that high yield strength is more important than high tensile strength. The approach is to lower carbon content while maintaining manganese. The advantage of high Mn:C ratio for impact toughness is well recognized. The significance of grain size has been established in this context. Grain refining addition of Al-N has been introduced. Impact strength is adversely affected by coarse as rolled grain size which could be avoided by using a low finishing temperature for rolling. To improve through thickness ductility and toughness it is required to avoid planar arrays of nonmetallic inclusions, which also cause lamellar tearing during welding. Thus, the objective of lowering carbon content in the pipes under investigation and compensating it by manganese to keep the strength level similar to SA333 Gr.6 has succeeded since the yield strength of all the pipes are greater than 280 MPa and the tensile strength is around 420 MPa. The percent elongation is more than 36% as specified.

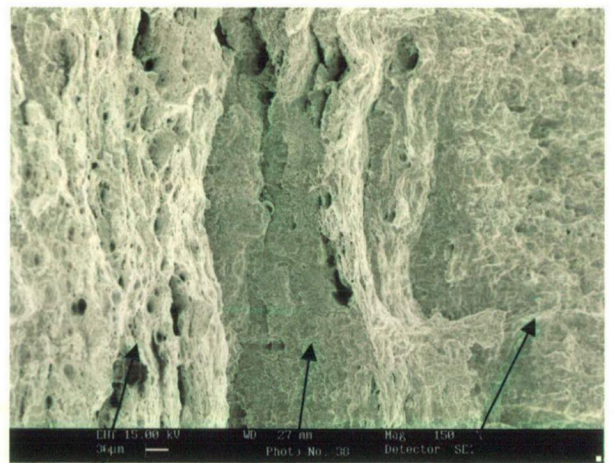
The stress-strain diagram for the base metal has been fitted with the help of Ramberg-Osgood equation given in Chapter 3 and the material parameters  $\alpha$  and  $n$  have been tabulated in Table 4.3.

The typical stress-strain plots of various specimens of SAILMA HI 410 from plate material are shown in Fig. 4.8. Tensile properties of SAILMA HI 410 material are shown in Table 4.4.



Ductile Fracture Stretched Zone Fatigue pre-crack

(a)



Ductile Fracture Stretched Zone Fatigue pre-crack

(b)

**Figs.4.9 Typical appearance of the SZW in SA333 Gr. 6 steel.**

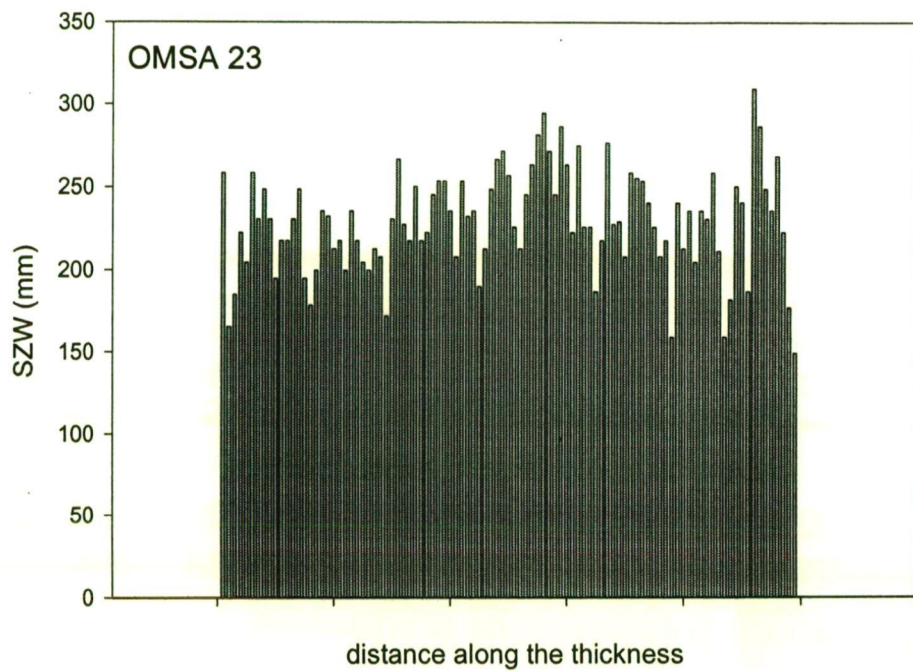
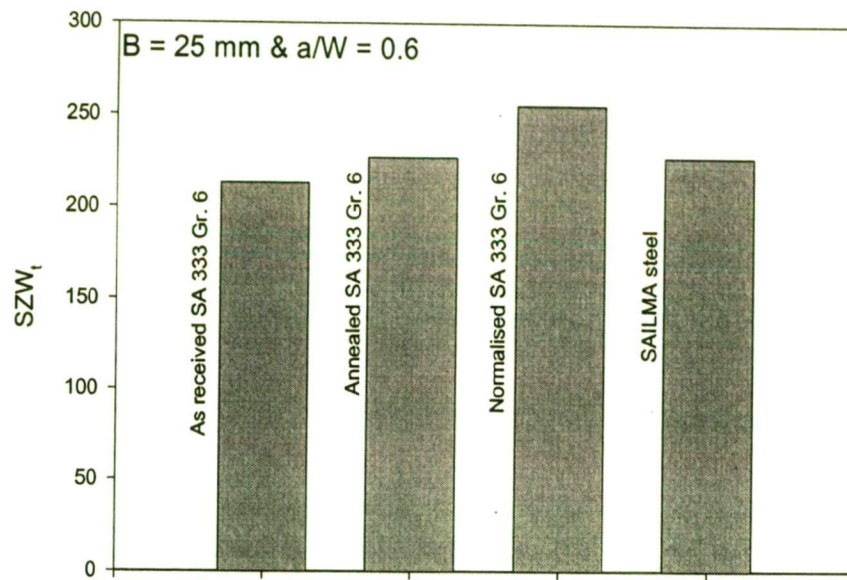
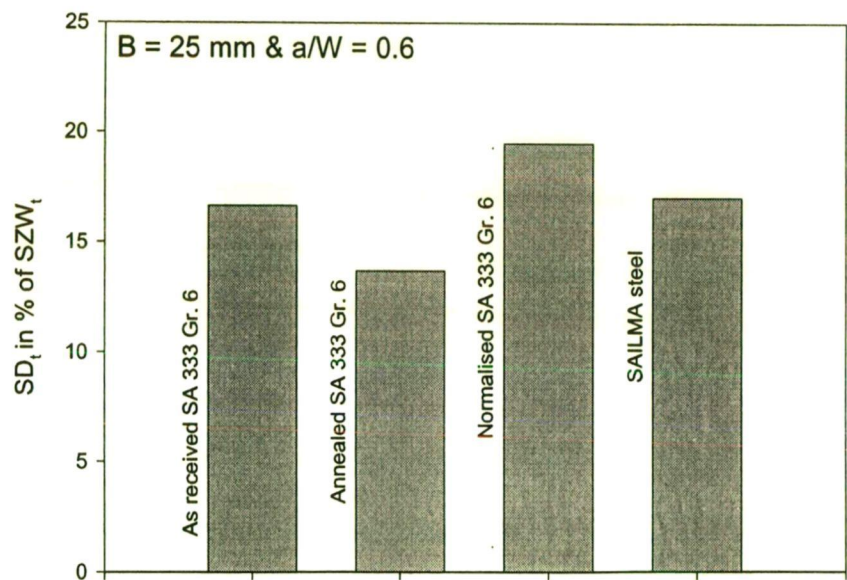


**Fig. 4.10** Variation of *SZW* measured at regular interval of 200 μm along the thickness of CT specimen of SA333 Gr. 6 steel at *a/W* ratio of 0.6 and specimen thickness of 25 mm.



(a)



(b)

**Fig. 4.11 Comparison of  $SZW_t$  and standard deviation of different steels, SA333 Gr. 6 steels with or without heat treatment and SAILMA steel in 25 mm thick CT specimens with pre-crack depth of  $a/W = 0.6$**

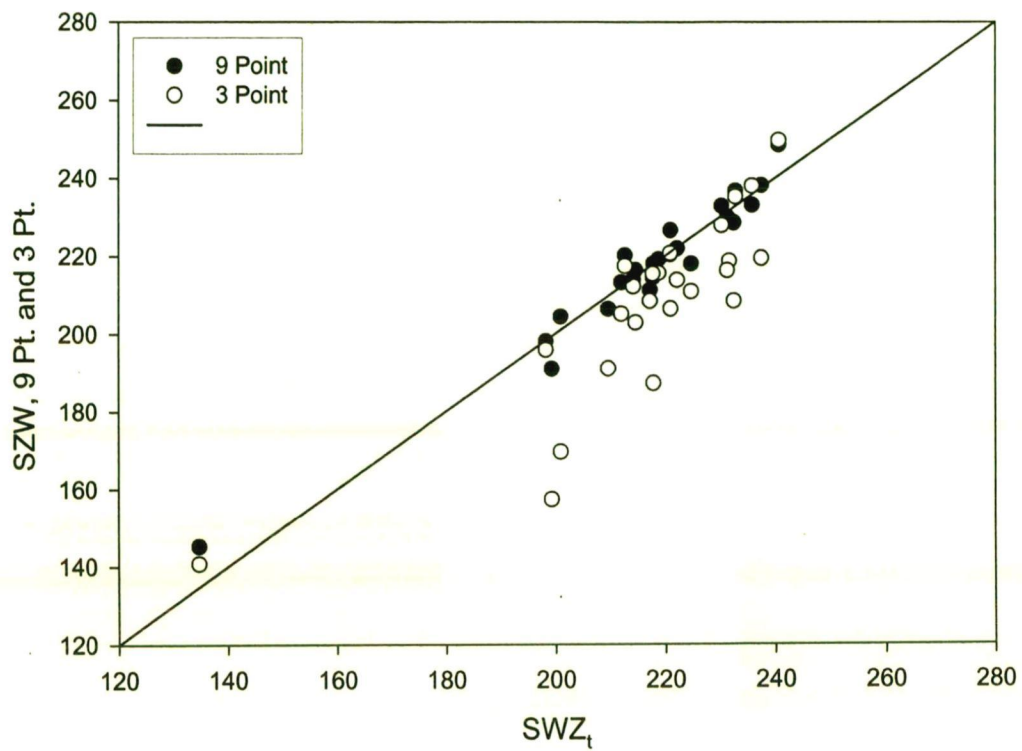


**Fig. 4.12** The comparison of stretched zone widths measured by nine point ( $SZW_9$ ) and three point methods ( $SZW_3$ ) with those given by average of measurements at close intervals ( $SWZ_t$ ) along the thickness on the fractured surface of CT specimens of SA333 Gr. 6 material.

independent of specimen thickness. Putatunda and Rigsbee [1985] has measured stretched zone width in the mid thickness region at 20-25 points on each half of the specimens and have reported that the specimen thickness has little influence on the stretched zone in AISI-4340 steel, which is in agreement with the results of present study.

Figures 4.23, 4.24 and 4.29 show that the changes in the pre-crack depth do not produce distinct variation in stretched zone width as the observed *SZW* values are within a close range for variations of  $a/W$  for different thickness. The standard deviation in the measurements are more than the extent of variations observed and so the variation could not be considered significant. This conclusion is in agreement with that of Zheng *et al* [2000a] who have tested the fracture toughness in TPB specimens of St 69 steel by changing the crack length ( $a/W$ ) and it has been observed that the stretched zone size is independent of the relative precrack size. Shen *et al* [2001] has also reported that there is no effect of pre-crack depth on *SZW*. Hyatt and Matthews [1994] have also shown that the changes in the pre-crack depth do not produce significant change in stretched zone width.

The present investigation indicates that the stretched zone width measured by nine point method is more representative than the measurement by three point method when the results are compared with more exhaustive but time consuming measurements at close intervals of 200  $\mu\text{m}$  along the thickness of the fractured CT and TPB specimens. However, the standard deviation of the measurements by nine point method is relatively lower than that observed in the measurements at close intervals. The present study has also indicated that the stretched zone width is relatively insensitive to constraints as imposed by specimen thickness or pre-crack depth. Therefore, it may be possible to arrive at a characteristic stretched zone width for a material of a given composition and microstructure. Wide difference in the mechanical properties of the constituent phases in a material results in larger standard deviation in *SZW* measurement.



## Chapter 5

# RESULTS AND DISCUSSIONS: FRACTURE TOUGHNESS

This chapter describes the experimental results of the  $J$ - $R$  curve, its necessary corrections and the method of determining the initiation fracture toughness ( $J_{IC}$ ). The variations of initiation fracture toughness in two steel - SA333 Gr. 6 steel and SAILMA steel, with changing thickness and pre-crack depth have been investigated. The effect of constraints imposed by specimen thickness and pre-crack depth on the  $J$ - $R$  curves have been examined. The effect of heat treatment on both  $J_{IC}$  and  $J$ - $R$  curve has been investigated in SA333 Gr. 6 steel. At the end, the results have been discussed to evolve a coherent understanding of the effect of constraints and heat treatment on the fracture toughness of steels investigated in the present investigation.

### 5.1 DETERMINATION OF INITIATION FRACTURE TOUGHNESS ( $J_{IC}$ )

Figure 5.1 shows a typical  $J$ - $R$  curve indicated by circular points, for SA333 Gr. 6 steel specimen having thickness 25 mm and width of 50 mm, pre-fatigued to  $a/W$  ratio of 0.4. The  $J$ - $R$  curve has been obtained for a single CT specimen by compliance technique using the compliance equation for crack extension. In this case, the initiation fracture toughness ( $J_{IC}$ ) could not be determined from ASTM blunting line equation with 0.2 mm offset (indicated by dotted line in Fig. 5.1), since this offset line based on material flow stress does not intersect the  $J$ - $R$  curve within the valid region as prescribed by ASTM standard. It may be noted that the crack extension at the beginning of  $J$ - $R$  curve is not truly a crack extension but represents stretching and blunting of the fine crack created by pre-fatiguing. Direct measurement of

stretched zone width shows that the end of blunting as indicated by the onset of stable crack propagation occurs at an average distance of 0.212 mm for  $SZW_t$ . Therefore, it is expected that the ASTM prescribed procedure to identify the end of blunting and beginning of crack extension by construction of blunting line with the offset should intersect  $J$ - $R$  curve at an apparent crack extension similar to the average stretched zone width  $SZW_t$ . However, for highly ductile material like SA333 Gr. 6 steel, the intersection of blunting line with  $J$ - $R$  curve has taken place at a considerable large distance than  $SZW_t$ . Faced with this problem, many investigators have done away with the 0.2 mm offset in the ASTM procedure and drawn a blunting line from the origin, as shown in Fig. 5.1 by the firm line which also does not intersect the  $J$ - $R$  curve anywhere near the observed  $SZW$ . Thus, it is evident that the blunting line equation based on flow stress does not represent the blunting behaviour of the fatigue pre-crack and so there is a need to evolve a procedure which may establish an accurate blunting line equation for the highly ductile materials.

ASTM standard defines the blunting line using the equation

$$J = 2M\sigma_f\Delta a \quad (5.1)$$

where  $M = 1$  and  $\sigma_f = \frac{1}{2}(\sigma_Y + \sigma_U)$  [ASTM -813-89] which determine the slope of the blunting line. Subsequently ASTM [ASTM 1820] has revised its recommendation for the initial slope of the  $J$ - $R$  curve. It has been recognized that the slope could be steeper than  $2\sigma_f$  for certain materials. For these materials, it is recommended that initiation fracture toughness value may be determined using  $M$  evaluated by experiment taking into consideration the effect of strain hardening as indicated by strain hardening coefficient.

The equation of the  $m = 0.2$  mm offset blunting line which is used to determine initiation fracture toughness,  $J_{IC}$ , may be derived from the blunting line equation (5.1) as

$$J = 2M\sigma_f(\Delta a - m) \quad (5.2)$$

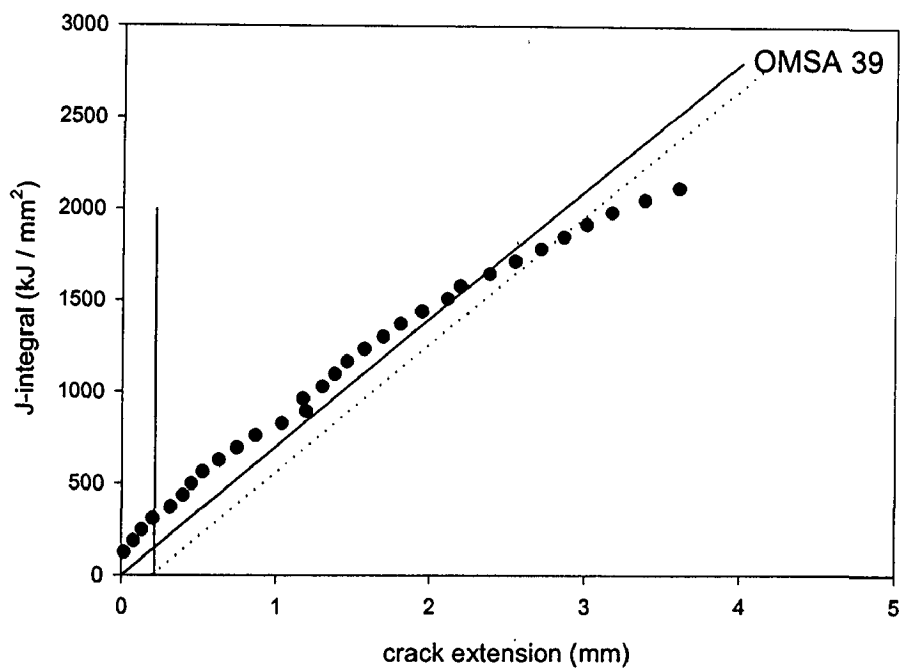


**Fig. 5.1** Typical *J-R* curve of SA333 Gr. 6 having thickness of 25 mm and *a/W* ratio of 0.4 with the blunting line drawn by ASTM procedure

*J-R* curves of the different steels (SA333 Gr. 6, Annealed SA333 Gr. 6, Normalized SA333 Gr. 6 and SAILMA steel) have been fitted by nonlinear regression in term of crack extension ( $\Delta a$ ), upto  $\Delta a = SZW_i$  value from the larger  $\Delta a$  side of the curve. From the fitted *J-R* curves of different steels, initiation fracture toughness ( $J_{SZW}$ ) have been determined for different materials by putting the  $SZW_i$  values as the average crack extension corresponding to the end of blunting. Table 5.1 gives the values of initiation fracture toughness ( $J_{SZW}$ ) determined on the basis of  $SZW_i$  for different steels, as received and after different heat treatments, along with the corresponding strain hardening coefficient ( $n$ ) for each of these materials, as evaluated by Ramberg Osgood equation.  $M$  has been evaluated by putting in equation (5.2) the value of initiation fracture toughness determined on the basis of  $SZW$  for different materials for different offset distances of  $m = 0.2, 0.15, 0.1$  and  $0$  mm as indicated by subscript of  $M$ . These values of  $M$  are also summarized in Table 5.1. Since the limiting value of  $M$  has been claimed by ASTM to be unity,  $\log (M_{0.2} - 1)$  has been plotted with  $\log$  of inverse of strain hardening coefficient,  $\log (1/n)$ , for the purpose of linear least square fit as shown in Fig. 5.2 (a) where dotted line represents the experimental values and the firm line shows the fitted curve with coefficient of correlation ( $R^2$ ) of 0.9592. A change in the offset of the blunting line equation affects the value of  $M$  significantly when evaluated using both *J-R* curve and stretched zone width. The slope of the blunting line  $2M\sigma_f$  decreases with decreasing offset distance as shown in Table 5.1. It may be noted that  $M_{0.2}$  determined on the basis of  $SZW$  is resulting in a steep slope as high as 36.29. Thus, it may be recommended to use 0.1 mm offset which will keep the slope in a relatively lower range of values. The variation of  $\log (M_{0.1} - 1)$  with  $\log (1/n)$  is shown in Fig. 5.2 (b). In the present investigation slope of the blunting line is evaluated using offset 0.2 mm. The intersection of the stretched zone width and the *J-R* curve provides an estimation of the true value of  $M$  for a particular material and thereby a corrected  $J_{IC}$ .

one typical diagram includes

why

The resulting equations for  $M$  corresponding to 0.2 mm and 0.1 mm offset line from the fit may be written respectively as,

$$M_{0.2} = 1 + 4.53 \times 10^7 (1/n)^{9.59}$$

$$M_{0.1} = 1 + 2.93 \times 10^5 (1/n)^{7.74} \quad (5.3)$$

Roos *et al* [1991] has measured the fracture toughness of structural steel KS 17 having yield strength and ultimate tensile strength of 395 and 519 MPa respectively, on the basis of *SZW*. The stretched zone width for this material is 238  $\mu\text{m}$  and fracture toughness is 472 N/mm. The value of  $M$  calculated on the basis of 0.2 mm offset blunting line is 34.73.

For as received SA333 Gr.6 steel,  $M$  has been estimated from equation (5.3) as 32.75. Figure 5.3 shows the typical *J-R* curve of SA333 Gr. 6 steel specimen having thickness of 25 mm and width of 50 mm pre-fatigued to  $a/W$  ratio of 0.4, has been drawn at an enlarged scale for crack extension so that the offset blunting line and the *SZW* with 95 % confidence interval could be distinctly observed. The offset blunting line intersects *J-R* curve within the 95 % confidence interval around average stretched zone width.

The initiation fracture toughness determined by the offset blunting line using  $M$  given by equation (5.3) is found 317.04  $\text{kJ/m}^2$  and that determined on the basis of *SZW* is found to be 316.50  $\text{kJ/m}^2$ . Within 95 % confidence limit of *SZW* the fracture toughness value may lie in the range between 304.26 to 328.52  $\text{kJ/m}^2$ .

Figure 5.4 gives a typical *J-R* curve of SA333 Gr. 6 steel specimen having thickness 25 mm and width of 50 mm pre-fatigued to  $a/W$  ratio of 0.4, shown by circular points.

**Table: 5.1 Slope of the blunting line with offset distance.**

Material		Strain hardening coefficient ( <b>n</b> )	$J_{SZW}$	$SZW$	$M_{0.2}$	$M_{0.15}$	$M_{0.1}$	$M_0$
SA333	As received	4.37	324.59	0.21274	36.29	7.37	4.10	2.17
Gr. 6 Steel	Annealed	4.83	252.77	0.2267	15.23	4.57	2.77	1.55
	Normalised	5.23	227.32	0.25512	5.47	3.56	2.42	1.47
Sailma	As received	5.5	222.78	0.23948	5.40	2.38	1.53	0.89

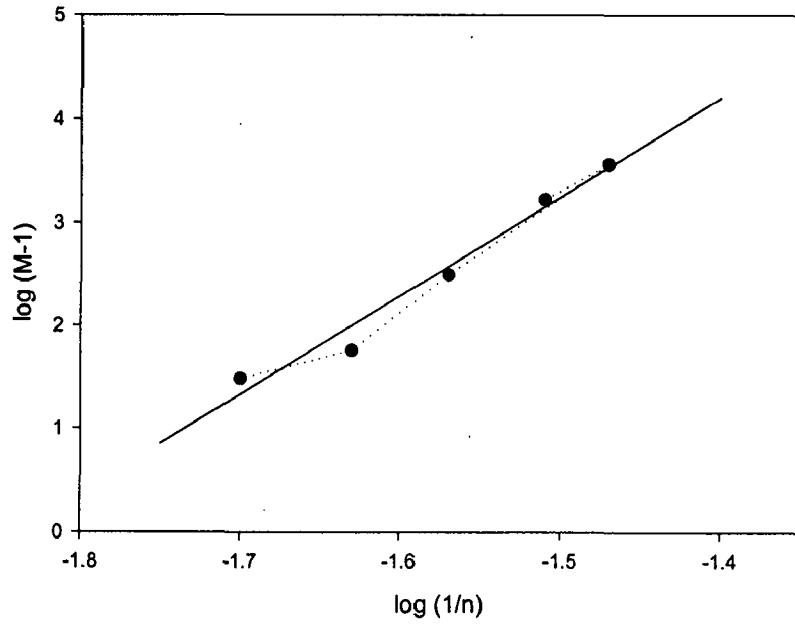


**Fig. 5.2 (a) Relationship of  $M$  with strain hardening coefficient ( $n$ ) when value of offset is taken as 0.2 mm**

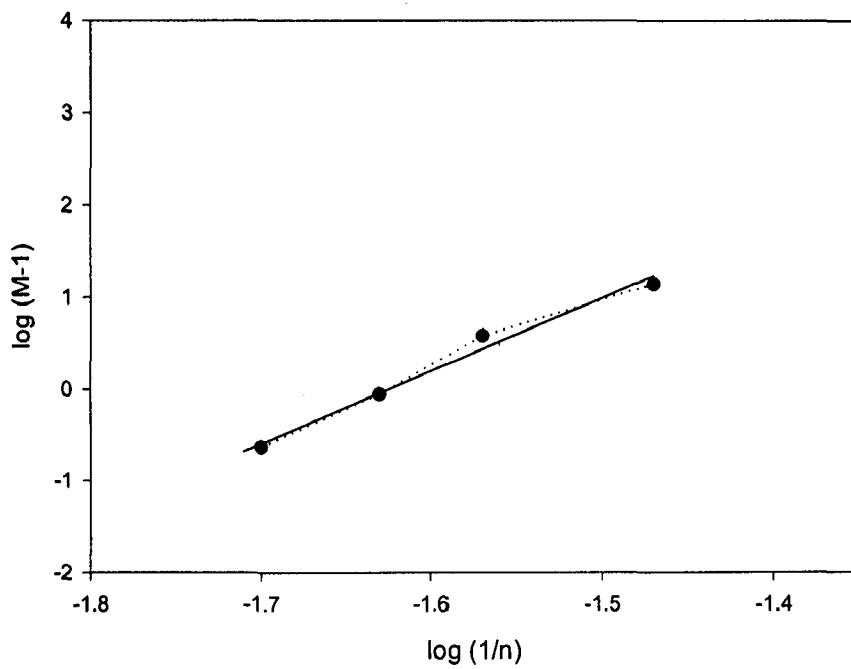


**Fig. 5.2 (b) Relationship of  $M$  with strain hardening coefficient ( $n$ ) when value of offset is taken as 0.1 mm**

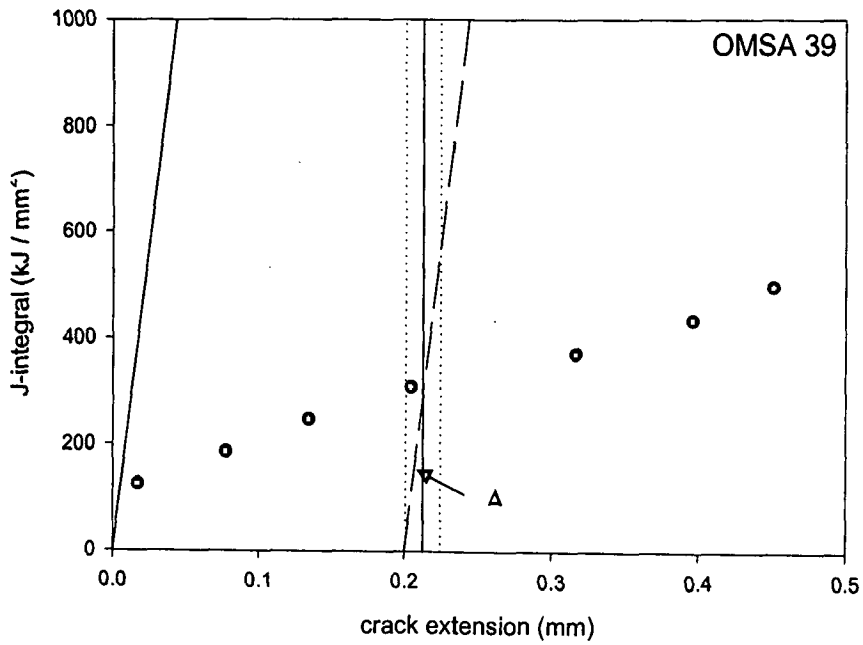


Fig. 5.3 Typical  $J$ - $R$  curve of SA333 Gr. 6 having thickness of 25 mm and  $a/W$  ratio of 0.4 with the blunting line drawn by Equation 5.3. Line A indicates the stretched zone width and the dotted line on both sides indicate the 95 % confidence interval.

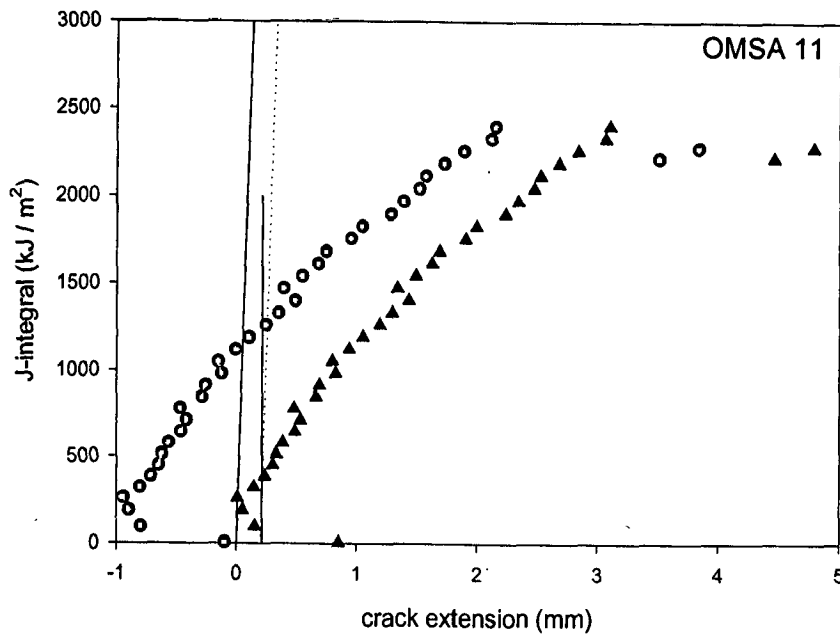


Fig. 5.4 Typical  $J$ - $R$  curve of SA333 Gr. 6 having thickness of 25 mm and  $a/W$  ratio of 0.4 with the blunting line drawn by Equation 5.3.

or 5.37.



In some of the  $J$ - $R$  curve obtained from experiment the initial crack extension ( $\Delta a$ ) data points have anomalous negative values, which are often encountered in ductile materials during partial unloading compliance test. This is an artifact of the method of measurement. ASTM standard does not discuss this problem of the apparent negative crack growth phenomenon or specify any procedure for treating  $J$ - $R$  curve with such features. In many laboratories dealing with  $J$ - $R$  testing, this problem is treated by eliminating the negative data points or by shifting the resistance-curve to a new zero in an ad-hoc manner to correspond to the most negative point. Such treatment has been termed as arbitrary and undesirable, since it depends on the decision of the analyst [Rosenthal *et al*, 1990]. Previous investigations [Rosenthal *et al* 1990, Bowman *et al* 1988, Voss and Mayville, 1985] have shown that the negative crack growth phenomenon occurs perhaps due to various effects such as friction, misalignment in the loading train, balancing and zero adjustment of electronic equipment and physical blunting behavior etc. In the present study, precautions were taken to minimize extraneous causes and no plastic indentations or bending of the pins at the load points could be observed. Therefore, the possible source of error leading to negative crack growth could be due to compressive residual stresses during unloading process caused by the plastic zone around crack tip. Seok [2000] has proposed offset technique that may be used for correcting the apparent negative crack growth. Figure 5.4 shows the  $J$ - $R$  curve in which all  $J$  versus  $\Delta a$  data are shifted along the  $\Delta a$  direction by such an extent that the most negative  $\Delta a$  point falls on the blunting line from origin as proposed by Seok [2000]. The corrected data points are represented by triangle shaped points in Fig. 5.4, which gives the corrected  $J$ - $R$  curve. The initiation fracture toughness ( $J_{IC}$ ) as determined from the 0.2 mm offset blunting line method is found to be 293.58 kJ/mm<sup>2</sup> and from  $SZW$  it is 292.05 kJ/mm<sup>2</sup>. Within 95 % confidence limit of  $SZW$ , the fracture toughness value lies in the range between 304.28 and 281.35 kJ/m<sup>2</sup>.

The initiation fracture toughness for specimens of as received SA333 Gr. 6 material for CT and TPB specimens determined by the offset blunting line using  $M$  given by equation (5.3) and that determined on the basis of  $SZW$  are compared in Table 5.2 and 5.3.  $J_{SZW}$  and  $J_{SZW+}$  are the values of initiation fracture toughness at the limits of the 95 % confidence limit of  $SZW$ .

Figures 5.5 and 5.6 shows the comparison of fracture toughness measured by the 0.2 mm offset blunting line method and fracture toughness measured by *SZW* method in CT and TPB specimens of SA333 Gr. 6 steel. These figures show that the fracture toughness measured by the *SZW* method and fracture toughness measured by the blunting line are comparatively similar in both CT and TPB specimens of SA333 Gr. 6 steel.

Figure 5.7 shows the circular points which belong to a typical *J-R* curve of SAILMA steel specimen having thickness 25 mm and width of 50 mm pre-fatigued to  $a/W$  ratio of 0.4. This *J-R* curve shown in Fig. 5.7 has been obtained by testing a single CT specimen by compliance technique using the compliance equation for crack extension. There are no negative data points in the measured *J-R* curve.

The blunting line (shown by firm sloping line) is drawn by using the blunting line equation drawn by equation (5.3) and that with 0.2 mm offset is shown by the dotted line. The initiation fracture toughness values measured by the 0.2 mm offset blunting line is  $200.78 \text{ kJ/m}^2$  while the fracture toughness value measured by *SZW* method is found to be  $200.75 \text{ kJ/m}^2$ . Within 95 % confidence limit of *SZW*, the fracture toughness value lies in the range between  $194.76$  and  $209.35 \text{ kJ/m}^2$ .

Figure 5.8 shows the data point represent by filled circles belonging to typical *J-R* curve determined by compliance technique by testing a CT specimen of SAILMA steel having thickness 25 mm and width of 50 mm, pre-fatigued to  $a/W$  ratio of 0.4. This curve shows that some initial data points showing negative crack extension. The curve is corrected by shifting the most negative data point to the blunting line and the corrected curve is represented by open circles as shown in Fig. 5.8. The initiation fracture toughness ( $J_{IC}$ ) as determined from the 0.2 mm offset blunting line is found to be  $222.95 \text{ kJ/m}^2$  and fracture toughness measured by *SZW* method is  $219.67 \text{ kJ/m}^2$ . Within 95 % confidence limit of *SZW*, the fracture toughness value lies in the range between  $200.45$  and  $227.59 \text{ kJ/m}^2$ .

**Table 5.2 Initiation Fracture toughness based on stretched zone width method and blunting line equation of CT specimens of SA333 Gr. 6 steel**

Specimen Designation	Thickness (mm)	Effective Thickness (mm)	$a/W$	$J_{0.2}$	$J_{SZW-}$	$J_{SZW}$	$J_{SZW+}$
OMSA 21	25	20	0.41	298.44	310.94	298.44	285.94
OMSA 11	25	20	0.39	293.58	304.28	292.05	281.35
OMSA 23	25	20	0.37	353.40	361.11	348.77	337.96
OMSA 39	25	20	0.40	373.42	381.33	367.09	354.43
OMSA 40	25	20	0.40	310.40	322.63	310.40	301.22
				<b>325.85</b>	<b>336.06</b>	<b>323.35</b>	<b>312.18</b>
OMSA 15	25	20	0.60	302.22	325.95	291.14	253.17
OMSA 16	25	20	0.62	385.09	408.39	369.57	318.32
OMSA 44	25	20	0.61	214.98	234.54	208.95	180.33
OMSA 45	25	20	0.60	269.11	290.52	258.41	226.30
OMSA 46	25	20	0.59	240.80	262.27	234.66	202.45
				<b>282.44</b>	<b>304.33</b>	<b>272.55</b>	<b>236.11</b>
OMSA 12	25	20	0.81	230.89	249.24	247.71	246.18
OMSA 19	25	20	0.81	220.18	238.53	237.00	235.47
OMSA 41	25	20	0.81	246.18	263.00	264.53	263.00
OMSA 43	25	20	0.80	224.77	241.59	241.59	240.06
				<b>230.50</b>	<b>248.09</b>	<b>247.71</b>	<b>246.18</b>
OMSA 32	15	12	0.40	455.66	478.59	478.59	477.06
OMSA 33	15	12	0.39	342.45	371.50	371.50	368.44
				<b>399.05</b>	<b>425.05</b>	<b>425.05</b>	<b>422.75</b>
OMSA 30	15	12	0.59	284.40	302.75	293.58	285.93
OMSA 31	15	12	0.59	377.68	391.44	382.26	373.09
				<b>331.04</b>	<b>347.09</b>	<b>337.92</b>	<b>329.51</b>
OMSA 28	15	12	0.80	276.08	280.69	266.83	252.96
OMSA 29	15	12	0.80	483.18	474.01	461.77	443.43
				<b>379.63</b>	<b>377.35</b>	<b>364.30</b>	<b>348.19</b>
OMSA 48	10	8	0.39	206.42	226.30	212.54	198.78
OMSA 49	10	8	0.41	362.38	377.67	366.97	356.27
OMSA 50	10	8	0.40	356.27	370.03	360.86	350.15
OMSA 35	10	8	0.42	362.39	379.21	368.50	353.21
				<b>321.87</b>	<b>338.30</b>	<b>327.22</b>	<b>314.60</b>
OMSA 51	10	8	0.60	197.25	206.42	201.84	197.25
OMSA 52	10	8	0.60	211.01	221.71	212.54	209.48
OMSA 53	10	8	0.60	207.95	217.13	211.01	204.89
OMSA 34	10	8	0.59	290.52	298.17	292.05	287.46
				<b>226.68</b>	<b>235.86</b>	<b>229.36</b>	<b>224.77</b>

OMSA 54	10	8	0.80	206.42	233.95	221.71	212.54
OMSA 55	10	8	0.80	249.24	275.23	263.00	253.82
OMSA 36	10	8	0.81	211.01	235.47	224.77	217.13
				<b>222.22</b>	<b>248.22</b>	<b>236.49</b>	<b>227.83</b>

**Table 5.3 Initiation Fracture toughness based on stretched zone width method and blunting line equation of TPB specimens of SA333 Gr. 6 steel**

Specimen Designation	Thickness (mm)	Effective Thickness (mm)	$a/W$	$J_{0.2}$	$J_{SZW}$	$J_{SZW}$	$J_{SZW+}$
OMSAT 1	25	20	0.408	288.82	290.52	298.14	302.75
OMSAT 2	25	20	0.401	302.80	310.40	315.22	324.16
				<b>295.81</b>	<b>300.46</b>	<b>306.68</b>	<b>313.46</b>
OMSAT 3	25	20	0.614	318.32	314.99	321.43	327.22
OMSAT 4	25	20	0.603	327.64	336.39	344.72	353.21
				<b>322.98</b>	<b>325.69</b>	<b>333.07</b>	<b>340.21</b>
OMSAT 5	25	20	0.810	389.75	370.03	378.88	386.85
OMSAT 6	25	20	0.804	368.01	368.50	374.22	380.73
				<b>378.88</b>	<b>369.27</b>	<b>376.55</b>	<b>383.79</b>
OMSAT 7	15	12	0.402	298.14	287.46	293.48	296.64
OMSAT 8	15	12	0.405	291.93	287.46	296.58	299.69
				<b>295.03</b>	<b>287.46</b>	<b>295.03</b>	<b>298.17</b>
OMSAT 9	15	12	0.600	307.45	282.88	290.37	296.64
OMSAT 10	15	12	0.597	301.24	275.23	282.61	287.46
				<b>304.35</b>	<b>279.05</b>	<b>286.49</b>	<b>292.05</b>
OMSAT 11	15	12	0.799	302.53	292.05	299.45	308.87
OMSAT 12	15	12	0.805	310.56	301.22	310.56	318.04
				<b>306.54</b>	<b>296.64</b>	<b>305.01</b>	<b>313.46</b>
OMSAT 13	10	8	0.386	312.11	301.22	301.24	308.87
OMSAT 14	10	8	0.402	307.69	299.69	304.20	313.46
				<b>309.90</b>	<b>300.46</b>	<b>302.72</b>	<b>311.16</b>
OMSAT 15	10	8	0.601	315.22	298.17	304.35	310.40
OMSAT 16	10	8	0.598	321.43	316.51	324.53	330.28
				<b>318.32</b>	<b>307.34</b>	<b>314.44</b>	<b>320.34</b>
OMSAT 17	10	8	0.802	322.98	314.99	318.32	325.69
OMSAT 18	10	8	0.797	325.81	324.16	329.03	334.86
				<b>324.39</b>	<b>319.57</b>	<b>323.68</b>	<b>330.28</b>

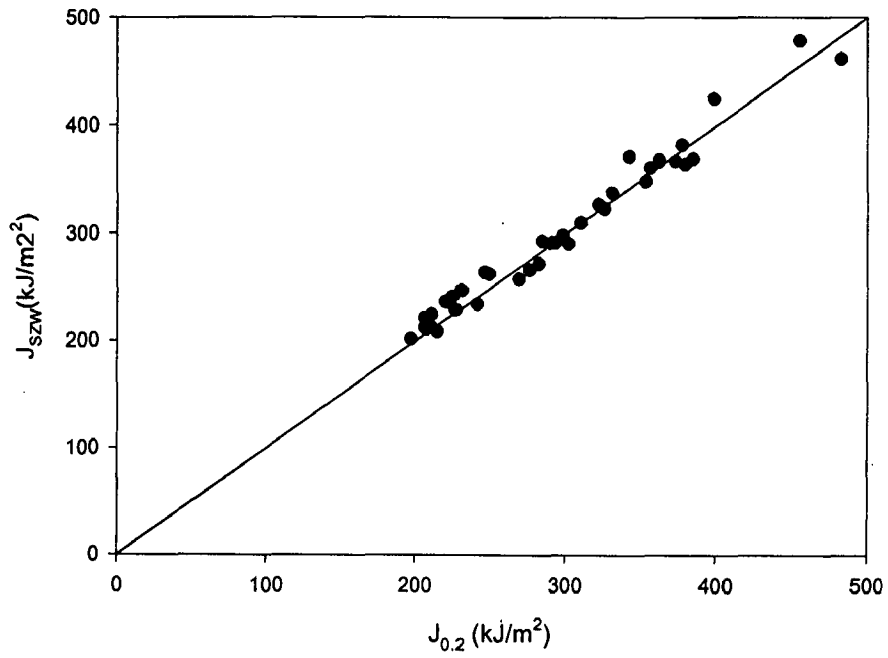


**Fig. 5.5** The comparison of the fracture toughness measured by blunting line method and *SZW* method in the CT specimens of SA333 Gr. 6 steel material.

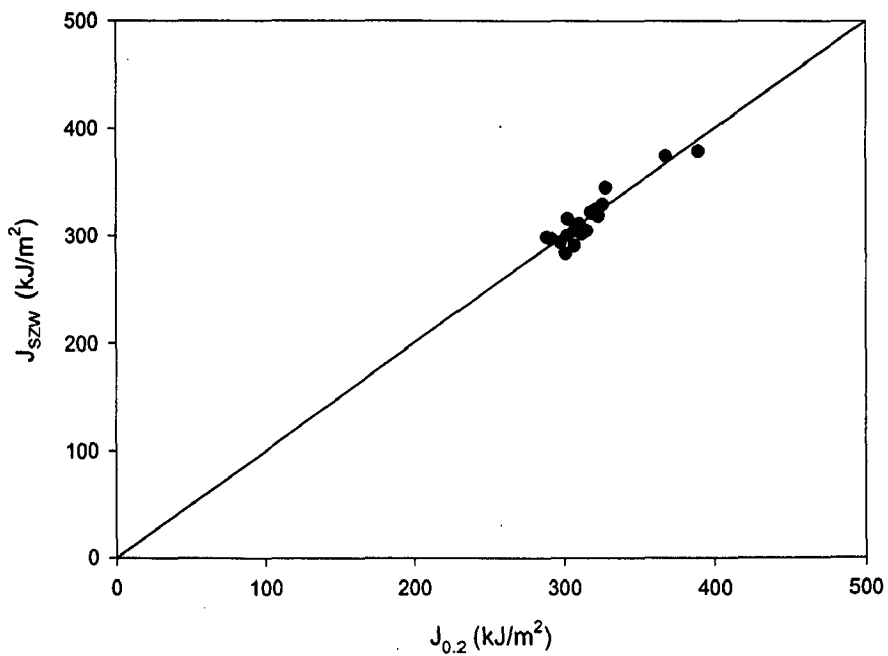


**Fig. 5.6** The comparison of the fracture toughness measured by blunting line method and *SZW* method in the TPB specimens of SA333 Gr. 6 steel material.

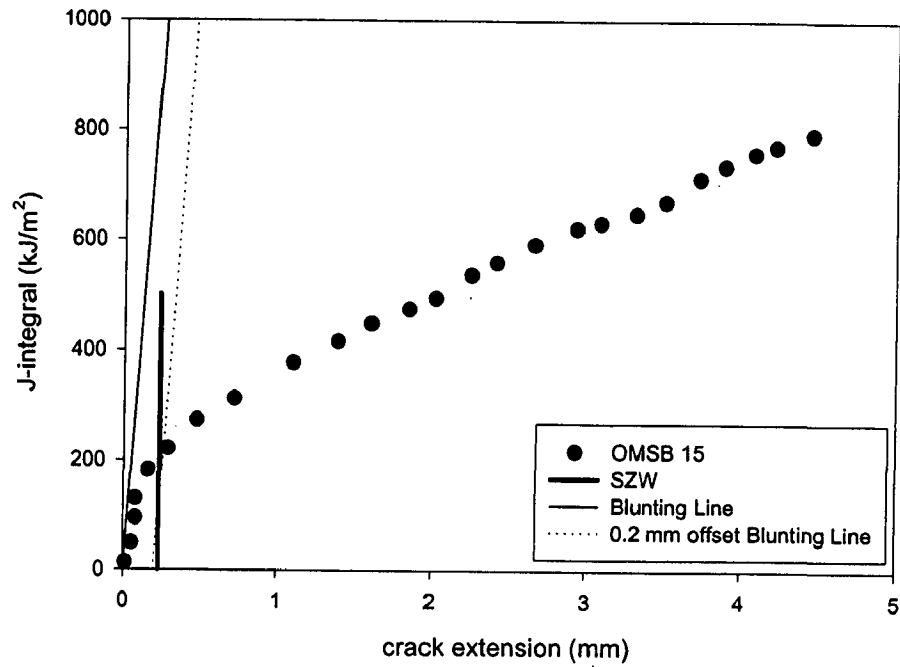


Fig. 5.7 Typical *J-R* curve of SAILMA steel having thickness of 25 mm and *a/W* ratio of 0.4

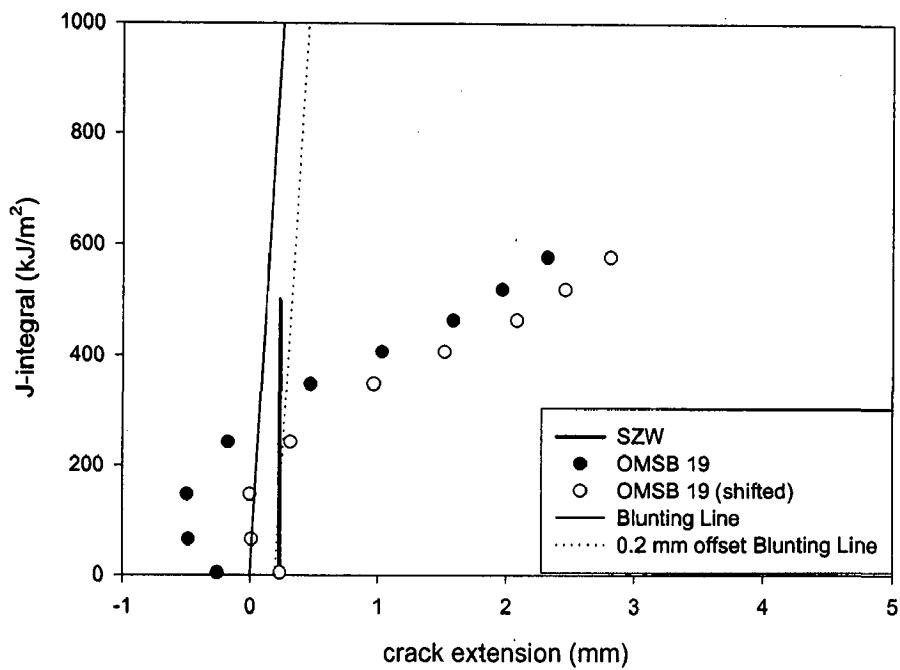


Fig. 5.8 Typical *J-R* curve of SAILMA steel having thickness of 25 mm and *a/W* ratio of 0.4

The initiation fracture toughness based on stretched zone width method and 0.2 mm blunting line equation are evaluated from  $J$ - $R$  curves of CT specimens of SAILMA steel of different  $a/W$  ratio and thickness. The results are summarized in Table 5.4. Table 5.4 reports the value of initiation fracture toughness values evaluated on the basis of 0.2 mm blunting line equation ( $J_{0.2}$ ) and initiation fracture toughness values based on  $SZW_i$  ( $J_{SZW}$ ) for CT specimens of SAILMA steel. Fracture toughness values measured by the stretched zone width method are similar to the fracture toughness values measured by 0.2 mm blunting line equation method.

Figure 5.9 shows the comparison of fracture toughness measured by the 0.2 mm offset blunting line method and fracture toughness measured by  $SZW$  method in CT specimens of SAILMA steel. This figure shows that the fracture toughness measured by the  $SZW$  method and fracture toughness measured by the blunting line are fairly similar.

## **5.2 INFLUENCE OF SPECIMEN THICKNESS AND PRE-CRACK DEPTH ON INITIATION FRACTURE TOUGHNESS ( $J_{IC}$ )**

### **5.2.1 Fracture toughness of SA333 Gr. 6 steel**

The variation of the initiation fracture toughness ( $J_{IC}$ ) with the pre-crack depth ( $a/W$  ratio) for CT specimens of SA333 Gr. 6 steel having thickness of 25 mm, 15 mm and 10 mm are shown in Figs. 5.10, 5.11 and 5.12. Figure 5.10 shows that the initiation fracture toughness values measured by either 0.2 mm blunting line or  $SZW$  method in CT specimens of thickness 25 mm, decreases continuously from around  $\sim 320$  kJ/m<sup>2</sup> to  $\sim 240$  kJ/m<sup>2</sup> as the pre-crack depth increases from 0.4 to 0.8. The drop in the value of  $J_{IC}$  is more when  $a/W$  ratio increases from 0.6 to 0.8 compared to that observed between  $a/W = 0.4$  to  $a/W = 0.6$ .



Figure 5.11 shows that the initiation fracture toughness values measured by either 0.2 mm blunting line or *SZW* method in 15 mm thick CT specimens decreases from  $\sim 410 \text{ kJ/m}^2$  to  $\sim 340 \text{ kJ/m}^2$  as the pre-crack depth increases from 0.4 to 0.6 but in the specimens having pre-crack depth 0.8, the initiation fracture toughness increases to  $\sim 378 \text{ kJ/m}^2$ .

Figure 5.12 shows that the initiation fracture toughness values measured by either 0.2 mm blunting line or *SZW* method in 10 mm thick CT specimens of SA333 Gr. 6 steel decreases drastically from  $\sim 330 \text{ kJ/m}^2$  to  $\sim 230 \text{ kJ/m}^2$  as the pre-crack depth increases from 0.4 to 0.6 but in the specimens having pre-crack depth 0.8 it increases marginally to  $\sim 235 \text{ kJ/m}^2$ .

From the results on initiation fracture toughness for CT specimens of SA333 Gr. 6 steel it appears that in a relatively thin specimens there is drastic reduction in  $J_{IC}$  when pre-crack depth increases from  $a/W$  ratio of 0.4 to 0.6 and  $J_{IC}$  changes marginally from  $a/W$  ratio of 0.6 to 0.8. But at larger thickness of 25 mm, there is significant reduction in  $J_{IC}$  with increasing  $a/W$  ratio in the entire range from 0.4 to 0.8. However, the extent of reduction of  $J_{IC}$  with increasing  $a/W$  ratio from 0.6 to 0.8 is relatively more compared to that between  $a/W = 0.4$  to  $a/W = 0.6$ .

The variation of the initiation fracture toughness ( $J_{IC}$ ) with the pre-crack depth ( $a/W$  ratio) for TPB specimens of SA333 Gr. 6 steel having thickness of 25 mm, 15 mm and 10 mm are shown in Figs. 5.13, 5.14 and 5.15. Figure 5.13 shows that the initiation fracture toughness values measured by either 0.2 mm blunting line or *SZW* method in TPB specimens, increases continuously as the pre-crack depth increases from 0.4 to 0.8. The initiation fracture toughness increases  $\sim 300 \text{ kJ/m}^2$  to  $\sim 330 \text{ kJ/m}^2$  with increasing pre-crack depth of 0.4 to 0.6 from. However, the increase of fracture toughness is relatively larger  $\sim 50 \text{ kJ/m}^2$  when the pre-crack depth increases from 0.6 to 0.8.

**Table 5.4 Initiation Fracture toughness based on stretched zone width method and blunting line equation of CT specimens of SAILMA steel**

Specimen Designation	Thickness (mm)	Effective Thickness (mm)	Width (mm)	$a/W$	$J_{0.2}$	$J_{SZW+}$	$J_{SZW}$	$J_{SZW-}$
OMSB 19	25	20	50	0.397391	200.656	195.41	194.098	194.098
OMSB 20	25	20	50	0.402227	233.443	228.197	225.574	224.262
OMSB 15	25	20	50	0.395391	201.967	201.967	199.344	198.033
					<b>212.022</b>	<b>208.5247</b>	<b>206.3387</b>	<b>205.4643</b>
OMSB 11	25	20	50	0.601672	217.705	213.77	209.836	208.525
OMSB 12	25	20	50	0.604711	188.852	183.607	180.984	179.672
OMSB 14	25	20	50	0.60417	188.852	184.918	183.607	182.295
					<b>198.4697</b>	<b>194.0983</b>	<b>191.4757</b>	<b>190.164</b>
OMSB 16	25	20	50	0.806888	200.656	198.033	195.41	194.098
OMSB 17	25	20	50	0.806716	163.934	161.311	160	158.689
OMSB 18	25	20	50	0.797602	187.541	184.918	183.607	182.295
					<b>184.0437</b>	<b>181.4207</b>	<b>179.6723</b>	<b>178.3607</b>
OMSB 21	20	16	50	0.395621	247.869	240	234.754	228.197
OMSB 22	20	16	50	0.39399	285.902	270.164	264.918	259.672
OMSB 28	20	16	50	0.398949	226.885	226.885	222.951	219.016
					<b>253.552</b>	<b>245.683</b>	<b>240.8743</b>	<b>235.6283</b>
OMSB 9	20	16	50	0.604195	162.623	162.623	161.311	160
OMSB 10	20	16	50	0.607114	125.902	131.148	128.525	127.213
OMSB 27	20	16	50	0.615701	149.508	150.82	148.197	146.885
					<b>146.011</b>	<b>148.197</b>	<b>146.011</b>	<b>144.6993</b>
OMSB 23	20	16	50	0.798423	145.574	142.951	144.262	140.328
OMSB 24	20	16	50	0.79908	145.574	146.885	145.574	144.262
OMSB 29	20	16	50	0.784719	175.738	174.426	171.803	170.492
					<b>155.6287</b>	<b>154.754</b>	<b>153.8797</b>	<b>151.694</b>
OMSB 37	10	8	50	0.403621	139.016	133.77	131.148	128.525
OMSB 38	10	8	50	0.39799	146.885	142.951	137.705	137.705
OMSB 39	10	8	50	0.402549	172.131	167.213	165.574	162.295
					<b>152.6773</b>	<b>147.978</b>	<b>144.809</b>	<b>142.8417</b>
OMSB 31	10	8	50	0.798903	119.344	120.656	119.344	114.098
OMSB 32	10	8	50	0.79488	125.902	135.082	129.836	127.213
OMSB 33	10	8	50	0.794719	132.459	137.705	133.77	128.525
					<b>125.9017</b>	<b>131.1477</b>	<b>127.65</b>	<b>123.2787</b>
OMSB 34	10	8	50	0.603195	98.361	98.361	95.738	95.738
OMSB 35	10	8	50	0.602594	100.984	100.984	99.672	98.361
OMSB 36	10	8	50	0.59957	106.23	110.164	107.541	103.607
					<b>101.8583</b>	<b>103.1697</b>	<b>100.9837</b>	<b>99.23533</b>

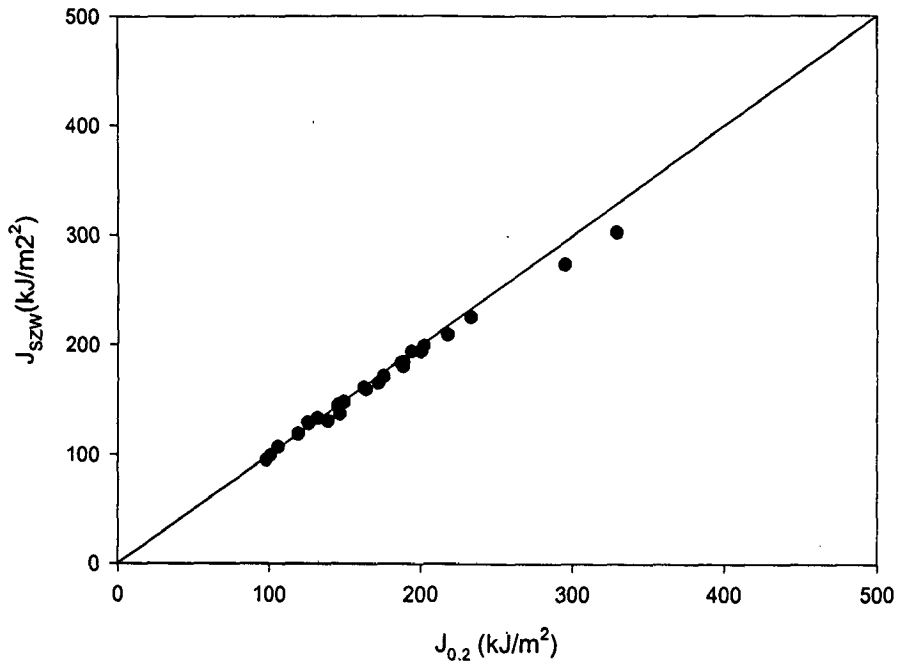


**Fig. 5.9** The comparison of the fracture toughness measured by blunting line method and *SZW* method in the CT specimens of SAILMA steel material.

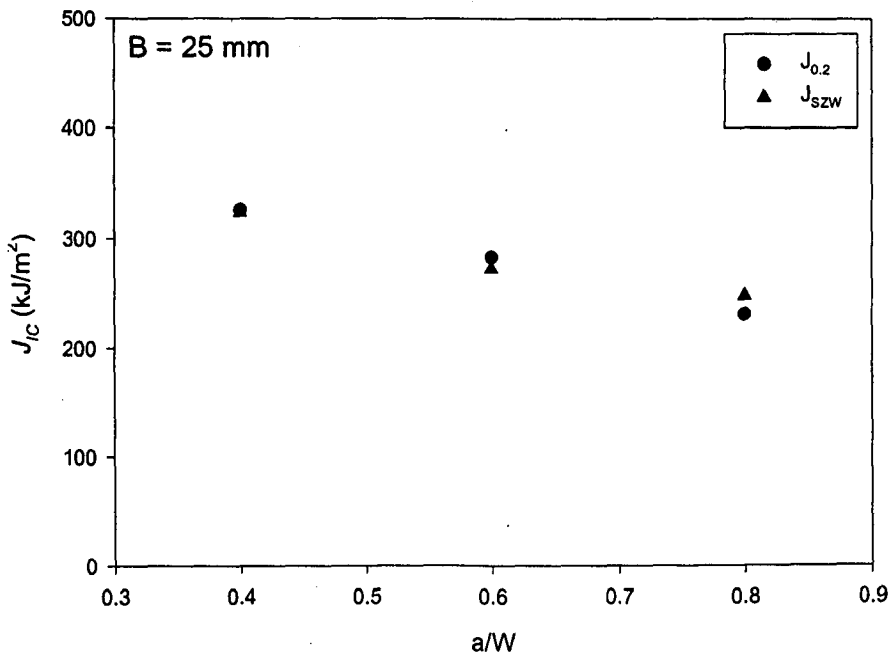


**Fig. 5.10** The variation of the fracture toughness ( $J_{IC}$ ) with the pre-crack depth ( $a/W$  ratio) for 25 mm thickness of the CT specimens of SA333 Gr. 6 steel.

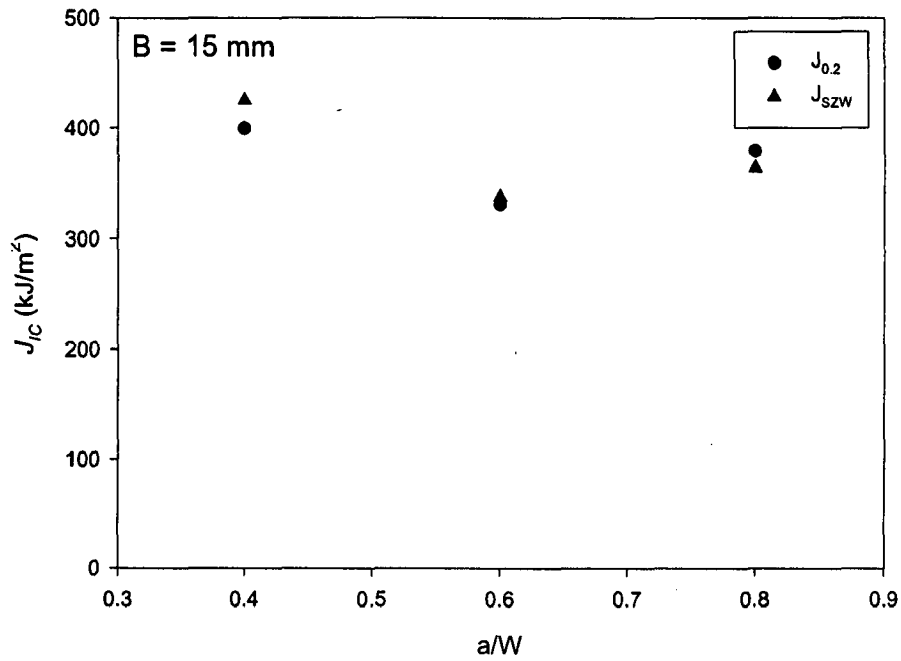


**Fig. 5.11** The variation of the fracture toughness ( $J_{IC}$ ) with the pre-crack depth ( $a/W$  ratio) for 15 mm thickness of the CT specimens of SA333 Gr. 6 steel.

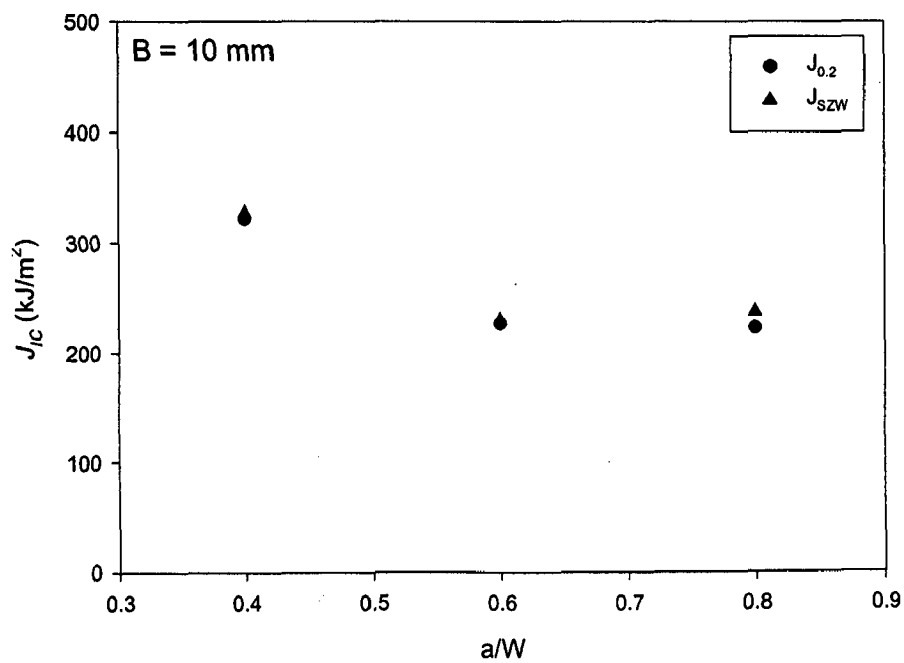


**Fig. 5.12** The variation of the fracture toughness ( $J_{IC}$ ) with the pre-crack depth ( $a/W$  ratio) for 10 mm thickness of the CT specimens of SA333 Gr. 6 steel.

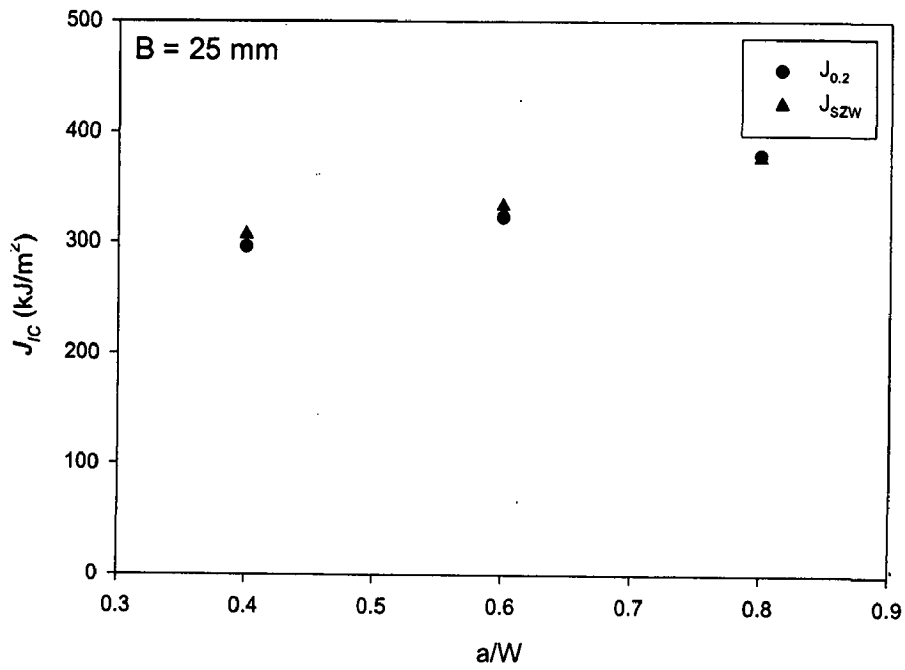


**Fig. 5.13** The variation of the fracture toughness ( $J_{IC}$ ) with the pre-crack depth ( $a/W$  ratio) for 25 mm thickness of the TPB specimens of SA333 Gr. 6 steel.

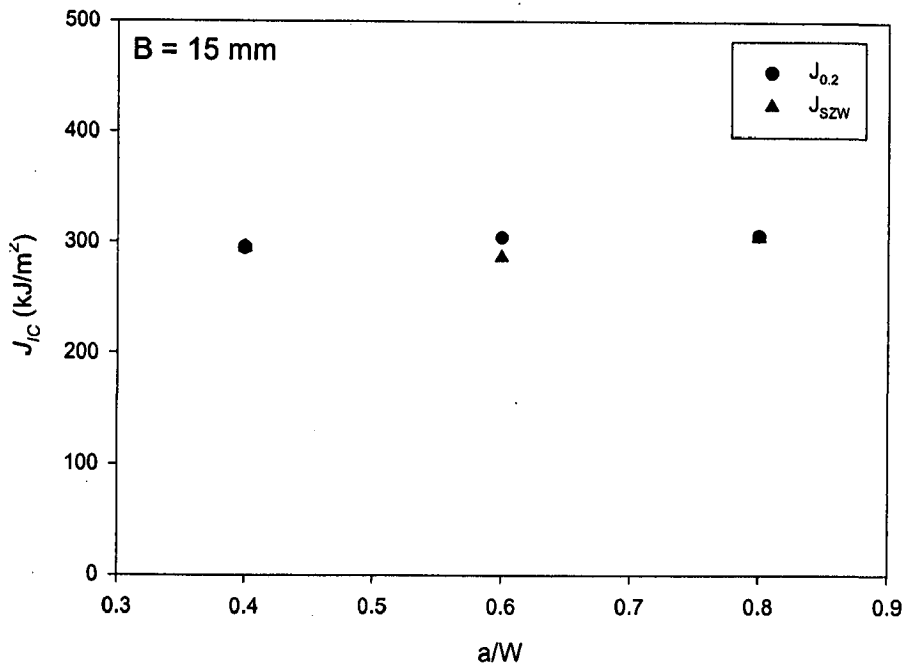


**Fig. 5.14** The variation of the fracture toughness ( $J_{IC}$ ) with the pre-crack depth ( $a/W$  ratio) for 15 mm thickness of the TPB specimens of SA333 Gr. 6 steel.

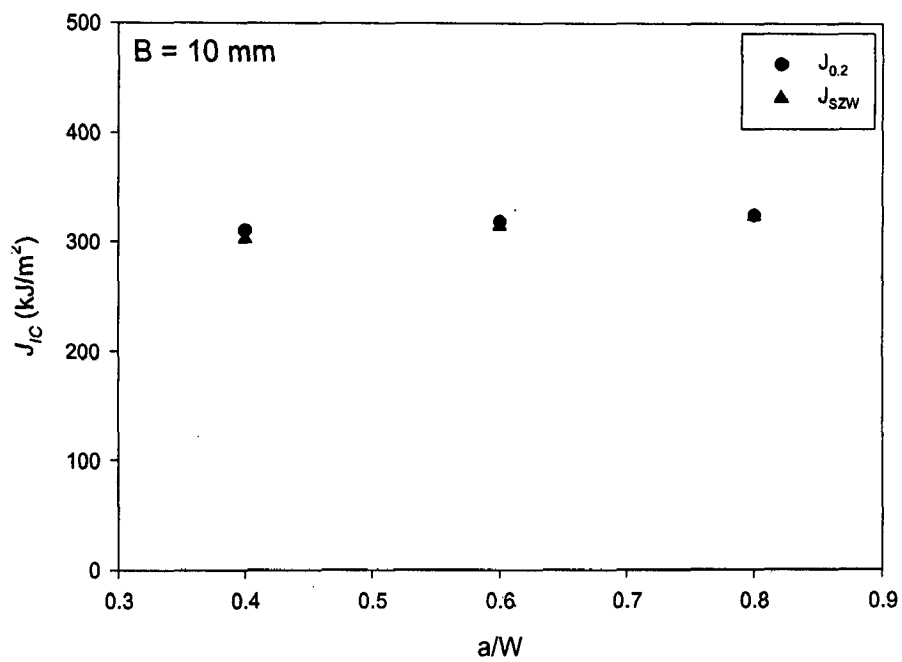


**Fig. 5.15** The variation of the fracture toughness ( $J_{IC}$ ) with the pre-crack depth ( $a/W$  ratio) for 10 mm thickness of the TPB specimens of SA333 Gr. 6 steel.

Figure 5.14 shows that the initiation fracture toughness values measured by either 0.2 mm blunting line or *SZW* method in 15 mm thick TPB specimens increases marginally with the pre-crack depth. The increase in the initiation fracture toughness is about 10 kJ/m<sup>2</sup> for increasing pre-crack depth from 0.4 to 0.8.

Figure 5.15 shows that the initiation fracture toughness values measured by either 0.2 mm blunting line or *SZW* method in 10 mm thick TPB specimens increases with the pre-crack depth. The initiation fracture toughness increases from ~300 kJ/m<sup>2</sup> to ~315 kJ/m<sup>2</sup> for increasing pre-crack depth from 0.4 to 0.6. A further increase in pre-crack depth to 0.8 increases  $J_{IC}$  to ~330 kJ/m<sup>2</sup> which shows nearly linear variation in initiation fracture toughness with pre-crack depth.

From the results described above, it is evident that the initiation fracture toughness measured on TPB specimens are comparatively less sensitive to variation in pre-crack depth as compared to these measured on CT specimens of SA333 Gr. 6 steel. It is also interesting to note that the fracture toughness generally decreases with increasing  $a/W$  ratio (particularly from 0.4 to 0.6) in CT specimens but it increases with increasing  $a/W$  ratio in TPB specimens.

The variation of the initiation fracture toughness,  $J_{IC}$ , increasing the specimen thickness of CT specimens of SA333 Gr. 6 steel at given pre-crack depths ( $a/W$  ratio) of 0.4, 0.6 and 0.8 are shown in Figs. 5.16, 5.17 and 5.18 respectively. Figure 5.16 shows that for a pre-crack depth of 0.4, the initiation fracture toughness measured on CT specimens by 0.2 mm offset blunting line or *SZW* method, increases from ~320 kJ/m<sup>2</sup> to ~400 kJ/m<sup>2</sup> when the specimen thickness increases from 10 mm to 15 mm but a further increase in thickness to 25 mm results in a decrease of the initiation fracture toughness to about ~330 kJ/m<sup>2</sup>.

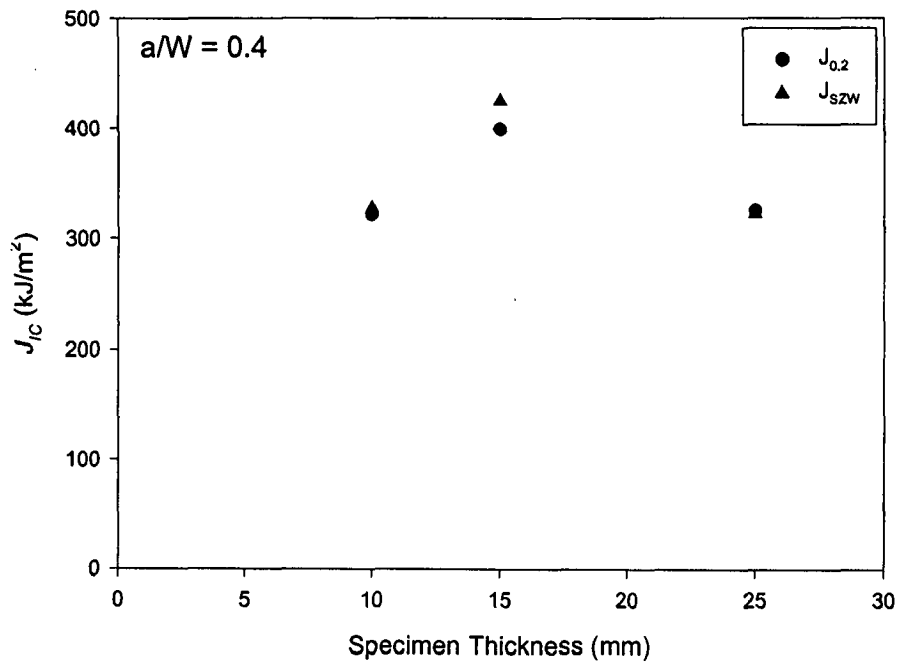
Figure 5.17 shows that for a pre-crack depth of 0.6, the initiation fracture toughness measured on CT specimen by either of 0.2 mm offset blunting line or *SZW* method, increases from  $\sim 230 \text{ kJ/m}^2$  to  $\sim 330 \text{ kJ/m}^2$  as the specimen thickness increases from 10 mm to 15 mm but a further increase of thickness to 25 mm results in decreasing the initiation fracture toughness to about  $\sim 290 \text{ kJ/m}^2$ .

Figure 5.18 shows that for a pre-crack depth of 0.8, the initiation fracture toughness measured on CT specimens by either methods of 0.2 mm offset blunting line or *SZW* method increases from  $\sim 220 \text{ kJ/m}^2$  to  $\sim 370 \text{ kJ/m}^2$  when specimens of pre-crack depth 0.8, increases as the specimen thickness increases from 10 mm to 15 mm a further increases in thickness to 25 mm results in decreasing initiation fracture toughness.

From the results it appears that the initiation fracture toughness measured on CT specimens of lower thickness increases significantly with increasing specimen thickness but as the thickness increases from 15 mm to 25 mm, the initiation fracture toughness decreases for a given pre-crack depth.

The variation of the initiation fracture toughness,  $J_{IC}$ , measured on TPB specimens of SA333 Gr. 6 steel, with increasing specimen thickness at a given pre-crack depth ( $a/W$  ratio) of 0.4, 0.6 and 0.8 are shown in Figs. 5.19, 5.20 and 5.21 respectively. These figures show that the initiation fracture toughness measured by either 0.2 mm offset blunting line or *SZW* method, increase by about  $10 \text{ kJ/m}^2$  as the specimen thickness increases from 15 mm to 25 mm. However, the trend reverses when the specimen thickness decreases from 15 mm to 10 mm and the initiation fracture toughness increases by about  $20 \text{ kJ/m}^2$ . In general, it appears that the fracture toughness is TPB specimen is relatively insensitive to the variation of thickness compared to that measured on CT specimens.





**Fig. 5.16** The variation of the fracture toughness ( $J_{IC}$ ) with the specimen thickness at  $a/W$  ratio of 0.4 in the CT specimens of SA333 Gr. 6 steel.

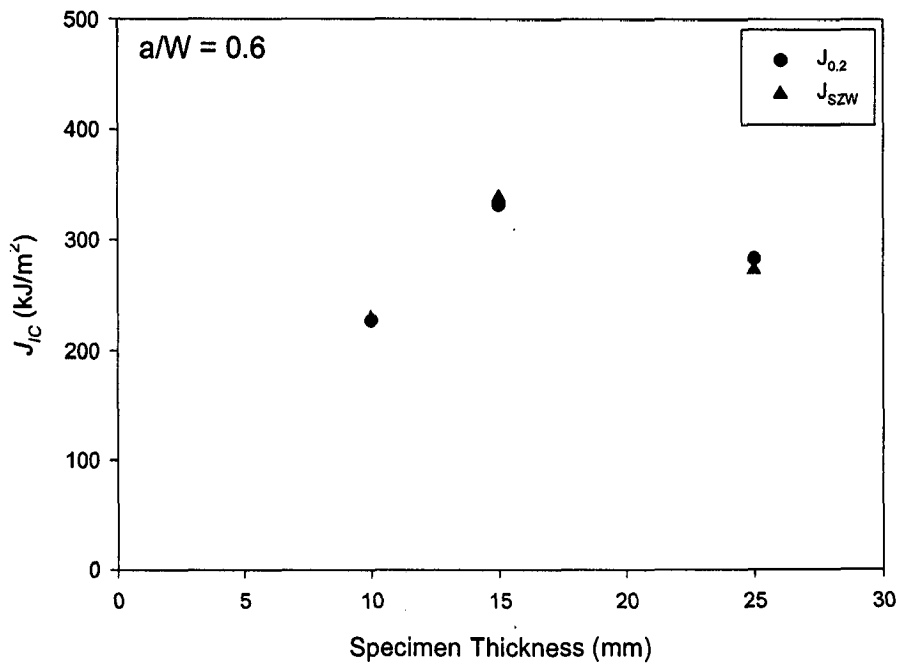


**Fig. 5.17** The variation of the fracture toughness ( $J_{IC}$ ) with the specimen thickness at  $a/W$  ratio of 0.6 in the CT specimens of SA333 Gr. 6 steel.

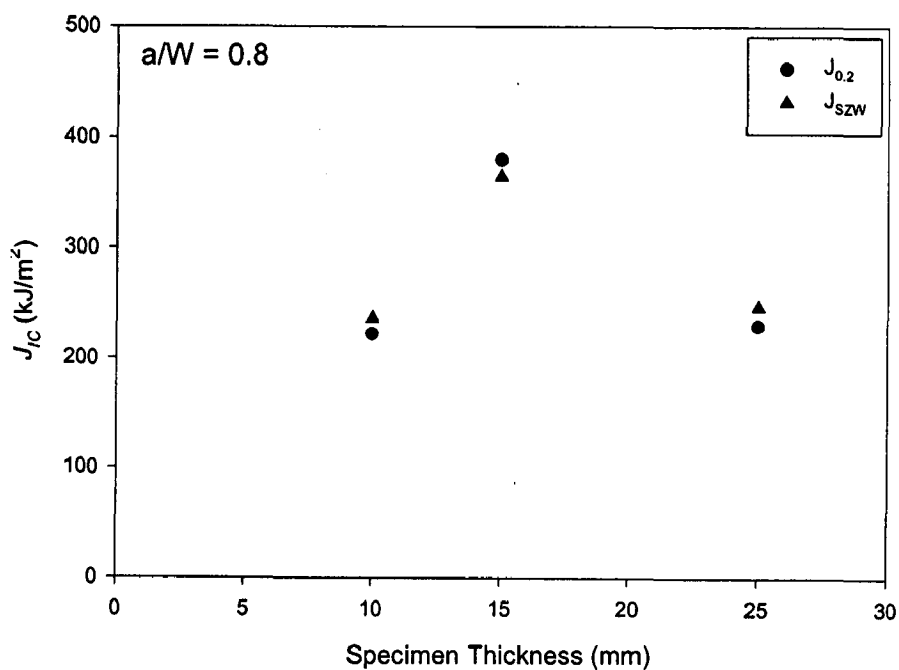


**Fig. 5.18** The variation of the fracture toughness ( $J_{IC}$ ) with the specimen thickness at  $a/W$  ratio of 0.8 in the CT specimens of SA333 Gr. 6 steel.

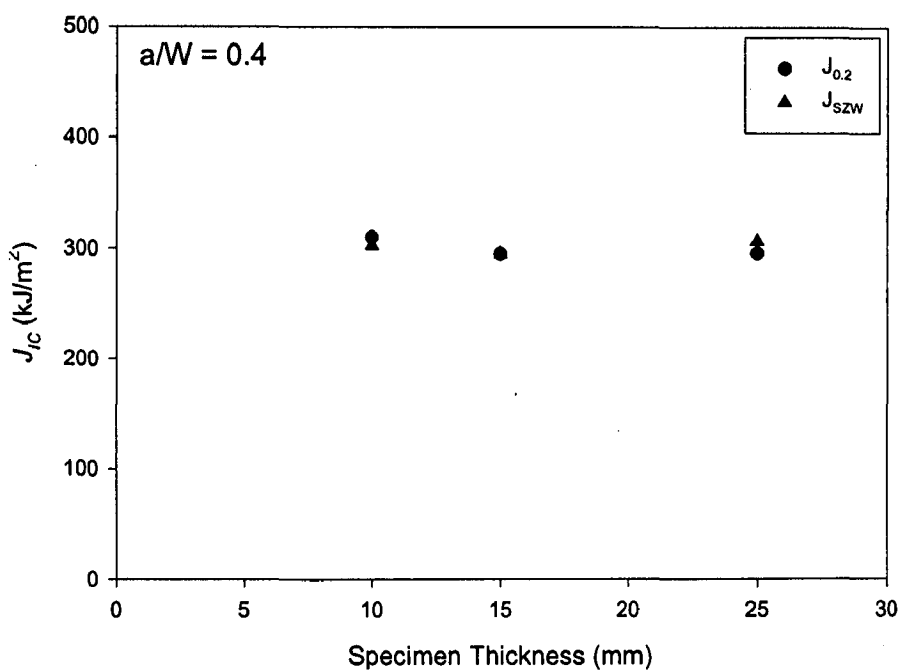


**Fig. 5.19** The variation of the fracture toughness ( $J_{IC}$ ) with the specimen thickness at  $a/W$  ratio of 0.4 in the TPB specimens of SA333 Gr. 6 steel.

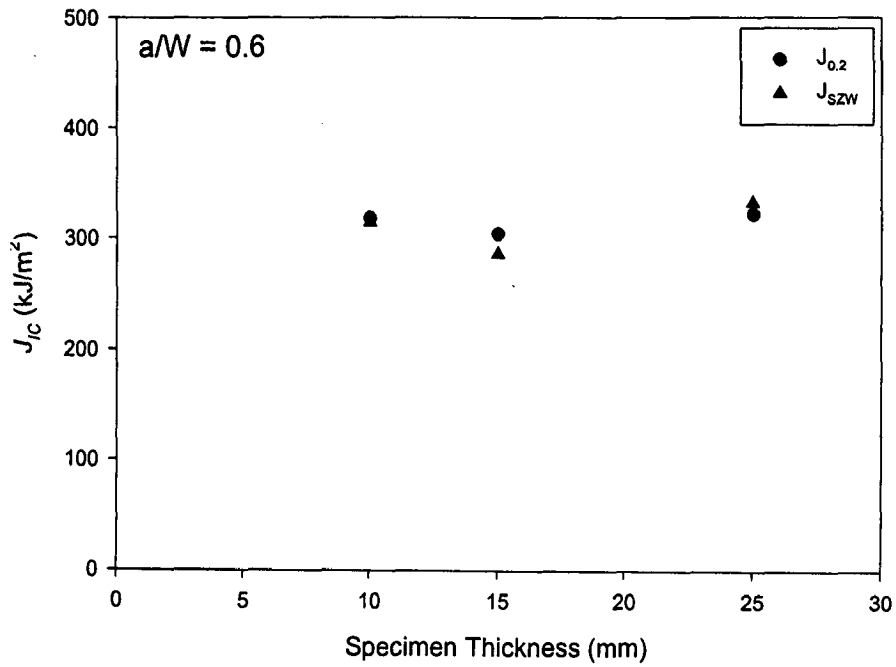


**Fig. 5.20** The variation of the fracture toughness ( $J_{IC}$ ) with the specimen thickness at  $a/W$  ratio of 0.6 in the TPB specimens of SA333 Gr. 6 steel.

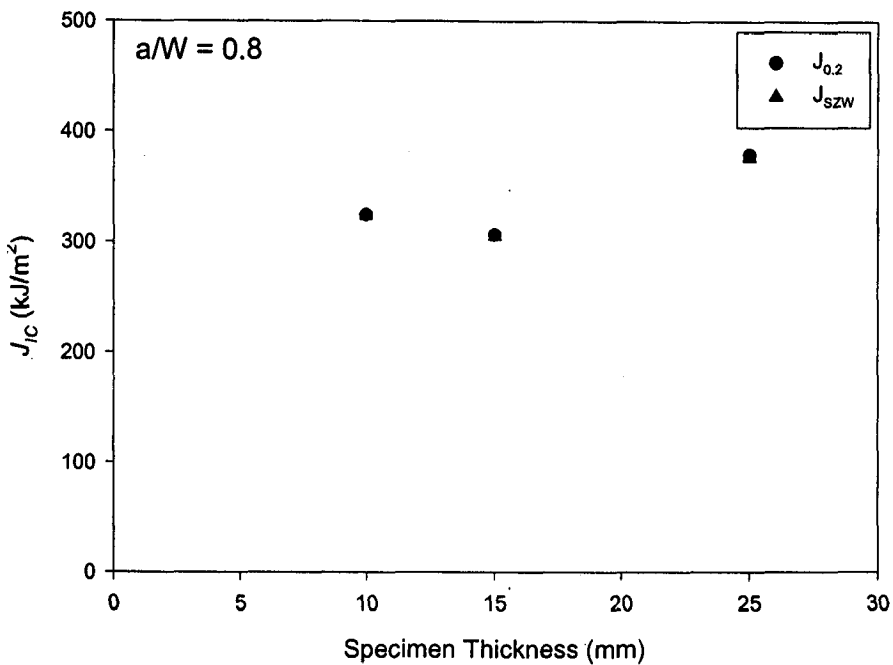


**Fig. 5.21** The variation of the fracture toughness ( $J_{IC}$ ) with the specimen thickness at  $a/W$  ratio of 0.8 in the TPB specimens of SA333 Gr. 6 steel.

## 5.2.2 Fracture toughness of SAILMA steel

The variation of the initiation fracture toughness ( $J_{IC}$ ) with the pre-crack depth ( $a/W$  ratio) for CT specimens of SAILMA steel having thickness of 25 mm, 20 mm and 10 mm are shown in Figs. 5.22, 5.23 and 5.24. Figure 5.22 shows that the initiation fracture toughness values measured by either 0.2 mm blunting line or *SZW* method in CT specimens decreases as the pre-crack depth increases similarly as observed in Fig. 5.10 for CT specimens of SA333 Gr. 6 steel but the extent of lowering is about 30 kJ/m<sup>2</sup>, much less than that observed in SA333 Gr. 6 steel.

Figure 5.23 shows that for specimens of 20 mm thickness the initiation fracture toughness values,  $J_{IC}$ , measured by either 0.2 mm blunting line method or *SZW* method, decreases drastically from ~253 kJ/m<sup>2</sup> to ~146 kJ/m<sup>2</sup> when the specimen pre-crack depth increases from 0.4 to 0.6 but thereafter,  $J_{IC}$  increases only marginally for increasing pre-crack depth to 0.8. This behavior is similar to that observed for 15 mm thick specimen of SA333 Gr. 6 steel as shown in Fig. 5.11.

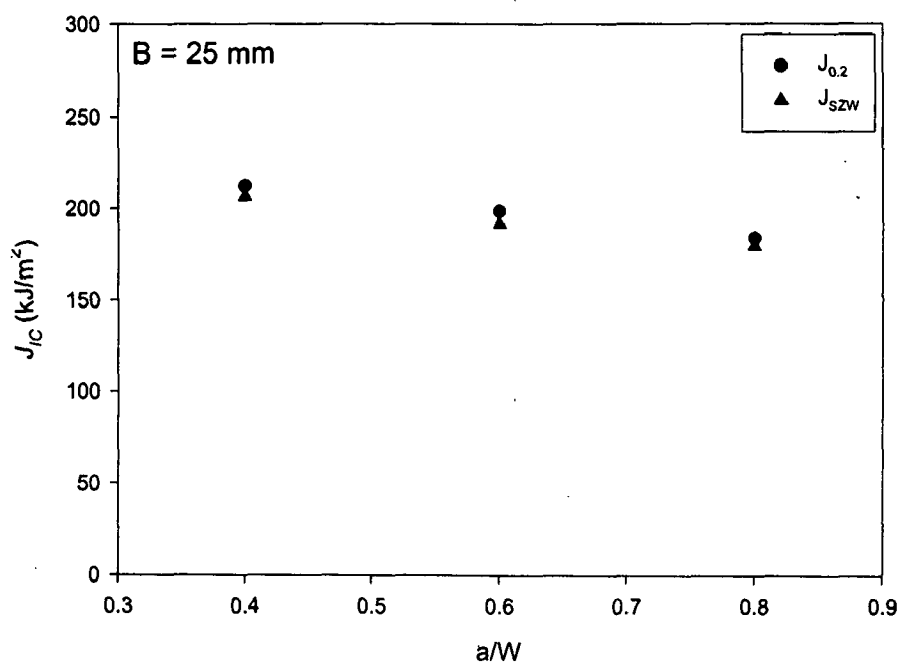
Figure 5.24 shows that for specimens of 10 mm thickness, the initiation fracture toughness values measured either by 0.2 mm blunting line method or *SZW* method, decreases from ~152 kJ/m<sup>2</sup> to ~101 kJ/m<sup>2</sup> when pre-crack depth increases from 0.4 to 0.6, but thereafter,  $J_{IC}$  increases to 125 kJ/m<sup>2</sup> for increasing pre-crack depth to 0.8. This behavior is again similar to that observed in 10 mm thick specimen of SA333 Gr. 6 steel as shown in Fig. 5.12

From the results on  $J_{IC}$  described above it appears that at higher thickness, the effect of changing pre-crack depth is relatively small at higher thickness but at lower thickness, there is a drastic reduction in  $J_{IC}$  when pre-crack depth increases from  $a/W$  ratio of 0.4 to 0.6. The variation of initiation fracture toughness with pre-crack depth in SAILMA steel follows similar trends for different thickness as observed SA333 Gr. 6 steel.

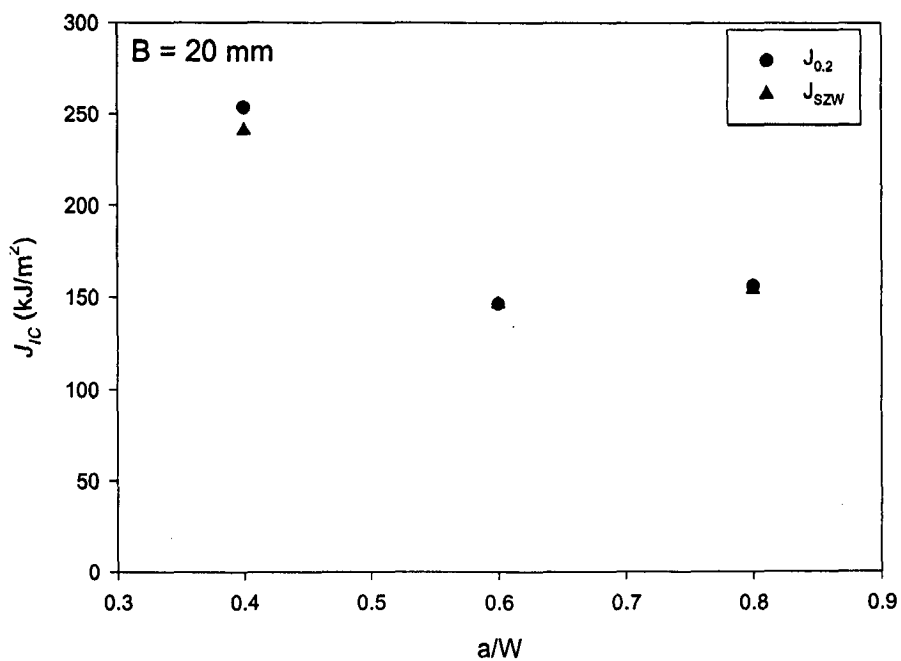
The variation of the initiation fracture toughness,  $J_{IC}$ , with the specimen thickness of CT specimens of SAILMA steel at pre-crack depths ( $a/W$  ratio) of 0.4, 0.6 and 0.8 are shown in Figs. 5.25, 5.26 and 5.27 respectively. Figure 5.25 shows that the fracture toughness increases from  $\sim 150 \text{ kJ/m}^2$  to  $\sim 250 \text{ kJ/m}^2$  when the specimen thickness increases from 10 mm to 20 mm but on increasing the thickness further to 25 mm, the fracture toughness decreases to  $\sim 210 \text{ kJ/m}^2$ . The trend of variation in Fig. 5.25 is similar to that observed for CT specimens of SA333 Gr. 6 steel as shown in Fig. 5.16.

Figure 5.26 shows that the fracture toughness at pre-crack depth of 0.6, measured either by 0.2 mm offset blunting line or *SZW* method, increases significantly with increasing specimen thickness. The initiation fracture toughness is  $\sim 100 \text{ kJ/m}^2$  in 10 mm thick specimens and it increases almost linearly to  $\sim 200 \text{ kJ/m}^2$  observed in the specimens of 25 mm thickness. It may be noted that for a pre-crack depth of 0.6, fracture toughness of SA333 Gr. 6 steel decreases when thickness increases from 15 to 25 mm as shown in Fig. 5.17 but here in SAILMA steel the fracture toughness goes on increasing with increasing thickness even upto 25 mm.

Figure 5.27 shows the variation of initiation fracture toughness with increasing thickness as measured either by the methods of 0.2 mm offset blunting line or *SZW* method, in the specimens of pre-crack depth 0.8. This figure shows similar trend as that observed in the specimens of pre-crack depth of 0.6 where the initiation fracture toughness increases almost linearly with the specimen thickness. At the same pre-crack of 0.8, the fracture toughness measured on CT specimens of SA333 Gr.6 steel decreases when the thickness increases for 15 mm to 25 mm as shown in Fig. 5.18 but there is not much decrease observed in SAILMA steel when thickness increases from 20 mm to 25 mm.



**Fig. 5.22** The variation of the fracture toughness ( $J_{IC}$ ) with the pre-crack depth ( $a/W$  ratio) for 25 mm thickness of the CT specimens of SAILMA steel.



**Fig. 5.23** The variation of the fracture toughness ( $J_{IC}$ ) with the pre-crack depth ( $a/W$  ratio) for 20 mm thickness of the CT specimens of SAILMA steel.

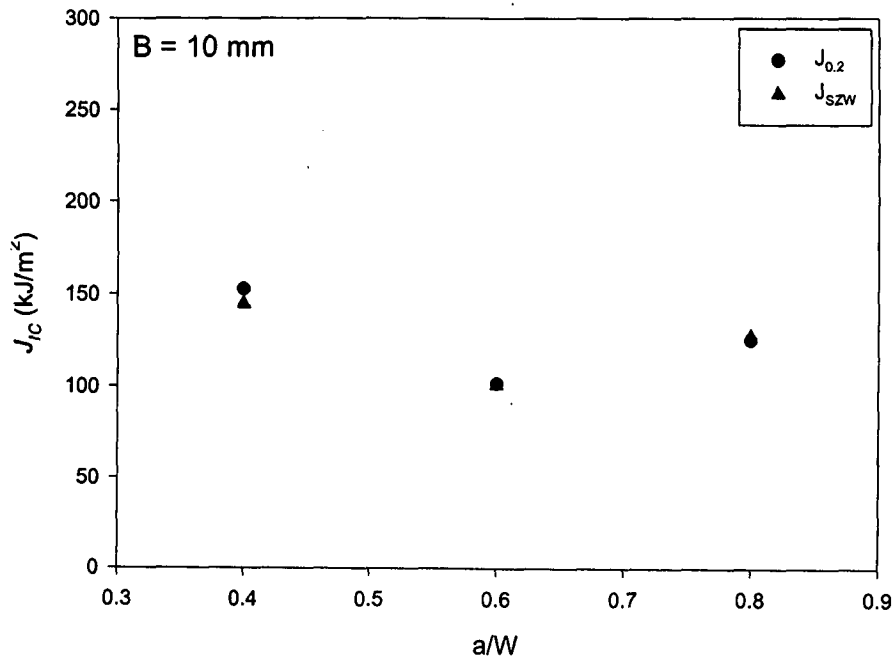


Fig. 5.24 The variation of the fracture toughness ( $J_{IC}$ ) with the pre-crack depth ( $a/W$  ratio) for 10 mm thickness of the CT specimens of SAILMA steel.

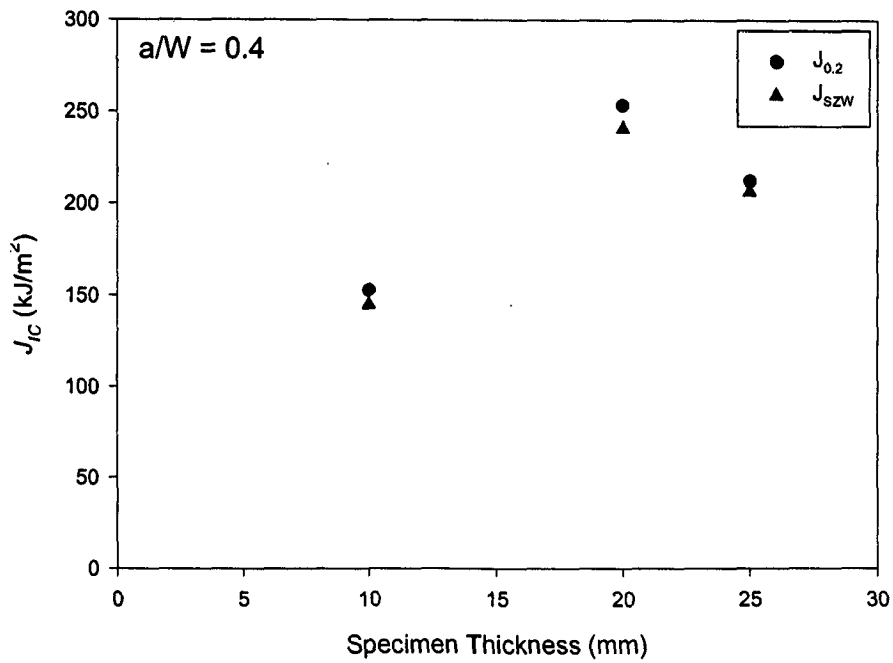
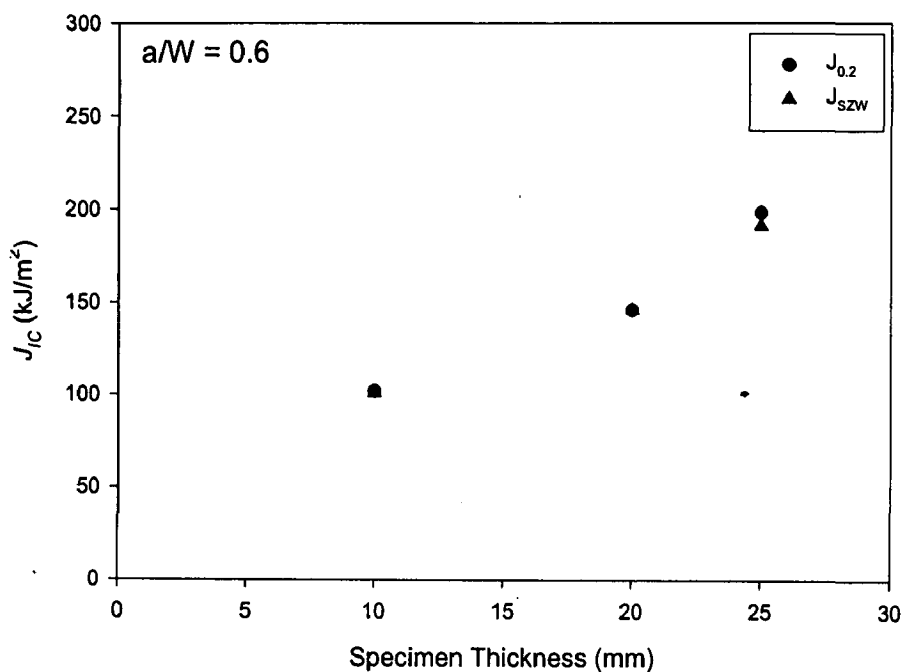
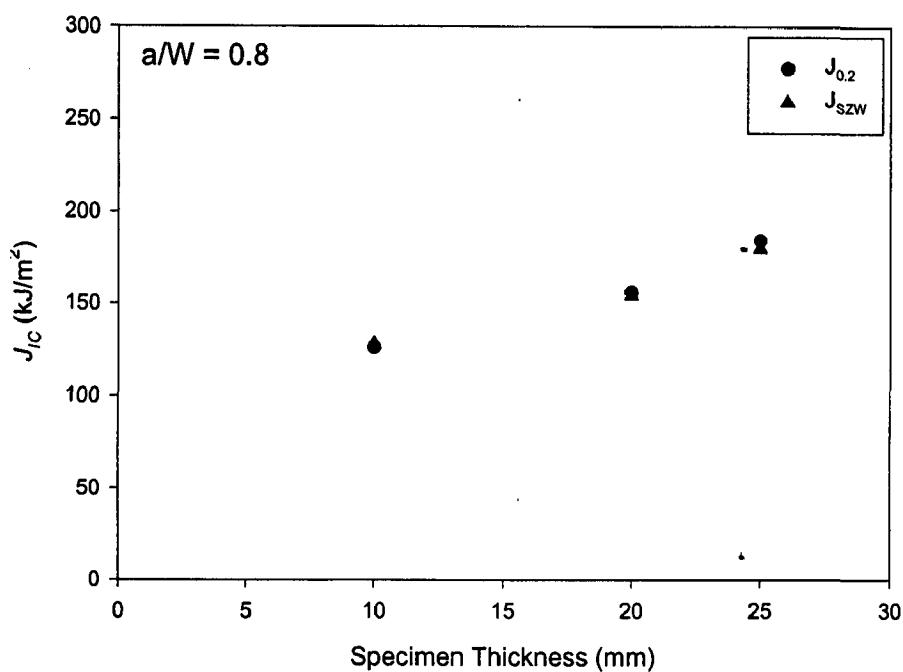


Fig. 5.25 The variation of the fracture toughness ( $J_{IC}$ ) with the specimen thickness at  $a/W$  ratio of 0.4 in the CT specimens of SAILMA steel.



**Fig. 5.26** The variation of the fracture toughness ( $J_{IC}$ ) with the specimen thickness at  $a/W$  ratio of 0.6 in the CT specimens of SAILMA steel.



**Fig. 5.27** The variation of the fracture toughness ( $J_{IC}$ ) with the specimen thickness at  $a/W$  ratio of 0.8 in the CT specimens of SAILMA steel.



### 5.3 INFLUENCE OF COMPOSITION AND HEAT TREATMENT ON $J_{IC}$

The ferritic-pearlitic steels investigated in the present study has a spectrum of mechanical properties obtained either through variation in composition or different heat treatments as described in the previous chapter. Table 5.5 gives the initiation fracture toughness as observed in different low carbon steels along with their mechanical properties. It is observed that with the limited variation of composition and heat treatment in low carbon steels investigated here, initiation fracture toughness closely follows the observed ductility, obliterating the variations in strength.

**Table 5.5 The initiation fracture toughness as observed in different low carbon steels along with their mechanical properties.**

Material		$J_{IC}$ (kJ/m <sup>2</sup> )	YS (MPa)	TS (MPa)	% elong.	Strain hardening coefficient (n)
SA333 Gr. 6 Steel	As received	324.59	318.47	445.86	38.0	4.37
	Annealed	285.68	306.00	415.00	36.7	4.83
	Normalised	227.32	327.00	428.00	34.2	5.23
Sailma	As received	222.78	440.43	574.30	28.8	5.5

change in ductility in FT  
Small but in FT  
change in ductility  
but not in

Figure 5.28 shows the initiation fracture toughness in SA333 Gr. 6 steel measured either by 0.2 mm blunting line or *SZW* method in CT specimens of 25 mm thickness and pre-crack depth of 0.6 after different heat treatments like annealing and normalizing. The initiation fracture toughness in as received SA333 Gr. 6 steel is ~325 kJ/m<sup>2</sup> but it decreases to ~290 kJ/m<sup>2</sup> and ~220 kJ/m<sup>2</sup> after annealing and normalizing respectively. The initiation fracture toughness in as received SAILMA steel is ~222 kJ/m<sup>2</sup>.

## 5.4 INFLUENCE OF SPECIMEN THICKNESS AND PRE-CRACK DEPTH ON *J*-*R* CURVE

### 5.4.1 *J*-*R* curves for SA333 Gr. 6 Steel

The experimental points of fracture toughness,  $J$ , and the corresponding crack extension,  $\Delta a$ , after making correction for negative crack growth, are fitted using a two parameter power law  $J = C_1(\Delta a)^{C_2}$ , where  $C_1$  and  $C_2$  are constants. Figure 5.29 shows the typical experimental points in a CT specimen of SA333 Gr. 6 steel and the fitted *J*-*R* curve shown by the continuous curve. The fitting has been carried out considering the points beyond stretched zone width. The figure shows that the experimental data fit fairly well. Fig. 5.30 shows the *J*-*R* curve plotted after averaging the coefficients of fitted experimental curves of different CT specimens of as received SA333 Gr. 6 steel having thickness of 25 mm and pre-crack depth close to 0.4.

Figures 5.31, 5.32 and 5.33 show *J*-*R* curves plotted after averaging the coefficients of fitted experimental curves obtained from different CT specimens of as received SA333 Gr. 6 steel having pre-crack depths of around 0.4, 0.6 and 0.8 respectively for thicknesses of 10, 15 and 25 mm. Figure 5.31 shows that at a pre-crack depth of 0.4, the crack extension in 15 and 25 mm thick specimens takes place at a higher rate of increase in  $J$  but that in 10 mm thick specimens crack extension takes place more readily at relatively lower rate of increasing  $J$ . For a given value of crack extension, it is interesting to note that 15 mm thick specimen requires a higher value of  $J$  but close to that required in 25 mm thick specimen, which may be due to uncertainty in averaging but 10 mm thick specimen requires a much lower value of  $J$ .

For a pre-crack depth of 0.6, the situation has somewhat altered as shown in Fig. 5.32. For a large crack extension, the  $J$  values of the thickest sample is the highest and the next one is for the thinnest one. The specimen with intermediate thickness shows the lowest  $J$  values. However, it is interesting to note that 15 mm thick specimen requires a higher

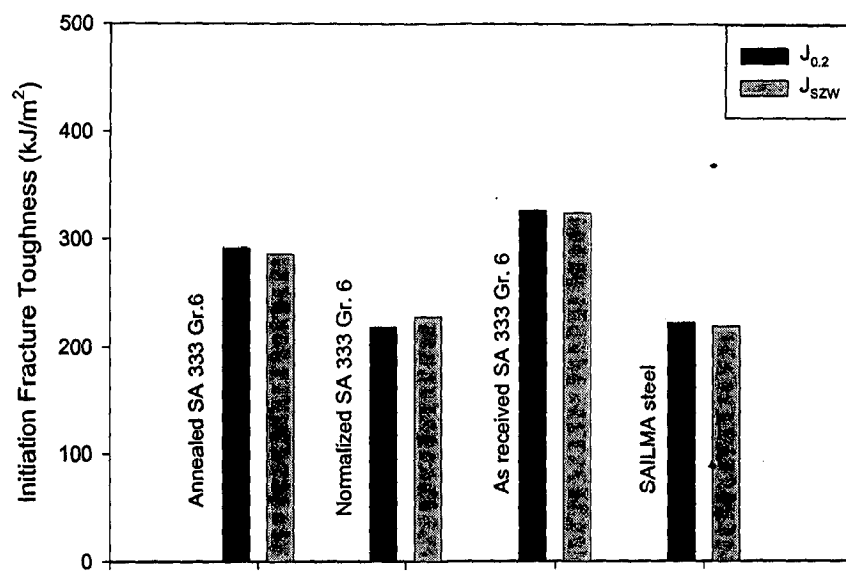


**Fig. 5.28** The initiation fracture toughness of SA333 Gr. 6 steel with or without heat treatment and SAILMA steel as observed in CT specimens of 25 mm thickness and pre-crack depth of 0.6.

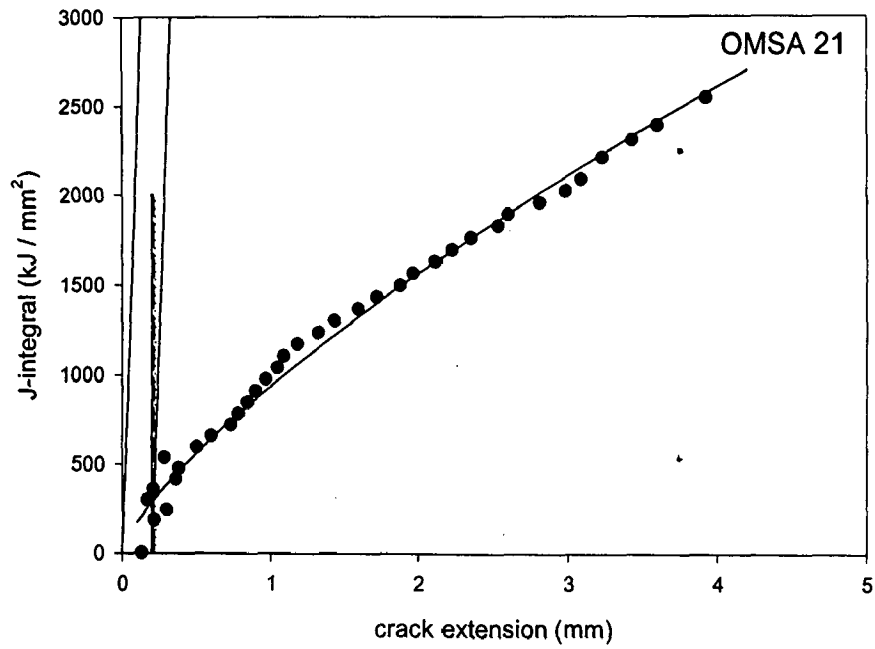


**Fig. 5.29** Power law fit for a Typical *J-R* curve in CT specimen of SA333 Gr. 6 steel.

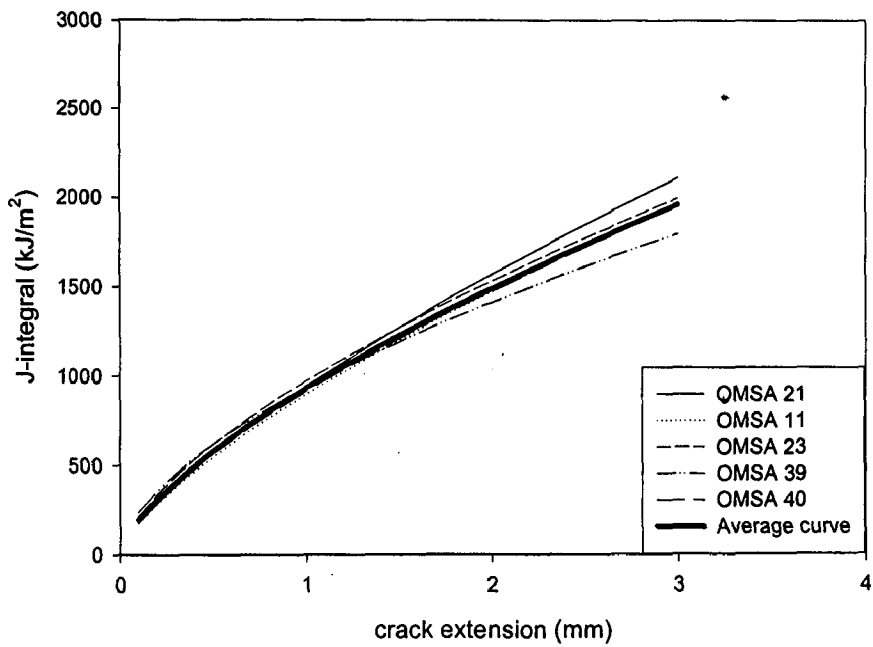


**Fig. 5.30** *J-R* curve plotted after averaging the coefficients of fitted experimental curves of similar parameter from different CT specimens of as received SA333 Gr. 6 steel.

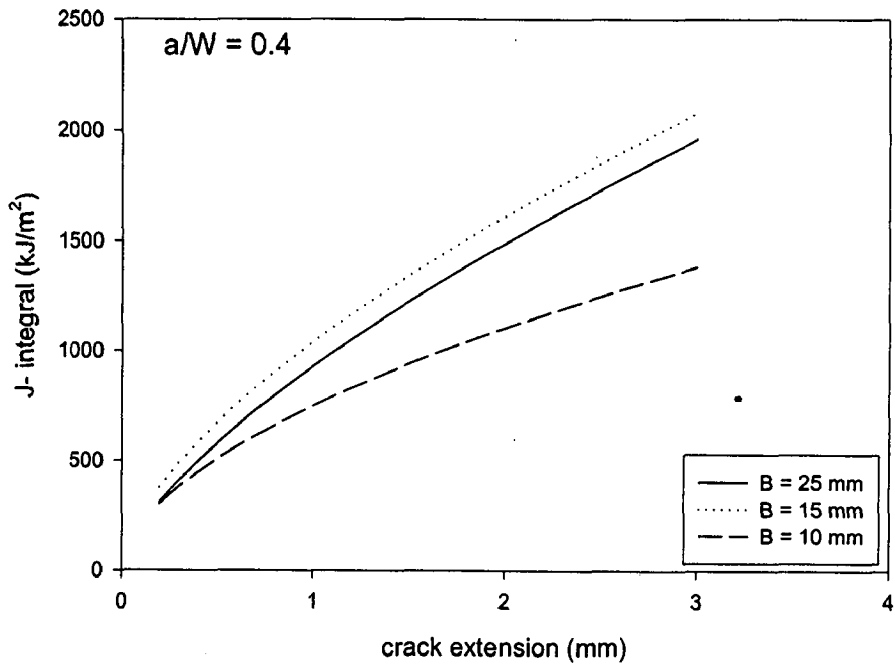


Fig. 5.31 The averaged  $J$ - $R$  curve at pre-crack depth of 0.4 at different thickness of the CT specimens of SA333 Gr. 6 steel.

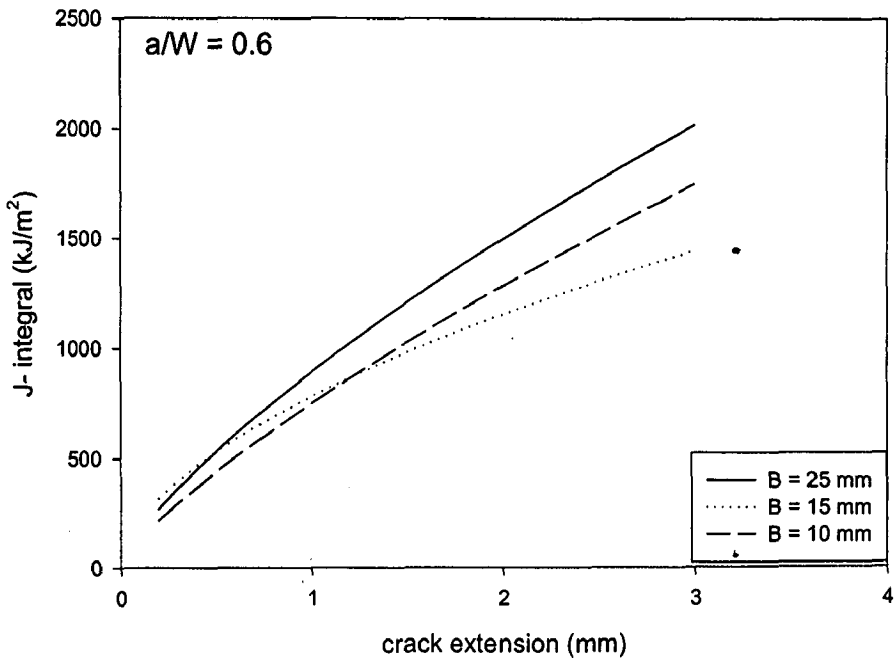
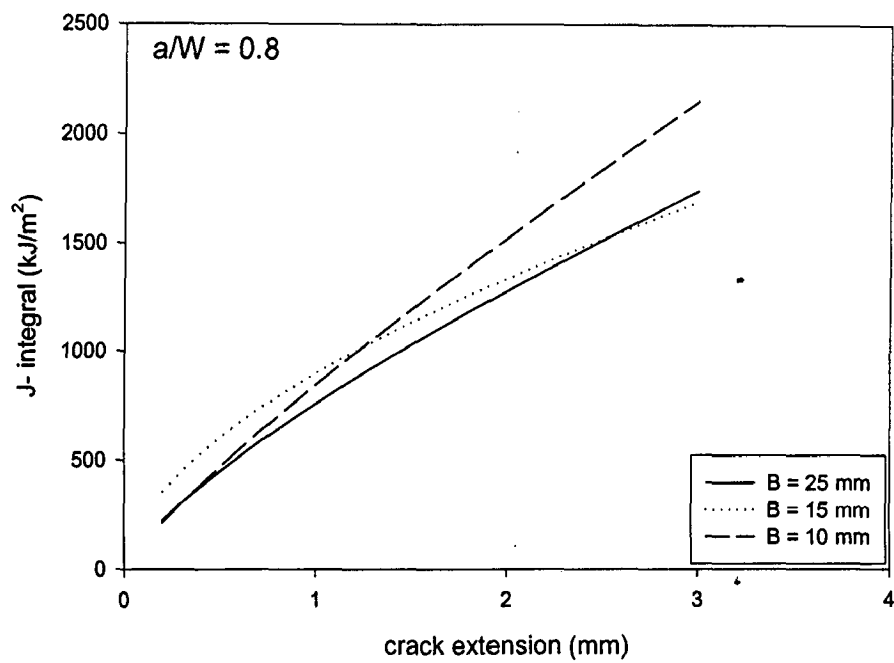


Fig. 5.32 The averaged  $J$ - $R$  curve at pre-crack depth of 0.6 at different thickness of the CT specimens of SA333 Gr. 6 steel.



**Fig. 5.33** The averaged *J-R* curve at pre-crack depth of 0.8 at different thickness of the CT specimens of SA333 Gr. 6 steel.

value of  $J_{IC}$  compared to that in either 25 mm thick or 10 mm thick specimen as shown in Fig. 5.17. The  $J$ - $R$  curve for intermediate thickness starts with a higher slope in the beginning of crack extension and then crosses both the  $J$ - $R$  curves for 25 and 10 mm thick specimens.

Figure 5.33 shows that for a pre-crack depth of 0.8, the rate of increase in  $J$  with crack extension in 10 mm thick specimen is relatively higher at higher crack extension than those observed in either 15 or 25 mm specimens. However, it is observed that the onset of crack propagation takes place at a higher  $J$  in 15 mm thick specimen compared to that in either of 25 mm or 10 mm thick specimens as shown in Fig. 5.18. Although the  $J$ - $R$  curve of specimens of intermediate thickness starts initially at higher  $J$ , it crosses the  $J$ - $R$  curves of specimens of 10 mm and 25 mm thickness. It is interesting to note that  $J$ - $R$  curve of 10 mm and 25 mm thick specimens are very close initially. At higher crack extension, the  $J$ - $R$  curve for 10 mm specimens is at the top, followed by that in 25 mm and 15 mm specimens.

Figures 5.34, 5.35 and 5.36 show  $J$ - $R$  curves plotted after averaging the coefficients of fitted experimental curves obtained from different CT specimens of as received SA333 Gr. 6 steel, for given pre-crack depths of 0.4, 0.6 and 0.8 at thicknesses of 25 mm, 15 mm and 10 mm respectively. Figure 5.34 shows that in the specimens of 25 mm thickness, the  $J$ - $R$  curves at pre-crack depths of 0.4 and 0.6 are very similar, with a higher rate of increase in  $J$  with crack extension. But in specimens of pre-crack depth of 0.8, crack extension takes place more readily at relatively lower rate of increasing  $J$  with crack extension. In terms of absolute value, it is noted that pre-crack depth of 0.4 and 0.6 requires a higher value of  $J$  for the onset of crack propagation compared to that for pre-crack depth of 0.8.

Figure 5.35 shows that in the specimens of 15 mm thickness, there is a higher rate of increase in  $J$  with crack extension for pre-crack depth of 0.8 compared to that for pre-crack depth of either 0.4 or 0.6. When thickness has decreased from 25 mm to 15 mm, the  $J$ - $R$  curve for pre-crack depth of 0.8 has shifted from the bottom position to the top. But the  $J$ - $R$  curve

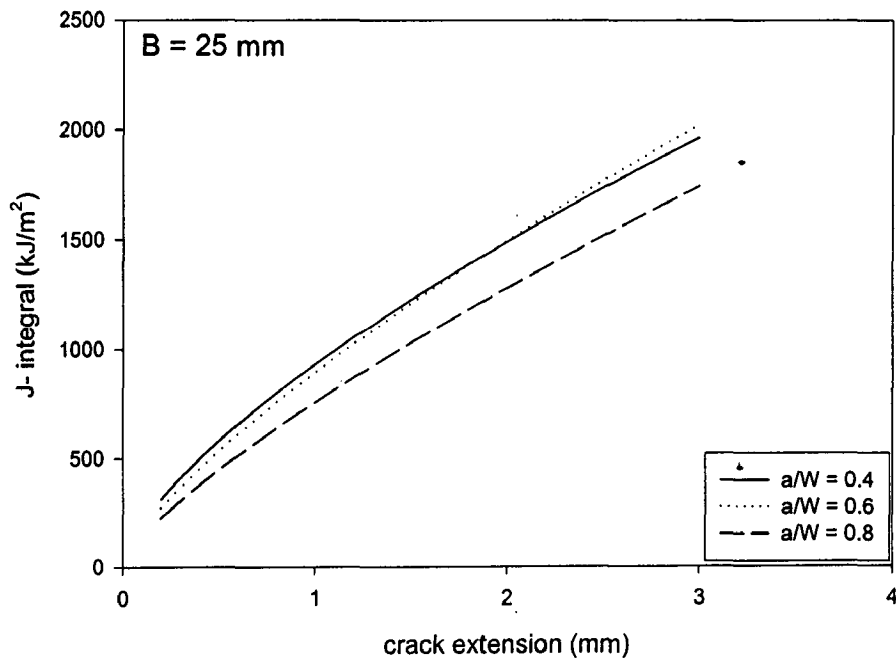
for pre-crack depth of 0.4 has taken a distinct and higher position compared to that for pre-crack depth of 0.6.

Figure 5.36 shows that in the specimens of 10 mm thickness, the rate of increase in  $J$  at higher crack extension increases as pre-crack depth increases from 0.4 to 0.8. Thus, the  $J$ - $R$  curve for pre-crack depth of 0.8 is at the highest similar to that in Fig. 5.35 but only at higher crack extension, the  $J$ - $R$  curve at pre-crack depth 0.6 lies above that at pre-crack depth 0.4 contrary to that observed in Fig. 5.35. However, in the region of relatively lower crack extension the  $J$ - $R$  curve for pre-crack depth of 0.4 is at top and it crosses the  $J$ - $R$  curve for pre-crack depth of 0.8 and 0.6, to reach the bottom position at higher crack extension. However, it is observed that the specimen at pre-crack depth of 0.4 requires higher value of  $J$  to initiate the crack compared to those in specimens of 0.6 and 0.8 pre-crack depths.

Figures 5.34, 5.35 and 5.36 clearly shows that as the thickness decreases from 25 mm to lower values,  $J$ - $R$  curve for the higher pre-crack depths comes to the top position and the  $J$ - $R$  curve for a pre-crack depth of 0.4 eventually reaches the bottom position.

Figures 5.37, 5.38 and 5.39 show  $J$ - $R$  curves plotted after averaging the coefficients of fitted experimental curves obtained from different TPB specimens of as received SA333 Gr. 6 steel, for different thicknesses of 10, 15 and 25 mm tested at different pre-crack depths of 0.4, 0.6 and 0.8 respectively. These figures shows that as the specimen thickness increases crack extension takes place at a higher rate of increase in  $J$  placing  $J$ - $R$  curve of relatively thicker specimens them above the  $J$ - $R$  curve of thinner specimens right from the initial stage. This scenario remains unaltered for the range of pre-crack depth investigated.





**Fig. 5.34** The averaged *J-R* curve of 25 mm thickness at different *a/W* ratio of the CT specimens of SA333 Gr. 6 steel.

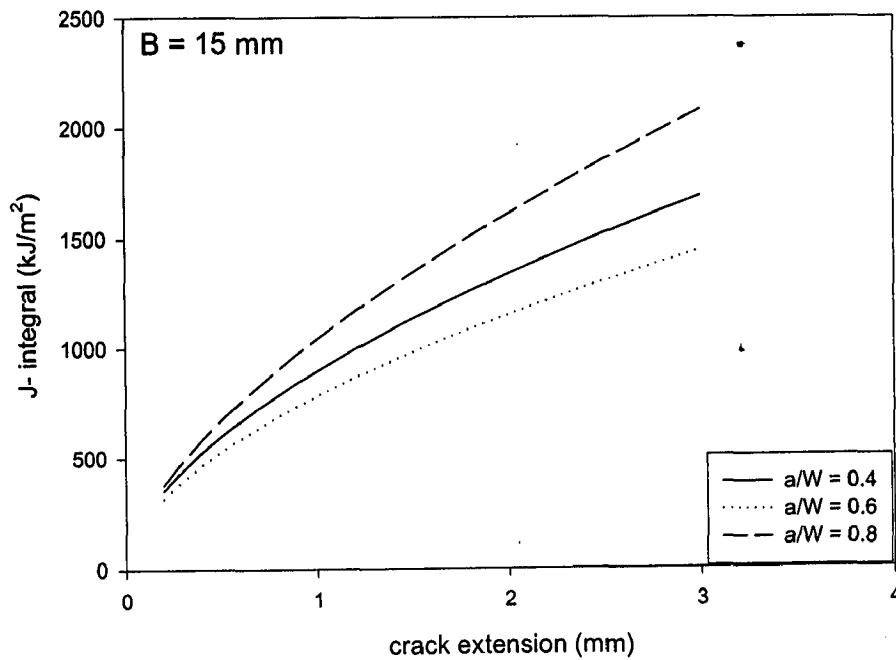


**Fig. 5.35** The averaged *J-R* curve of 15 mm thickness at different *a/W* ratio of the CT specimens of SA333 Gr. 6 steel.

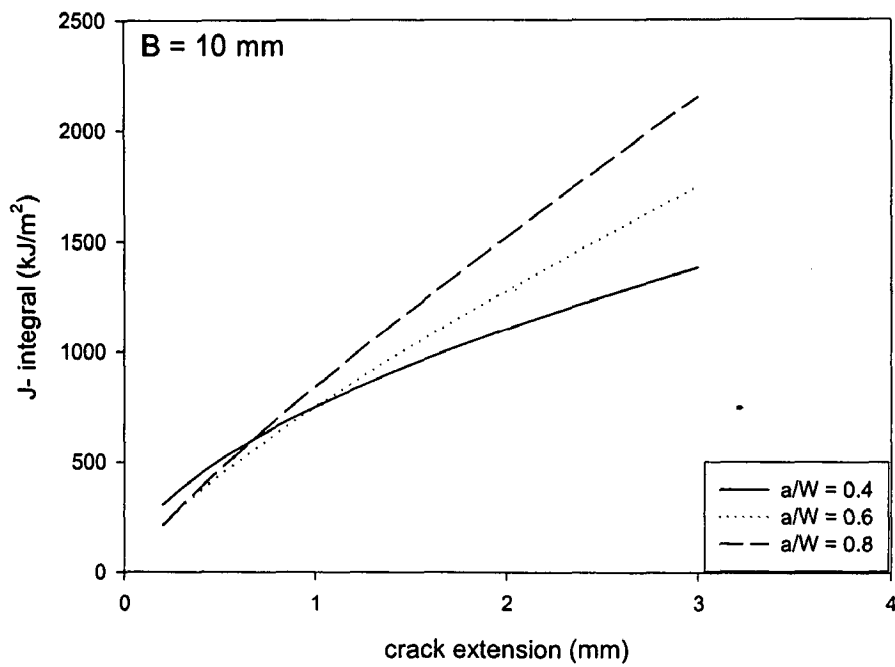


**Fig. 5.36** The averaged  $J$ - $R$  curve of 10 mm thickness at different  $a/W$  ratio of the CT specimens of SA333 Gr. 6 steel.

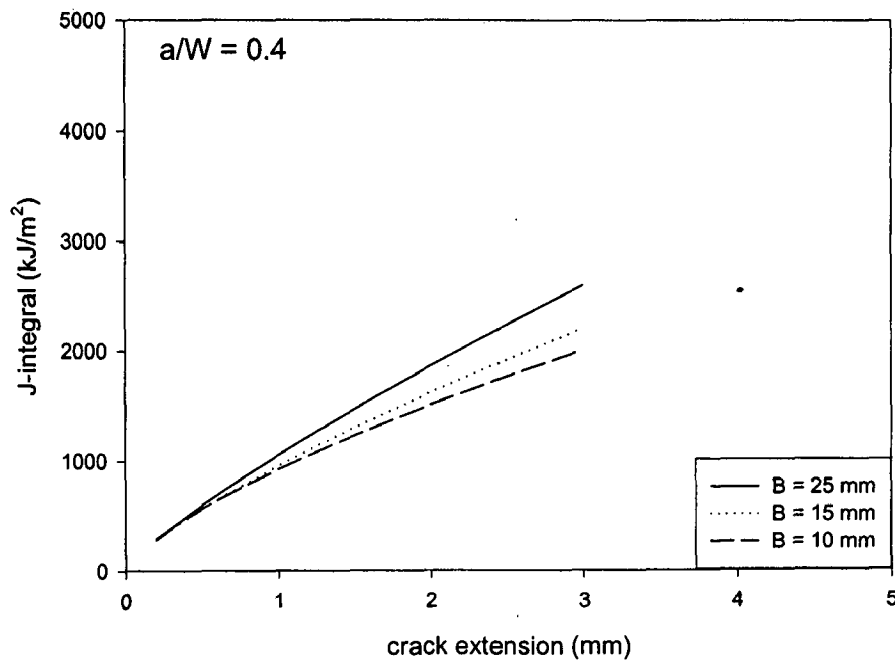


**Fig. 5.37** The averaged  $J$ - $R$  curve at pre-crack depth of 0.4 at different thickness of the TPB specimens of SA333 Gr. 6 steel.

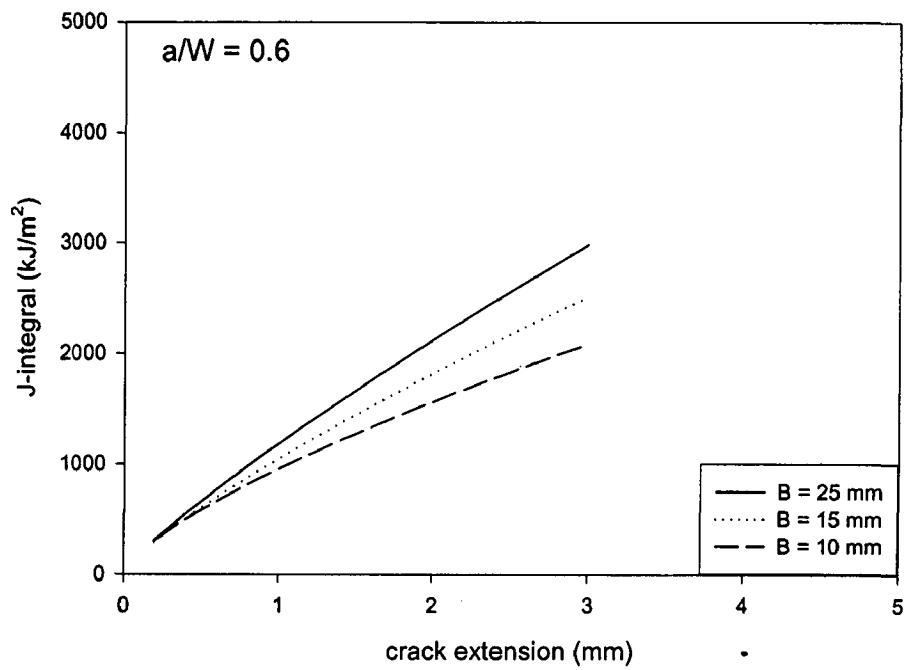


**Fig. 5.38** The averaged *J-R* curve at pre-crack depth of 0.6 at different thickness of the TPB specimens of SA333 Gr. 6 steel.

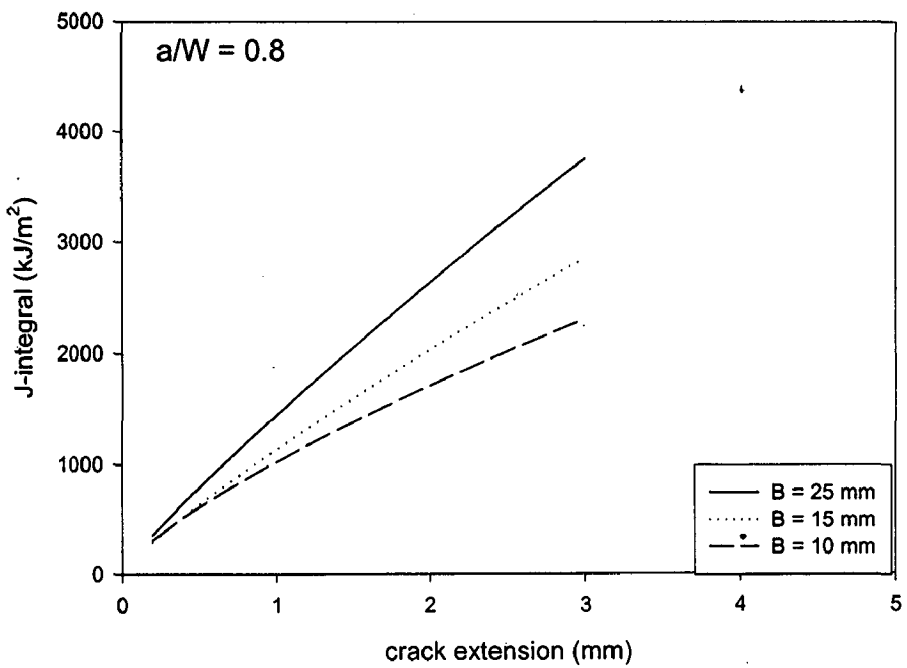


**Fig. 5.39** The averaged *J-R* curve at pre-crack depth of 0.8 at different thickness of the TPB specimens of SA333 Gr. 6 steel.

Figures 5.40, 5.41 and 5.42 show  $J$ - $R$  curves plotted after averaging the coefficients of fitted experimental curves obtained from different TPB specimens of as received SA333 Gr. 6 steel, for pre-crack depths of 0.4, 0.6 and 0.8 but at different thicknesses of 25 mm, 15 mm and 10 mm respectively. These figures show that as the pre-crack depth increases from 0.4 to 0.8 for specimens of thicknesses of 25 mm, 15mm and 10 mm crack extension takes place at a higher rate of increase in  $J$ , placing the  $J$ - $R$  curve of a specimen of given thickness but higher pre-crack depth above those observed in specimens of the same thickness with lower pre-crack depth. The divergence of the  $J$ - $R$  curves decreases as the specimen thickness decreases from 25 mm to 10 mm.

#### **5.4.2 $J$ - $R$ curves of SAILMA Steel**

Figures 5.43, 5.44 and 5.45 show  $J$ - $R$  curves plotted after averaging the coefficients of fitted experimental curves obtained from specimens of different CT specimens of SAILMA steel, with different thicknesses of 25mm, 20 mm and 10mm but for pre-crack depth of 0.4, 0.6 and 0.8 respectively. Figure 5.43 shows that in the specimens at pre-crack depth of 0.4, the crack extension takes place at a much higher rate of increase in  $J$  in specimens of 20 mm thickness than that observed in specimens of either 25 mm or 10 mm thicknesses where crack extension takes place more readily at relatively lower rate of increasing  $J$ , placing the  $J$ - $R$  curve for intermediate thickness of 20 mm at the top followed by that for 25 mm thick and 10 mm thick specimens.

Figures 5.44 and 5.45 show that at higher pre-crack depths of 0.6 and 0.8 crack extension takes place at a higher rate of increase in  $J$  in relatively thicker specimens compared to that in thin specimens, placing the  $J$ - $R$  curve for 25 mm thick specimens at the top, followed by that for 20 mm and 10 mm thick specimens. But the divergence between the  $J$ - $R$  curves at higher crack extension decreases as the pre-crack depth increases.

The  $J$ - $R$  curve of SAILMA steel follows the same trend as that of SA333 Gr. 6 steel at pre-crack depth of 0.4 as shown in Figs. 5.31 and 5.43 but at higher pre-crack depth, the  $J$ - $R$  curves for SA333 Gr. 6 steel has shown crossover between specimens of different thicknesses as shown in Figs. 5.32 and 5.33 but in SAILMA steel there is no crossover observed at similar pre-crack depths. Also, for SA333 Gr. 6 steel, the  $J$ - $R$  curve for specimens of relatively higher thickness is not always above that for smaller thickness even at higher crack extension.

Figures 5.46, 5.47 and 5.48 show  $J$ - $R$  curves plotted after averaging the coefficients of fitted experimental curves obtained for different CT specimens of SAILMA steel, with pre-crack depths of 0.4, 0.6 and 0.8 but for thickness of 25mm, 15 mm and 10mm respectively. For 25 mm thick specimens, as shown in Fig. 5.46, the crack extension in 0.6 pre-crack depth takes place at a higher rate of increase in  $J$  placing it at the top, followed by  $J$ - $R$  curves of specimens of pre-crack depths of 0.4 and 0.8.

Figures 5.47 and 5.48 show that for specimens of thickness 20 mm and 10 mm, the crack extension at pre-crack depth of 0.4 takes place at a higher rate of increase in  $J$ , followed by that in specimens of pre-crack depth of 0.8 and 0.6. It is interesting to note that the  $J$ - $R$  curve moves from the top position at pre-crack depth 0.4 to the lowest position at higher pre-crack depths while the  $J$ - $R$  curve at higher pre-crack depth of 0.8 moves from the bottom to intermediate position. In SA333 Gr. 6 steel, although the relative positions of  $J$ - $R$  curves are similar at pre-crack depth of 0.4 but the  $J$ - $R$  curve for pre-crack depth of 0.8 is at a higher position in thinner specimens.

## **5.5 INFLUENCE OF COMPOSITION AND HEAT TREATMENT ON $J$ - $R$ CURVE**

Figure 5.49 shows the  $J$ - $R$  curves of annealed and normalized SA333 Gr. 6 steel measured on CT specimens and compares these curves with that observed in as received steels of SA333 Gr. 6 and SAILMA. In the initial part of the  $J$ - $R$  curves at low crack

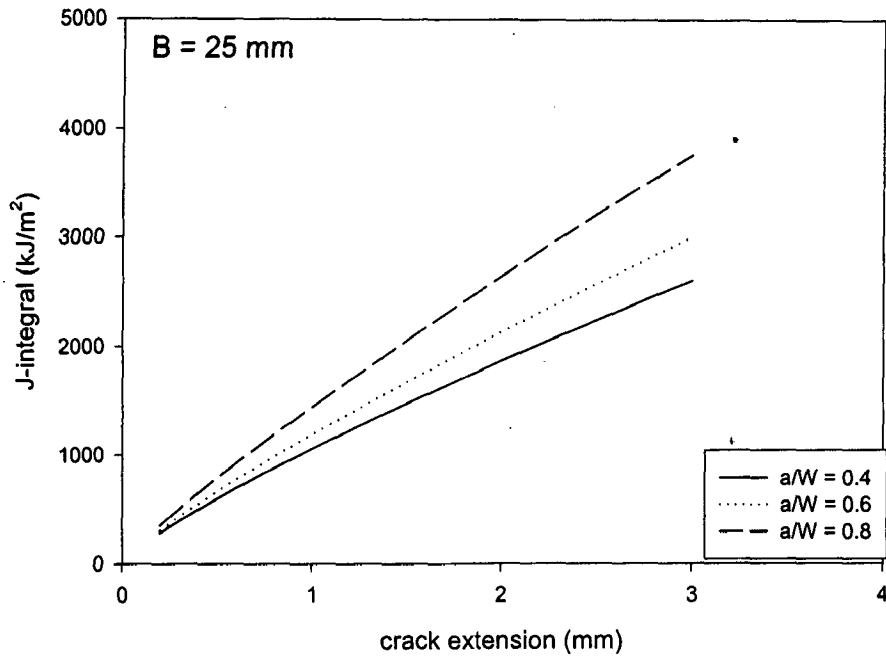


**Fig. 5.40** The averaged *J-R* curve of 25 mm thickness at different *a/W* ratio of the TPB specimens of SA333 Gr. 6 steel.

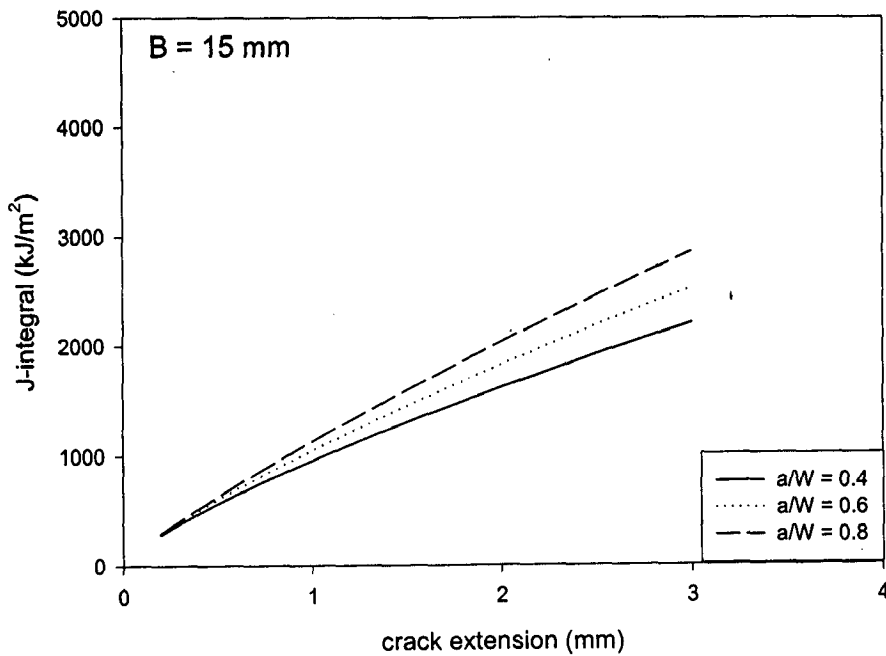


**Fig. 5.41** The averaged *J-R* curve of 15 mm thickness at different *a/W* ratio of the TPB specimens of SA333 Gr. 6 steel

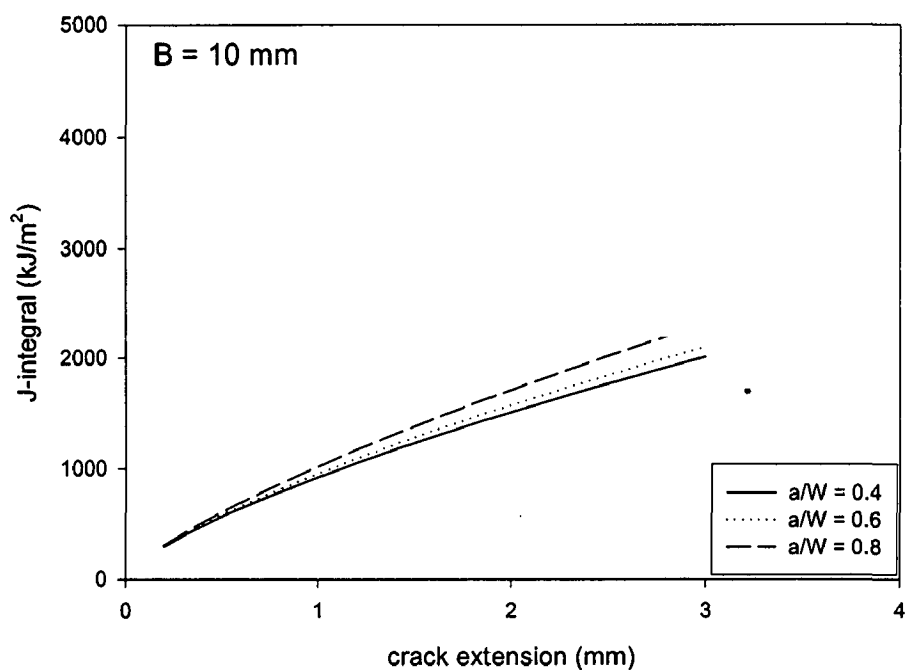


**Fig. 5.42** The averaged *J-R* curve of 10 mm thickness at different *a/W* ratio of the TPB specimens of SA333 Gr. 6 steel

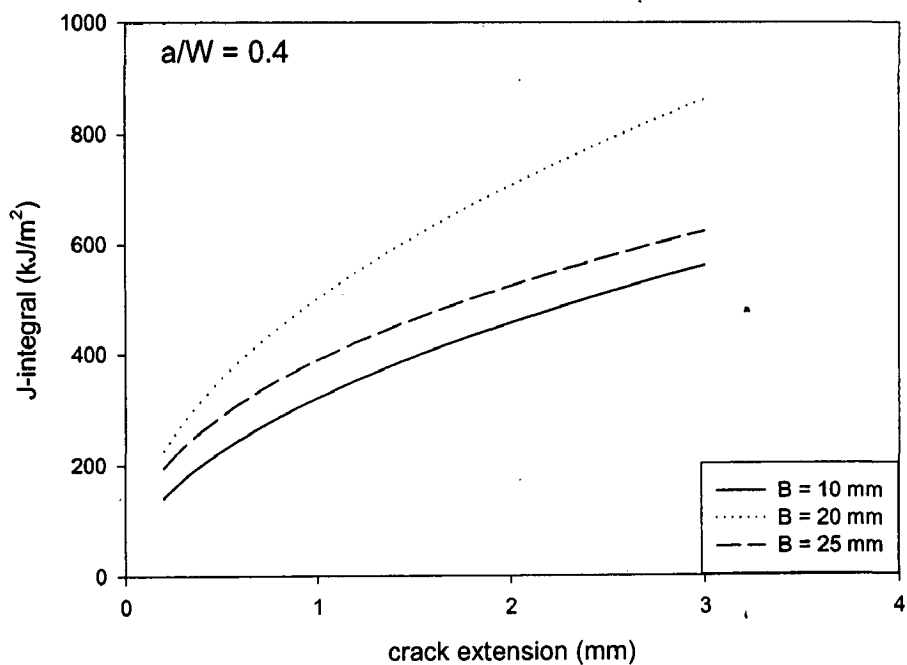


**Fig. 5.43** The averaged *J-R* curve at pre-crack depth of 0.4 at different thickness of the CT specimens of SAILMA steel.

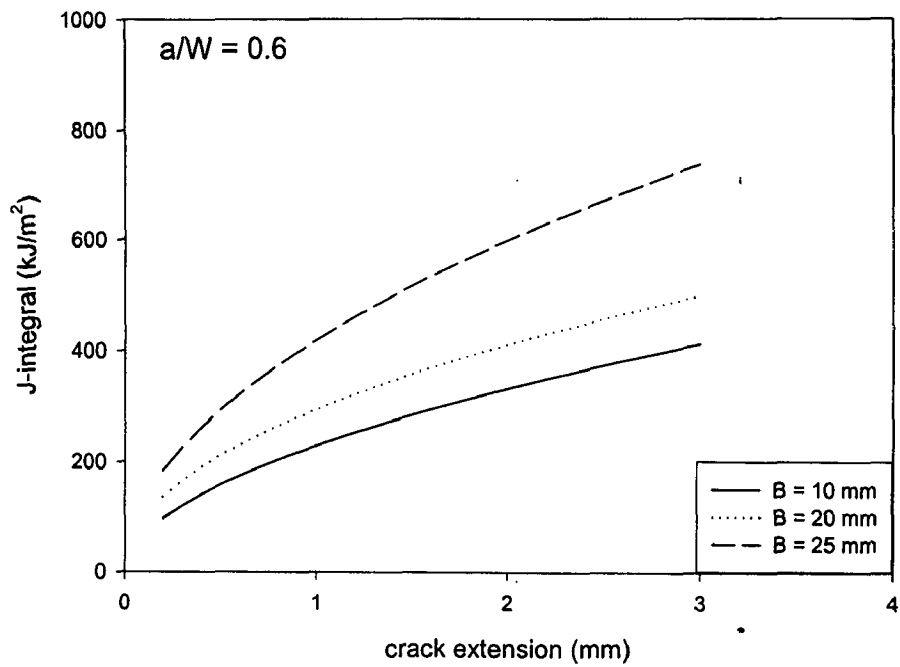


**Fig. 5.44** The averaged *J-R* curve at pre-crack depth of 0.6 at different thickness of the CT specimens of SAILMA steel.

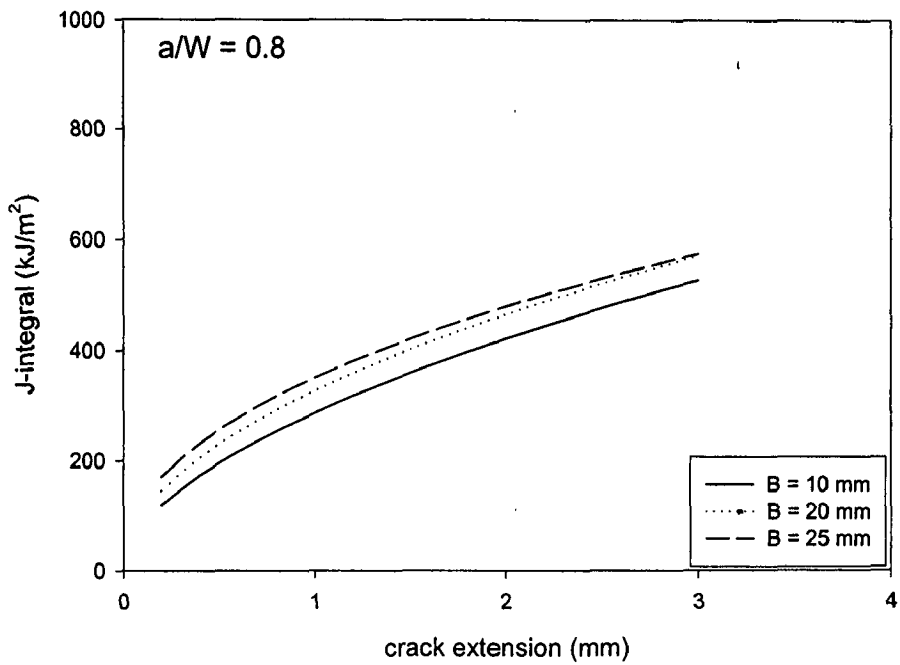


**Fig. 5.45** The averaged *J-R* curve at pre-crack depth of 0.8 at different thickness of the CT specimens of SAILMA steel.



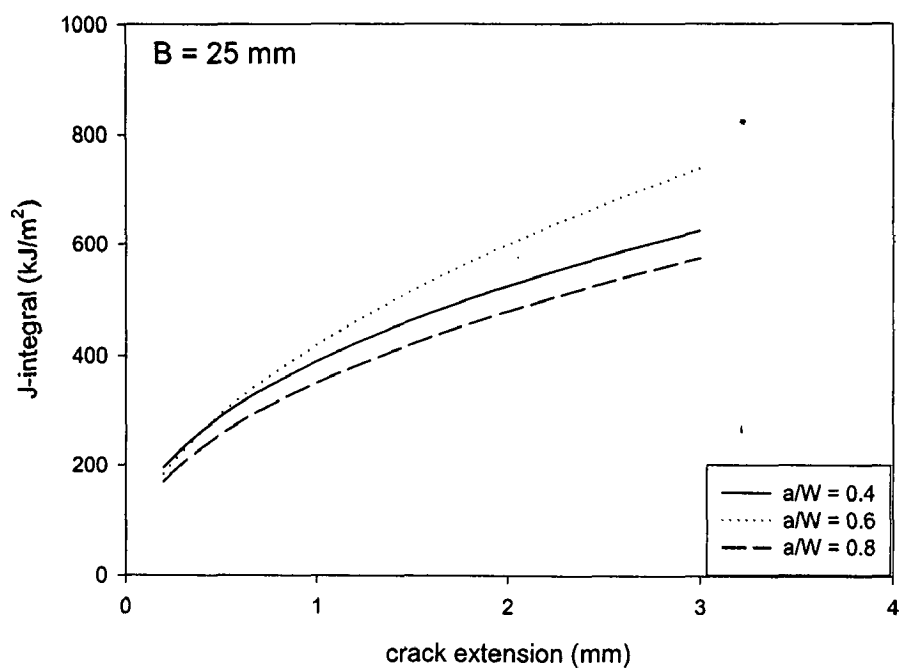


**Fig. 5.46** The averaged  $J$ - $R$  curve of 25 mm thickness at different  $a/W$  ratio of the CT specimens of SAILMA steel.

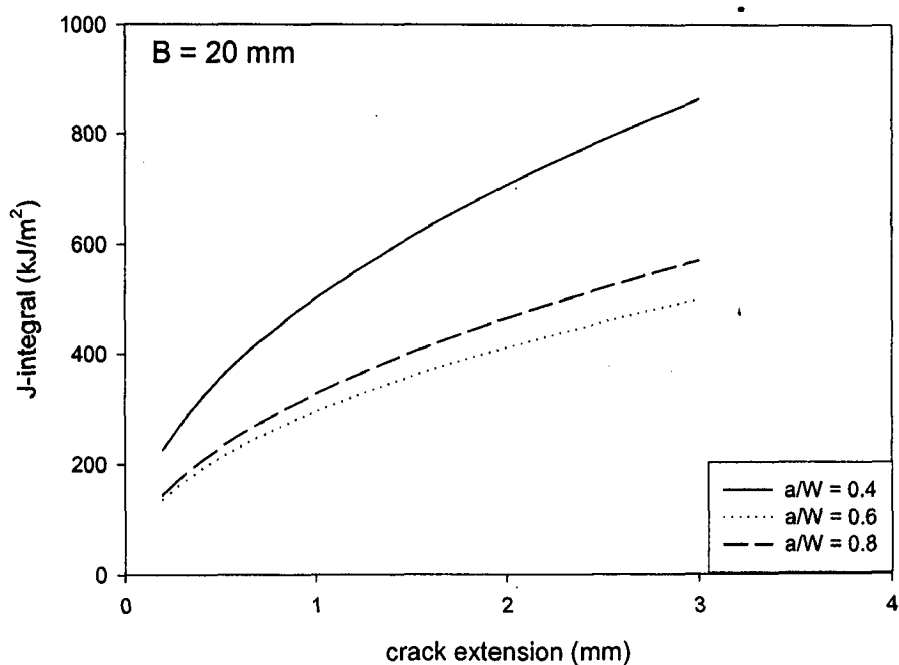


**Fig. 5.47** The averaged  $J$ - $R$  curve of 20 mm thickness at different  $a/W$  ratio of the CT specimens of SAILMA steel.

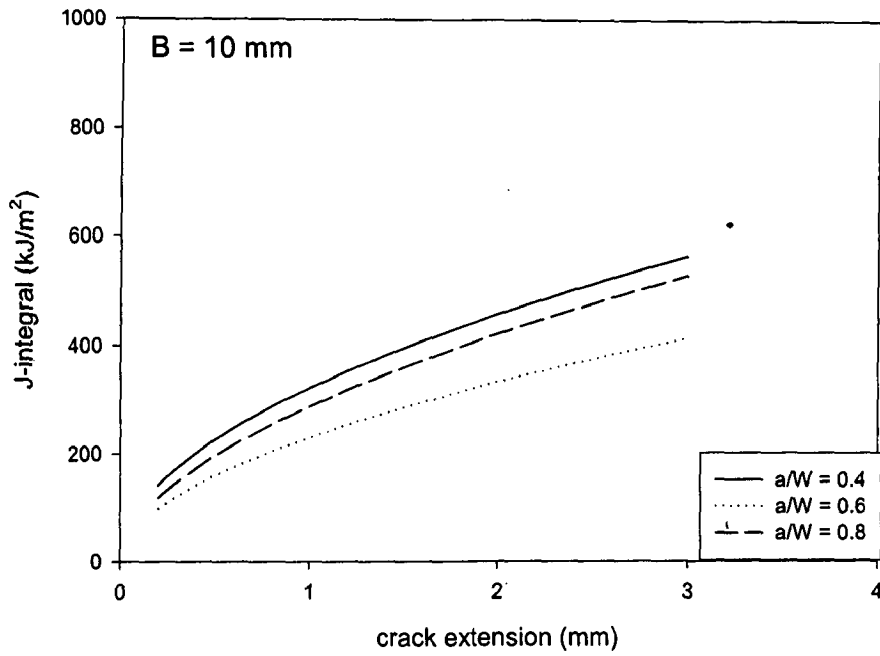


**Fig. 5.48** The averaged  $J$ - $R$  curve of 10 mm thickness at different  $a/W$  ratio of the CT specimens of SAILMA steel.

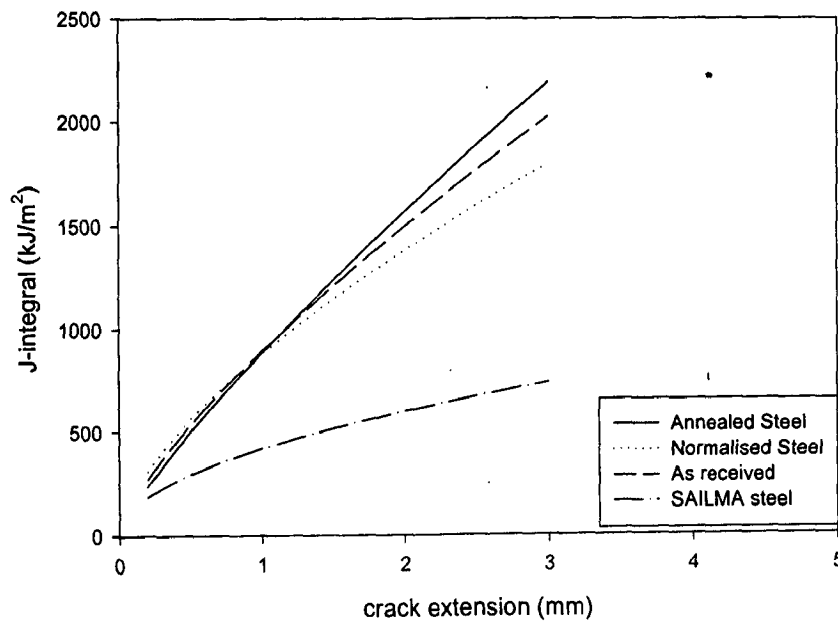


**Fig. 5.49** The averaged  $J$ - $R$  curve of SA333 Gr. 6 steel with or without heat treatment and SAILMA steel as observed in CT specimens of 25 mm thickness and pre-crack depth of 0.6.

Is it annealed? ?

extension all the three  $J$ - $R$  curves of SA333 Gr. 6 are very close although normalized one shows a relatively higher  $J$ - $R$  curve followed by that of as received as well as annealed SA333 Gr. 6 steel. But the difference between these curves are too small to have any confidence in their relative positions. Thereafter, crossover takes place at higher crack extension and the annealed steel shows higher resistance against crack extension, followed by that in as received and that in normalized steel. But SAILMA steel shows a considerably lower  $J$ - $R$  curve from the very beginning in crack extension. After cross over, all the three  $J$ - $R$  curves of SA333 Gr. 6 steel diverge with increasing crack extension. But the  $J$ - $R$  curve of SAILMA steel retains a considerably lower slope.

## 5.6 DISCUSSION

The development of failure arising out of stable or unstable crack propagation leading to fracture of pre-cracked large scale specimens and components, depends on the stress state as well as geometry. For a better prediction of failure by fracture mechanics, it is necessary to have a crack resistance curve corresponding to the component or at least, capable of representing conservatively the component behavior. In order to delineate the influence of the stress state on the course of the crack resistance curves, a comparison has been made between crack resistance curves determined from specimens of various sizes and geometries with the purpose of arriving at a lower bound crack resistance curve. The results of this segment of study, described in previous sections, are discussed here.

Elastic plastic fracture mechanics is concerned with safety against fracture of a cracked structure in the face of slow stable crack growth. The precise determination of value of  $J = J_{IC}$ , characterizing the onset of propagation of crack under monotonic load is necessary for a given material. For the determination of  $J_{IC}$ , ASTM prescribes the blunting line method in which the intersection of the 0.2 mm offset blunting line and the  $J$ - $R$  curve defines the initiation fracture toughness in a test specimen. ASTM standard defines the blunting line

using the equation  $J = 2M\sigma_f\Delta a$ , where  $M = 1$  and  $\sigma_f = \frac{1}{2}(\sigma_y + \sigma_u)$  [ASTM -813-89] determine the slope of the blunting line. For highly ductile materials like SA333 Gr. 6 steel, the initiation fracture toughness ( $J_{IC}$ ) could not be determined by the 0.2 mm offset blunting line proposed by the ASTM, as this offset line based on material flow stress does not intersect the  $J$ - $R$  curve within the valid region prescribed by ASTM standard, shown in Fig. 5.1. Figure 5.1 shows that the intersection of the blunting line with  $J$ - $R$  curve takes place at considerably larger distance than the stretched zone width, which measures the end of blunting of fatigue pre-crack directly by experiment. Thus, it is evident that the blunting line equation based on flow stress does not represent the blunting behavior of the fatigue pre-crack. It is obvious that any equation to represent blunting behavior should reflect the work hardening characteristics of the material as well. For highly ductile materials an accurate blunting line has been determined experimentally by ascertaining that the offset line intersects the  $J$ - $R$  curve at the observed stretched zone width in test specimens of materials having different strain hardening coefficient. The value of  $M$  calculated from the 0.2 mm offset on the basis of equation (5.3) for SA333 Gr. 6 steel is found to be 34.73, which shows a steep slope in the blunting line. Thus, it may be desirable to adopt a smaller offset of 0.1 mm and use the equation of  $M_{0.1}$  as the equation for determining the slope of the blunting line. It may be desirable to use 0.1 mm offset line for the purpose of limiting the slope of the blunting line within a range of single digit values.

The stretched zone width is clearly identified by the boundary of fatigue fracture obtained during pre-fatiguing and the ductile fracture obtained during crack propagation as discussed in the previous chapter. The stretched zone width has been used to identify the initiation of crack extension. This value of 'apparent' crack extension equivalent to blunting before initiation of actual crack extension, has been used to find the single-point fracture-toughness value  $J_{IC}$ . Figures 5.5 and 5.6 show the comparison of fracture toughness measured

by the 0.2 mm offset blunting line method, which is essentially derived on the basis of slope matching with the *SZW* observed for low carbon steels of various history, and the fracture toughness measured directly by *SZW* observed in CT and TPB specimens of SA333 Gr. 6 steel. These figures show that the values of initiation fracture toughness measured by the *SZW* method and those measured by the 0.2 mm offset blunting line show fairly good consistency of individual measurements in both CT and TPB specimens of SA333 Gr. 6 steel as shown respectively in Figs. 5.5 and 5.6. Fairly similar results are obtained also in SAILMA steel as shown in Fig. 5.9 for CT specimens.

The initiation fracture toughness ( $J_{IC}$ ) values observed for the 25 mm thick CT specimens of as received SA333 Gr. 6 steel is  $\sim 330 \text{ kJ/m}^2$  for a pre-crack depth of 0.6 while that for TPB specimens of the same steel specimen of the same thickness and pre-crack depth is  $\sim 320 \text{ kJ/m}^2$ . Tarafder *et al* [2003] has reported the initiation fracture toughness,  $J_{IC}$ , of  $315 \text{ kJ/m}^2$ , measured on the basis of stretched zone width in 25 mm TPB specimen of SA333 Gr. 6 steel without mentioning the corresponding pre-crack depth. However,  $J_{IC}$  value reported by Tarafder *et al* [2003] on the basis of ASTM blunting line without offset is  $567 \text{ kJ/m}^2$  which is much higher than the  $J_{IC}$  measured by *SZW* method in the same specimen. It is apparent that following the ASTM prescribed blunting line, the intersection with *J-R* curve is taking place at a point far beyond the stretched zone width. Singh *et al* [1998] have reported initiation fracture toughness of  $400 \text{ kJ/m}^2$  in 25 mm thick CT specimen of SA333 Gr. 6 steel, with pre-crack depth of 0.5, evaluated by the blunting line without offset based on the equation  $J = m \cdot \sigma_f \cdot \Delta a$  where  $m = 4.82$ . However, if the initiation fracture toughness is determined by 0.2 mm offset blunting line, it is  $675 \text{ kJ/m}^2$ .

The initiation fracture toughness ( $J_{IC}$ ) value observed is  $\sim 200 \text{ kJ/m}^2$  in 25 mm thick CT specimens of SAILMA steel, with pre-crack depth of 0.6, measured either by the 0.2 mm offset blunting line method or by *SZW* method. The observed value of initiation fracture

toughness is similar to  $\sim 190 \text{ kJ/m}^2$  reported by Sun *et al* [1989] for equivalent HY 80 steel measured by 0.2 mm offset blunting line in TPB specimens.

The variation of the initiation fracture toughness ( $J_{IC}$ ) with the pre-crack depth ( $a/W$  ratio) for CT specimens of SA333 Gr. 6 steel having thickness of 25 mm, 15 mm and 10 mm are shown in Figs. 5.10, 5.11 and 5.12. These figures show that in a relatively thin specimen there is drastic reduction in  $J_{IC}$  when pre-crack depth increases from  $a/W$  ratio of 0.4 to 0.6 but beyond 0.6,  $J_{IC}$  changes marginally till  $a/W$  ratio of 0.8. But at larger thickness of 25 mm, there is continuous reduction in  $J_{IC}$  with increasing  $a/W$  ratio in the entire range from 0.4 to 0.8.

The results on the effect of  $a/W$  ratio on  $J_{IC}$  in CT specimens of SAILMA steel show similar trends of variation in Figs. 5.22, 5.23 and 5.24 as it has been observed in Figs. 5.10, 5.11 and 5.12 for SA333 Gr. 6 steel. At higher thickness, the change in  $J_{IC}$  is relatively small but continuous with increasing  $a/W$  ratio but at lower thickness, there is a drastic reduction in  $J_{IC}$  when pre-crack depth increases from  $a/W$  ratio of 0.4 to 0.6. Thus, it is evident that in thicker specimens conforming to plain strain condition,  $J_{IC}$  will become smaller with increasing  $a/W$  ratio. Thus, depending on crack size, the design criteria for initiation fracture toughness may be fixed for savings in material use. Enhanced detection limit to lower crack size in quality control may be rewarded with higher value of  $J_{IC}$  for design. However, towards plane stress condition as prevailing in thinner specimens,  $J_{IC}$  values may reduce drastically with  $a/W$  ratio at lower depth of pre-crack but eventually becomes less sensitive at higher pre-crack depth.

The fracture toughness of three point bend specimen of SA333 Gr. 6 steel increases with increasing  $a/W$  ratio as shown in Figs. 5.13, 5.14 and 5.15, but the extent of increase is relatively small and becomes still smaller at lower thickness. This trend is contrary to that observed on CT specimens. The trend of variation of  $J_{IC}$  with increasing  $a/W$  ratio in either CT and TPB specimen will depend on the method of the determination of  $J_{IC}$  from the  $J$ - $R$  curve. In

the literature there are different types of trends reported for this behavior –starting from decreasing  $J_{IC}$  with increasing  $a/W$  to  $J_{IC}$  independent of  $a/W$ .

Zhang and Wang [1987] while studying the variation of  $J_{IC}$  with  $a/W$  in TPB specimens of structural steel in the range of 0.1 to 0.5 have observed that  $J_{IC}$  decreases with increasing  $a/W$  ratio. However, the authors have not indicated the method of determination of  $J_{IC}$ . Shen *et al* [2001] in their study on TPB specimens of CSA grade G40.21 350WT plate materials at  $-30^{\circ}\text{C}$  have similarly observed that  $J_{IC}$  decreases with increasing  $a/W$  ratio in the range between 0.2 to 0.7. In this study,  $J_{IC}$  has been determined by 0.2 mm offset blunting line with slope which has been taken as function of both strain hardening coefficient and  $a/W$  ratio. The slope increases with increasing  $a/W$  ratio and therefore, forcing an intersection offset blunting with  $J$ - $R$  curve at earlier crack extension point for higher  $a/W$ , thereby resulting in lower  $J_{IC}$ .

In the study carried out by Tarafder *et al* [2003] on the TPB specimens of the same SA333 Gr. 6 steel used in the current investigation, it has been found that on increasing  $a/W$  ratio,  $J_{IC}$  decreases initially and thereafter it increases before decreasing again at higher  $a/W$  ratio. This trend has been explained by these investigators in terms of recovery of fracture toughness around  $a/W= 0.35$  and renewed loss of constraint at higher  $a/W$  ratio. Li *et al* [1986] in their study on TPB specimens of high strength and high toughness alloy steel, have observed that  $J_{IC}$  is insensitive to  $a/W$  ratio when  $a/W$  is greater than 0.2. Jitsukawa *et al* [1999] have not found any appreciable change in  $J_{IC}$  value with increasing  $a/W$  ratio from 0.125 to 0.5 in TPB specimens of 7075-T6 high strength aluminum alloy. Joyce and Link [1995, 1997] have carried out an extensive study on A533B, HY-100 and HY-80 structural steels in different types of CT and TPB specimens in the range of  $a/W$  ratios from 0.13 to 0.83 but could not detect any effect of  $a/W$  ratio on  $J_{IC}$ . However, a large effect of  $a/W$  ratio on  $J$ - $R$  curve have been observed only at relatively large crack extension.

In the present study with TPB specimens,  $J_{IC}$  has been determined on the basis of mean  $SZW$  and 0.2 mm offset blunting line based on the slope, determined by matching with the observed mean  $SZW$  as stated earlier. Stretched zone width has a variation along the thickness of the specimen which originates from inhomogeneity of mechanical properties on microscopic scale and the standard error resulting due to this variation may give rise to an uncertainty in the determination of  $J_{IC}$ . 95 % confidence limit for the  $J_{IC}$  values are indicated by  $J_{+SZW}$  and  $J_{-SZW}$  in Tables 5.2, 5.3 and 5.4. The observed increase of  $J_{IC}$  in TPB specimens with increasing  $a/W$  ratio consistently for all the three thicknesses appears to be a genuine trend if initiation fracture toughness is measured on the basis of  $SZW$ . A strong defence for the measurement of  $J_{IC}$  on the basis of  $SZW$  lies in  $SZW$  being a directly measurable quantity and its variation along the thickness is a real effect originating from the property of the specimen. Thus, a host of contradictory trend in the variation of  $J_{IC}$  could be avoided if  $J_{IC}$  is measured on the basis of  $SZW$  which is directly measurable. The variation of  $J_{IC}$  in CT specimens with increasing  $a/W$  is distinctly different from that observed in TPB specimens. This difference in the trend of  $J_{IC}$  with  $a/W$  ratio in CT and TPB specimens could only be attributed to difference in mode of loading and the associated difficulties in experiments.

The influence of specimen thickness on the initiation fracture toughness  $J_{IC}$  have been shown in Figs. 5.16, 5.17 and 5.18 for CT specimens of SA333 Gr. 6 steel. Although it is expected that initiation fracture toughness should decrease with increasing thickness because one is moving towards plane strain conditions but it is observed only in the range of thickness between 15 and 25 mm. At relatively lower thickness initiation fracture toughness increases significantly with increasing specimen thickness between 10 and 15 mm. As the thickness decreases the plastic deformation in blunting will take place more readily due to lack of restraint, by absorbing energy before the plasticity is exhausted. In the thick specimens, it is expected that restraints from surrounding material will decrease the extent of plastic



deformation and thereby, decreasing the energy absorbed before the onset of crack propagation. However, it has to be realized that the size of plastic zone and the extent of energy absorbed for plastic deformation under a given state of stress are two different quantities. The size of plastic zone reduces as one move towards plain strain condition. But the trend of energy absorbed per unit volume of material may change the trend in the energy absorbed before the onset of crack extension from that observed for the size of plastic zone. It is, therefore, not inconceivable to find that an optimum  $J_{IC}$  is observed at intermediate thickness. Further, the energy required for shape change during stretching may also vary with thickness and pre-crack depth. Thus, the effect of pre-crack depth or thickness on  $J_{IC}$  may not involve merely the plastic zone size and it could be more complex as indicated by the results. The variation of the initiation fracture toughness,  $J_{IC}$ , measured on TPB specimens of SA333 Gr. 6 steel, with increasing specimen thickness have been shown in Figs. 5.19, 5.20 and 5.21, respectively. These figures show that the initiation fracture toughness measured by either 0.2 mm offset blunting line or *SZW* method, is more or less insensitive to increasing thickness particularly at lower  $a/W$  ratio of 0.4 and 0.6 but at higher  $a/W$  ratio 0.8, there is a slight increase in initiation fracture toughness as the thickness increases from 15 mm to 25 mm. The variation of the initiation fracture toughness,  $J_{IC}$ , with the specimen thickness of CT specimens of SAILMA steel are shown in Figs. 5.25, 5.26 and 5.27 respectively. Figure 5.25 shows that at a pre-crack depth of  $a/W = 0.4$ , the fracture toughness increases from  $\sim 150$   $\text{kJ/m}^2$  to  $\sim 250$   $\text{kJ/m}^2$  when the specimen thickness increases from 10 mm to 20 mm but on increasing the thickness further to 25 mm, the fracture toughness decreases to  $\sim 210$   $\text{kJ/m}^2$ . However, Figs. 5.26 and 5.27 show that at higher pre-crack depth of  $a/W = 0.6$  or  $0.8$  the initiation fracture toughness increases steadily with increasing specimen thickness. Mao [1991] has tested CT specimens of A533B-1 steel with thickness ( $B$ ) of 25, 10, 3 and 0.5 mm having width ( $W$ ) of 50, 20, 10 and 10 mm respectively and concluded that the initiation fracture toughness decreases with decreasing specimen thickness when the width of the specimen remains fixed. Ono *et al* [2004] have also studied the effect of specimen

size on initiation fracture toughness in CT specimens of reduced activation ferritic steel, JLF-1. However,  $J_Q$  values obtained for the 1T-1CT and 1/2T-1CT (different thickness, same width) specimens are found to be 404 and 623 kJ/m<sup>2</sup>, respectively, indicating that the  $J_Q$  value increases with decreasing specimen thickness, which is expected considering plane strain condition and plastic zone size. Jitsukawa *et al* [1999], however, have not found any appreciable change in  $J_Q$  value with specimen thickness (for the same width) on three point bend bar specimens of 7075-T6 high strength aluminum alloy. The variation of  $J_{IC}$  with thickness and pre-crack depth as observed in the present study is primarily due to the influence of these variables of thickness and pre-crack depth on  $J-R$  curve. This is evident from the observation in the previous chapter that stretched zone width does not vary significantly with either thickness or pre-crack width in either CT or TPB specimens.

The effect of different heat treatments like annealing and normalizing on SA333 Gr. 6 steel has been shown in Fig. 5.28. The initiation fracture toughness in as received SA333 Gr. 6 steel is ~325 kJ/m<sup>2</sup> but it decreases to ~290 kJ/m<sup>2</sup> and ~220 kJ/m<sup>2</sup> after annealing and normalizing respectively. The micrograph of as received SA333 Gr. 6 steel shows the presence of ferrite and pearlite with banded morphology as shown in Fig. 4.2. However, under annealed and normalized conditions, the microstructure of the steels consists of well distributed ferrite and pearlite in the microstructure. The increase in the cooling rate in passing from annealing to normalization reduces the grain size. It is observed that normalized steel has higher yield strength and tensile strength than those in the annealed SA333 Gr. 6 steel due to faster rate of cooling in normalization resulting in a finer scale of distribution of ferrite and cementite in pearlite. The fine pearlite in normalized steel has relatively higher strength. However, ductility reduces in normalized steel compared to annealed steel. Due to higher ductility, annealed steel is able to absorb more energy before the onset of crack propagation compared to that in both as received and normalized steel. Interestingly, as received steel with banded pearlite has a higher  $J_{IC}$ , possibly because entirely ferrite band has

much higher capability to absorb energy before the onset of crack propagation than that attained in well distributed ferrite-pearlite structure.

The results on  $J$ - $R$  curve show that the TPB specimens show a consistent variation with either thickness or pre-crack depth in SA333 Gr. 6 steel. For a given pre-crack depth, the  $J$ - $R$  curve for a specimen of higher thickness is higher compared to those of lower thicknesses. In other words, one may state that for the same crack extension, one will have to employ higher  $J$  in a relatively thicker specimens as shown in Figs. 5.37, 5.38 and 5.39. The divergence in  $J$  requirement in specimens of different thicknesses increases with increasing pre-crack depth. For a given thickness, the  $J$ - $R$  curve observed in a specimen with higher pre-crack depth is higher compared to those in specimens of relatively lower pre-crack depth as shown in Figs. 5.40, 5.41 and 5.42. Here, the divergence of the required  $J$  for the same crack extension in specimens of different pre-crack depth is more in relatively thicker specimens. Thus, it appears that the lowest  $J$ - $R$  curve which may be used for design purposes should be thinner with a shallow pre-crack depth. This conclusion, although contrary to present belief that  $J$ - $R$  curve should be lowest under plane strain condition, is inescapable from consistent trends obtained in the results on TPB specimens of SA333 Gr. 6 steel. Since the materials under investigation are highly ductile, one may have approached a situation where the development of plastic zone is limited by thickness at lower thickness and so, higher thickness may be resulting in larger plastic zone resulting in a higher  $J$ - $R$  curve for higher thickness. Similarly, with increasing pre-crack depth the ligament length is coming down and thereby, the plastic zone is increasing due to a lack of restraint in the width direction. The results are possible but careful FEM investigation is required to settle this issue.

The results on CT specimens of SA333 Gr. 6 steel show a complicated trend. During initial crack extension the  $J$ - $R$  curves for intermediate thickness of 15 mm are at the top for the given pre-crack depths of 0.4, 0.6 and 0.8 but at higher pre-crack depth of 0.6 and 0.8, the  $J$ - $R$  curve for 15 mm thick specimen crosses the  $J$ - $R$  curves of 10 mm and 25 mm thick

specimens to come to the bottom at higher crack extension as shown in Figs. 5.32 and 5.33. In SAILMA steel the trend for CT specimens are similar to those observed in TPB specimens of SA333 Gr. 6 steel at higher pre-crack depths of 0.6 and 0.8 as shown in Figs. 5.44 and 5.45. But the divergence in required  $J$  for the same crack extension in specimens of different thickness is more at relatively lower pre-crack depth of 0.6 than that for pre-crack depth of 0.8. But at lower pre-crack depth of 0.4, the  $J$ - $R$  curve for thinner specimen of 10 mm is higher than the  $J$ - $R$  curves for 20 and 25 mm specimens, which are close and parallel as shown in Fig. 5.41. For CT specimens of SA333 Gr. 6 steel of a given thickness, the relative positions of  $J$ - $R$  curves at higher crack extension for specimens with different pre-crack depths in the thinner specimen of 10 mm is similar to that observed in TPB specimens as shown in Fig. 5.36. This has happened because the  $J$ - $R$  curve for pre-crack depth 0.4 crossed the  $J$ - $R$  curves for specimens with pre-crack depth of 0.8 and 0.6. As the thickness of CT specimen increases to 15 mm, the  $J$ - $R$  curve for the lowest pre-crack depth of 0.4 occupies an intermediate position between the  $J$ - $R$  curves for pre-crack depth of 0.8, which is at the top, and for pre-crack depth of 0.6, which is at the bottom, as shown in Fig. 5.35. However, there is no crossover between the  $J$ - $R$  curves of different pre-crack depths.

At still higher thickness of 25 mm, the  $J$ - $R$  curve for pre-crack depth of 0.4 reaches the top at higher crack extension crossing the  $J$ - $R$  curve for pre-crack depth of 0.6 as shown in Fig. 5.34. Both these  $J$ - $R$  curves are however, very close. The  $J$ - $R$  curve for pre-crack depth of 0.8 is at the bottom but almost parallel to the other two  $J$ - $R$  curves at higher crack extension. In CT specimens of SAILMA steels, the  $J$ - $R$  curves shown in Figs. 5.46, 5.47 and 5.48, reveal that the curve for specimens with pre-crack depth of 0.8 is never at the top for specimens of any thickness studied here nor the  $J$ - $R$  curve for specimen with pre-crack depth of 0.4 is at the bottom, as observed in TPB specimens of SA333 Gr. 6 steel. However, except for specimen of thickness 25 mm, there is no cross over between  $J$ - $R$  curves of different pre-crack depths in relatively thinner specimens of 20 mm and 10 mm.

The trends of results obtained for  $J$ - $R$  curve in TPB specimens, although consistent are at variance with the accepted trends in the literature. It is generally observed that  $J$ - $R$  curve has relatively decreasing slope with increasing pre-crack depth for TPB specimens as observed by Lam *et al* [2003] and Shen *et al* [2001]. Similar variation has reported by Seok and Kim [2002] for CT specimens, Roos *et al* [1993] for DENT specimens. But a study carried out by Tarafder *et al* [2003] on the TPB specimens of SA333 Gr. 6 steel, has shown similar variation as observed in the present study for the TPB specimens of the same steel. Only in 25 mm thick CT specimens, the accepted trend of higher  $J$ - $R$  curve for lower pre-crack depth has been observed.

The results on the variation of  $J$ - $R$  curve with thickness have shown mixed trends. Seok and Kim [2002] have not observed any significant effect of thickness on  $J$ - $R$  curve of TPB specimens; Jitsukawa *et al* [1999] have also confirmed it. But Roos *et al* [1993] have observed that  $J$ - $R$  is lower in thicker SENT specimens and the same trend has been confirmed by Mao [1991] and Ono *et al* [2004] in CT specimens. In the present study, there is overwhelming indication that  $J$ - $R$  curve is higher in thicker specimens in TPB as well CT specimens of both SA333 Gr. 6 and SAILMA steels.

The discussion on the observed  $J$ - $R$  curves leads one to infer that the trends of  $J$ - $R$  curves for CT specimens of different thicknesses and pre-crack depths are not very consistent in both SA333 Gr.6 and SAILMA steel but TPB specimens of SA333 Gr. 6 steel show consistent trends in  $J$ - $R$  curves which are some times observed in CT specimens under limited circumstances. The nature of the test in TPB specimen makes it more reliable without any problem of specimen misorientation due to alignment of grips as encountered in tests of CT specimens. However, in SA333 Gr. 6 steel, the  $J$ - $R$  curve for 10 mm thick specimen with a pre-crack depth of  $a/W = 0.4$  results in the lowest  $J$ - $R$  curve both in CT and TPB specimens. In SAILMA steel, the lowest  $J$ - $R$  curve results in CT specimen of 10 mm thickness but with the pre-crack depth of 0.6.

The effect of different composition and heat treatments like annealing and normalizing on fracture behavior of different carbon steels under investigation has revealed that the initiation fracture toughness closely follows the trend in variation of ductility obliterating the effect of strength. This is because of limited variation of mechanical properties in the steels investigated. At relatively high crack extension, the annealed SA333 Gr. 6 steel has relatively much higher slope of  $J$ - $R$  curve although as received SA333 Gr. 6 steel has shown a relatively higher strength and ductility as shown in Fig. 5.49. It could only be attributed to banded microstructure of as received steel, although it has still a higher initiation fracture toughness. The normalized steel although has well distributed pearlite in the microstructure but fine pearlite and its relatively larger volume fraction make it suffer to have a relatively lower  $J$ - $R$  curve at high crack extension as well as relatively lower initiation fracture toughness.

The major conclusions of the present investigation are given here in two segments. The first segment includes conclusions related to materials characterization and stretched zone width observed on the fractured surface of the tested CT and TPB specimens of the two steels used in the present investigation. The conclusions pertaining to the initiation fracture toughness and  $J$ - $R$  curves are outlined in the second segment.

### A. MATERIAL CHARACTERIZATION AND STRETCHED ZONE

- (1) The steels used in the present investigation, has relatively low carbon contents of 0.16 wt. % and 0.14 wt. % respectively in SA333 Gr. 6 steel and SAILMA steel. SA333 Gr. 6 steel has major alloying elements of manganese and silicon but SAILMA steel is microalloyed with small amounts (0.01 to 0.05 wt%) of strong carbide formers like vanadium, titanium and niobium.
- (2) As received SAILMA steel has banded pearlite and extremely fine ferrite grains compared to as received SA333 Gr. 6 steel which also has banded pearlite and ferrite but ferrite grains are relatively coarser.
- (3) Annealed and normalized SA333 Gr. 6 steel have relatively coarser ferrite grains compared to that in as received steel. But the pearlite got well distributed in the microstructure due to heat treatment and the annealed microstructure is the coarsest due to slow cooling but the normalized microstructure has more pearlite, relatively finer than that in the annealed microstructure. In terms of increasing ferrite grain size, the order is as received SAILMA steel, as received SA333 Gr. 6 steel, normalized SA333 Gr. 6 steel and annealed SA333 Gr. 6 steel.

- (4) The yield strength increases in the order annealed SA333 Gr. 6 steel, as received SA333 Gr. 6 steel, normalized SA333 Gr. 6 steel and SAILMA steel, with observed yield strengths of 306, 318, 327 and 440 MPa respectively. The tensile strength increases in the order annealed SA333 Gr. 6 steel, normalized SA333 Gr. 6 steel, as received SA333 Gr. 6 steel and SAILMA steel, with observed tensile strength of 415, 428, 445 and 574 MPa respectively. The tensile strength maintains almost the same order as in yield strength excepting that as received SA333 Gr. 6 steel has relatively lower yield strength compared to that in normalized steel, which has been attributed to banded microstructure in as received steel.
- (5) The ductility decreases in the order of as received SA333 Gr. 6 steel, annealed SA333 Gr. 6 steel, normalized SA333 Gr. 6 steel and SAILMA steel with observed percent elongation of 38.0, 36.7, 34.2 and 28.8 respectively. It is interesting to note that SA333 gr. 6 steel has higher ductility in as received banded microstructure than even in the annealed microstructure, which has a coarser microstructure than the as received one.
- (6) Stretched zone has been identified as the region between the end of the fatigue crack front resulting during pre-cracking and the onset of the ductile tearing and its width is measured across the thickness at close interval of 200  $\mu\text{m}$ , using scanning electron microscope under tilted condition. In as received SA333 Gr. 6 steel, the mean stretched zone width in CT specimens vary between 201  $\mu\text{m}$  to 240  $\mu\text{m}$  with the maximum standard error of  $\pm 4\%$  which is a manifestation of inhomogeneity in mechanical properties across the crack front and the end effect from the sides of the specimen in the thickness direction.
- (7) In TPB specimens of SA333 Gr. 6 steel, the mean stretched zone width developed are of similar magnitude as in CT specimens but has a tendency to be a little lower in majority of the specimens of the same thickness and pre-crack depth.



- (8) In both the as received steels, having different alloying element, the measurements of the stretched zone width have shown similar mean width of 212  $\mu\text{m}$  and 227  $\mu\text{m}$  respectively in 25 mm thick CT specimens of SA333 Gr. 6 steel and SAILMA steel having the same pre-crack depth of 0.6. Thus, for the low carbon steels investigated, variation in composition of alloying elements does not results in significant variation of stretched zone width in the limited context of low carbon steels investigated.
- (9) In SA333 Gr. 6 steel, annealing and normalization causes distribution of banded pearlite in as received steel to a more uniform distribution in the microstructure but shows stretched zone width of 226  $\mu\text{m}$  and 255  $\mu\text{m}$  respectively. But annealed steel shows relatively lower standard deviation than that in normalized steel which has phase constituents of ferrite and fine pearlite, having wider variation in mechanical properties compared to ferrite and coarse pearlite in annealed steel.
- (10) Mean stretched zone width measured in either CT or TPB specimens by nine point method following ESIS procedure, is more representative of the mean obtained by measurements at close intervals of 200  $\mu\text{m}$ , than that obtained by three point method. However, the standard deviation of the measurements by nine point method is relatively lower than that observed in the measurements at close intervals. Nine point method could, therefore, be taken as an adequate procedure but three point method may result in large deviations from the results of mean at close interval.
- (11) Because of relatively larger standard deviation in the measurements of stretched zone width, arising out of microscope variation in mechanical properties, no significant trend of variation of stretched zone width with thickness could be inferred.
- (12) The trend of variation of stretched zone width with changes in the pre-crack depth could not be inferred again because of its marking by large standard deviation.

## B. FRACTURE BEHAVIOUR

- (13) The initiation fracture toughness ( $J_{IC}$ ) in SA333 Gr. 6 steel could not be determined from ASTM blunting line equation with 0.2 mm offset, since the slope of the blunting line based on material flow stress is fairly low and so, the offset blunting line does not intersect the  $J$ - $R$  curve within the valid region as prescribed by ASTM standard. So ASTM procedure for determining initiation fracture toughness based on a blunting line, whose slope depends on flow stress, could not be followed in the highly ductile SA333 Gr. 6 steel having relatively lower strength.
- (14) The slope of the 0.2 mm offset blunting line,  $M_{0.2}$ , has been determined such that the line intersects the  $J$ - $R$  curve at stretched zone width in different low carbon steels of varying strain hardening parameter,  $n$ , of Ramberg-Osgood equation and it is given by  $M_{0.2} = 1 + 4.53 \times 10^7 (1/n)^{9.59}$ .
- (15) The slope  $M_{0.2}$  is observed to vary over a large magnitude when  $n$  is limited to a range between 4.37 to 5.5. But if, the offset is limited to 0.1 mm the range of variation of slope,  $M_{0.1}$ , becomes rather limited. The variation of  $M_{0.1}$  with Ramberg-Osgood strain hardening parameter is given by  $M_{0.1} = 1 + 2.93 \times 10^5 (1/n)^{7.74}$ .
- (16) The initiation fracture toughness ( $J_{IC}$ ) observed for the 25 mm thick CT specimens of as received SA333 Gr. 6 steel is  $\sim 330 \text{ kJ/m}^2$  for a pre-crack depth of 0.6 while that for TPB specimens of the same steel specimen of the same thickness and pre-crack depth is  $\sim 320 \text{ kJ/m}^2$ , similar to that reported earlier [Tarafder *et al* 2003] on the basis of stretched zone width in 25 mm TPB specimen of SA333 Gr. 6 steel.
- (17) In 25 mm thick CT specimens of SAILMA steel, with pre-crack depth of 0.6, the initiation fracture toughness ( $J_{IC}$ ) is  $\sim 200 \text{ kJ/m}^2$ , similar to that observed in HY 80 steel measured by 0.2 mm offset blunting line in TPB specimens [Sun *et al* 1989].

- (18) The variation of the initiation fracture toughness ( $J_{IC}$ ) with the pre-crack depth ( $a/W$  ratio) for CT specimens of SA333 Gr. 6 steel having thickness of 25 mm, 15 mm and 10 mm show that in a relatively thin specimen there is drastic reduction in  $J_{IC}$  when pre-crack depth increases from  $a/W$  ratio of 0.4 to 0.6 but beyond 0.6,  $J_{IC}$  changes marginally till  $a/W$  ratio of 0.8. But at larger thickness of 25 mm, there is continuous reduction in  $J_{IC}$  with increasing  $a/W$  ratio in the entire range from 0.4 to 0.8.
- (19) The results on the effect of  $a/W$  ratio on  $J_{IC}$  in CT specimens of SAILMA steel show similar trends of variation as observed in SA333 Gr. 6 steel. At higher thickness, the change in  $J_{IC}$  is relatively small but continuous with increasing  $a/W$  ratio but at lower thickness, there is a drastic reduction in  $J_{IC}$  when pre-crack depth increases from  $a/W$  ratio of 0.4 to 0.6.
- (20) The fracture toughness of three point bend specimen of SA333 Gr. 6 steel increases with increasing  $a/W$  ratio, but the extent of increase is relatively small and becomes still smaller at lower thickness. This trend is contrary to that observed on CT specimens.
- (21) The influence of specimen thickness on the initiation fracture toughness  $J_{IC}$  for CT specimens of SA333 Gr. 6 steel show that fracture toughness decrease with increasing thickness but it is observed only in the range of thickness between 15 and 25 mm. At relatively lower thickness initiation fracture toughness increases significantly with increasing specimen thickness between 10 and 15 mm.
- (22) The variation of the initiation fracture toughness,  $J_{IC}$ , with the specimen thickness of CT specimens of SAILMA steel show that at a pre-crack depth of  $a/W = 0.4$ , the fracture toughness increases from  $\sim 150 \text{ kJ/m}^2$  to  $\sim 250 \text{ kJ/m}^2$  when the specimen thickness increases from 10 mm to 20 mm but on increasing the thickness further to 25 mm, the fracture toughness decreases to  $\sim 210 \text{ kJ/m}^2$ . However, at higher pre-crack depth of  $a/W = 0.6$  or  $0.8$  the initiation fracture toughness increases steadily with increasing specimen thickness.

- (23) The variation of the initiation fracture toughness,  $J_{IC}$ , measured on TPB specimens of SA333 Gr. 6 steel, with increasing specimen thickness show that the initiation fracture toughness measured by either 0.2 mm offset blunting line or *SZW* method, is more or less insensitive to increasing thickness particularly at lower  $a/W$  ratio of 0.4 and 0.6 but at higher  $a/W$  ratio 0.8, there is a slight increase in initiation fracture toughness as the thickness increases from 15 mm to 25 mm.
- (24) The results on  $J$ - $R$  curve show that TPB specimens show a consistent variation with either thickness or pre-crack depth in SA333 Gr. 6 steel. For a given pre-crack depth, the  $J$ - $R$  curve for a specimen of higher thickness is higher compared to those of lower thicknesses, resulting in higher  $J$  in relatively thicker specimens for the same crack extension. The divergence in  $J$  in specimens of different thicknesses increases with increasing pre-crack depth. For a given thickness, the  $J$ - $R$  curve observed in a specimen with higher pre-crack depth is higher compared to those in specimens of relatively lower pre-crack depth. The divergence of  $J$  in specimens of different pre-crack depth is more in relatively thicker specimens.
- (25) The results on  $J$ - $R$  curve for CT specimens of SA333 Gr. 6 steel show that during initial crack extension the  $J$ - $R$  curves for intermediate thickness of 15 mm are at the top for the given pre-crack depths of 0.4, 0.6 and 0.8 but at higher pre-crack depth of 0.6 and 0.8, the  $J$ - $R$  curve for 15 mm thick specimen crosses the  $J$ - $R$  curves of 10 mm and 25 mm thick specimens to come to the bottom at higher crack extension.
- (26) In SAILMA steel the trend of  $J$ - $R$  curve for CT specimens are similar to those observed in TPB specimens of SA333 Gr. 6 steel at higher pre-crack depths of 0.6 and 0.8. But the divergence in  $J$  in specimens of different thickness is more at relatively lower pre-crack depth of 0.6 than that for pre-crack depth of 0.8. But at lower pre-crack depth of 0.4, the  $J$ - $R$  curve for thinner specimen of 10 mm is higher than the  $J$ - $R$  curves for 20 and 25 mm thick specimens.

- (27) The observed  $J$ - $R$  curves leads one to infer that the trends of  $J$ - $R$  curves for CT specimens of different thicknesses and pre-crack depths are not very consistent in both SA333 Gr.6 and SAILMA steel but TPB specimens of SA333 Gr. 6 steel show consistent trends of lower  $J$ - $R$  curves for thinner specimens of higher pre-crack depth, which are some times observed in CT specimens as well under limited circumstances.
- (28) The effect of different composition and heat treatments like annealing and normalizing on fracture behavior of different carbon steels reveals that the variation in initiation fracture toughness in CT specimens of 25 mm thickness and pre-crack depth of 0.6, closely follows the trend of variation in ductility obliterating the effect of strength, possibly because of limited variation of mechanical properties in the steels investigated.
- (29) At relatively high crack extension, the annealed SA333 Gr. 6 steel having relatively lower strength, has relatively much higher slope of  $J$ - $R$  curve compared to that in as received SA333 Gr. 6 steel which has shown a relatively higher strength and ductility, possibly because of the difference in morphology of phases. The normalized SA333 Gr. 6 steel has a  $J$ - $R$  curve lower than that of as received steel at higher crack extension reflecting the importance of ductility, which is more emphasized in the lowest observed  $J$ - $R$  curve in SAILMA steel.



## REFERENCES

1. Alexander, D.J. [1993], "Fracture toughness measurements with sub-size Disk Compact Specimens," *Small Specimens Test Techniques Applied to Nuclear Reactor Vessel Thermal Annealing and Plant Life Extension, ASTM STP 1204*, American Society of Testing and Materials, Philadelphia, pp. 130-142.
2. Amouzouvi, K.F. and Bassim, M.N. [1982], "Determination of fracture toughness from stretch zone width measurement in predeformed AISI type 4340 steel," *Materials Science and Engineering*, Vol. 55, pp. 257-262.
3. Anderson, T.L. [1995], "Fracture Mechanics, Fundamentals and Applications," 2nd edn., CRC Press, Boca Raton.
4. ASTM E 399-70T [1970], "Standard Test Methods for Plane-Strain Fracture Toughness of Metallic Materials, *Annual Book of ASTM Standards*, Vol. 03.01.
5. ASTM E 399, "Standard Test Methods for Plane-Strain Fracture Toughness of Metallic Materials, *Annual Book of ASTM Standards*, Vol. 03.01.
6. ASTM E 1823-96 [1996], "Standard Test Method for  $J_{IC}$ , a Measure of Fracture Toughness," ASTM Standard E-1823-96, *Annual Book of ASTM Standard*, Vol. 03.01, pp. 732-746.
7. ASTM E 813 [1995], "Standard Test Method for  $J_{IC}$ , A Measure of Fracture Toughness", *Annual Book of ASTM Standards*, Vol. 03.01.
8. ASTM E 813-81 [1982], "Standard Test Method for  $J_{IC}$ , a Measure of Fracture Toughness," ASTM Standard E-813-89, *Annual Book of ASTM Standard*, pp. 732-746.
9. ASTM E 1820-01 [2001], "Standard Test Method for  $J$ -Integral Characterization of Fracture Toughness," *American Society for Testing and Materials*, Philadelphia.
10. Barsom, J.M. and Rolfe, S.T. [1987], "Fracture and Fatigue Control in Structures," 2nd edn., Prentice-Hall, Englewood Cliffs, NJ.

11. Bassim, M.N., Bayoumi, M.R. and Shum, D. [1987], "Study of the variation of fracture toughness with loading rate using compact tension specimens," *Engineering Fracture Mechanics*, Vol. 26, pp. 619-623.
12. Bassim, M.N., Matthews, J.R. and Hyatt, C.V. [1992], "Evaluation of fracture toughness of HSLA80 steel at high loading rates using stretch zone measurements," *Engineering Fracture Mechanics*, Vol. 43, pp. 297-303.
13. Bayoumi, M.R., Klepaczko, J.R. and Bassim M.N. [1984], "Determination of Fracture toughness  $J_{Ic}$  under quasi-static and dynamic loading conditions using wedge loaded specimens," *Journal of Testing and Evaluation*, Vol. 12, pp. 316-322
14. Begley, J.A. and Landes, J.D. [1972], "The J-integral as a Fracture Criterion. Fracture Toughness," *ASTM/STP 514, American Society for Testing and Materials*, pp. 1 -23.
15. Betegon, C. and Hancock, J.W. [1991], "Two parameter characterization of elastic-plastic crack-tip fields," *Journal of Applied Mechanics*, Vol. 58, pp. 104-10.
16. Bowman, R., Antolovich, S.D. and Brown, R.C. [1988], "A demonstration of problems associated with crack closure measurement techniques, *Engineering Fracture Mechanics*, Vol. 31(4), pp. 703-711.
17. Brocks, W., Eberle, A., Fricke, S. and Veith, H. [1994], "Large stable crack growth in fracture mechanics specimens," *Nuclear Engineering & Design*, Vol. 151, pp. 387-400
18. Broek, D. [1974], "Correlation between stretched zone size and fracture toughness," *Engineering Fracture Mechanics*, Vol. 6, pp. 173-174.
19. Broek, D. [1986], "Elementary Fracture Mechanics," 4<sup>th</sup> revised edn., Martinus Nijhoff Publishers, Dordrecht, The Netherlands.
20. Cao, Wei-Di, and Lu, Xiao-Ping [1984], "On the relationship between the geometry of deformed crack tip and crack parameters," *International Journal of Fracture*, Vol. 25, pp. 33-52.
21. Chao, Y.J. and Zhu, X.K. [1998], " $J-A_2$  Characterization of Crack-Tip Fields: Extent of  $J-A_2$  Dominance and Size Requirements," *International Journal of Fracture*, Vol. 89, pp. 285-307.

22. Chao, Y.J. and Zhu, X.K. [2000], "Constrain modified J-R curves and its application to ductile crack growth," *International Journal of Fracture*, Vol. 106, pp.135-160.
23. Chao, Y.J., Yang, S., and Sutton, M.A. [1994], "On the fracture of solids characterized by one or two parameters: theory and practice," *Journal of the Mechanics and Physics of Solids*, Vol. 42, pp. 629–647.
24. Clarke, G.A., Andrews, W.R., Paris, P.C. and Schmidt, D.W. [1976], "Single specimen tests for  $J_{Ic}$  determination," *Mechanics of crack growth, ASTM / STP 590*, American Society for Testing and Materials, pp. 27-42.
25. Dawes, M.G. [1979], "Elastic plastic fracture toughness based on J contour integral concepts," *STP 668*, American Society for Testing and Materials, pp. 307-333.
26. Decamp, K., Bauvineau, L., Besson, J., Pineau, A. [1997], "Size and geometry effects on ductile rupture of notched bars in a C-Mn steel: experiments and modeling," *International Journal of Fracture*, Vol. 88, pp. 1-18.
27. Dodds, Jr. R.H., Shih, C.F. and Anderson, T.L. [1993], "Continuum and micromechanics treatment of constraint in fracture," *International Journal of Fracture*, Vol. 64, pp. 101-33.
28. Dugdale, D.S. [1960], "Yielding in steel sheets containing slits," *Journal of the Mechanics of Physics and Solids*, Vol. 8, pp. 100-106.
29. Eisele, U., Roos, E., Seidenfuss, M. and Silcher, H. [1992], "Determination of J - integral-based crack resistance curve and initiation values for the assessment of cracked large-scale specimens," *Fracture Mechanics: Twenty Second Symposium (Volume I)*, ASTM STP 1133, American Society for Testing and Materials, Philadelphia, pp. 37–59.
30. Elliot, C., Emark, M., Lucas, G.E. [1991], "Development of disk compact tension specimens and test techniques for HFIR irradiation," *Journal of Nuclear Materials*, Vol. 179, pp. 434–437.
31. Eshelby, J.D. [1956], "The Continuum Theory of Lattice Defects," *Solid State Physics*, Vol. 3, pp. 79-141



32. **ESIS P1-92 [1992a]**, “ESIS recommendations for determining the fracture resistance of ductile materials,” January 1992, ESIS office, University of Technology, Delft, The Netherlands.
33. **ESIS P2-92 [1992b]**, “ESIS procedure for determining the fracture behaviour of materials: ESIS P2-92,” *European Structural Integrity Society*, Delft, The Netherlands.
34. **Faleskog J. [1995]**, “Effects of local constraint along three-dimensional crack fronts - a numerical and experimental investigation,” *Journal of the Mechanics of Physics and Solids*, Vol. 43, pp. 447-493.
35. **Gibson, G.P. [1987]**, “The use of alternating current potential drop for determining J-crack resistance curves,” *Engineering Fracture Mechanics*, Vol. 26, pp. 213-222.
36. **Gilbert, C.J., Cao, J.J., De Jonghe, L.C., and Ritchie, R.O. [1997]**, “Crack-growth resistance-curve behaviour in silicon carbide: small versus long cracks,” *Journal of American Ceramics Society*, Vol. 80, pp. 2253–2261.
37. **Gilmore, C.M., Provenzano, V., Smidt, F.A.Jr. and Hawthorne, J. R [1983]**, “Influence of thickness and temperature on stretched zone size in  $J_{Ic}$  tests,” *Metal Science*, Vol. 17, pp. 177-185.
38. **Gordon, J.R. [1986]**, “An assessment of the accuracy of the unloading compliance method for measuring crack growth resistance curve,” 325-1986, The Welding Institute, Abington, Cambridge.
39. **Griffith, A.A. [1920]**, “The Phenomena of Rupture and Flow in Solids”, *Philosophical Transactions, Series A*, Vol. 221, pp. 163-198.
40. **Gullerud, A.S., Doods Jr, H.R. Hampton R.W. and Dawicke D.C. [1999]**, “Three dimensional modeling of ductile crack growth in thin sheet metals: computational aspects and validation,” *Engineering Fracture Mechanics*, Vol. 63, pp. 347-374.
41. **Halim, A., Dahl, W. and Hagedorn, K.E. [1988]**, “Measurements of stretched zone width (SZW)—A round robin program of European group on fracture” *Engineering Fracture Mechanics*, Vol. 31, pp. 857-866.

42. **Hancock, J.W., Reuter, W.G., and Parks, D.M.**, [1993], "Constraint and Toughness Parameterized by  $T$ ," *Constraint Effects in Fracture, ASTM STP-1171*, American Society of Testing and Materials, Philadelphia, pp.21–40.
43. **Haynes, M.J., Gangloff, R.P.** [1997], "High resolution R-curve characterization of the fracture toughness of thin sheet aluminum alloys," *Journal of Testing and Evaluation*, Vol. 25, pp. 82-98.
44. **Heerens, J., Cornec, A. and Schwalbe, K.H.** [1988], "Results of a round robin on stretch zone width determination," *Fatigue Fract. Engng. Mater. Struct.*, Vol. 11, pp. 19–29.
45. **Henry, B.S., Luxmoore A.R., Sumpter J.D.G.** [1996], "Elastic-plastic fracture mechanics assessment of low constraint aluminium test specimens," *International Journal of Fracture*, Vol. 81, pp. 217-234.
46. **Hertzberg, R.W.** [1983], "Deformation and Fracture Mechanics of Engineering Materials," 4th edn., Wiley.
47. **Hsing-Shih, C. and Ji-Liang, D.** [1983], "Influence of precracking load on critical stress intensity factor of mild steel," *Journal of Materials Science*, Vol. 18, pp. 2305–2310.
48. **Hutchinson J.W.** [1968a], "Plastic Stress and Strain Fields at a Crack Tip", *Journal of Mechanics and Physics of Solids*, Vol. 16, pp. 337-347.
49. **Hutchinson, J.W.** [1968b], "Singular Behavior at the End of a Tensile Crack Tip in a Hardening Material," *Journal of Mechanics and Physics of Solids*, Vol. 16, pp. 13-31.
50. **Hutchinson, J.W. and Paris, P.C.** [1979], "Stability Analysis of J-Controlled Crack Growth," *Elastic-Plastic Fracture*, ASTM STP 668, American Society for Testing and Materials, pp. 37-64.
51. **Hyatt, C.V. and Matthews, J.R.** [1994], "Variation of stretch zone width with  $J$ , loading rate, temperature and pre-crack depth," *International Journal of Fracture*, Vol. 66, pp. 19-32.
52. **Inglis, C.E.** [1913], "Stress in Plate Due to the Presence of Cracks and Sharp Corners", *Transactions of the Institute of Naval Architects*, Vol. 55, pp. 219-241.

53. Irwin G.R. [1948], "Fracture Dynamics", *Fracturing of Metals*, American Society for Metals, pp. 147-166.
54. Irwin G.R. [1957], "Analysis of Stresses and Strains Near the End of a Crack Traversing a Plate" *Mechanics*", *Journal of Applied Mechanics*, Vol. 24, pp. 361-364.
55. Jitsukawa S., Naito A. and Segawa J. [1999], "Effect of size and configuration of 3- point bend bar specimens on J-R curves," *Journal of Nuclear Materials*, Vol. 271&272, pp. 87-91.
56. Joyce J.A. and Link R.E. [1997], "Application of two parameter elastic-plastic fracture mechanics to analysis of structures," *Engineering Fracture Mechanics*, Vol. 57, pp. 431-446.
57. Joyce J.A. and Link R.E., [1995], "Effects of Constraint on Upper Shelf Fracture Toughness," *Fracture Mechanics: 26th Vol., ASTM STP-1256*, American Society of Testing and Materials, Philadelphia, pp. 142-177.
58. Kaufman, J.G., Schilling, P.E. [1973], "Influence of Stress Intensity Level During Fatigue Precracking on Results of Plane-Strain Fracture Toughness," *Progress in Flaw Growth and Fracture Toughness Testing*, ASTM STP 536, pp. 312-319.
59. Kfourri, A.P. [1986], "Some evaluations of the elastic T-term using Eshelby's method", *International Journal of Fracture*, Vol. 30, pp. 301-315
60. Kikuchi, M. [1997], "Study of the effect of the crack length on the  $J_{IC}$  value," *Nuclear Engineering and Design*, Vol. 174, pp. 41-49.
61. Klemm, W., Memhard, D. and Schmitt, W. [1991], "Experimental and numerical investigation of surface cracks in plates and pipes," In: *Kussmaul K, editor. Fracture Mechanics Verification by Large-Scale Testing, EGF/ESIS8*, pp. 139-150.
62. Knott, J.F. [1980], *Metal Science*, Vol. 14, pp 327.
63. Kobayashi, H., Hirano. K., Nakamura, H. and Nakazawa, H. [1977], "A Fractographic study on Evaluation of Fracture Toughness," *Fracture 1977*, Vol. 3, ICF4, Waterloo, Canada, June 19- 24, pp. 583-592.

64. Kobayashi, H., Nakamura, N. and Nakazawa, H., [1979], "A relation between crack tip blunting and the J integral" *Int. Conf. on Materials*, Vol. 3, pp. 529-538. Cambridge, England (August 1979).
65. Kolednik, O. and Stüwe, H.P. [1986], "An extensive analysis of a  $J_{IC}$ -test," *Engineering Fracture Mechanics*, Vol. 24, pp. 277-290.
66. Kordisch, H., Sommer, E. and Schmitt, W. [1989], "The influence of triaxiality on stable crack growth," *Nuclear Engineering Design*, Vol. 112, pp. 27-35.
67. Krasovskii, A. Ya [2000], "Stereoscopic measurements of the stretched zone as an independent method for metal fracture toughness control" *Strength of Materials*, Vol. 32, pp. 476-479.
68. Krasowsky, A.J., Vainshtok, V.A. [1981], "On the relationship between stretched zone parameters and fracture toughness of ductile structural steels," *International Journal of Fracture*, Vol. 17, pp. 579-592.
69. Lam, P.S., Chao, Y.J., Zhu, X-K., Kim, Y. and Sindelar, R.L. [2003], "Determination of Constraint- Modified J-R Curves for Carbon Steel Storage Tanks," *Journal of Pressure Vessel Technology*, Vol. 125, pp. 136-143.
70. Lam, P.S., Kim, Y. and Chao, Y.J. [2005], "Crack tip opening displacement and angle for a growing crack in carbon steel," *WSRC-MS-2005-00059*, U.S. Department of Energy, pp. 1-18.
71. Landes, J.D. and Begley, J.A. [1972], "The Effects of Specimen Geometry on  $J_{IC}$ " Fracture Toughness, *ASTM STP - 514*, American Society for Testing and Materials, pp. 24-39.
72. Landes, J.D. and Begley, J.A. [1974], "Test results from J integral studies: An attempt to establish a  $J_{IC}$  testing procedure" *American Society for Testing and Materials STP- 560*, pp.170-186.
73. Larsson, S.G. and Carlsson, A.J. [1973], "Influence of non-singular stress terms and specimen geometry on small-scale yielding at crack tips in elastic-plastic materials," *Journal of the Mechanics of Physics and Solids*, Vol. 21, pp. 263-.

74. Li, Q., Zhou, L. and Li, S. [1986], "The effect of  $a/W$  ratio on crack initiation values of COD and  $J$ -integral," *Engineering Fracture Mechanics*, Vol. 23, pp. 925-928.
75. Lloyd, and McClintock, [2003], "Microtopography for ductile fracture process characterization Part 2: application for CTOA analysis", *Engineering Fracture Mechanics*, Vol. 70, pp. 403-415.
76. Luo, L.G., and Embury, J. D. [1988], "An investigation of crack blunting processes under plane strain conditions" *Engineering Fracture Mechanics*, Vol. 30, pp. 177-190.
77. Mao, X. [1991], "Influence of specimen size on I–III mixed mode fracture, fracture toughness  $J_{IC}$  and plastic dissipation with crack growth  $dW_p/da$ ," *Engineering Fracture Mechanics*, Vol. 38, pp. 241-254
78. Marengo, A.A. and Ipina, J.E.P. [1996], "Pressure vessel steel fracture toughness in the regime from room temperature to 400 °C," *Nuclear Engineering and Design*, Vol. 167, pp. 215-222.
79. Marschall, C.W., Papaspyropoulos, V. and Landow, M.P. [1989], "Evaluation of attempts to predict large-crack growth  $J - R$  curves from small specimen tests," *Nonlinear Fracture Mechanics: Volume II – Elastic Plastic Fracture*, ASTM STP 995, American Society of Testing and Materials, Philadelphia, pp.123–143.
80. May, M.J. [1970], "British experience with plane strain fracture toughness ( $K_{IC}$ ) testing," *Review of Developments in Plane Strain Fracture Toughness Testing*, ASTM STP 463, pp. 41–62.
81. McClintock, F.A. [1971], "Plasticity Aspects of Fracture", *Fracture – An Advanced Treatise*, Vo. 3, H. Liebowitz, editor, Academic Press, New York, pp. 47-255
82. Mills, W. J. [1981], "On the relationship between stretch zone formation and  $J$ -integral for high strain hardening materials" *Journal of Testing and Evaluation*, Vol. 9, pp. 56-62.
83. Mott, N.F. [1948], "Fracture of Metals: Theoretical Considerations", *Engineering*, Vol. 165, pp. 16-18.
84. Moyer, E.T., McCoy, H. and Sarkani, S. [1997], "Prediction of stable crack growth using continuum damage mechanics," *International Journal of Fracture*, Vol. 86, pp. 375–384.

85. Nguyen-Duy, P. and Bayard, S. [1981], "Fracture toughness of 4130 quenched and tempered steel" *Journal of Engineering Materials and Technology*, Vol. 103, pp. 55-61
86. Nikishkov, G.P., Bruckner-Foit, A. and Munz, D. [1995], "Calculation of the second fracture parameter for finite cracked bodies using a three-term elastic-plastic asymptotic expansion," *Engineering Fracture Mechanics*, Vol. 52, pp. 685-701.
87. O'Dowd, N.P. [1995], Applications of two parameter approaches in elastic-plastic fracture mechanics. *Engineering Fracture Mechanics*, Vol. 52, pp. 445-465.
88. O'Dowd, N.P. and Shih, C.F. [1991], "Family of crack-tip fields characterized by a triaxiality parameter - I. Structure of fields," *Journal of the Mechanics and Physics of Solids*, Vol. 39, pp. 989-1015.
89. O'Dowd, N.P. and Shih, C.F. [1992], "Family of crack-tip fields characterized by a triaxiality parameter - II. Fracture applications," *Journal of the Mechanics and Physics of Solids*, Vol. 40, pp. 939-963.
90. O'Dowd, N.P. and Shih, C.F. [1994], "Two-parameter fracture mechanics: Theory and Applications," *Fracture Mechanics: twenty-fourth volume, ASTM STP 1207*, American Society for Testing and Materials, Philadelphia, pp. 21-47.
91. Ohji, K., Ogura, K., Mutoh, Y., Itogawa, H., Uchida, H., and Honki, M., [1978], *J. Mater. Sci. Soc. Jpn.*, Vol. 27, pp. 31
92. Okumura, N., Venkatasubramanian, T.V., Unvala, B.A. and Baker, T.J., [1981], "Application of the ac potential drop technique to the determination of R curves of tough ferritic steels", *Engineering Fracture Mechanics*, Vol. 14, pp. 617-625.
93. Omidvar, B., Michael P. Wnuk and Choroszynski, M. [1997], "Relationship between the CTOD and the J-integral for stationary and growing cracks: Closed-form solutions," *International Journal of Fracture*, Vol. 87, pp. 331-343.
94. Ono, H., Kasada, R., and Kimura, A. [2004], "Specimen size effects on fracture toughness of JLF-1 reduced-activation ferritic steel," *Journal of Nuclear Materials*, Vol. 329-333, pp. 1117-1121.

95. Orowan, E. [1948], "Fracture and Strength of Solids", *Reports on Progress in Physics*, Vol. XII, pp. 185-232.
96. Pandey, R.K. and Banerjee, S. [1973], "Studies of fracture toughness and fractographic features in Fe-Mn base alloys," *Engineering Fracture Mechanics*, Vol. 5, pp. 965-975.
97. Pickles, B.W. and Cowan, A. [1983], "A review of warm prestressing studies," *International Journal of Pressure Vessel and Piping*, Vol. 14, pp. 95-131.
98. Pluvinage, G. and Lanvin, A. [1993], "Stretch zone geometrical measurement, a particular way to measure fracture toughness," *Fatigue Frac. Eng Mater Struct*, Vol. 16, pp.955- 972.
99. Putatunda, S.K. and Rigsbee, J.M. [1985], "Influence of specimen size on the crack-opening stretch zone," *Materials Science and Engineering*, Vol. 70, pp. 111-122.
100. Putatunda, S. K. [1986], "A comparison of various fracture toughness testing methods," *Engineering Fracture Mechanics*, Vol. 25, pp. 429-439
101. Rice, J.R. [1968], "A Path Independent Integral and the Approximate Analysis of Strain Concentration by Notches and Cracks," *Journal of Applied Mechanics*, Vol. 35, pp. 379-386.
102. Rice, J.R. and Rosengren, G.F. [1968], "Plane Strain Deformation near a Crack Tip in a Power-Law Hardening Material," *Journal of Mechanics and Physics of Solids*, Vol. 16, pp. 1-12.
103. Robinson, J.N. and Tetelman, A.S. [1976], "Comparison of various methods of measuring  $K_{IC}$  on small precracked bend specimens that fracture after general yield," *Engineering Fracture Mechanics*, Vol. 8, pp. 301-313.
104. Roos, E., Eisele, U. and Silcher, H. [1993], "Effect of stress state on the ductile fracture behaviour of large scale specimens," *Constraint effects in fracture, ASTM STP 1171*, American Society for Testing and Materials, Philadelphia, pp. 41-63.

105. Roos, E., Eisels, U. and Stumpfrock, L. [2000] "Transferability of results of PTS experiments to the integrity assessment of reactor pressure vessel," *Nuclear Engineering and Design*, Vol. 198, pp. 173-183.
106. Roos, E., Eisels, U., Silcher, H. and Eckert, W. [1991], Impact of the stress state on the fracture mechanics of heavy section steel component failure mechanics. *Fracture Mechanics Verification by Large-Scale Testing, EGF/ESIS8* (Edited by K Kussmaul), pp. 65–85.
107. Rosenthal, Y.A., Tobler, R.L. and Purtscher, P.T. [1990], JIC data analysis methods with a 'negative crack growth' correction procedure, *Journal of Testing and Evaluation* Vol. 18, pp. 301–304.
108. Saxena, A. and Hudak, Jr. S.J., [1978], "Review and Extension of Compliance Relationships for Common Crack Growth Specimens," *International Journal of Fracture*, Vol. 14, pp. 453-469.
109. Schwalbe, K.H., Hayes, B, Baustian, K., Cornec, A., Gordon, R., Homayun, M. and Voss, B. [1993], "Validation of the fracture mechanics test method EGF P1-87D (ESIS P1-90 / ESIS P1-92)," *Fatigue Fract. Engng. Mater. Struct.*, Vol. 16, pp. 1231–1284.
110. Scibetta, Marc, Enricolucon, Walle E.V. and Valo, M. [2002], "Towards a uniform precracking procedure for fracture toughness tests," *International Journal of Fracture*, Vol. 117, pp. 287-296.
111. Seok, Chang-Sung [2000], "Correction methods of an apparent negative crack growth phenomenon," *International Journal of Fracture*, Vol. 102, pp. 259-269.
112. Seok, Chang-Sung and Kim, Soo-Yong [2002], "Effect of specimen configurations on the fracture resistance Curve," *Nuclear Engineering and Design*, Vol. 214, pp. 47–56.
113. Sham T-L. [1991], "The determination of the elastic T-term using higher order weight functions," *International Journal of Fracture*, Vol. 48, pp. 81–102.
114. Shan, G.X., Kolednik, O. and Fischer, F.D. [1996], "A numerical study on the crack growth behaviour of a low and a high strength steel," *International Journal of Fracture*, Vol. 78, pp. 335–346.



115. Sharma, S.M., Aravas, N. and Zelman, M.G. [1995] "Two-parameter characterization of crack tip fields in edgedcracked geometries: Plasticity and creep solutions," *Fracture Mechanics: 25th Volume, ASTM STP 1220*, American Society for Testing and Materials, Philadelphia, pp. 309–327.
116. Shen, G., Xu, S. and Tyson, W.R., [2001], "Constraint Effects on Fracture Toughness", *Defence R & D Canada, Contract Report, DREA CR 2001-091*, Defence Research Establishment Atlantic.
117. Sherry A.H., France C.C. and Goldthorpe M.R. [1995], "Compendium of T-stress solutions for two and three dimensional cracked geometries," *Fatigue and Fracture of Engineering Materials & Structures*, Vol. 18, pp 141-155.
118. Shih, C.F., Delorenzi, H.G. and Andrews, W.R. [1979], "Studies on crack initiation and stable crack growth," *Elastic-Plastic Fracture*, ASTM STP 668, American Society for Testing and Materials, pp. 65-120.
119. Shih, C.F. [1981], "Relationship between Crack Tip Opening Displacement for Stationary and Extending Cracks," *Journal of Mechanics and Physics of Solids*, Vol. 29, pp. 305-326.
120. Singh, P.K., Chattopadhyay, J., Kushwaha, H.S., Tarafder, S. and Ranganath, V.R. [1998], "Tensile and fracture properties evaluation of PHT system piping material of PHWR," *International Journal of Pressure Vessels and Piping*, Vol. 75, pp. 271-280.
121. Sivaprasad, S., Tarafder, S., Ranganath, V. R., Das, S. K. and Ray, K. K.[2002], "Effect of Prestrain on stretch- zone Formation during Ductile Fracture of Cu-Strengthened High-Strength Low-Alloy Steels" *Metallurgical and Materials Transactions A*, Vol. 33A, pp. 3731-3740.
122. Smith, J., Bassim, M.N. and Liu, C.D. [1995], "Effects of fatigue precracking on stretch zone formation" *Engineering Fracture Mechanics*, Vol. 52, pp. 401-408.
123. Spitzig, W.A. [1968], "A fractographic feature of plane- strain fracture in 0.45C- Ni-Cr-Mo steel," *Trans. ASTM*, Vol. 61, pp.344.
124. Sreenivasan, P.R., Ray, S.K., Vaidyanathan, S. and Rodriguez, P. [1996], "Measurement of stretch zone height and its relationship to crack tip opening

- displacement and initiation J-value in an AISI 316 stainless steel," *Fatigue and Fracture of Engineering Materials & Structures*, Vol. 19, pp 855-868.
125. Srinivas, M. and Kamat, S.V., [1992], "Effect of notch root radius on ductile fracture toughness of Armco Iron," *International Journal of Fracture*, Vol. 58, pp. R15- R21.
  126. Srinivas, M., Kamat, S.V. and Rao, P.R. [1994], "A Fractographic Technique for the Estimation of Initiation Fracture Toughness  $J_{Ic}$  for Ductile Materials," *Journal of Testing and Evaluation*, Vol. 22, pp. 302-308.
  127. Srinivas, M., Malakondaiah, G. and Rama Roa, P. [1987], "Influence of polycrystal grain size on fracture toughness of and fatigue threshold in Armco iron," *Engineering Fracture Mechanics*, Vol. 28, pp. 561-576
  128. Sun, D.Z., Li, Z. and Tu, M. [1989], "Constraint Intensity in crack tip field and elastic-plastic fracture criterion," *Engineering Fracture Mechanics*, Vol. 34, pp. 413-418.
  129. Sun, D.Z. and Schmitt, W. [1990], "Application of micro-mechanical models to analysis of ductile fracture resistance behaviour," *Numerical Methods in Fracture Mechanics* (Eds. AR Luxmoore and DRJ Owen), Proceedings of the 5th international conference in Freiburg, pp. 275-286.
  130. Sun, D.Z., Sester, M. and Schmitt, W. [1997], "Development and application of micro-mechanical material models for ductile fracture and creep damage," *International Journal of Fracture*, Vol. 86, pp. 75-90.
  131. Talug, A. and Reifsnider, K. [1977], "Analysis and Investigations of Small Flaws", *ASTM STP 637*, pp. 81-96.
  132. Tarafder, S. and Ranganath, V.R, Sivaprasad, S. and Johri, P. [2003], "Ductile fracture behaviour of primary heat transport piping material of nuclear reactors," *Sadhana*, Vol. 28, pp. 167-186.
  133. Tobler, R.L. and Shimada, M. [1991], "Warm precracking at 295 K and its effects on the 4-K toughness of austenitic steels," *Journal of Testing and Evaluation*, Vol. 19, pp. 312-320.

134. Voss, B. and Mayville, R.A. [1985], "The use of the partial unloading compliance method for the determination of  $J$ - $R$  curve and  $J_{IC}$ ", *ASTM STP 856*, pp. 117–130.
135. Wallin, A. [2001], "Quantifying  $T_{\text{stress}}$  controlled constraint by the master curve transition temperature  $T_0$ ," *Engineering Fracture Mechanics*, Vol. 68, pp. 303-328.
136. Wallin, K. [1985], "The size effect in  $K_{IC}$  results," *Engineering Fracture Mechanics*, Vol. 22, pp. 149-163.
137. Westergaard, H.M. [1939], "Bearing Pressure and Cracks", *Journal of Applied Mechanics*, Vol. 6, pp. 49-53.
138. Wells, A.A. [1961], "Unstable Crack Propagation in Metals: Cleavage and Fast Fracture," *Proceedings of the Crack Propagation Symposium*, Vol. 1, Paper 84, Cranfield, U.K., 1961.
139. Williams M.L., [1957], "On the Stress Distribution at the Base of a Stationary Crack", *Journal of a Applied Mechanics*, Vol. 24, pp. 109-114.
140. Wu, Shang-Xian [1984], "Crack length calculation formula for three point bend specimens," *International Journal of Fracture*, Vol. 24, pp. R33–R35.
141. Wu, S.-X., Mai, Y.-W. and Cotterell, B. [1995] "Prediction of the initiation of ductile fracture," *Journal of the Mechanics of Physics and Solids*, Vol. 43, pp. 793–810.
142. Xia, L. and Shih, C.F. [1995a], "Ductile crack growth - I. A numerical study using computational cells with microstructurally – based length scales," *Journal of the Mechanics of Physics and Solids*, Vol. 43, pp. 233–259.
143. Xia, L. and Shih, C.F. [1995b], "Ductile crack growth - II. Void nucleation and geometry effects on macroscopic fracture behaviour," *Journal of the Mechanics of Physics and Solids* Vol. 43, pp. 1953–1981.
144. Xia, L., Shih, C.F. and Hutchinson, J.W. [1995], "A computational approach to ductile crack growth under large scale yielding conditions," *Journal of the Mechanics of Physics and Solids*, Vol. 43, pp. 389–413.

145. Yan, C. and Mai, Y.W. [1997], "Effect of constraint on ductile crack growth and ductile – brittle fracture transition of a carbon steel," *International Journal of Pressure Vessels and Piping*, Vol. 73, pp. 167–173.
146. Yang, S., Chao, Y.J. and Sutton, M.A. [1993], "Higher order asymptotic crack tip fields in a power-law hardening material," *Engineering Fracture Mechanics*, Vol. 45, pp. 1-20.
147. Yin, S. W., Gerbrands, R.A. and Hartevelt, M. [1983], "An investigation of the blunting line" *Engineering Fracture Mechanics*, Vol. 18, pp. 1025-1036.
148. Yuan, H. and Brocks, W. [1989], "Numerical investigation on the significant of  $J$  for large stable crack growth," *Engineering Fracture Mechanics*, Vol. 32, pp. 459-468.
149. Yuan, H. and Brocks, W. [1998], "Quantification of constraint effects in elastic-plastic crack front fields," *Journal of Mechanics and Physics of Solids*, Vol. 46, pp.219-41.
150. Zhang, D.Z. and Wang, H. [1987], "On the effect of the ratio  $a/W$  on the values of  $\delta_i$  and  $J_i$  in a structural steel," *Engineering Fracture Mechanics*, Vol. 26, pp. 247-250.
151. Zhang, D.Z. and Huang, X.D. [1988], "The crack initiation and plastic work," *Engineering Fracture Mechanics*, Vol. 29, pp. 415-421.
152. Zheng, M., Zhou, G., Zacharopoulos, D.A., and Kuna, M., [2000a], "Crack initiation behavior in StE690 steel characterized by strain energy density criterion," *Theoretical and Applied Fracture Mechanics*, Vol. 36, pp. 141-145.
153. Zheng, M., Lauschke, U. and Kuna, M. [2000b], "A damage mechanics based approach for fracture of metallic components," *Computational Materials Science*, Vol. 19, pp. 170-178.
154. Zhu, X.K. and Chao, Y.J. [1999], "Characterization of constraint of fully plastic crack-tip fields in non-hardening materials by the three-term solution," *International Journal of Solids and Structures*, Vol. 36, pp. 4497–4517.